

**NEW ASSESSMENT CRITERIA FOR  
DURABILITY EVALUATION OF  
HIGHLY REPELLENT SURFACES**

A thesis submitted for the degree of Doctor of  
Philosophy

by  
Anna Maria Wojdyła-Cieślak

Department of Mechanical Aerospace and Civil Engineering  
Brunel University  
November 2016

## Declarations

I declare that this thesis was composed by myself, that the work contained herein is my own except where explicitly stated otherwise in the text, and that this work has not been submitted for any other degree or professional qualification except as specified

Signed:

Anne Marie Wojcylta - Cieślak

Date:

2nd May 2017

## ABSTRACT

Highly repellent surfaces are constantly being sought in a number of industrial sectors, where accumulation of unwanted material (ice, debris, insects etc...) can cause seriously detrimental effects on these function. The chemistry and physics of such surfaces is relatively well-understood, yet their industrial adoption is still very limited, due to their poor durability. Emerging technologies for nanostructured coatings have significant potential for the development of advanced surfaces, where high repellency can be combined with mechanical robustness. However, lack of understanding of the wear mechanism in such coatings and lack of recognised test methodologies to enable comparison of various approaches hinders effective progress in advanced surfaces development. Furthermore, there is no comprehensive classification system that allows categorization of highly repellent surfaces.

New multi-variable analysis methodology for the evaluation of durability in highly repellent coatings was developed in this study. Key coating parameters were identified, including initial wettability, abrasive wear, adhesive wear and ability to retain repellency. Coating characteristics were examined with FTIR, SEM, AFM, DSA, Taber Abrader, roughness profilometer and goniometer. Furthermore, these characteristics were presented in a form of spider diagrams and performance indices and are used to generate plot of performance indices. In this study, six types of TWI coating anti-soiling materials (based on patented TWI's Vitolane® technology, containing silsesquioxanes and functionalized silica nanoparticles) and two commercial easy clean products were prepared and subjected to new assessment methodology.

It has been found that this novel methodology for evaluation of highly repellent surfaces allows comparison and categorizing different families of coatings. The data obtained from plot of performance indices supports the statement that there is an inverse relation between repellency and durability of hydrophobic surfaces. It has been found that coatings with low Ra value (no more than 10nm) and symmetric distribution of peaks and valleys are the most durable, yet their WCA value doesn't exceed more than 105°. It has been also found that some nanostructured coatings behave beyond this inverse relationship. Addition of novel inorganic building blocks

with controlled size (Ra in a range of 200nm and symmetric distribution in roughness profile) and functionalities (3-(trimethoxysilyl)propyl methacrylate and 1H 1H 2H 2H-perfluorooctyltriethoxysilane) improves overall coating performance by linking mechanical robustness with desired wetting characteristics (WCA reaches 112°C).

The progress in testing and classification criteria of repellent coatings enables further development of next generation of materials. This novel knowledge-based approach for highly repellent coatings validation has the potential to accelerate uptake. The findings open a promising new direction in materials development, where advanced coatings and surface treatments can be developed by design, reducing the number of development iterations, ultimately leading to reduced cost and development time.

## ACKNOWLEDGEMENT

First and foremost I would like to express my gratitude to my supervisor Dr Alan Taylor, who has supported me throughout my thesis with his patience and knowledge whilst giving me freedom to work in on my way. His has been a constant source of motivation during all the time of research and writing of this thesis. I could not have imagined having a better advisor and mentor for my PhD study.

I'm also very grateful to Professor Ian Boyd for his scientific advice and knowledge and many insightful discussions and suggestions. It was a pleasure to work with him.

I would also like to thank Dr Alec Gunner and Dr George Fern for providing advice, information and support on different aspects of project. I'm also very thankful to Professor Wamadeva Balachandran for good advice, support and constructive suggestions during all PhD programme.

I'm also very grateful to my fantastic team from TWI, Dr Geraldine Durand, Gillian Dixon-Payne, Laura Vivar, Maria Linzoain, Marion Bourebrab, Marta Alvarez, and Nadia Sid. My research would not have been possible without their support and help. I will be forever thankful to Steve Mycock, Alexander Russell, Jacob Greenwood and Ashley Spencer for their invaluable help with the experiments. I would also like to thank Evan Keller and Karthik Selvaraj for advice and suggestions in FTIR analysis and Colin Graves for his help in statistics.

I would like to thank my colleagues form Experimental Technique Centre for all administrative help and support with experiments. Special thanks to Ashely Howkins for his help in SEM analysis and Nico Nelson for his guidance with AFM experiments.

Finally, I would like to thank my parents, husband, family and friends for their encouragement, support and invaluable help.

## GLOSSARY OF TERMS AND ACRONYMS

<b>Abhesion</b>	The ability of the surfacve to prevent or greatly decrease adhesion
<b>Abrasion resistance</b>	The ability of a coating to resist degradation due to mechanical wear
<b>Absorbance</b>	A measure of the capacity of a substance to absorb light of a specified wavelength
<b>Acrylate</b>	The salt or esther of acrylic acid, a monomer
<b>Adhesion</b>	Force of attraction that causes two different materials to join togetreher
<b>Anodizng</b>	An electrolytic passivation process used to increase the thickness of the natural oxide layer on the surface of metal parts
<b>Anti-soiling properties</b>	The ability of materials to resist adhesion of dirt and other forms of surface contamination
<b>Blast cleaning</b>	The cleaning and roughing of a surface by the use of sand, artificial grit, or fine metal shot which is projected at a surface by a compressed gas
<b>Bottom-up approach</b>	Assembly method based on progressing from small or subordinate units to larger or more important units, as in an organization or process
<b>Cassie-Baxter</b>	The model of wetting used to predict the apparent contact angle on heterogenous interfaces
<b>Chemical resistance</b>	The strength of a material to resist chemical attack/degradation
<b>Coating</b>	A layer or film spread over a surface for protection or decoration
<b>Cohesion</b>	The ability of sticking together of particles and molecules of the same surface
<b>Contact angle CA</b>	Angle formed by a droplet of liquid of a solid and measured at the intersection of the liquid-solid interface and the liquid-vapor interface
<b>Crosslinking</b>	The setting up or arragement of chemical links between molecular or macromolecular structures usually to form a three dimensional network
<b>Dichroic</b>	Type of filter, which exhibits significantly different reflection or transmission in two differnet wavelengths, used in UV curing lamps to minimise transmission of IR to temperature sensitive subsstrates
<b>Fish eyes</b>	Circular voids or separations in the coating usually caused by surface low energy materials such as silicone or oily spots

<b>Gloss</b>	The sheen or ability to reflect light.
<b>HMDS</b>	Hexamethyldisilazane $(\text{CH}_3)_3\text{SiNH}\text{Si}(\text{CH}_3)_3$
<b>Hydrophilic</b>	The term used to describe surfaces having strong affinity to water with a water contact angle lower than $90^\circ\text{C}$
<b>Hydrophobic</b>	The term used to describe surfaces tending to repel water with a water contact angle greater than $90^\circ\text{C}$
<b>IMS</b>	Industrial methylated spirits
<b>IPA</b>	Isopropyl alcohol, in IUPAC notation propan-2-ol
<b>Methacrylate</b>	The salt or ester of methacrylic acid, a monomer
<b>MPTMA</b>	3-(trimethoxysilyl)propyl methacrylate $\text{H}_2\text{C}=\text{C}(\text{CH}_3)\text{CO}_2(\text{CH}_2)_3\text{Si}(\text{OCH}_3)_3$
<b>NPTMS</b>	n-propyl trimethoxy silane $\text{CH}_3\text{CH}_2\text{CH}_2\text{Si}(\text{OCH}_3)_3$
<b>Parahydrophilic</b>	The term used to describe the surface, on which high wettability is achieved due to roughness, beyond the effect of the surface chemistry
<b>Parahydrophobic</b>	The term used to describe the surface, on which reduced wettability is achieved due to roughness, beyond the effect of the surface chemistry
<b>Self-cleaning surfaces</b>	The materials that are working by being extremely repellent to water, keeping the surfaces free of contaminants and other debris
<b>Silsesquioxane</b>	An oligomer with an empirical chemical formula $\text{RSiO}_{1.5}$ , where R is either hydrogen or an alkyl, alkene, aryl or arylene group
<b>Sliding angle (SA)</b>	The minimum slope, measured in degrees from the horizontal, at which loose solid material will start to slide or flow.
<b>Soiling</b>	An accumulation of solid particles on the top of the surface, such as debris, ice, bacteria causing detriment of function
<b>Solvent</b>	A chemical used to dissolve another material.
<b>Superhydrophilic</b>	The terms used to describe complete spreading on the surface. The superhydrophilic surfaces have a water contact angle lower than $35^\circ$
<b>Superhydrophobic</b>	A type of surface that is very difficult to wet and have a water contact angle greater than $150^\circ$
<b>Surface energy SE</b>	A measure of the tendency of a surface to repel a coating. Low surface energy indicates a tendency to repel, while high surface energy indicates a tendency to attract.
<b>TEOS</b>	Tetraethyl orthosilicate $\text{Si}(\text{OC}_2\text{H}_5)_4$
<b>Top-down approach</b>	Creation of small structure from large parent entity

<b>Wavelength</b>	A fundamental descriptor of electromagnetic energy, including light. It is a distance between corresponding points of a propagated wave.
<b>Wavenumber</b>	It is the spatial frequency of a wave, either in cycles per unit distance or radians per unit distance
<b>Wenzel</b>	The model of wetting used to predict apparent contact angles on homogenous interfaces
<b>Wettability</b>	The ability of a liquid to spread on a solid
<b>UV light</b>	Ultraviolet light. Light that is invisible to the naked eye because it consists of wavelengths shorter than those of visible light, UV range 400 – 100nm (UVA 400-315 nm, UVB 315-280 nm, UVC 280-100 nm)

## LIST OF SYMBOLS AND ABBREVIATIONS

Symbols:

F	Force [N]
$\gamma$	Surface energy [N*m <sup>-1</sup> ]
L	Length [m]
W	Work [J]
AS	Surface area [m <sup>2</sup> ]
G	Gibbs free energy [kJ*K <sup>-1</sup> *mol <sup>-1</sup> ]
$\theta_Y$	Young contact angle [degree]
S	Spreading parameter
E	Energy [J]
$\theta_W$	Wenzel contact angle [degree]
r	Roughness parameter {-}
$\theta_{CB}$	Cassie-Baxter contact angle [degree]
f	Fraction of surface area
H	Contact angle hysteresis
PI	Performance index
h	Planck's constant [m <sup>2</sup> *kg*s <sup>-1</sup> ]
c	Speed of light [m*s <sup>-1</sup> ]
$\lambda$	Wavelength [m]
$\nu$	Wavenumber [cm <sup>-1</sup> ]
T	Transmittance
A	Absorbance
I	Intensity of light [W*m <sup>-2</sup> ]
dp	Depth of penetration [m]
n	Refractive index
Ra	Roughness average [m]
Rq	Roughness root mean squared average [m]
Ku	Surface kurtosis
Sk	Surface skewness

Aberivations:

ACA	Advanced contact angle
RCA	Receding contact angle
WCA	Water contact angle
DCA	Diiodo contact angle
RR	Retention of repellency

## LIST OF FIGURES

FIGURE 2.1 FORCE BALANCE IN A THREE PHASE SYSTEM – CONTACT ANGLE PRINCIPLE ...9	
FIGURE 2.2 WETTING PHENOMENA IN CORRELATION TO SURFACE CHEMISTRY AND SURFACE ROUGHNESS .....	13
FIGURE 2.3 WETTING REGIMES ON THE ROUGH SURFACES (NOSONOVSKY M., 2011) .....	14
FIGURE 2.4 THE PRINCIPLE OF DYNAMIC CONTACT ANGLE .....	15
FIGURE 2.5 SURFACE TYPES ACCORDING TO THE WETTING BEHAVIOUR .....	15
FIGURE 2.6 THE RELATIONSHIP BETWEEN WORK OF ADHESION AND WETTABILITY OF THE SURFACE. THE AUTHOR APPROXIMATES THE WORK OF ICE ADHESION TO SURFACE ENERGY OF WATER AND THE CONTACT ANGLE OF WATER THEREFORE, THE RATIO $W_A/Y_W$ DOESN'T HAVE AN UNIT (MAKKONEN L., 2012) .....	16
FIGURE 2.7 THE LOTUS LEAF EFFECT .....	17
FIGURE 2.8 THE PETAL EFFECT – STICKY MODE (MILIONIS A., 2013).....	19
FIGURE 2.9 SOL-GEL STRUCTURAL EVOLUTION (ASSINK R.A., 1994) .....	25
FIGURE 2.10 STATE OF THE ART – INDUSTRIAL NEED FOR NANOSTRUCTURED COATINGS .....	34
FIGURE 2.11 STRUCTURAL VARIANTS OF SILSESQUIOXANES: CAGE AND LADDER FORMATION (TAYLOR A. B. L., 2011).....	35
FIGURE 2.12 COMPARISON OF “BREAKTHROUGH VALUE” .....	36
FIGURE 3.1 GLOSS MEASUREMENT GEOMETRIES USED IN STANDARD EVALUATION OF SURFACE VISUAL APPEARANCE.....	43
FIGURE 3.2 TABER ROTARY PLATFORM ABRASION TESTER (PIC. SOURCE FALEX TRIBOLOGY).....	43
FIGURE 3.3 WEAR PATTERN RESULTING FROM ROTARY ABRASION TABER TEST.....	44
FIGURE 3.4 NOVEL APPROACH TO TEST DURABILITY OF HIGHLY REPELLENT SURFACES – ABRASION AND WATER CONTACT ANGLE TESTING ROUTINE.....	45
FIGURE 3.5 NOVEL APPROACH TO TEST DURABILITY OF HIGHLY REPELLENT SURFACES – FINAL DURABILITY POINT DEFINITION .....	46
FIGURE 3.6 ABRASION CONDITIONS (TYPES OF ABRASIVE WHEELS AND LOAD) APPLIED IN ROTARY TABER TEST.....	46
FIGURE 3.7 SPIDER DIAGRAM SCHEME PROPOSED FOR EVALUATION OF HIGHLY REPELLENT SURFACES.....	48
FIGURE 3.8 COATING CLASSIFICATION CRITERIA BY MATERIALS CATEGORY .....	52
FIGURE 3.9 PLOT OF PERFORMANCE INDICES OF EASY CLEAN COATINGS – GENERAL PRINCIPAL.....	55
FIGURE 4.1 BP AND 184 EMISSION SPECTRA (SIGMA-ALDRICH).....	60
FIGURE 4.2 SYNTHESIS PROCEDURE FOR MONO-FUNCTIONAL SILSESQUIOXANES (PART OF TWI'S VITOLANE® TECHNOLOGY).....	61
FIGURE 4.3 PARTICLE SIZE DISTRIBUTION – TSS4 SILICA STÖBER SPHERES .....	62
FIGURE 4.4 PARTICLE SIZE DISTRIBUTION – TSS5 SILICA STÖBER SPHERES .....	63
FIGURE 4.5 FUNCTIONALIZATION PROCESS OF TSS5 STÖBER SPHERES – TRIPLE FUNCTIONALIZATION .....	64
FIGURE 4.6 CALIBRATION PROCEDURE OF SELECTED UV CURING SYSTEM .....	67
FIGURE 4.7 THE PRINCIPLE OF ATTENUATED TOTAL REFLECTANCE SPECTROSCOPY.....	69
FIGURE 4.8 CORRELATION BETWEEN TWO TECHNIQUES FOR THICKNESS MEASUREMENTS. TWO SEM IMAGES SHOWS THE GENERAL PRINCIPLE OF THICKNESS EVALUATION DONE WITH MICROSCOPIC TECHNIQUE .....	70
FIGURE 4.9 FTIR SPECTRA OF TWI FORMULATION A MEASURED IN RANGE OF 4000-650 $CM^{-1}$ (ABS – ABSORBANCE).....	73
FIGURE 4.10 FTIR SPECTRA OF TWI FORMULATION B MEASURED IN RANGE 4000-650 $CM^{-1}$ (ABS – ABSORBANCE).....	73
FIGURE 4.11 FTIR SPECTRA OF TWI FORMULATION C MEASURED IN A RANGE 4000-650 $CM^{-1}$ (ABS – ABSORBANCE).....	74
FIGURE 4.12 FTIR SPECTRA OF TWI FORMULATION D MEASURED IN RANGE 4000-650 $CM^{-1}$ (ABS – ABSORBANCE).....	74
FIGURE 4.13 FTIR SPECTRA OF TWI FORMULATION E MEASURED IN A RANGE OF 4000-650 $CM^{-1}$ (ABS – ABSORBANCE).....	75

FIGURE 4.14 FTIR SPECTRA OF TWI FORMULATION D RESIN AND IMS MEASURED IN A RANGE OF 4000-650 $\text{CM}^{-1}$ (ABS – ABSORBANCE) .....	77
FIGURE 4.15 FTIR SPECTRA OF TWI FORMULATION B FOR DIFFERENT AMOUNTS OF ENERGY ABSORBED MEASURED IN A RANGE OF 4000-650 $\text{CM}^{-1}$ (ABS – ABSORBANCE) .....	79
FIGURE 4.16 DEGREE OF CONVERSION ASSESSMENT MEASURED BASED ON DISAPPEARANCE OF C=C PEAK– TWI FORMULATION B – C=O AND C-H STANDARD PEAKS.....	80
FIGURE 4.17 DEGREE OF CONVERSION ASSESSMENT MEASURED BASED ON DISAPPEARANCE OF C=C PEAK – TWI FORMULATION B – ABSORBANCE RATIO.....	80
FIGURE 4.18 RELATIONSHIP BETWEEN THE COATING THICKNESS AND THE DEGREE OF CONVERSION (TWI FORMULATION B, 5.5 $\text{J}/\text{CM}^2$ ENERGY ABSORBED) .....	81
FIGURE 4.19 HARDNESS AND REDUCED MODULUS AT 0.1MN LOAD FOR DIFFERENT DEGREES OF CONVERSION (TWI FORMULATION B) .....	82
FIGURE 4.20 DEGREE OF CONVERSION ANALYSIS – TWI FORMULATION D – POTASSIUM PERMANGANATE REACTION.....	85
FIGURE 4.21 DEGREE OF CONVERSION ASSESSMENT BY FTIR AND POTASSIUM PERMANGANATE REACTION – TWI FORMULATION D .....	85
FIGURE 4.22 DEGREE OF CONVERSION ASSESSMENT BY FTIR AND POTASSIUM PERMANGANATE REACTION – TWI FORMULATION A.....	86
FIGURE 5.1 DROP SHAPE ANALYSER FROM KRÜSS .....	95
FIGURE 5.2 CROSS CUT TAPE TEST CUTTING PATTERN.....	97
FIGURE 5.3 PULL-OFF TEST SETUP.....	98
FIGURE 5.4 INFLUENCE OF SURFACE PREPARATION TECHNIQUE ON WATER CONTACT ANGLE OF 3003 H14 ALUMINIUM ALLOY .....	98
FIGURE 5.5 INFLUENCE OF SURFACE PREPARATION TECHNIQUE ON DIIDOMETHANE CONTACT ANGLE OF 3003 H14 ALUMINIUM ALLOY .....	99
FIGURE 5.6 INFLUENCE OF SURFACE PREPARATION TECHNIQUE ON TOTAL SURFACE ENERGY OF 3003 H14 ALUMINIUM ALLOY. SURFACE ENERGY CALCULATED WITH OWRK METHOD.....	100
FIGURE 5.7 SURFACE CLEANLINESS VERIFICATION BY DIFFUSIVE REFLECTANCE SPECTROSCOPY (REFLECTED FTIR, ABS - ABSORBANCE) .....	101
FIGURE 5.8 DETECTION LIMITATION FOR AGILENT 4100 EXOSCAN FTIR (DIFFERENT LEVELS OF IMS CONCENTRATION IN WATER, LIQUID SAMPLES).....	102
FIGURE 5.9 THE CLASS OF ADHESION – PRISTINE CONDITIONS WITH ACCORDANCE TO ASTM D 3359 – 97.....	103
FIGURE 5.10 ADHESION STRENGTH – PRISTINE CONDITIONS WITH ACCORDANCE TO ASTM D4541.....	103
FIGURE 5.11 THE CLASS OF ADHESION – AGEING CONDITIONS WITH ACCORDANCE TO ASTM D 3359 – 97.....	104
FIGURE 5.12 ADHESION STRENGTH – AGEING CONDITIONS WITH ACCORDANCE TO ASTM D4541 .....	104
FIGURE 5.13 THE INFLUENCE OF SURFACE PREPARATION ON THE SURFACE TOPOGRAPHY (IMAGES TAKEN WITH UNDERTAKEN WITH OLYMPUS BX41M METALLURGICAL MICROSCOPE, 10X MAGNIFICATION) .....	106
FIGURE 5.14 INFLUENCE OF BOND POLARITY ON THE ADHESION STRENGTH .....	108
FIGURE 5.15 PULL-OFF TEST SETUP – VERSION FOR EASY CLEAN COATINGS .....	110
FIGURE 6.1 DIAGRAM REPRESENTING THE RELATION BETWEEN COATING COMPOSITION, STRUCTURE AND PROPERTY .....	112
FIGURE 6.2 WCA (LEFT) AND DCA (RIGHT) MEASUREMENTS PRINCIPLE TAKEN USING A DSA100 FROM KRÜSS.....	115
FIGURE 6.3 EFFECT OF MATERIAL SYSTEM PARAMETERS ON THE MECHANICAL PERFORMANCE OF A COATING .....	116
FIGURE 6.4 INITIAL WETTABILITY CHARACTERISTICS OF SELECTED COATING SYSTEMS (BOX PLOT PRINCIPLE EXPLAINED IN CHAPTER 5) .....	118
FIGURE 6.5 LIPOPHOBIC CHARACTERISTICS IN PRISTINE STATE OF SELECTED COATING SYSTEMS BOX PLOT PRINCIPLE EXPLAINED IN CHAPTER 5) .....	118
FIGURE 6.6 VISUAL APPEARANCE (GLOSS, HAZE AND DOI) TAKEN WITH 20° GEOMETRY OF SELECTED COATING SYSTEMS .....	119

FIGURE 6.7 WATER CONTACT ANGLE RETENTION AS A FUNCTION OF ABRASION CYCLES – TWI FORMULATION A (C1 – CS10 WHEELS/500 G LOAD; C2 – CS10 WHEELS/1000 G LOAD; C3 – H18 WHEELS/500 G LOAD; C4 – H18 WHEELS/1000 G LOAD) .....	119
FIGURE 6.8 SEM IMAGES OF PRISTINE TWI FORMULATION A (LEFT) AND WEAR SCARS (RIGHT) AFTER ABRASION TESTING (CONDITION 2, 3500 CYCLES). RA REPRESENTS ROUGHNESS LEVEL IN NANOMETRES FOR SPECIFIED CONDITIONS .....	120
FIGURE 6.9 WATER CONTACT ANGLE RETENTION AS A FUNCTION OF ABRASION CYCLES – TWI FORMULATION B (C1 – CS10 WHEELS/500 G LOAD; C2 – CS10 WHEELS/1000 G LOAD; C3 – H18 WHEELS/500 G LOAD; C4 – H18 WHEELS/1000 G LOAD) .....	120
FIGURE 6.10 SEM IMAGES OF PRISTINE TWI FORMULATION B (LEFT) AND WEAR SCARS (RIGHT) AFTER ABRASION TESTING (CONDITIONS 2, 3500 CYCLES). RA REPRESENTS ROUGHNESS LEVEL IN NANOMETRES FOR SPECIFIED CONDITIONS .....	120
FIGURE 6.11 WATER CONTACT ANGLE RETENTION AS A FUNCTION OF ABRASION CYCLES – TWI FORMULATION C (C1 – CS10 WHEELS/500 G LOAD; C2 – CS10 WHEELS/1000 G LOAD; C3 – H18 WHEELS/500 G LOAD; C4 – H18 WHEELS/1000 G LOAD) .....	120
FIGURE 6.12 SEM IMAGES OF PRISTINE TWI FORMULATION C (LEFT) AND WEAR SCARS (RIGHT) AFTER ABRASION TESTING (CONDITIONS 2, 250 CYCLES). RA REPRESENTS ROUGHNESS LEVEL IN NANOMETRES FOR SPECIFIED CONDITIONS .....	121
FIGURE 6.13 WATER CONTACT ANGLE RETENTION AS A FUNCTION OF ABRASION CYCLES – TWI FORMULATION D (C1 – CS10 WHEELS/500 G LOAD; C2 – CS10 WHEELS/1000 G LOAD; C3 – H18 WHEELS/500 G LOAD; C4 – H18 WHEELS/1000 G LOAD) .....	121
FIGURE 6.14 SEM IMAGES OF PRISTINE TWI FORMULATION D (LEFT) AND WEAR SCARS (RIGHT) AFTER ABRASION TESTING (CONDITIONS 2, 5 CYCLES). RA REPRESENTS ROUGHNESS LEVEL IN NANOMETRES FOR SPECIFIED CONDITIONS .....	121
FIGURE 6.15 WATER CONTACT ANGLE RETENTION AS A FUNCTION OF ABRASION CYCLES – TWI FORMULATION E (C1 – CS10 WHEELS/500 G LOAD; C2 – CS10 WHEELS/1000 G LOAD; C3 – H18 WHEELS/500 G LOAD; C4 – H18 WHEELS/1000 G LOAD) .....	121
FIGURE 6.16 SEM IMAGES OF PRISTINE TWI FORMULATION E (LEFT) AND WEAR SCARS (RIGHT) AFTER ABRASION TESTING (CONDITIONS 2, 3000 CYCLES). RA REPRESENTS ROUGHNESS LEVEL IN NANOMETRES FOR SPECIFIED CONDITIONS .....	122
FIGURE 6.17 WATER CONTACT ANGLE RETENTION AS A FUNCTION OF ABRASION CYCLES – TWI FORMULATION F (C1 – CS10 WHEELS/500 G LOAD; C2 – CS10 WHEELS/1000 G LOAD; C3 – H18 WHEELS/500 G LOAD; C4 – H18 WHEELS/1000 G LOAD) .....	122
FIGURE 6.18 SEM IMAGES OF PRISTINE TWI FORMULATION F (LEFT) AND WEAR SCARS (RIGHT) AFTER ABRASION TESTING (CONDITIONS 2, 3500 CYCLES). RA REPRESENTS ROUGHNESS LEVEL IN NANOMETRES FOR SPECIFIED CONDITIONS .....	122
FIGURE 6.19 WATER CONTACT ANGLE RETENTION AS A FUNCTION OF ABRASION CYCLES – COMMERCIAL PRODUCTS GP101 (LEFT) AND NEVER WET (RIGHT) (C1 – CS10 WHEELS/500 G LOAD; C2 – CS10 WHEELS/1000 G LOAD; C3 – H18 WHEELS/500 G LOAD; C4 – H18 WHEELS/1000 G LOAD) .....	122
FIGURE 6.20 SEM IMAGES OF PRISTINE COMMERCIAL PRODUCT GP101 (LEFT) AND WEAR SCARS (RIGHT) AFTER ABRASION TESTING (CONDITION 2, 5 CYCLES). RA REPRESENTS ROUGHNESS LEVEL IN NANOMETRES FOR SPECIFIED CONDITIONS .	123
FIGURE 6.21 SEM IMAGES OF PRISTINE COMMERCIAL PRODUCT NEVER WET (LEFT) AND WEAR SCARS (RIGHT) AFTER ABRASION TESTING (CONDITIONS 2, 75 CYCLES). RA REPRESENTS ROUGHNESS LEVEL IN NANOMETRES FOR SPECIFIED CONDITIONS .	123
FIGURE 6.22 PRINCIPLE FOR ASSESSING THE RESISTANCE OF COATINGS TO SEPARATION FROM SUBSTRATES (1 WEEK IN 5%NACL, LEFT – TWI FORMULATION E, RIGHT – TWI FORMULATION A) .....	124
FIGURE 6.23 CHEMICAL RESISTANCE MEASURED IN A FUNCTION OF INITIAL ADHESION STRENGTH AND SURFACE QUALITY AFTER SPECIFIED AGEING CONDITIONS (1 WEEK IN 1% $H_2SO_4$ SOLUTION) .....	124
FIGURE 6.24 CHEMICAL RESISTANCE MEASURED IN A FUNCTION OF INITIAL ADHESION STRENGTH AND SURFACE QUALITY AFTER SPECIFIED AGEING CONDITIONS (1 WEEK IMS SOLUTION) .....	124
FIGURE 6.25 CHEMICAL RESISTANCE MEASURED IN A FUNCTION OF INITIAL ADHESION STRENGTH AND SURFACE QUALITY AFTER SPECIFIED AGEING CONDITIONS (1 WEEK 4.95%NACL SOLUTION) .....	125
FIGURE 6.26 CHANGES IN WCA AS A RESULT OF ACCELERATED CHEMICAL AGEING PROCESS (ONE WEEK OF IMMERSION IN: CR1 – 1% $H_2SO_4$ , CR2 – IMS, CR3 – 4.95%NACL) .....	125

FIGURE 6.27 SEM IMAGES OF TWI FORMULATION B (LEFT) AND E (RIGHT) – CROSS-SECTIONING AND TOP SURFACE VIEW (500X MAGNIFICATION, BS DETECTOR).....	126
FIGURE 6.28 KURTOSIS AND SKEWNESS OF SURFACE PROFILE OF THE SELECTED COATING SYSTEMS (PRISTINE STATE).....	128
FIGURE 6.29 SEM CROSS-SECTIONAL IMAGES AND AFM ROUGHNESS PROFILE OF TWI FORMULATIONS C (LEFT) AND D (RIGHT) .....	128
FIGURE 6.30 INFLUENCE OF THE ROUGHNESS PROFILE (GEOMETRICAL MEAN OF SURFACE PEAKS (RQ)) ON SURFACE REFLECTION (GLOSS) MEASURED WITH 20° ANGLE OF INCIDENCE.....	130
FIGURE 6.31 EFFECT OF SURFACE PREPARATION CONDITIONS ON SURFACE REFLECTION IN TWI FORMULATION B MEASURED WITH 20° ANGLE.....	131
FIGURE 6.32 KURTOSIS AND SKEWNESS OF SURFACE PROFILE IN SELECTED COATING SYSTEMS AFTER SUBJECTING THEM TO ABRASION CONDITION 2.....	134
FIGURE 6.33 EFFECT OF SURFACE PREPARATION PROCEDURE ON THE INTERFACE INTEGRITY BETWEEN ALUMINIUM AND TWI FORMULATION F (ONE WEEK OF IMMERSION IN 5%NaCl SOLUTION) – ACETONE WIPING (LEFT SIDE) AND ETCHING COMBINED WITH ANODIZING (RIGHT SIDE) .....	138
FIGURE 7.1 TWI FORMULATION A – SPIDER DIAGRAM.....	144
FIGURE 7.2 TWI FORMULATION B – SPIDER DIAGRAM.....	145
FIGURE 7.3 TWI FORMULATION C – SPIDER DIAGRAM .....	146
FIGURE 7.4 TWI FORMULATION D – SPIDER DIAGRAM .....	147
FIGURE 7.5 TWI FORMULATION E – SPIDER DIAGRAM.....	148
FIGURE 7.6 TWI FORMULATION F – SPIDER DIAGRAM.....	149
FIGURE 7.7 GP101 ANTI-GRAFFITI SYSTEM – SPIDER DIAGRAM.....	150
FIGURE 7.8 NEVER WET SYSTEM – SPIDER DIAGRAM .....	151
FIGURE 7.9 COATING PERFORMANCE PROFILE BASED ON THE SIX SEPARATE PERFORMANCE INDICES ASSOCIATED WITH THE SELECTED GROUP OF KEY PROPERTIES.....	153
FIGURE 7.10 PLOT OF PERFORMANCE INDICES FOR EASY CLEAN COATINGS (FOR FIVE TEST SPECIMENS PER COATING TYPE). RELATION BETWEEN PRISTINE WCA ( $PI_{1A}$ – PERFORMANCE INDEX FOR INITIAL REPELLENCY) AND MECHANICAL DURABILITY ( $PI_2$ – PERFORMANCE INDEX FOR ABRASION RESISTANCE (COMBINATION OF FOUR SPECIFIED ABRASION CONDITIONS)).....	153
FIGURE 7.11 SUPPORT FOR NULL HYPOTHESIS – INVERSE RELATIONSHIP BETWEEN INITIAL WCA ( $PI_{1A}$ ) AND MECHANICAL DURABILITY ( $PI_2$ ) (FOR ALL SELECTED COATING SYSTEMS WITHOUT DISTINCTION BETWEEN FAMILIES OF COATING).....	154
FIGURE 7.12 PLOT OF PERFORMANCE INDICES FOR EASY CLEAN COATINGS. RELATION BETWEEN PRISTINE WCA ( $PI_{1A}$ – PERFORMANCE INDEX FOR INITIAL REPELLENCY) AND CHEMICAL DURABILITY ( $PI_4$ – PERFORMANCE INDEX FOR ADHESION PERFORMANCE UNDER CHEMICAL DEGRADATION).....	154
FIGURE 7.13 PLOT OF PERFORMANCE INDICES FOR EASY CLEAN COATINGS. RELATION BETWEEN INITIAL REPELLENCY ( $PI_A$ ) AND INDIRECT DURABILITY REFERRED AS ABILITY TO RETAIN INITIAL REPELLENCY UNDER ABRASIVE CONDITIONS ( $PI_3$ ).....	155
FIGURE 7.14 PLOT OF PERFORMANCE INDICES FOR EASY CLEAN COATINGS. RELATION BETWEEN MECHANICAL DURABILITY UNDER ABRASIVE CONDITIONS ( $PI_2$ ) AND CHEMICAL DURABILITY ( $PI_4$ – PERFORMANCE INDEX FOR ADHESION PERFORMANCE UNDER CHEMICAL DEGRADATION).....	155
FIGURE 7.15 PLOT OF PERFORMANCE INDICES FOR EASY CLEAN COATINGS. RELATION BETWEEN COATING REPELLENT CHARACTERISTICS OVER LIFETIME (AVERAGE OF INITIAL WCA ( $PI_{1A}$ ) AND RETENTION RATION UNDER ABRASIVE CONDITION ( $PI_3$ )) AND MECHANICAL DURABILITY UNDER ABRASIVE CONDITIONS ( $PI_2$ ).....	156
FIGURE 7.16 PROPOSED MODEL OF GRAPH PREDICATING BEHAVIOURAL PATTERN OF EASY CLEAN COATINGS. F1-5 REFERS TO CHANGES IN TYPE OF SILICA NANOPARTICLES FUNCTIONALITY, S1-3 SYMBOLISES TYPE OF SILICA NANOPARTICLES SIZE AND LL1-2 CORRESPONDS TO SILICA NANOPARTICLES LOADING LEVEL.....	159
FIGURE 7.17 ROUGHNESS PROFILE TRENDS OF SELECTED COATING SYSTEMS AND ITS INFLUENCE ON PERFORMANCE CHARACTERISTICS PRESENTED ON A PLOT OF PERFORMANCE INDICES (AVERAGE OF INITIAL WCA ( $PI_{1A}$ ) AND RETENTION RATION UNDER ABRASIVE CONDITION ( $PI_3$ )) AND MECHANICAL DURABILITY UNDER ABRASIVE CONDITIONS ( $PI_2$ ) .....	164

*FIGURE 7.18 EFFECT OF COATING COMPOSITION IN TWI FORMULATIONS A, B AND E ON  
QUALITY OF SURFACE UNDER ABRASIVE CONDITIONS (CS10 WHEELS, 1000G LOAD  
AND 3500 CYCLES) ..... 165*

## LIST OF TABLES

TABLE 2.1 EQUILIBRIUM WATER CONTACT ANGLE VALUES FOR VARIOUS SURFACES.....	11
TABLE 2.2 WETTING TERMINOLOGY PROPOSED BY MARMUR (MARMUR A., 2012).....	15
TABLE 2.3 TWO TIER GRADING SYSTEM FOR THE DURABILITY EVALUATION OF EASY CLEAN COATINGS.....	30
TABLE 2.4 TYPICAL PROPERTIES OF ORGANIC AND INORGANIC MATERIALS (KICKELBICK G., 2007).....	32
TABLE 3.1 EASY CLEAN COATINGS – PROPOSED SELECTION CRITERIA.....	40
TABLE 3.2 GENERAL PRINCIPLE OF GLOSS MEASUREMENTS.....	43
TABLE 3.3 SUMMARY OF THE PROPERTIES MEASURED, MEASUREMENT TECHNIQUES AND ACCOMPANYING STANDARD PROCEDURES.....	48
TABLE 3.4 WCA AND DCA (INITIAL VALUES) CLASSIFICATION CRITERIA FOR SPIDER DIAGRAM.....	49
TABLE 3.5 GLOSS AND HAZE (PRISITNE STATE) CLASSIFICATION CRITERIA FOR SPIDER DIAGRAM.....	49
TABLE 3.6 ABRASION CLASSIFICATION CRITERIA FOR SPIDER DIAGRAM.....	50
TABLE 3.7 RETENTION RATIO AND ADHESION CLASSIFICATION CRITERIA FOR SPIDER DIAGRAM.....	50
TABLE 3.8 CHEMICAL RESISTANCE CLASSIFICATION (WITH THE RESPECT TO RETENTION RATE) CRITERIA FOR SPIDER DIAGRAM.....	51
TABLE 3.9 CHEMICAL RESISTANCE CLASSIFICATION (ADHESIVE FAILURE ANALYSIS) CRITERIA FOR SPIDER DIAGRAM (BASED ON THE IDEA TAKEN FROM ASTM D3359) ...	51
TABLE 4.1 TWI FORMULATION A COMPOSITION (WT%).....	60
TABLE 4.2 CHEMICAL FORMULAS OF SILICA NANOPARTICLES FUNCTIONALIZING AGENTS	64
TABLE 4.3 TWI FORMULATIONS SUMMARY (COMPOSITION BY WT% AND FUNCTIONALITIES) .....	66
TABLE 4.4 THICKNESS MEASUREMENTS CARRIED OUT WITH TWO DIFFERENT TECHNIQUES (EDDY CURRENT AND SEM) FOR THREE DIFFERENT COATING THICKNESSES (10, 20 AND 50 MM).....	70
TABLE 4.5 ANOVA SINGLE FACTOR FOR THICKNESS MEASUREMENTS OBTAINED BY EDDY CURRENT GAUGE AND SEM FOR PANELS COATED WITH 10 MM BAR.....	71
TABLE 4.6 ANOVA SINGLE FACTOR FOR THICKNESS MEASUREMENTS OBTAINED BY EDDY CURRENT GAUGE AND SEM FOR PANELS COATED WITH 20 MM BAR.....	71
TABLE 4.7 ANOVA SINGLE FACTOR FOR THICKNESS MEASUREMENTS OBTAINED BY EDDY CURRENT GAUGE AND SEM FOR PANELS COATED WITH 50 MM BAR.....	71
TABLE 4.8 INFRARED ABSORPTION FREQUENCIES FOR SELECTED COATING SYSTEMS (PANORAMA SOFTWARE LIBRARY).....	72
TABLE 4.9 CORRELATION BETWEEN ABSORPTION BANDS AND RESIN COMPOSITION (F1, F2 AND F3 CORRESPONDS TO FUNCTIONALITY TYPE IN SILICA SYSTEM) (IR FREQUENCIES DATABASE FROM PANORAMA SOFTWARE LIBRARY).....	78
TABLE 4.10 H/E AND H3/E2 RATIO AS A FUNCTION OF DEGREE OF CONVERSION DURING UV EXPOSURE (TWI FORMULATION B).....	82
TABLE 4.11 VISUAL APPEARANCE AS A FUNCTION OF DEGREE OF CONVERSION (TWI FORMULATION B).....	83
TABLE 5.1 DISPERSIVE AND POLAR COMPONENTS OF SURFACE ENERGY AFTER SELECTED SURFACE PREPARATION ROUTINES.....	100
TABLE 5.2 CONCENTRATIONS OF IMS DISSOLVED IN DEIONIZED WATER.....	102
TABLE 6.1 COATING APPLICATION METHODOLOGY.....	117
TABLE 6.2 SURFACE ROUGHNESS LEVEL, CORRESPONDING WATER CONTACT ANGLE AND DIIDO CONTACT ANGLE (IN SELECTED COATING SYSTEMS, ROUGHNESS PARAMETERS ASSESSED WITH TALYSURF).....	118
TABLE 7.1 SUMMARY OF THE PROPERTIES MEASURED, MEASUREMENT TECHNIQUES AND ACCOMPANYING STANDARD PROCEDURES.....	142
TABLE 7.2 SUMMARY OF SPIDER DIAGRAM POINTING SYSTEM.....	142
TABLE 7.3 CHEMICAL RESISTANCE CLASSIFICATION (ADHESIVE FAILURE ANALYSIS) CRITERIA FOR SPIDER DIAGRAM (ADDITIONAL INFORMATION TO THE TABLE 7.2) ....	143
TABLE 7.4 TWI FORMULATION A PROPERTIES REPRESENTED BY NUMERICAL VALUE (SPIDER DIAGRAM BANDING) (% AA - % OF AFFECTED AREA).....	144
TABLE 7.5 TWI FORMULATION B PROPERTIES REPRESENTED BY NUMERICAL VALUE (SPIDER DIAGRAM BANDING) (% AA - % OF AFFECTED AREA).....	145

TABLE 7.6 TWI FORMULATION C PROPERTIES REPRESENTED BY NUMERICAL VALUE (SPIDER DIAGRAM BANDING) (% AA - % OF AFFECTED AREA) .....	146
TABLE 7.7 TWI FORMULATION D PROPERTIES REPRESENTED BY NUMERICAL VALUE (SPIDER DIAGRAM BANDING) (% AA - % OF AFFECTED AREA) .....	147
TABLE 7.8 TWI FORMULATION E PROPERTIES REPRESENTED BY NUMERICAL VALUE (SPIDER DIAGRAM BANDING) (% AA - % OF AFFECTED AREA) .....	148
TABLE 7.9 TWI FORMULATION F PROPERTIES REPRESENTED BY NUMERICAL VALUE (SPIDER DIAGRAM BANDING) (% AA - % OF AFFECTED AREA) .....	149
TABLE 7.10 TWI FORMULATION GP101 PROPERTIES REPRESENTED BY NUMERICAL VALUE (SPIDER DIAGRAM BANDING) (% AA - % OF AFFECTED AREA) .....	150
TABLE 7.11 TWI FORMULATION NEVER WET PROPERTIES REPRESENTED BY NUMERICAL VALUE (SPIDER DIAGRAM BANDING) (% AA - % OF AFFECTED AREA).....	151
TABLE 7.12 PERFORMANCE INDICES FOR SELECTED COATING SYSTEMS .....	152

## TABLE OF CONTENT

<b>ABSTRACT</b>	<b>III</b>
<b>ACKNOWLEDGEMENT</b>	<b>V</b>
<b>GLOSSARY OF TERMS AND ACRONYMS</b>	<b>VI</b>
<b>LIST OF SYMBOLS AND ABBREVIATIONS</b>	<b>IX</b>
<b>LIST OF FIGURES</b>	<b>XI</b>
<b>LIST OF TABLES</b>	<b>XVI</b>
<b>1 Introduction</b>	<b>1</b>
1.1 <i>Project background</i>	1
1.2 <i>Research need</i>	1
1.3 <i>Aim of research</i>	3
1.4 <i>Objectives</i>	3
1.5 <i>Organization of the thesis</i>	3
1.6 <i>Contributions to knowledge</i>	4
<b>2 Easy Clean Coatings</b>	<b>8</b>
2.1 <i>Introduction to Wetting Phenomena</i>	8
2.1.1 <i>Surface energy and contact angle</i>	8
2.1.2 <i>Wetting regimes and terminology of the wettability</i>	10
2.2 <i>Attributes of Easy Clean Coatings</i>	18
2.2.1 <i>Self-cleaning</i>	19
2.2.2 <i>Anti-icing</i>	19
2.2.3 <i>Anti-graffiti</i>	20
2.2.4 <i>Anti-fingerprints/oleophobic</i>	20
2.2.5 <i>Aerodynamic drag reduction</i>	21
2.2.6 <i>Anti-corrosive</i>	21
2.3 <i>Advanced Easy Clean Coatings</i>	22
2.3.1 <i>Fluoropolymers</i>	22
2.3.2 <i>Polysiloxanes</i>	23
2.3.3 <i>Inorganic-organic hybrid coatings</i>	23
2.4 <i>Durability assessment of easy clean coatings</i>	25

2.5	<i>Novel Inorganic Building Blocks for Durability Improvement</i>	31
2.5.1	<i>Silsesquioxanes</i>	34
2.5.2	<i>Silica nanoparticles</i>	36
2.6	<i>Summary</i>	38
<b>3</b>	<b>New Assessment Criteria for Durability Evaluation of Highly Repellent Surfaces</b>	<b>39</b>
3.1	<i>Introduction – coating selection criteria</i>	39
3.2	<i>Experimental – methods</i>	42
3.3	<i>Classification criteria</i>	47
3.4	<i>Plot of performance indices</i>	53
3.5	<i>Summary</i>	55
<b>4</b>	<b>Assessment of the Degree of Conversion of selected Coatings systems</b>	<b>57</b>
4.1	<i>Overview</i>	57
4.2	<i>Introduction – Fundamentals of UV Radiation Curing</i>	57
4.3	<i>Experimental</i>	59
4.3.1	<i>Materials</i>	59
4.3.2	<i>Methods</i>	66
4.4	<i>Results and discussion</i>	70
4.4.1	<i>Dry film thickness</i>	70
4.4.2	<i>Structural characterization</i>	72
4.4.3	<i>Degree of conversion</i>	78
4.5	<i>Summary</i>	86
<b>5</b>	<b>Adhesion of Easy Clean Coatings to 3003 H14 Aluminium Alloy</b>	<b>88</b>
5.1	<i>Introduction – Fundamentals of Coating Adhesion</i>	88
5.1.1	<i>Theories of adhesion</i>	88
5.1.2	<i>Factors affecting coating adhesion</i>	89
5.2	<i>Experimental</i>	91
5.2.1	<i>Surface preparation</i>	91
5.2.2	<i>Surface cleanliness verification</i>	94
5.2.3	<i>Adhesion measurements</i>	96
5.3	<i>Results</i>	98
5.3.1	<i>Surface cleanliness verification</i>	98
5.3.2	<i>Adhesion bonding measurements</i>	102

5.4	<i>Discussion</i>	105
5.5	<i>Summary</i>	110
<b>6</b>	<b>Advanced Easy Clean Coatings – Performance Characteristics</b>	<b>112</b>
6.1	<i>Introduction</i>	112
6.2	<i>Experimental</i>	113
6.2.1	<i>Materials</i>	113
6.3	<i>Results</i>	117
6.3.1	<i>Initial performance characteristics</i>	117
6.3.2	<i>Abrasion resistance and water contact angle retention</i>	119
6.3.3	<i>Adhesive wear and chemical resistance</i>	123
6.4	<i>Discussion</i>	125
6.5	<i>Summary</i>	139
<b>7</b>	<b>Classification of Easy Clean Coatings</b>	<b>141</b>
7.1	<i>Spider diagrams</i>	141
7.2	<i>Performance profile and Figures of Merit</i>	151
7.3	<i>Discussion</i>	156
7.4	<i>Summary</i>	166
<b>8</b>	<b>Conclusions and recommendation for future work</b>	<b>168</b>
8.1	<i>Conclusions</i>	168
8.2	<i>Recommendation for future work</i>	170

# 1 INTRODUCTION

## 1.1 Project background

This project was carried out under PhD programme in High Performance Materials in Brunel University's Department of Mechanical Aerospace and Civil Engineering with the partnership with TWI Ltd and NSIRC. Additional founding was provided by Engineering and Physical Sciences Research Council (EPSRC).

TWI is independent research and technology organisation (RTO) that develops new technologies in the field of materials, joining and structural integrity. National Structure Integrity Research Centre (NSIRC) is established and managed by TWI, working closely with lead academic partners. The mission of NSIRC is to train next generation of engineers and scientists to support UK's R&D and accelerate uptake of research. The PhD programme under NSIRC is a new model of postgraduate research driven by the need of industry.

Over last years, TWI had been developing its expertise in high performance coatings both through European founded projects and through sponsorship of PhDs, with an extensive focus laid on development and fabrication of advanced materials (Taylor A. D. G., 2015) (Taylor A., 2011). These novel materials are the baseline for the reaserch carried out in this thesis.

## 1.2 Research need

The industrial need for multifunctional coatings with anti-soiling (easy clean) properties is significant and will continue to grow over the next few years (Sanchez C. B. P., 2011). Structures designed for dynamic outdoor applications are constantly prone to the environmental factors and soiling is one of them. "Soiling" is a general term that includes any kind of deposit or extraneous material that appears upon the surface during its lifetime (ice, insects, algae etc...) (Random House Webster's College Dictionary, 2005). There are a number of examples showing the evidence of loss of functional performance associated with the effect of the soiling. Biofouling on hulls of ships results in them burning 40% more fuel due to the increase in frictional drag (Townsin R.L., 2003). Ice build-up can affect wind turbine performance, reducing power production and causing structural failures in extreme situations (Dalili, 2009). In oil & gas industry, potential losses for abandoned fields due to the pipeline blockage as a result of wax build-up are greater than €75M (Singh P., 2000).

Surface chemistry and its structure are two important features that regulate wetting and soiling of surfaces and therefore, control over these parameters is a crucial step in successful designing highly repellent coatings. The main coating materials offering hydrophobic surface are currently based on fluoropolymers, polysiloxanes and inorganic-organic hybrids. Techniques involved in controlling roughness are mainly based on top-down (plasma treatments, etching and lithography) and bottom-up (self-assembly) approaches. Despite the fact that chemistries and fabrication routines of highly repellent coatings are well-understood (Sanchez C. B. P., 2011), their industrial adoption is still limited (Verho T., 2011). A key bottleneck for technology transfer from laboratory to outdoor applications lies in poor durability of conventional anti-soiling materials (Verho T., 2011). Moreover, the lack of recognised test methodology that enables repellent properties to be examined against environmental and mechanical degradation hamper further progress of advanced multifunctional coatings (Malavasi I., 2014).

The emergence of nanotechnology brings new opportunities in the field of materials design. The potential of nanostructures lies in the fact that they may improve coating performance, by linking things together, such as mechanical robustness and repellency, opening up the potential direction for research with benefit to transportation, construction and power generation field (Sanchez C. B. P., 2011). Tuning of nanoparticles properties through controlled surface chemistries and texturing should allow for combination of multi-functionality within one coating system. Nevertheless, the novelty of such material by design approach highlights the need of expanding fundamental knowledge about nanostructured coatings. Greater focus is required to understand their wear mechanisms and the relationship between surface, composition and functional performance.

The ability to understand the mechanisms of surface failure and the ability to assess coating lifetime has its bases in properly selected testing methodology. Current approaches used for durability evaluation of highly repellent coatings are focused only on one of the functional attribute and don't allow for direct comparison between different materials families, which hampers further progress of nanostructure coatings. Likewise, none of these approaches focus on measuring the polymodal nature of material durability. Not only should the overall lifetime of the coating be taken under consideration, but also its ability to retain main functional performance, which in case of highly repellent surfaces is determined by anti-soiling properties. Another obstacle in the characterization of advanced materials lies in the lack of

classification criteria that enable the categorizing and comparison of these surfaces that come from very different material families. The term “durability” of the coating system is not clearly defined, which hampers surface failure investigation and in consequence, transfer of novel coating from laboratory to industrial applications.

### **1.3 Aim of research**

The work presented within this thesis addresses the need for new assessment criteria for durability evaluation of highly repellent surfaces, so that knowledge translation of research findings can be accelerated.

### **1.4 Objectives**

The specific objectives of this work were:

- To develop new assessment criteria for durability evaluation of multifunctional coatings that allows for comparison of different types of anti-soiling coatings
- To test and compare selected anti-soiling coatings (TWI formulation A-F and two commercial products, GP101 and Never Wet)
- To establish and monitor the degree of conversion using real-time infrared spectroscopy and reaction with potassium permanaganate for selected coating systems (TWI formulation A-E) in order to ensure that coating failure is not the effect of the lack of cure
- To choose the best-practise available surface preparation method of aluminium alloy 3003 H14 that increases the adhesion strength between metal and coating (model coating system - TWI formulation B)
- To investigate structure-composition-property relationships in selected coating systems, especially the relationship between structure and composition and its influence on abrasive wear and ability to keep anti-soiling properties
- To enable novel classification criteria of highly repellent coatings based on the relation between coating durability and anti-soiling properties over coatings lifetime.

### **1.5 Organization of the thesis**

The work of this thesis is presented in following order.

**Chapter 2** provides general background of surface wetting. Methods and chemistries for developing highly repellent surfaces are discussed. The attributes and benefits of easy clean coatings are outlined and the limitations associated with

their poor durability are examined. The current approaches taken to evaluate the lifetime of the coating are presented.

**Chapter 3** introduces new assessment methodology for the evaluation of the durability of easy clean coatings. The key functional parameters of easy clean coatings are selected and presented in a form of spider diagram. This approach allows for expressing polymodal nature of materials durability within one graph and helps to identify performance indices of easy clean coatings. The performance indices are used as basis for the development of global plot of performance indices of easy clean coatings.

**Chapter 4** describes procedures of preparation of TWI formulations. Structural changes in coating system associated with degree of cure are examined with FTIR analysis. The effect of the degree of conversion on final properties of the coating, including visual appearance and hardness are discussed.

**Chapter 5** presents the influence of surface preparation methodology on the bonding quality between the coating and aluminium alloy 3003 H14 substrate. The best-practise available surface treatment approach is selected, in order to reduce the effect of adhesive wear on the further coating failure investigation.

**Chapter 6** examines the assessment of selected easy clean surfaces. Key coatings parameters are validated according to a novel approach, including initial repellency, lipophobicity, and visual appearance in pristine state, abrasion resistance, retention ratio and ability to withstand in chemical environments. The relation between mechanical lifetime of coating and its ability to retain main functional attribute is investigated based on the changes in surface roughness profile.

**Chapter 7** provides a global plot of performance indices of selected coating systems. The significance of plot of performance indices is discussed in the context of its scientific and industrial value.

**Chapter 8** presents general conclusions of the thesis and provides recommendation for future work, in order to suggest the direction for further development of materials in the process of design by approach in order to accelerate research uptake.

## **1.6 Contributions to knowledge**

A summary of contributions to new knowledge is given below:

- The main contribution to knowledge of this research is in terms of presenting new assessment methodology for durability evaluation of highly repellent surfaces. This new approach allows for a direct comparison

between many different families of anti-soiling coating based on their different properties. The novelty of the assessment methodology presented in this thesis is the ability to compare anti-soiling properties of the surface with its durability (direct and indirect).

- Characterisation of structure-composition-property relationship is selected coating systems (TWI formulations A-F, GP101 and Never Wet) revealed that wear mechanisms of these materials have polymodal nature and can be measured on direct and indirect level. The changes in coating structure resulted from abrasion affect the anti-soiling abilities of this coating. However, the rate of changes in terms of abrasion resistance and anti-soiling abilities are strongly dependent upon initial coating roughness profile. In terms of abrasive wear, the highest survivability was found in coating systems that have low value of arithmetic means of roughness profile and symmetric distribution of peaks and valleys (TWI formulation A and B). Nevertheless, similar survivability was found in surfaces with relatively high value of arithmetic means of roughness profile and symmetry in roughness profile. This indicates that symmetry in roughness profile in coating systems evaluated in this thesis plays an important role on extending the lifetime of these materials.
- The amount of energy absorbed during UV curing of TWI formulation B influences its degree of cross-linking and as consequence, mechanical and optical properties. It was found that TWI formulation B (with 20  $\mu\text{m}$  wet thickness) fully develops its mechanical and optical properties when surface absorbs more than 5.5  $\text{J}/\text{cm}^2$ . It was also found that addition of functionalized silica nanoparticles into matrix resin (TWI formulation A) decreases the rate of cross-linking and TWI formulation D (with 20  $\mu\text{m}$  wet thickness) needs to absorb 13.5  $\text{J}/\text{cm}^2$  in order to break all C=C bonds in the system.
- Surface preparation of aluminium alloy 3003 H14 prior to deposition of TWI formulation B increases the adhesion strength at the interface. Nevertheless, simple removal of the greases and fats by alcohol or acetone wiping is not enough in order to significantly enhance the adhesion quality. In order to boost the adhesion strength at the interface it is necessary to remove and replace aluminium oxide layer.

- Designed plot of performance indices supports the null hypothesis, which stated that there is an inverse relation between initial anti-soiling characteristics and abrasion resistance. This plot of performance indices also improves classification and ranking of highly repellent surfaces and help to select right coating for right application.

## LIST OF PUBLICATIONS AND CONFERENCE PROCEEDINGS

Wojdyla A., Durand G.G., Taylor A., Boyd Ian W., “Advanced low energy durable coatings” NANOSMAT conference 2013, Spain

Wojdyla A., “Advanced low energy durable coatings” Research Student Conference, Brunel University 2013

Wojdyla A., “Advanced low energy durable coatings” ResCon, Brunel University 2014

Wojdyla A., Durand G.G., Taylor A., Boyd Ian W., “Advanced low energy durable coatings” International Journal of Energy Research, 2015 (published)

Wojdyla A., Durand G.G., Taylor A., Boyd Ian W., “Advanced easy clean durable coatings” Advanced Nanomaterials Conference, Portugal 2014

Wojdyla A., Durand G.G., Taylor A., Boyd Ian W., “Advanced easy clean durable coatings” NSIRC conference, Cambridge 2015

Wojdyla A., Taylor A., Boyd Ian W., “New Assessment Criteria for Durability Evaluation of Highly Repellent Surfaces” Progress in Surface Science (article in progress)

Wojdyla A., Taylor A., Boyd Ian W., “New Assessment Criteria for Durability Evaluation of Highly Repellent Surfaces” ACS Spring Meeting, San Diego, U.S 2016

Wojdyla A., Taylor A., Boyd Ian W., “New Assessment Criteria for Durability Evaluation of Highly Repellent Surfaces”, ETCC, Birmingham 2016

Wojdyla A., Taylor A., Boyd Ian W., “New Assessment Criteria for Durability Evaluation of Highly Repellent Surfaces” NSIRC conference, Cambridge 2016

## 2 EASY CLEAN COATINGS

This chapter introduces general background to the chemistry and physics of surface wetting phenomena. Models used to explain wetting regimes on heterogeneous surfaces are presented. The key approaches currently used to achieve easy clean coatings are described and the attributes of such coatings are outlined. The issue of the durability of highly repellent surfaces is described, followed by the presentation of test methodologies used to determine the lifetime of the coating. Finally, two routes to enhance the resilience of easy clean surfaces are proposed.

### 2.1 Introduction to Wetting Phenomena

#### 2.1.1 Surface energy and contact angle

The atoms at interfaces are exposed to different environment than the atoms within the bulk and therefore, they also have a different distribution of energy arising from intermolecular forces. Atoms within the bulk are surrounded by similar ones and they have balanced net force, whereas atoms at interface are faced with unbalanced force due to the lack of neighbouring atoms (Lyklema J., 1991). Differences between these energies (forces) of atoms from interior and from the bulk of the material are called surface tension  $\gamma$  or surface free energy and can be explained by two equivalent definitions (Lyklema J., 1991). The first one describes surface tension as a force, which acts perpendicular and inward from the interface. The resistance against extension of a free surface shows that the surface has an internal surface tension which is measured in force ( $\delta F$ ) per unit length ( $\delta L$ ) [N/m] (Eq.2.1).

$$\gamma = \frac{\delta F}{\delta L} \quad (2.1)$$

On the other hand, thermodynamic definition expresses surface tension in terms of the work ( $\delta W$ ) done per unit area and is measured in [J/m<sup>2</sup>]. In order to increase a surface area by an amount ( $\delta A_s$ ), a quantity of work is needed:

$$\delta W = -\gamma \delta A_s \quad (2.2)$$

Work done by the system is equivalent to decrease in surface area (negative  $\delta A$ ), while increase in surface means that work was done on the system (positive  $\delta A$ ). Finally, this work corresponds to Gibbs free energy for reversible process, under constant temperature ( $T$ ) and pressure ( $p$ ) in a closed system (Gibbs J.W., 1873):

$$\gamma = \left( \frac{\partial G}{\partial A} \right)_{T,p} \quad (2.3)$$

Two terms surface energy and surface tension can be used interchangeably in the case of liquids. However, it is important to remember that for solids the term “surface tension” is not appropriate, since an increase in surface area of solids leads to work acting against the elastic forces and plastic resistance (Good R.J., 1979). The characterization of surface properties and surface free energy components of solids is the key to understanding the mechanism of surface-based phenomena, such as molecular self-assembly, wetting, spreading etc. Quantitatively, these properties can be indirectly estimated by the measurement of the contact angle, which describes the interaction between liquid, vapour and solid interface (Figure 2.1).

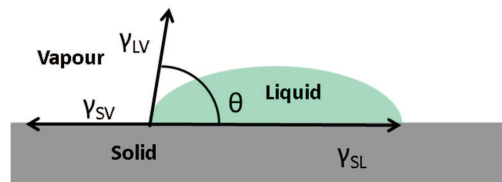


Figure 2.1 Force balance in a three phase system – contact angle principle

The link between surface energy and contact angle was first described by Thomas Young in 1805 (Young T., 1805):

$$\cos \theta_Y = \frac{\gamma_{SV} - \gamma_{SL}}{\gamma_{LV}} \quad (2.4)$$

Where  $\gamma$  is the surface energy of the interface and the subscripts L, S, V refer to the liquid, solid and vapour phases respectively and  $\theta_Y$  is the observed (equilibrium) Young contact angle (Fowkes F.M., 1964) (Neumann A.W., 1979) (Van Oss C.J., 1988). The force equilibrium at the triple point between these phases is a trade-off between adhesive and cohesive forces. Adhesive forces will seek to increase the surface area between the droplet and solid, causing the droplet to spread out. On the contrary, when the force of cohesion between liquid molecules exceeds the force of adhesion between solid and liquid, a drop of liquid placed onto the solid surface will form a finite contact angle. Shifting of this force balance gives a basis to the wetting classification.

### 2.1.2 *Wetting regimes and terminology of the wettability*

Surfaces are divided into categories corresponding to their wetting abilities. Wetting on the ideal surface (smooth, uniform etc.) depends only on intrinsic chemistries of the solid-liquid-vapour system. It is usual practice to call a surface “hydrophilic” (from Greek “hydro” – water and “philic” – love), when its equilibrium contact angle  $\theta_Y$  with water is less than  $90^\circ$ . In this scenario the surface energy of the solid is higher than the solid-liquid interfacial tension  $\gamma_{SV} > \gamma_{SL}$  and wetting of the surface is favourable in terms of decreasing Gibb’s free energy. A less wettable surface with an equilibrium water droplet contact angle higher than  $90^\circ$  means that  $\gamma_{SV} < \gamma_{SL}$  and is defined as “hydrophobic” (“phobic” – fear) (Zisman W.A., 1964) (Adamson A.W., 1976) (Butt H., 2003). For classification of the wettability of solids, water is the most commonly used liquid, due to its high surface tension. Nevertheless, other liquids should be also taken under consideration. In general, most of the used liquids have surface energy lower than water and their equilibrium contact angle on a smooth surface will be smaller than  $\theta_Y$  of water. Marmur has proposed a classification system based on the terms hygro from the Greek (“hygro – liquid) (Marmur A., 2012). In Marmur’s classification surfaces are hygrophilic or hygrophobic.

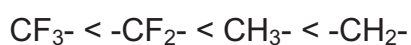
Every surface has characteristic surface energy value, which gives characteristic contact angle with liquids. The values of equilibrium water contact angle for various surfaces are given in Table 2.1 (Arkles B., 2006).

Table 2.1 Equilibrium water contact angle values for various surfaces

Surface/surface treatment	Water contact angle (WCA)
Polytetrafluoroethylene	108° – 112°
Polypropylene	108°
Polyethylene	88° – 103°
Human skin	75° – 90°
Diamond	87°
Graphite	86°
Silicon (etched)	86° – 88°
Steel	70° – 75°
Gold (typical)	66°
Platinum	40°
Gold (clean)	< 10°

The data in the Table represents values for smooth surfaces. The highest water contact value that can be achieved by surface chemistry is approximately 112°. Fluorinated surfaces are the one with the lowest surface energy and therefore, they are capable of displaying high water contact angles.

Great repellency displayed by fluorinated surfaces finds its explanation in Zisman's work (Zisman W.A., 1964). Zisman studied the wettability of polytetrafluoroethylene (PTFE) with different liquids and found out the linear relationship for cosine of contact angle  $\theta$  and surface tension of n-alkanes solvents. Furthermore, he attributed this linear relationship to van der Waals interactions between n-alkanes and PTFE surface. The deviation from linearity for high surface tension liquids was associated with strong molecular interactions, such as dipolar and H-bonding. Zisman established critical solid surface tension (for  $\cos\theta=1$ ) that is the value of highest surface tension, which the liquid fully wets the solid surface and he found out that critical surface tension of single-carbon based molecules increases in order:



Nevertheless, the work of Zisman focuses only on Van der Waals interactions and doesn't consider the nature of interaction between phases. Further work, by Owens and Wendt and Rabel and Kaelble (OWRK method) expanded on these

ideas by introducing considerations of dispersive, polar, hydrogen, induction and acid-base bonding (Owens D., 1969) (Kaelble D.H., 1970):

$$\gamma_s = \gamma_s^d + \gamma_s^p + \gamma_s^h + \gamma_s^i + \gamma_s^{ab} \quad (2.5)$$

Due to the fact that fluorine is the most electronegative element, it is very difficult to polarize. Fluorine can form a stable bonding with carbon and hydrogen and rigidity of created C-F (C-H) bonding hampers the molecule from the further reactions (Kissa, 1994). As a result perfluorinated compounds have very weak intermolecular forces with non-polar, polar, and ionic compounds, which make them insoluble by most of the liquids.

In the real life, the phenomenon of wetting is more than just a static state. Young's equation applies only to the ideal (equilibrium) situation at the triple point, where three thermodynamic parameters  $\gamma_{LV}$ ,  $\gamma_{SV}$ , and  $\gamma_{SL}$  determine a single and unique contact angle  $\theta_Y$ . Young's theory assumes that solid surface is homogenous, smooth and non-porous. In reality, wetting process is much more complicated. This comes from the non-ideality of solid surfaces, which are typically chemically heterogeneous and possess surface roughness.

In general, wetting is divided into different regimes: total and partial wetting. The spreading parameter  $S$  introduced by de Gennes allows to distinguish these two regimes (de Gennes P.G., 1985):

$$S = E_{\text{substrate dry}} - E_{\text{substrate wet}} = \gamma_{SV} - (\gamma_{SL} + \gamma_{LV}) \quad (2.6)$$

When  $S > 0$ , the energy ( $E$ ) of the dry surface is higher than that of the wet surface, the liquid completely spreads to reduce the energy of the system. In this case, total wetting occurs in the system. In the opposite situation, when  $S < 0$ , only partial wetting takes place, meaning the liquid will form a drop on the substrate. Specified equilibrium contact angle (previously defined as  $\theta_Y$ ) splits partial wetting into two regimes, namely "mostly non-wetting" (hydrophilic) and "mostly wetting" (hydrophobic). Furthermore, mostly wetting and mostly non-wetting regimes will be dependent upon the surface roughness. Wetting phenomena are governed by two factors: surface chemistry and surface roughness and its summarised diagrammatically, in Figure 2.2 (Spori D., 2010).

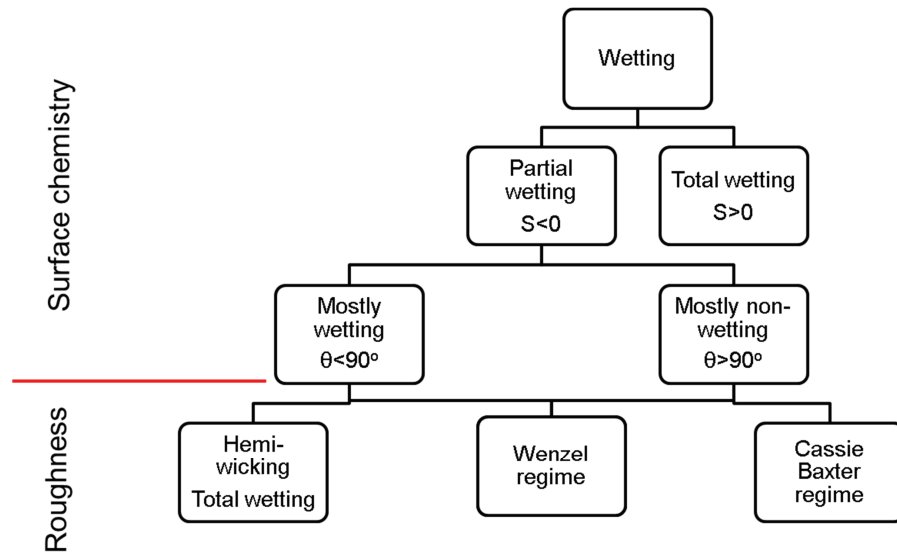


Figure 2.2 Wetting phenomena in correlation to surface chemistry and surface roughness

Surface roughness affects the apparent contact angle. It has been first spotted by Wenzel that liquid droplet penetrates the corrugation of the surface and spreads until it finds its equilibrium (Wenzel R.N., 1936). Wenzel assumed that there is no air layer entrapped between solid and liquid (Figure 2.2) and therefore, the observed contact angle – Wenzel contact angle ( $\theta_W$ ) will be proportional to the equilibrium Young contact angle ( $\theta_Y$ ) by a roughness factor ( $r$ ):

$$\cos \theta_W = r \cos \theta_Y \quad (2.7)$$

According to Wenzel's theory, in the case of hydrophilic surfaces the contact angle should be reduced by the presence of surface roughness ( $r$  factor larger than 1,  $\theta_W < \theta_Y$ ). The opposite situation happens in the case of hydrophobic surfaces. For such surfaces, the introduction of roughness in the system will lead to an increase in observed contact angle ( $\theta_W > \theta_Y$ ).

A more complex situation has been further studied by Cassie and Baxter (Cassie A.B.D., 1948). In their study they assumed that roughness traps the air in the valleys beneath the liquid and droplet rests on the surface (Figure 3.3). As a result of that, apparent contact angle (Cassie-Baxter contact angle  $\theta_{CB}$ ) is given as:

$$\cos \theta_{CB} = f(\cos \theta_Y + 1) - 1 \quad (2.8)$$

By examining the Cassie-Baxter equation, it can be seen that increasing the surface fraction  $f$  (fraction of solid area wet by the liquid), yields higher apparent contact angles ( $\theta_{CB}$ ) regardless of the value of equilibrium Young contact angle ( $\theta_Y$ ).

As has been mentioned before, the highest contact angle achieved by a flat surface is  $\sim 112^\circ$  and it's only achievable by fluorinated surfaces or fully reacted hydrocarbons (Table 2.1). Nevertheless, as discussed surface roughness can lead to much higher values. It has been proposed by Marmur to use the prefix para- (“para” – beyond, “parahydrophilic” and “parahydrophobic”) for cases where apparent contact angle is the effect of surface chemistry and surface roughness (Marmur A., 2012).

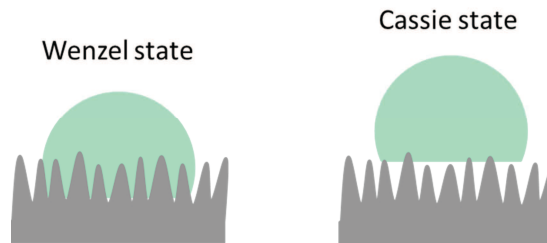


Figure 2.3 Wetting regimes on the rough surfaces (Nosonovsky M., 2011)

There are also two extremities in wetting regimes, caused by the effect of surface chemistry and surface roughness. When a hydrophilic surface is very rough, wicking of the liquid through the furrows may occur. A thin film layer is formed on the surface and contact angle can reach even  $0^\circ$ . This process of extreme wetting is called “superhydrophilic” and is reserved only for surfaces with contact angles lower than  $10^\circ$  (Marmur A., 2012) (Drelich J., 2011) (Roach P., 2008).

On the other hand, combination of hydrophobic chemistry and surface roughness can yield to very high contact angles. In some case, roughness may not only affect the apparent contact angle but also the way how the droplet will move when three-phase contact line is in actual motion. In general, dynamic contact angle is formed by extracting (advancing contact angle) and contracting (receding contact angle) the liquid on a heterogeneous surface (Figure 2.4). The difference between maximum contact angle (advancing CA,  $\theta_{ACA}$ , wetting of the surface) and minimum contact angle (receding CA,  $\theta_{RCA}$ , de-wetting of the surface) is called contact angle hysteresis and the greater the difference is, the more drops will adhere to the surface (Cassie A.B.D., 1948) (Gao L., 2006) (Marmur A., Thermodynamic aspects of contact angle hysteresis, 1994). The diagram below represents the principle of dynamic contact angle, including tilting angle, which corresponds to inclination of solid surface.

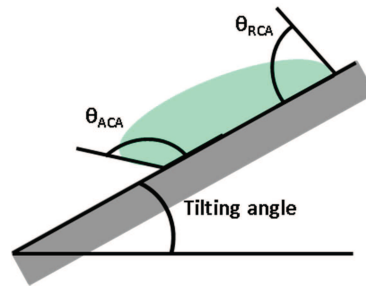


Figure 2.4 The principle of dynamic contact angle

As the contact angle hysteresis gets smaller, it is easier to remove the droplet from the surface. Therefore, the state represented by high apparent contact angles and low contact angle hysteresis represent the other extremity in wetting regimes. In general, it has been proposed to term the surface “superhydrophobic” when its apparent contact angle exceeds  $150^\circ$  while its contact angle hysteresis (sometimes called roll-off angle) is less than  $\leq 10^\circ$  (Arkles B., 2006) (Lafuma A., 2003) (Wang S., 2007). A wettability classification is further explained in Figure 2.5 whereas Table 2.2 provides a summary of generally accepted wetting terminology.

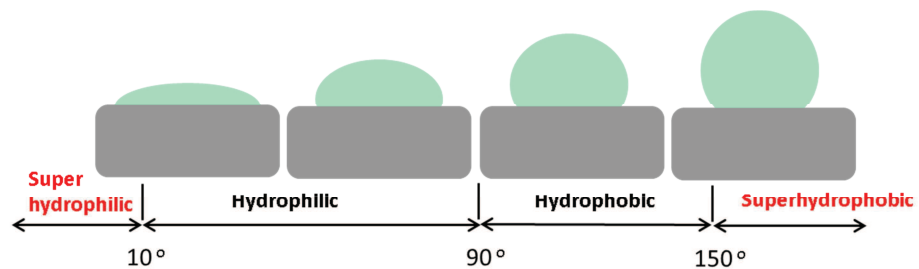


Figure 2.5 Surface types according to the wetting behaviour

Table 2.2 Wetting terminology proposed by Marmur (Marmur A., 2012)

Roughness level of the surface	Wettability classification	Definition based on water CA in air, $\theta_{smooth} = \theta_Y$ or $\theta_C$	Process
Smooth	Hydrophilic	$0^\circ \leq \theta_{smooth} \leq 90^\circ$	Wetting of the smooth surfaces
	Hydrophobic	$\theta_{smooth} \geq 90^\circ$	
Rough	Parahydrophilic	$0^\circ < \theta_W < \theta_{smooth}$	Wetting of the rough surfaces
	Parahydrophobic	$\theta_W$ or $\theta_C \geq \theta_{smooth}$	
Very Rough	Superhydrophilic	$\theta_W = 0^\circ < \theta_{smooth}$	Complete wetting
	Superhydrophobic	Very low hysteresis on parahydrophobic surfaces	Non-wettable surfaces

Superhydrophobic surfaces are often called easy clean, self-cleaning, anti-soiling, highly repellent and/or low energy surfaces. The origin of these names stems from the fact that water does not wet these surfaces.

The relation between extraordinary repellency and contact angle was investigated in the work of Makonnen (Makonnen L., 2012). According to Makonnen's studies, there is a relationship between the water adhesion and wettability of the surface (Eq. 2.9).

$$W_a \approx Y_w(1 + \cos\theta) \quad (2.9)$$

From the above equation, that thermodynamic work of adhesion ( $W_a$ ) is closely approximated to the surface energy of water ( $Y_w$ ) and contact angle of water that created on the specified surface ( $\theta$ ). Further explanation of Makonnen's work can be found in Figure 2.6. As wettability of surface decreases, the adhesion between this surface and water should be reduced as well. When contact angle exceeds 150 degrees, very little adhesion should be expected in the system and therefore, water is repelled from the surface.

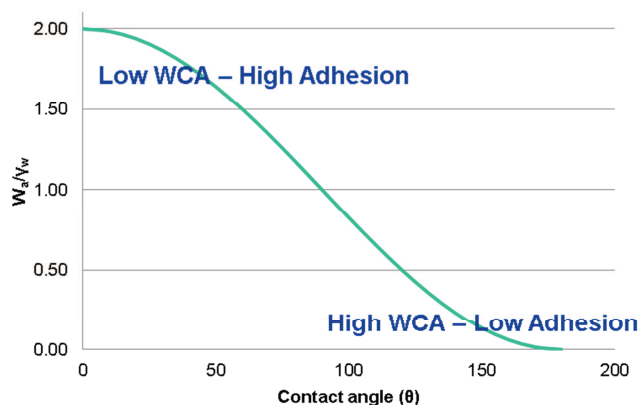


Figure 2.6 The relationship between work of adhesion and wettability of the surface. The author approximates the work of ice adhesion to surface energy of water and the contact angle of water therefore, the ratio  $W_a/Y_w$  doesn't have an unit (Makonnen L., 2012)

As has been mentioned before, in order to create a surface with extraordinary repellent characteristic, surface chemistry has to be supported by surface roughness. Some work has been carried out regarding the texturing model for highly repellent surfaces (Nosonovsky M. N. , 2007) (Bhushan B., 2008) (Bhushan B J. Y., 2006). Most of these studies are based on the conviction that in order to achieve superhydrophobicity, it is necessary to provide multiscale roughness. Such design ideas have been inspired by the observation of super water-repellency and self-cleaning ability of the Lotus flower (Bhushan B J. Y., 2009).

Due to the hierarchical structure of Lotus leaf (a combination of micro- and nano-structures with optimized geometry), the water droplet in contact with the surface will touch only the top of the micro-papillae covered with wax tubes, enclosing the air in the space in between (Figure 2.7). Therefore, contamination (such as dust particles etc.) sits on top of the micro-papillae, resulting in a very small actual contact area with the leaf. Consequently, the adhesion forces attaching the particle to the surface will be small. Water will wet such contamination by not the leaf and so water droplets will “collect” such contaminants as they roll off the leaf giving rise to the description of self-cleaning behaviour (Marmur A, The Lotus Effect: superhydrophobicity and metastability, 2004) (Bhushan B J. Y., 2009), although since the water is from external sources this description is not strictly accurate.

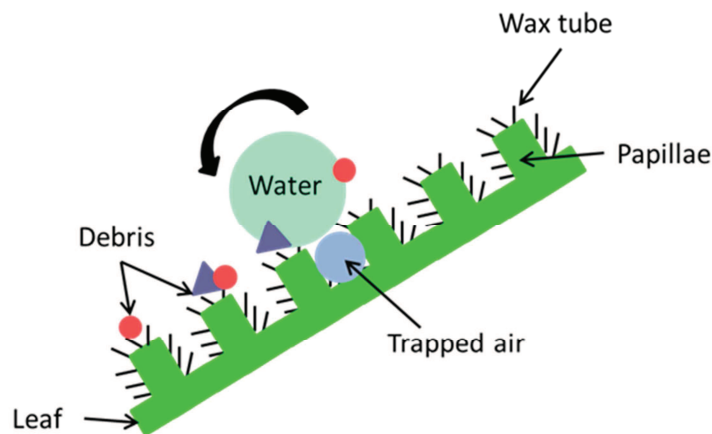


Figure 2.7 The Lotus leaf effect

As has been discovered recently, dual-scale roughness combined with the proper surface chemistry is not the only way to achieve highly repellent materials. Kim et al. has shown in his studies that uniformly nanostructured surfaces can provide an excellent non-wetting characteristic (Kim P., 2013). Furthermore, as it turned out, such way of designing roughness can lead to superior performance compared to traditional hierarchical texturing.

There are two broad strategies for generating the nanostructured surfaces. They can be classified as “top-down” (patterning nanoscale features on a substrate) and “bottom-up” (assembling atomic or molecular building blocks into nanoscale structures in a solution phase) (Teo B.K., 2006) (Sanchez C. B. P., 2011). In top-down techniques, large pieces of materials are reduced all the way down to the nanoscale (for example, by electron beams, and then by applying appropriate etching or lithography processes). On the contrary, bottom-up approach involves

processing or building up a material from the atomic scale or nanoclusters into structures such as sheets, tubes, wires (Whitesides G.M., 2002) (Shevchenko V.Y., 2003). Self-assembling of building blocks into well-organized structures is dependent on the ability to control their size, shape and surface properties. Therefore a primary aim of self-assembly is to synthesize building blocks with specified dimensions and form, and through chemical control of their surface properties (i.e. charge, hydrophobicity, hydrophilicity, functionality), in order to create an integrated systems with fixed function and utility (Cademartiri L., 2009). In general, bottom-up approach involves a high degree of complexity and it is sometimes difficult to control. Top-down techniques give the better control over the manufacturing process and it is easier to predict the final result. Nevertheless, these techniques are time-consuming and very expensive, which makes self-assembling the primary choice of nano-fabrication.

## **2.2 Attributes of Easy Clean Coatings**

Different pinning phenomena designated by homogenous (Wenzel) and heterogeneous (Cassie-Baxter) wetting, influence the way how the droplet moves on the surface. In general, movement mechanisms on the superhydrophobic or parahydrophobic surfaces can be either “slippery” or “sticky” (Figure 2.8) (Lafuma A., 2003) (Arkles B., 2006). Slippery mode of such surfaces can be compared to lotus leaf, where droplet rolls off very easily with little contact angle hysteresis (Koch K., 2010) (Bhushan B J. Y., 2006) (Marmur A, The Lotus Effect: superhydrophobicity and metastability, 2004). This slippery mechanism exhibits unique attributes, such as self-cleaning, anti-soiling, anti-icing, anti-graffiti, anti-fingerprints, anti-corrosive, aerodynamics (friction reduction) (Cao M., 2015). On the other hand, sticky surfaces (parahydrophobic surfaces with high contact angles and also large contact angle hysteresis) may be associated with a petal effect, where droplet does not roll off from the surface, even if it placed upside down (Bhushan B N. M., 2010) (Feng L., 2008). Such sticky surfaces with the affinity to water have the potential application in liquid transportation, ink-jet printing and microfluidic devices (Hong X., 2007) (Calvert P., 2001) (Cho W.K., 2008). This sub-chapter covers description of the attributes of highly repellent coatings with the slippery mode.

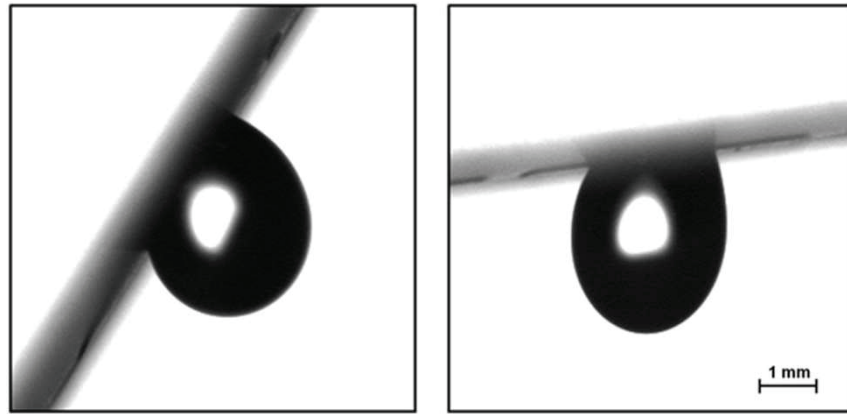


Figure 2.8 The petal effect – sticky mode (Milionis A., 2013)

### 2.2.1 Self-cleaning

In last decades, surfaces mimicking nature (i.e. lotus leaf) have been constantly attracting scientists and engineers and have found their applicability in exterior paints, windows and solar panels production (Zhu W., 2012) (Smitha V.S., 2013) (Parkin L.P., 2005). When a self-cleaning coating is applied, water from the rain is sufficient to clean the surface. Nevertheless, in order for surface to maintain fully self-cleaning property, it is necessary for this surface to display omniphobicity (the ability to repel both, oil and water). If material is not oil repellent, oils and fats from environment can accumulate in the surface textures, thereby blocking self-cleaning mechanisms.

### 2.2.2 Anti-icing

Atmospheric icing from supercooled droplets in the atmosphere, also known as "freezing rain" is a notorious problem in many fields, such as power lines, aircrafts, wind turbines (Laforte J.L., 1998) (Heinrich A., 1991) (Dalili, 2009), etc. Traditional methods of ice removal include simple mechanical scraping, melting by heating or applying anti-freezing substances like salt or glycol. Although, these methods are successful in de-icing, they require continuous supply of chemicals, hot air, they can cause abrasive damage to the surface or they are usually toxic to the environment. The development of superhydrophobic or parahydrophobic coatings with extraordinary water-repellency might offer an effective replacement for the current anti-icing systems (Makkonen L., 2012) (Dodiuk H. K. S., 2012) (Boinovich L.B., 2013)

The conception, description and examination of "icephobic" coatings have appeared many times in scientific works (Anderson D.N., 1997) (Menini R. F. M., 2009) (Menini R. F. M., 2011) (Antonini C., 2011). In general, it is expected that

the air enclosed below the water droplet will create a thermal barrier which can delay and may even prevent accumulation and adhesion of ice (Jung S., 2011). Even though superhydrophobic and parahydrophobic surfaces have proven lower ice adhesion strength, their ice-repellent mechanism seems to degrade gradually (Kulinich S.A., 2011).

### *2.2.3 Anti-graffiti*

Due to its rising prevalence in many areas and the high costs associated with clean-up and prevention, graffiti is often viewed as problem of society (Manczyk K., 2008). In principle there are two different types of anti-graffiti systems: temporary and permanent. Temporary anti-graffiti protection contains acrylates, waxes or sugar-based polysaccharides are applied to form a line interface between the coating and the surface. In result, cleaning the surface of graffiti involves removing the protective coating layer, which should be replaced. The development of permanent anti-graffiti systems is currently based on the water-borne low energy coatings with fluoro, perfluoro or silicones components (Wu X., 2008). These coatings do not allow the graffiti to stick properly to the surface. Therefore, as an effect of the poor adhesion, graffiti is easily removable from the surface (Rabea A.M., 2012) (Steidl N., 2003) (Aizenberg J., 2011).

### *2.2.4 Anti-fingerprints/oleophobic*

Recently, touch panels have dominated wide range of market products, including car navigation systems, phones, and computers, and their production is expanding every year. Due to such interest from the industry, scientists are constantly trying to find a way to solve the problem with fingerprints, which leaves unaesthetic, dirty appearance on the surface. A lot of research has been carried out regarding anti-fingerprint coatings, commonly known as the “oleophobic” systems (from Latin “oil fear”) (Liu X., 2012) (Wu L.Y., 2011).

Generally speaking, these surfaces are poorly wettable by the low surface tension liquids (or non-wettable in case of “superoleophobic” surfaces) (Marmur A., 2012). Oleophobic coatings do not completely prevent formation of fingerprints, although they reduce the adhesion between the surface and the oils, which makes them easy to clean. Conventional way of making coatings with water and oil repellency is generally based on the fluorine-based (Uyanik M., 2006) or silicone (Lakshmi R.V., 2012) materials.

### 2.2.5 Aerodynamic drag reduction

The aerospace and marine industries are constantly seeking ways to lower fuel consumption. One possible way to that is to reduce the air/fluid drag. Turbulent flows can occur in the boundary layer near solid surfaces due to the higher friction associated with increased flow velocity. In a consequence, the energy losses and self-noise arising from the turbulence friction can be of very high. The main purpose of drag reduction is to delay the onset of turbulent flows. Generally speaking, a drag reducing agent is able to shift the transition from a laminar to a turbulent flow to higher flow velocity (Hoyt J.W., 1985).

Highly repellent surfaces are known to exhibit reduced viscous drag due to the “slip” associated with the layer of air trapped beneath the droplet. This slip will lead to reduced turbulent drag flow in external flows. Besides that, surface irregularities (dirt, ice, and insects) can cause the boundary layer transition from laminar to turbulent flow in a very short distance. Easy clean coatings are able to remove (self-clean) debris, and thus extend the distance of the laminar flow (Kanagasabapathy S., 2012) (Srinivasan S., 2013) (Dong H., 2013).

### 2.2.6 Anti-corrosive

Control of corrosion has always been an important subject of interest in many areas of science and industry. There is a wide variety of protective coatings in use, which offers high resistance to wear and oxidation (Sørensen P.A., 2009). Traditional anti-corrosive coatings systems stabilize the potential of the metal in a passive regime, maintaining a protective oxide layer on the surface (Gelling V.J., 2001). Nevertheless, most of these coatings are likely to be limited in the future, due to the fact that they contain hexavalent chromium. Like most heavy metals,  $\text{Cr}^{6+}$  is toxic and a suspected carcinogen, the release of which is regulated by many environmental agencies (OCHA) (ECHA). Therefore, the prospect of producing highly repellent surfaces able to repel water has potential to bring great opportunities in the area of corrosion inhibitors for metal components. The surfaces having low energy promote the formation of the thin air film between the water and the coating. This layer acts like a barrier and thereby decreases the transport of the ions from the water to the metal (Ejenstam L., 2013) (Zhang F.Z., 2008).

In summary, highly repellent surfaces have recently shown great interest both in fundamental research and practical applications. Different methods of fabrication

such surfaces are constantly developed; bearing in mind that superhydrophobicity can be achieved only when the right surface chemistry is combined with specified roughness level. The degree and shape of roughness can be tailored with “top-down” or “bottom-up” approaches. An overview of surface chemistries necessary for the design of highly repellent materials is described in the following section.

### **2.3 Advanced Easy Clean Coatings**

In general, there are three main coatings that provide hydrophobic species, necessary to build-up easy clean (anti-soiling) systems. These include fluoropolymers, polysiloxilanes based coatings, and inorganic-organic hybrid materials.

#### *2.3.1 Fluoropolymers*

The dominant anti-soiling market is currently based on fluoropolymers. These surfaces display hydrophobicity and oleophobicity at the same time, which makes them not readily wettable. Due to that fact, clean-up is easier and more thorough than in other anti-soiling systems. Nevertheless, they are likely to be limited in future as a result of concern about their safety (Gallo V., 2012) (ECHA European Chemical Agency, 2014).

Fluoropolymers are the polymer materials which contain fluorine atoms in their structure. Generally, there are two types of fluoropolymer materials, perfluoropolymers (PTFE) ( $\text{CF}_2=\text{CF}_2$ ) and partially fluorinated polymers ( $\text{CH}_2=\text{CF}_2$ ) (Drobny J.G., 2001). The high thermal stability and chemical resistance of fluorine-carbon bond, combined with low coefficient of friction, wear resistance and excellent dielectric properties have made the fluoropolymer based materials widely used in the aerospace, automotive, construction and textiles (Teng H., 2012) (Jones B., 2008). Despite their high quality properties, fluoropolymer based easy clean coatings have some limitations. The PTFE and similar products require high temperature processing which can influence their final market price. Another disadvantage of fluoropolymer coatings is associated with their toxicity. Perfluoropolymers (C8) raw materials, such as perfluorooctanoic acid (PFOA) and perfluorooctanesulfonic acid (PFOS) have been the subject of legislation issue since 2000. Studies have shown that these components are persistent, with long-term accumulation and toxic for human population and wildlife nationwide (UNEP (United Nations Environmental Programme), 2006) (Gallo V., 2012) (EPA (Environmental Protection Agency), 2012).

### 2.3.2 *Polysiloxanes*

Another well-known class of materials with easy clean properties belongs to polydimethylsiloxane (PDMS). The development and success of silicone based coatings have been originated from the need of materials with low VOC (volatile organic compounds) and high performance attributes, as will be discussed.

Polysiloxane coatings are mainly built of alkoxy (RO) and silanol ( $\text{SiO}(\text{Me})_2$ ) functional groups. These polymers display high resistance to sunlight, elevated temperatures and chemicals (Pham Q.T., 2013) (Foscante R.E., 1997) (Keijman J.M., 2002). Such advantages stem from their covalent silicon-oxygen bonding, which gives a strong polymeric backbone and makes these materials more resistant to degradation mechanisms. Besides that, silicon in the polysiloxane polymer core is already 50%-75% oxidized and therefore, further oxidative degradation cannot occur (Brown L. H., 1972). Moreover, due to the very low viscosity level, polysiloxane coatings can be formulated with high solid content and low VOC. For coatings having more than 90% of solid content, VOC level can be kept below 100 g/l (Andriot M., 2008). Finally, most of the silanes used in formulating polysiloxane binders act as an adhesion promoters and form a strong bonding on the coating-substrate interface. All of these different properties of polysiloxanes make them a material of choice for various applications, such as heavy duty OEM, constructions, marine and industrial maintenance, medicine and electronics (Mowrer N. R., 2003) (Abbasi F., 2001) (Kawakami Y., 2006). Nevertheless, silicone based coatings have also some disadvantages. First of all, they have poor stability in solvent free systems (R. Valeri, 2009). Secondly, polysiloxanes that have good anti-soiling properties, tend to have poor durability (Taylor A, 2014).

### 2.3.3 *Inorganic-organic hybrid coatings*

The growth of interest for inorganic-organic hybrids has originated from the need of combining properties of organic (processability, flexibility, toughness) and inorganic (abrasion resistance, hardness, chemical resistance, weatherability and UV-resistance) polymers. A diversity of inorganic-organic hybrids have been developed and investigated in different fields of industry (Arkles B, 2001). Generally, these materials can be classified into two groups, depending on the forces acting between polymers. In class I organic and inorganic parts interact only through weak bonding (hydrogen, Van der Waals, electrostatic), whereas in class II inorganic-organic phase is linked by the strong bonding (covalent) (Sanchez C.

B. P., 2011). Class I materials are obtained by embedding organic materials in an inorganic matrix. Class II hybrids present the opposite situation, where the core is organic and it's filled with inorganic additives. Despite the fact that this taxonomy of inorganic-organic materials has been used extensively in the scientific literature, different types of classification can be also found (Nowak B.M., 1993) (Wen J.Y., 1996).

Inorganic-organic materials are generally prepared through sol-gel processing. Starting from molecular precursors (building blocks), such as metal or semi-metal alkoxides, through hydrolysis (i) and condensation (ii) reactions, metal oxide-based network is generated (Brinker C.J., 1990) (Hench L.L., 1990) (Sanchez C. R. F., 1994).



The range of hybrid coatings and their potential applications is enormous. In particular, these coatings have been used for adhesion enhancement, corrosion protection and easy clean surface properties (Schmidt H., 1986) (Izumi K., 1993) (Zheng S.X., 2010) (Messori M., 2006). Nevertheless, one of their main limitations is high content of solvent, necessary to avoid premature gelation (Brinker C.J., 1990). Besides that, due to the complex distribution of hydrolysis and condensation reactions during sol-gel process, the number of structural variants that can be created is huge and therefore, this complexity leads to variability, sub-optimised performance and the lack of reproducibility (Taylor A. H. D., 1993). One way of describing this is by a matrix based nomenclature (Figure 2.9). The sol-gel transition of tetraethylorthosilicate (TEOS) was studied using high resolution  $^1H$  NMR spectroscopy (Assink R.A., 1994). The matrix proposed by Assink and Kay displays all species of TEOS, from its starting position  $Si(OR)_4$  (4,0,0), to the fully hydrolysed and condensed anhydrous silica,  $Si(OSi)_4$  (0,0,4). These can also be described using 'Q' notation, where Q refers to the quatra functionality of silicon. If silicon has no siloxane bond (SiOSi) it is referred to as  $Q_0$ , if it has one siloxane it is referred to as  $Q_1$  etc. It can be seen from the matrix that there are multiple species that can be referred to as  $Q_0$ , since there are a number of partially hydrolysed molecules.

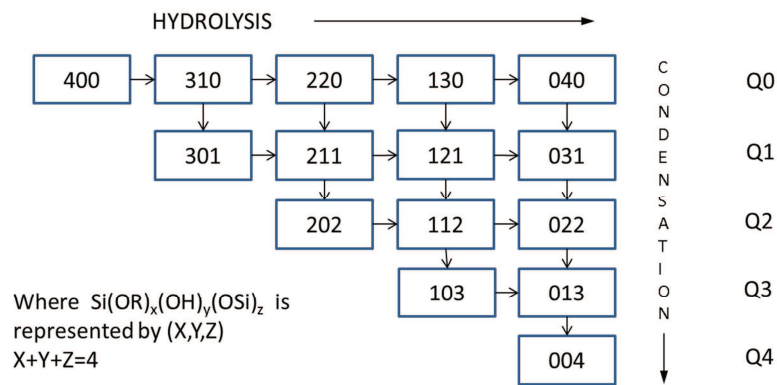


Figure 2.9 Sol-gel structural evolution (Assink R.A., 1994)

All above described coatings provide surface chemistry (hydrophobicity) in order to design highly repellent materials. Nevertheless, as has been mentioned before, non-wetting surfaces can be only achievable by combination of surface chemistry with surface roughness. Microscopic surface topography that is essential for very large contact angles has an impact on mechanical stability of material. As a result of that all presented convectional coatings display high performance (non-wetting properties) only when they are new. Situation changes when these surfaces are subjected to harsh environments and due to abrasion they lose their microstructuring and ability to repel water. Despite the importance of mechanical durability in applications, comparatively little attention has been paid to this issue, especially in case of highly repellent surfaces. The lack of understanding of the wear mechanism in such coatings and lack of recognised test methodologies enables that comparison of various approaches to achieve repellence, hinders effective progress of advanced coatings and surface treatments. An overview of current approaches used for durability validation for easy clean coatings has been presented in the following section.

## 2.4 Durability assessment of easy clean coatings

During its service life, coating is constantly prone to different challenging operating conditions, such as high temperature, abrasive wear, erosion, corrosion et cetera. Mechanical durability of highly repellent surfaces is therefore a crucial issue in developing successful easy clean coatings. Despite the fact that myriad of reports have been published regarding the routes to fabricate such coatings, majority of these methodologies offer limited mechanical resilience. Relatively little attention has been paid to wear mechanism of advanced easy clean surfaces, and as a result of that, their use in real world applications is still very limited. Furthermore, objective comparison of durability of highly repellent materials has been hampered

by the lack of recognised single test procedure. Although some efforts have been done in the direction of assessing durability of easy clean surfaces, no systematic procedure has been developed so far. Most of the current tests utilize in-house apparatus and focus on only one type of wear mechanisms.

In many cases, durability of the coating is predicted by coating ageing analysis. Li et al. have reported an approach for assessing the durability of easy clean surfaces by measuring their resistance against UV irradiation (200-400 nm for 30 min), to elevated and sub-zero temperatures (200°C for 1h followed by -30°C for 1h), to high water pressure (6000 Pa for 5 min). This study also covers chemical durability assessment, such as immersion in weak basic (0.1M NaOH, 1h) and acidic solutions (0.1M HCl, 1h). Resistance of the coatings have been classified in a function of change in static and dynamic contact angle (Li B., 2013). Boinovich et al. studied long-term durability of repellent properties under continuous contact with deionised water (Boinovich L., 2010). The studies of Bayer et al combine the chemical and mechanical durability evaluation (Bayer I.S., 2009). The durability test consists of exposure to basic (pH:10) and acidic (pH:2) aqueous solutions and gentle surface polishing (3M 1000 grit aluminium oxide sand paper mounted on a rotating platform applying approx. 0.6kg/cm<sup>2</sup>). Long-term durability assessment can be also found in studies of Zimmermann et al. (Zimmermann J., 2007). Natural and artificial weathering has been performed. Outdoor exposure has been conducted for a total duration of 12 months. Artificial weathering focused on ADF test (Acid Dew and Fog) and exposure to UV radiation.

Some of the studies report that degree of adhesion between the coating and the underlying substrate is the critical aspect in order to achieve a successful, durable surface. Steele et al. investigated adhesion strength between some superhydrophobic coatings and aluminium substrate. Evaluation was undertaken via a 90° tape test (3850 N/m maximum, applied force) and has been analysed with respect to changes in surface morphology and wetting characteristics (Steele A., 2012). Dodiuk et al. used variety of techniques to evaluate the coating resilience (Dodiuk H. R. P., 2008). Coating durability was characterized by indoor (T=25°C, RH=60%, 1month) and outdoor tests (QUV accelerated weathering test chamber, 500 hr using UVA 340 fluorescent lamps with a cycle comprising 8 hr radiation at 60°C and 4 hr condensation at 50°C), immersion in distilled water followed by immersion in IPA and paper rubbing. In addition, the degree of

adhesion between substrate and coating has been controlled. Similar approach to test durability can be found in Deng's work (Deng, 2012). In his study, he investigates the influence of adhesion strength and sand impingement on the wettability properties of easy clean coatings.

The combination of high repellency and mechanical durability is rarely found in nature. While the surface of the lotus leaf is non-wettable, it is not really prone to harsh abrasive conditions and therefore, its mechanical durability is not an issue. In technological applications, the situation is completely different. Coatings are constantly subjected to various kinds of abrasive wear. Abrasion durability should be therefore the key criterion in coating performance requirements. Many of the reported durability assessment methods concentrate on surface abrasion and erosion resilience. In these studies, different approaches are used, in order to investigate anti-soiling characteristics as a function of mechanical damage. The most common methodology involves rubbing the test specimen against some kind of abrasive material (cloth, abrasive paper) under a certain load. Li et al. have measured the scratch resistance of coatings with a homemade scratch tester that comprises a piece of 1500-mesh abrasive paper and weights of different mass (Li Y., 2010). The abrasive paper had a contact area of  $1 \times 1 \text{ cm}^2$  and was dragged with a speed of  $1 \text{ cm s}^{-1}$  over underlying easy clean coating. The scratching has been performed under applied pressure, ranging from 10 to 20kPa. Jin et al. has evaluated the wear resistance of the produced coatings by simply abrading the surface with abrasive paper (Jin H., 2013). Some kind of in-house abrasive apparatus has been presented in the work of Cho (Cho H., 2013). In order to assess the durability, fabricated easy clean coatings were tested using abrasive film (1 micron grade Imperial™ lapping film). Different weights have been applied to the test specimen and the surface was moved in one direction with 5mm/s at the stroke of 15cm. Zhu et al. investigate the resilience of produced easy clean surfaces with the combination of scratch and friction tests (Zhu X., 2011). The scratch resistance has been evaluated with a homemade scratch tester (1500 mesh abrasive paper) and friction has been studied using ball-on-plate tribometer under reciprocating motion. In addition, deterioration of WCA has been measured after being touched by a finger. This finger touching test is definitely a good approach, due to the fact that finger contact not only causes the damage to surface texture, but also introduces oily contamination to the material. Homemade scratch tester has been also used in the study of Wang et al. (Wang F.J., 2013). In

this case, 320 grit abrasive paper has been used, 30 kPa pressure was applied and the test specimen moved over 20 cm with the speed  $10 \text{ cm s}^{-1}$ .

Some testing approaches relate coating durability with its hardness. Therefore, nanoindentation measurements have been used as classification criteria for resilience of highly repellent surfaces. Verma et al. have performed nanoindentation with Berkovich diamond indenter tip to calculate coating surface hardness and scratch resistance (Verma G., 2013). All experiments were carried out under the displacement control mode. The rates of loading and unloading were both  $100 \text{ nm/s}$  and a 10 s holding was applied at the maximum indentation depth of  $1 \text{ }\mu\text{m}$ . Similar practise has been adopted by Zhou et al. (Zhou S., 2013). The micro-mechanical performance was determined using a nanoindentation tester (CSM Instruments, Switzerland) with a Berkovich diamond indenter. The indenter was penetrated into the coatings with a constant load rate of  $1 \text{ mN/min}$ , until a depth of  $3000 \text{ nm}$  was reached; the maximum load was held for 30s. Nevertheless, in Zhou's work, hardness measurements are not the only one indicator of coating durability. In addition to the mechanical resilience evaluation, accelerated ageing (QUV artificial weathering) and resistance to organic contaminants are measured. Schutzius et al. classifies the highly repellent surfaces based on their elastic behaviour (Schutzius T.M., 2011). Test specimens were mounted between two linear clamps and stretched using a programmable linear actuator (Velmex). Coatings water droplet roll-off angle has been measured in a function of increase in strain.

Easy clean surfaces are desirable in industry sectors, such as wind turbines and aerospace. Due to the fact that aircrafts and turbine blades work in a constant motion, several authors have decided to assess coating durability based on their wettability behaviour as a function of dynamic contact with water or air. Nahum et al. measure the CAs and SAs before and after air drag test was carried out (air gun has been used with the velocity of  $300 \text{ km/h}$ ) (Nahum T., 2014).

Remer et al. have evaluated dynamic contact of droplet with easy clean coatings in conditions favouring icing (Remer M., 2014). The droplet behaviour has been studied in "flight-like" conditions (from  $-30^{\circ}\text{C}$  to  $25^{\circ}\text{C}$ ), during contact with varying phases of ice formation and during frosting. Such an approach to test the durability of highly repellent surfaces is definitely a very useful methodology since it closely resembles real world conditions. Nevertheless, the range of possible applications

for highly repellent surfaces is enormous and one testing routine cannot be applied in all of the cases, due to the fact that different applications involve different challenges in terms of mechanical durability. Therefore, some of authors have decided to use application-based test routines. Zhang et al. evaluated fabricated easy clean coatings on stainless steel in field test at a paper machine (Zhang X., 2012). Specimens were tested near the size roll in the real paper machine producing release base paper for labelling. The function of this machine is to remove water in different steps in order to obtain dry and homogenous paper. The test lasted for 6 weeks consisting of two running periods of 16 days. Furthermore, after the field testing, durability of fabricated coatings has been evaluated by using nanoindentation technique. Application based testing such as this method have a lot of advantages, nonetheless, it is potentially labour-intensive and requires access to real world application fields.

The number of test routines that can be used to measure the durability of highly repellent surfaces is relatively high and therefore, it is hard to develop one all-encompassing standard protocol. Most of these tests have been developed in the recent years, show that there is a growing concern regarding evaluation of lifetime of easy clean coatings. Nevertheless, there is still a technological gap in this particular area. First of all, too much focus is laid on the materials composition and roughness and their properties in initial state, but not on their wear mechanisms and lose of initial properties. Second, test methodologies were designed for the purpose to evaluate some specified easy clean coatings, but not for the purpose to compare the different highly repellent surfaces. The absence of general classification criteria for the assessment of durability of highly repellent surfaces, not only stop the further progress of emerging coatings, but also do not provide useful guidance for designing and developing new materials.

Hohne et al. have identified a tier grading system, in order to classify fabricated easy clean materials (Hohne S., 2009). Mechanical tests were carried out using a homemade apparatus; abrasion and hardness were studied together with the surface wettability properties. Abrasion resilience of highly repellent materials was then evaluated using a two tier grade system. Table 2.3 presents the classification system designed by Hohne.

Table 2.3 Two tier grading system for the durability evaluation of easy clean coatings

Tier grade X	Tier grade Y	Applied load [N]
Abrasion resistance	Wettability characteristics	
Class 5	Class 5	0.05
Class 4	Class 4	0.1
Class 3	Class 3	0.2
Class 2	Class 2	0.5
Class 1	Class 1	1
Class 0	Class 0	>1

One of the grades represents abrasion resilience of the coating, whereas the second one describes the wettability characteristics. Both of the grades range from 5 to 0 and for example, when X=1, it means that abrasion is visible after mechanical testing is done with 1N applied load. In a case of repellent properties, Y=2 when a water droplet sticks to the surface after a load of 0.5N was applied (simplify by measuring the changes in sliding contact angle). Grade 0 corresponds to the best performing coatings, with no visible signs of abrasion (x) or loss of water droplets roll-off (y) under 1N of load applied. The studies of Hohne introduce some kind of durability classification criteria for highly repellent surfaces. Nevertheless, the presented procedure has some limitations. First of all, it's only a semiquantitative assessment and therefore, some quantitative precision can be lost. Second of all, abrasion is evaluated based on the results obtained with homemade apparatus, which makes it difficult to compare wear results obtained from different laboratories. Malavasi et al. have proposed a global plot of performance indices and ranking for different easy clean coatings, to help to identify those surfaces that fulfil durability requirements for specific applications (Malavasi I., 2014). Different tests have been performed (chemical and mechanical durability), in order to evaluate the resistance of surfaces in different operating conditions. The decrease of receding contact angle below 135° and an increase of contact angle hysteresis above 10° have been used as a borderline for wettability characteristics. The concept of presenting such protocol is a good idea nonetheless, there are some limitations. The main issue lies in the fact that this approach is only applicable for

very highly repellent surfaces and it doesn't help to assess the durability of just repellent surfaces. Despite the fact that coating resilience is evaluated, these figures of merit do not categorize the surface as durable or non-durable. Moreover, the final durability point of characterized surfaces in terms of mechanical resilience is not clearly defined. It is not specified if these surfaces lose their film integrity while losing or retaining their wetting characteristics which makes it difficult to use this protocol as a complete plot of performance indices.

In the last decade, the number of articles raising the issue of durability of highly repellent surfaces has significantly increased. Recent studies have begun to address not only the initial properties of easy clean coatings, but also their resilience in operating conditions, which is definitely a big step towards successful development of advanced coating systems. Nevertheless, despite all the work carried out regarding the durability of easy clean surfaces, no standard procedure or classification criteria have been developed so far and therefore, performance of emerging materials and coatings can hardly be compared. Application driven test methodologies seem to be a promising way of measuring mechanical properties of the coatings. Ability of recognizing the wear mechanism under specified operating condition, may give the answers how to enhance the durability of selected coating systems.

There is still a lack of an agreed approach or direction to achieve durability of highly repellent surface. Nevertheless, there is hope that this subject will receive more attention in the near future. The development of nanotechnology brings the hope that new generation of materials will have the ability to restore their repellent characteristic for a long period of time, even when the surface will be quite damaged. Following section presents the development of these new materials.

## **2.5 Novel Inorganic Building Blocks for Durability Improvement**

Nanotechnology is a novel approach that refers to understanding and analysing the properties of matter at the atomic level (nano-scale): one nano-meter (one billionth of meter) is the length of a small molecule (Drexler K.E., 1986) (NRC (National Research Council), 2006). Nanomaterials, defined by European Commission as "natural, incidental or manufactured material containing particles, in an unbound state or as an aggregate or as an agglomerate and where, for 50 % or more of the particles in the number size distribution, one or more external dimensions is in the size range 1 nm - 100 nm" (European Commission, 2015).

This new field of study involves not only the miniaturization but also the precise manipulation of atoms and molecules, in order to design and control the properties of the whole materials and systems. Scaling materials down into the nano-regime, it has been observed that material properties become completely different (optically, mechanically, and physically) than those possessed by the bulk materials. This knowledge gave the technology new capabilities, which cannot be found in bulk materials or in nature, or even the possibility to replicate some of natural processes that have not been currently achieved through synthetic materials (Tjong S.C., 2004).

The development of nanostructured coatings is driven by the market need for new materials with combined properties, providing anti-soiling performance and improving erosion/abrasion resistance, yet cost-effective and cost-efficient (Davison C., 2013). Such advanced coatings combined in the nanometer range, derived from clearly dissimilar organic and inorganic components (Table 2.4) offer the potential for significant improvements in engineering properties, such as mechanical (Mammeri F., 2005), optical (Smietana M., 2010), thermal (Vasiliev L.L., 2013) electronic (Malkov A.A., 2006) and tribological (Pham D.C., 2011) (Pazderova M., 2011).

*Table 2.4 Typical properties of organic and inorganic materials (Kickelbick G., 2007)*

Property	Organic materials	Inorganic materials
Bonding nature	covalent (C-C), Van der Waals, hydrogen	ionic, covalent
Thermal stability	Low	high
Density	Low	High
Refractive index	Low	High
Mechanical properties	elastic,  flexible	hard,  strong,  brittle
Electronic properties	Insulating, conductive and semiconductors	Insulating, conductive and semiconductors
Magnetic properties	non-magnetic	magnetic
Physical considerations	hydrophilic or hydrophobic	hydrophilic or hydrophobic
Processability	at low T and p	at high T and p

As has been previously mentioned, nanostructure materials can be obtained using “top-down” or “bottom-up” approach (Sanchez C. B. P., 2011). High complexity and costs of top-down techniques, makes bottom-up method the preferable way of designing nano-coatings (Zhang S., 2003). There is a big range of nanoparticles that can be incorporated into the coating, in order to upgrade the properties of the whole system. This approach opens a new direction for science and industry, a possibility to design novel materials with unique combination of properties.

By common consent, durable coatings are not particularly repellent and the more repellent the behaviour the lower the durability particularly to mechanical damage, but also to chemical attack. A lack of durability can be described as either as loss of coating integrity or as loss of a key functionality such as repellent behaviour. Such an inverse relationship has been previously postulated (Taylor A, 2014), this is illustrated schematically in Figure 2.10, which follows a materials selection chart type format. Conventional isotropic and non-structured materials can be considered by family. The fluoropolymers form the largest family of repellent materials (Taylor A, 2014), due in no small part to the fact that the  $CF_3$  and  $CF_2$  chemical groups are the most repellent. Silicones form the next largest groups due to the water repellence of the  $Si-CH_3$  chemical group and then the silanes and mixed polymer/inorganic hybrids. Lower polymer content hybrids, polysiloxanes and highly cross-linked hardcoats typically have much greater durability but typically are not very repellent to water. It has been shown that the introduction of nanostructure and particularly dual scale nanostructure enables very high levels of repellence to water and other liquids. The introduction of nanoscale reinforcement has also been demonstrated to improve abrasion resistance [Vu, 2006]. Therefore, the ability to design the coating from nano-level might offer the solution to bridge the gap between highly repellent performance and mechanical durability, leading to the target family of nanostructured coatings which are both durable and highly repellent (Vu C., 2005).

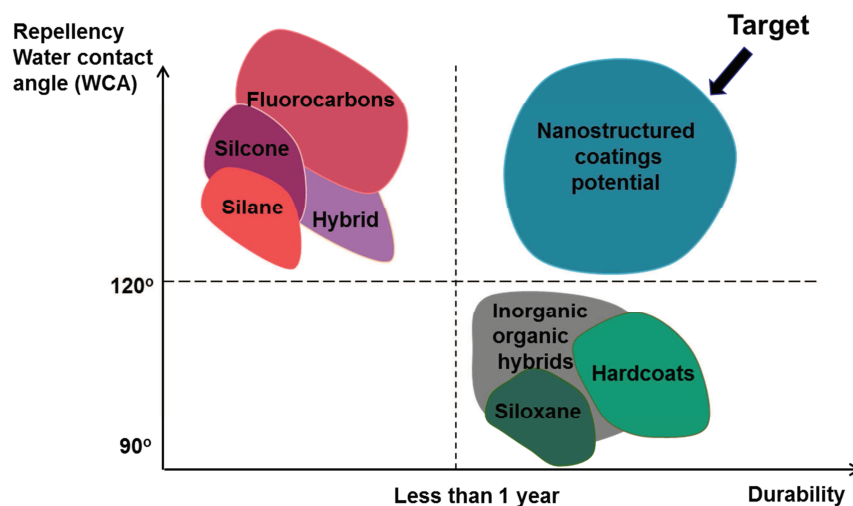


Figure 2.10 State of the art – industrial need for nanostructured coatings

One objective for TWI is to bridge this gap in the state-of-the-art. The approach to achieve this is to develop new functional building blocks that can be incorporated into current class-leading formulations to tailor performance of the whole coating system. A series of chemical assembly methods that can be used to fabricate these building blocks are currently under development. The core of this emerging technology is based on sol-gel technique and therefore, silica is the material that creates the skeleton of these new coatings. There are two elements in the approach undertaken by TWI, namely fabrication of silsesquioxanes and functionalization of silica nanoparticles.

### 2.5.1 Silsesquioxanes

One of the two methodologies proposed in this research is based on the part of Vitolane® technology, an innovation developed by TWI which allows low cost manufacturing of inorganic-organic hybrid materials such as silsesquioxanes (SSQs), which are picometer scale building blocks, oligomers (Taylor A. B. L., 2011).

Silsesquioxanes are defined as materials with the composition  $\text{RSiO}_{1.5}$ , consisting of ceramic backbone (silica-oxygen) surrounded by hydrogen atoms and organic groups (including epoxy, acrylate, vinyl, fluorocarbon etc...) (Figure 2.11).

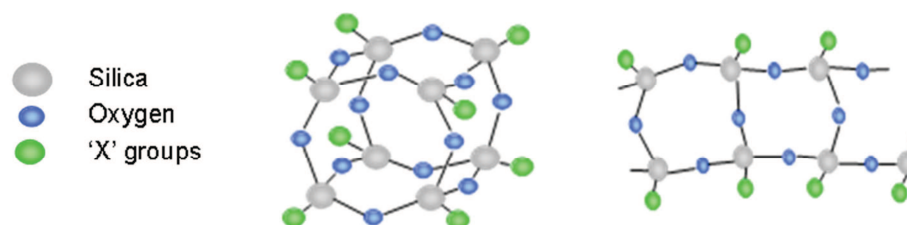


Figure 2.11 Structural variants of silsesquioxanes: cage and ladder formation (Taylor A. B. L., 2011)

Silsesquioxanes (SSQs) building blocks were first reported in 1946 (Scott D.W., 1946). Since then, there was a lot of work done in this area (Voronkov M.G., 1982) (Lichtenhan J.D.). Nevertheless, their use has been limited due to the high cost, resulting from complex route of preparation (Schottner G., 2001). Vitolane® technology offers a new, less complicated and cost-effective, two steps hydrolysis/condensation reaction followed by subsequent drying of the resulting composition. At the beginning, precursor materials (alkoxysilanes) are hydrolysed into cyclic siloxane structures and partially condensed, to form inorganic oligomers that are core building blocks for the final organosilsesquioxanes molecules. The second step involves quenching the inorganic oligomers by addition of large amount of water, which causes further condensation of the structures. Time and concentration are the key parameters in the determining the achieved degree of condensation. Finally, when the composition is dried, it can be added to traditional coatings, additives and bulk polymers, in order to enhance material properties such as mechanical, chemical resistance and barrier properties. The versatility of the Vitolane® process allows siloxane oligomers to be compatibilised with the resin matrix, which enables high loading levels without segregation or aggregation. Besides that, due to the nature of SSQs, certain properties can be tailored by selecting appropriate functionalities (organic groups) to meet specific demands of particular applications (Gnanasekaran D., 2009).

Vitolane® approach presents the possibility of achieving multi-functionality, where hydrophobicity and durability can be introduced in the one coating. Initial work focussed on the improvement of the abrasion resistance of the easy clean coating was done. In this preliminary study, the influence of the silsesquioxanes on coating durability was evaluated by assessing the retention of anti-soiling properties under abrasion conditions. TWI coating, containing silsesquioxanes was compared with the commercially available easy clean coatings (Wojdyla A., 2014). Linear abrasion testing of the coated substrates were undertaken (100, 250 and 500 rubs with 0000 wool wire). Performance was assessed by measuring the water contact

angle (WCA). In the pristine state all coatings showed good repellence considerable changes in the water contact angle were observed after linear abrasion test. The number of rubs required to achieve “breakthrough point” were compared (Figure 2.12). “Breakthrough point” indicates the point, at which the measured surface energy is the same as the substrate material indicating that the coating was no longer present. The data shows significantly enhanced abrasion resistance associated with incorporation of SSQs into organic matrix.

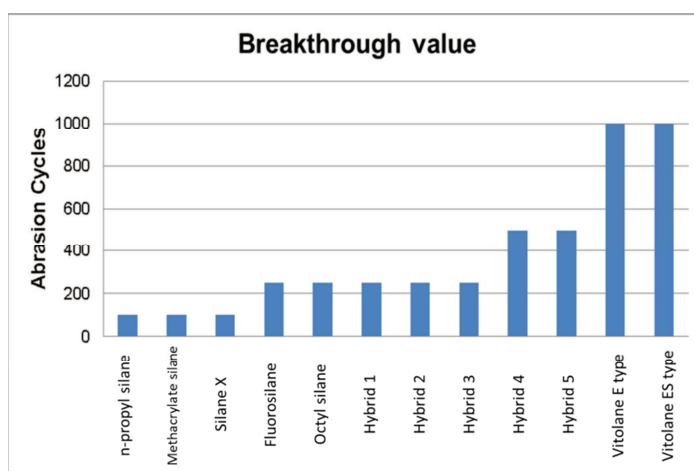


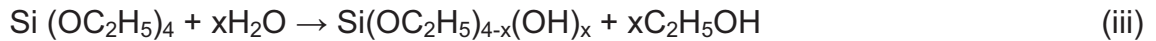
Figure 2.12 Comparison of “breakthrough value”

Moreover, the data highlighted in Figure 2.12 do not present full mechanical capabilities of TWI’s coating. Abrasion testing was stopped after 1000 cycles nonetheless, the coating containing SSQs molecules has not been removed from the substrate indicating that it can survive harsher operating conditions.

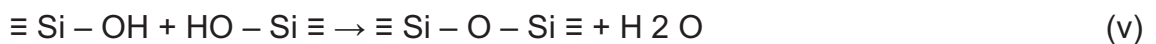
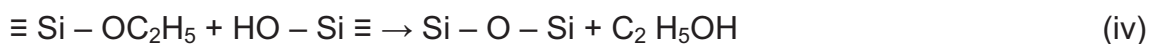
### 2.5.2 Silica nanoparticles

The second TWI self-assembly approach is also a part of the Vitolane® technology family and is based on the functionalization of silica nanoparticles. Silica nanoparticles (SiNPs) are used in coatings in different forms: colloidal, fumed (pyrogenic) and Stöber silica. Fumed silica is formed by reaction of water vapour produced by a hydrogen-oxygen flame with silicon tetrachloride to produce small, essentially spherical primary particles which subsequently collide to form rigid, covalently bound aggregates (Boldridge D., 2010) (Iler R.K., 1979). Colloidal silica (silica sol) is most often produced in a multi-step process in which the sodium ions are removed by solvent evaporation mineral acid (Lim H.M., 2010). The method of fabrication of some type of silica was introduced by Stöber, and it’s based on the hydrolysis and condensation of silica precursor (such as TEOS) in alcoholic solutions using ammonia (Stöber W., 1968). The hydrolysis and condensation

reactions provide precursor species and the necessary supersaturation for the formation of nanoparticles. In the first step, the ethoxy group of TEOS reacts with the water to form the intermediate  $[\text{Si}(\text{OC}_2\text{H}_5)_{4-x}(\text{OH})_x]$  with hydroxyl group substituting ethoxy groups (iii) (Brinker C.J., 1990):



Condensation reaction occurs after the hydrolysis is finished. Formation of Si-O-Si bridges can be initiated by reaction of the hydroxyl group of an intermediate species [e.g.  $\text{Si}(\text{OC}_2\text{H}_5)_{4-x}(\text{OH})_x$ ] with the ethoxy group of other TEOS (alcohol condensation) (iv) or by reaction of the hydroxyl group of an intermediate species [e.g.  $\text{Si}(\text{OC}_2\text{H}_5)_{4-x}(\text{OH})_x$ ] with another intermediate product (water condensation) (v):



Using the Stöber method, the particle size distribution is relatively narrow and can be easily tailored to different diameters. In general, the size of colloidal silica Stöber spheres range from 20nm to 1µm. Various studies were published to show how the type of precursor and reaction conditions can affect the final size and distribution of silica spheres (Blaaderen A., 1992) (Bogush G.H., 1988). Moreover, the ability to disperse silica nanoparticles in liquid phase (alcohol) makes these silica Stöber spheres easily processable in terms of subsequent treatment.

Nanoparticles are often functionalized, in order to prevent the flocculation and phase separation of Stöber spheres in solution. The behaviour of functionalized nanoparticles depends strongly on the attached groups and forces created between these nanoparticles in solution (Lane J. M., 2009). At the atomic scale, the forces observed between particles include: electrostatic, van der Waals, torsion forces. It has been found that exactly the same forces can be assigned for hydrodynamic drag, lubrication and depletion forces at the nanoscale (Min J., 2008). Therefore, the ability to functionalise silica nanoparticles offers the opportunity to tailor and tune the attributes they display, such as cross-linking, repellence, reaction rate and environmental response (Durand G.G., 2014). In the case of easy clean surfaces, the main role of functionalization is to provide

compatibility with the organic resin (allowing effective cross-linking) and at the same time, to keep highly hydrophobic character.

## **2.6 Summary**

This chapter introduces the requirements that need to be fulfilled in order to develop easy clean coatings. It was found out that conventional highly repellent surfaces are not capable of providing anti-wetting performance for extended periods of time. In general, practical use of such coatings is hampered by the poor mechanical stability of microscopic surface topography. Current approaches to test the durability of such surfaces were presented and it was found out that there is still a big gap in evaluating easy clean coatings. A lack of understanding of wear mechanisms under specified conditions and the lack of standardised test methodologies that enable comparison between different classes of highly repellent coatings hinders the progress. A more specific set of assessment criteria is needed, and there is a need to answer the question why existing methods fail or are limited. At the end of this chapter, new approaches of reinforcing easy clean materials were presented. Nevertheless, the area of using novel inorganic building blocks in order to enhance the properties of coating system is still in a very beginning stage and a lot of work needs to be done. Therefore, the purpose of this study is twofold. The aim is to develop new assessment criteria for durability assessment of easy clean surfaces. The second purpose of this study is to extend the existing knowledge about new materials containing inorganic building blocks with organic functionalities.

### **3 NEW ASSESSMENT CRITERIA FOR DURABILITY EVALUATION OF HIGHLY REPELLENT SURFACES**

Selecting the correct coating system for protection in specific industrial applications requires a variety of factors to be taken under consideration to ensure that the most economical and best technical solutions are achieved. This chapter introduces new assessment criteria for durability evaluation of easy clean coatings. The presented methodology helps to classify coatings not only in terms of their repellent characteristics, but also in terms of mechanical resilience and ability to retain their functional performance. The aim of this study is to provide a global plot of performance indices that enables meaningful comparison of different types of coatings in order to help select the right coating for the right application particularly those that are not currently served by the established chemistries.

#### **3.1 Introduction – coating selection criteria**

Choosing an easy clean coating for a specific application, there will be undoubtedly a primary motivation and reason behind the selection. Mechanical resistance of material is very often the crucial parameter that needs to be taken under consideration prior the application. Despite the importance of surface durability, there are many other factors that influence final selection of coating, such as degree of repellency, required appearance, multifunctionality, product cost, processing conditions, health and safety regulations (REACH) etc. In general, materials selection can be divided into two broad categories, namely coatings processability and coatings performance. Table 3.1 presents the most important identifiable parameters taken under consideration while selecting easy clean coatings.

Table 3.1 *Easy clean coatings – proposed selection criteria*

Processability	Performance
Solvent content	Repellency
Deposition method	
Processing temperature	Abrasion resistance
Rate of cure	Erosion resistance
Degree of cure	Scratch resistance, hardness
Quality (i.e. fish eyes, defects)	Resistance to chemical attack
Inorganic content	Retention rate
Viscosity	Gloss, haze, DOI
Thickness	Transparency
Adhesion	Roughness

The processability of coating is a measure of its ability to be worked and transformed into final product. Processability of material has some impact on the final performance of the coating; nonetheless these kinds of properties will not be discussed in this thesis. The assessment criteria presented below focus on the key operational and/or performance properties. With the respect to easy clean coatings, their ability to repel liquids is one of the most significant parameters that should be taken under consideration. In this case the optimisation and retention of their functional properties is the key to the development herein. All evaluation techniques for repellency concentrate on measurement of repellence to provide comparative data, or some assessment of mechanical performance (pencil hardness or scratch resistance). None have yet coupled assessment of repellence with an abrasion or erosion environment in a manner that it applicable to both thick fluoropolymer coatings and self-assembled monolayers and all the other possible approaches to coating design/synthesis. Furthermore, coating selection should be based on its ability to resist damage. Material durability is a very broad and multi-disciplined technology and there are many variables that affect the resilience of material, including:

- Chemistry and physics of substrate
- Chemistry and physics of coating
- Adhesion between coating and substrate
- Application and service environment

Therefore, before choosing a successful durability test that will allow on a combined assessment of all the key functional characteristics, few aspects need to be deliberated:

- The test must be suitable for substrate-coating system
- The test should replicate failure mechanisms observed in the real-world applications
- The test should also allow a detailed understanding of the structure-property behaviours of different coatings
- Where possible, accelerated life testing should be performed

On the other side, durability of coating system is not only its ability to resist mechanical, chemical and physical damage, but can be also referred to its ability to retain its main functional performance. Therefore, when measuring durability of easy clean surfaces, two types of variables need to be evaluated simultaneously, namely material resistance under some specified conditions and its ability to retain initial wetting characteristics (retention rate) under the same specified conditions.

Repellency and durability might be the most important parameters of easy clean surfaces, yet there are also other criteria that influence final selection of coatings. For some applications, visual appearance of the material plays an important role in coating selection routine (Karlović I., 2010). In general, aesthetic classification of material is dependent upon two variables, its colour and texture.

Chapter 2 provides some current approaches undertaken to test and classify easy clean coatings. With regard to recent advances in evaluating durability of highly repellent surfaces, few conclusions can be drawn:

- There is a lack of understanding wear mechanisms (too much attention is placed on initial functional performance and less on functional performance against the damage and time)
- Lack of systematic approach for assessing durability of advanced coatings
- Lack of robust generalized failure criteria of highly repellent coatings (What defines durability? What defines failure?)
- Current durability tests were designed to evaluate specific highly repellent surfaces, they do not allow comparing different families of easy clean materials

- There is an emerging need for standard protocol/procedure that will enable different easy clean coatings to be compared and classified (Malavasi I., 2014)

As a response to these needs, this chapter introduces novel approaches for assessing applicability of advances coatings. Focus is mainly laid on three parameters namely, initial wettability, ability to resist damage (direct durability) and ability to retain main functional property (indirect durability).

### **3.2 Experimental – methods**

The new approach to evaluate materials, involves characterizing material repellency (water), lipophobicity (oils repellency) visual appearance, mechanical properties (abrasive wear), retention of initial repellency and chemical resistance. Direct durability measurements that referred to abrasive wear were conducted such as to provide a wide range of abrasive conditions with the respect to different load and contact surface.

#### **Repellence and lipophobic performance**

Drop shape analyser DSA100 from KRÜSS GmbH was used to study the degree of wettability by polar and nonpolar liquids. Sessile drop static contact angles of deionised water and diiodomethane (purchased from Sigma-Aldrich) were measured in order to provide information about initial repellency characteristic of coatings and to provide an assessment of the surface energy of the coatings. Indirect durability evaluation (assessing retention ratio of initial contact angle) was carried out with the respect to deionised water contact angle only. Specification of water and diiodomethane contact angle measurements will be further provided in Chapter 6 and 7.

#### **Visual appearance**

Gloss and haze measurements were undertaken using a Novo-Gloss IQ Goniometer from Rhopoint Instruments, according to ASTM D523 – 08 (for the gloss) and ASTM E430 (for the haze) (ASTM D523-08, 2008) (ASTM E430-11, 2011) . In general, gloss is measured by shining a known amount of light at a surface and quantifying the reflectance. Depending of the type and roughness level of surface, three different angles of incidence were used to measure the shininess of material. Table 3.2 provides the commonly used principal of gloss measurement geometry selection. Schematic gloss examination is illustrated in Figure 3.1.

Table 3.2 General principle of gloss measurements

Gloss Range with 60° Gloss Meter	Measure With:
Gloss between 10 and 70 GU	60°
>70 GU	20°
<10 GU	85°

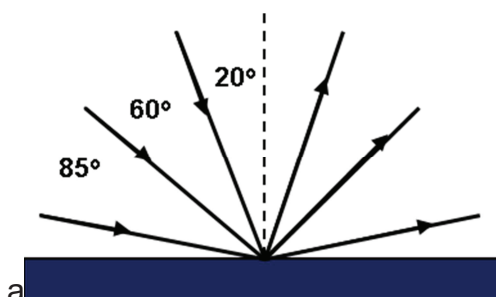


Figure 3.1 Gloss measurement geometries used in standard evaluation of surface visual appearance

Nevertheless, in order to have clear comparison between different types of surfaces, it was decided to measure gloss and haze only at the angle of 20°.

### Durability – abrasive wear

Abrasive wear was studied with Taber Rotary Platform Abrasion Tester (Model 5135, Figure 3.2). Auxiliary weights of 500/1000 g on each CS10/H18 wheel and a rotation rate of 60 rpm were used. CS-10 calibrase resilient wheels (composed of rubber and aluminium oxide particles) offer a mild - medium abrading action like that of normal handling, cleaning, and polishing, whereas H18 calibrade non-resilient wheels (composed of vitrified clay and silicon carbide particles) provide a medium coarse abrasive action.



Figure 3.2 Taber rotary platform abrasion tester (pic. Source Falex Tribology)

Taber tests involve mounting a test specimen approximately 100 mm across to a turntable platform that rotates horizontally at a fixed speed. Two Taber abrasive wheels, which are applied at a specific pressure, are lowered onto the specimen surface. The abrasive wear action is produced by contact of the coated sample against the sliding rotation of the two wheels. As the platform starts to rotate, the wheels are driven by the sample in opposite directions. While one abrading wheel rubs the specimen outward toward the periphery and the other inward toward the centre, a connected vacuum system removes loose debris produced during abrasion. The wheels traverse a complete circle on the specimen surface, revealing abrasion resistance at all angles. The resulting wear pattern forms a closed circle on the test specimen (Figure 3.3).

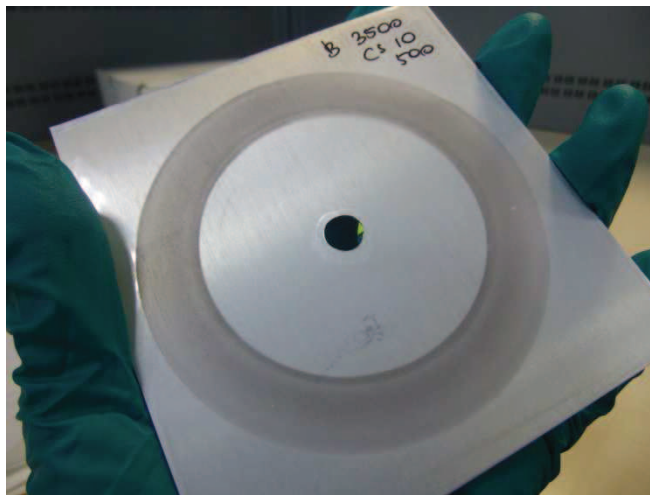


Figure 3.3 Wear pattern resulting from rotary abrasion Taber test

The number of abrasion cycles required to reach final durability point were studied. Maximum of 3500 cycles were studied, which refers to almost 1 h of constant abrasion. Some procedure was also applied wheels re-facing. The wheels were re-faced using S-11 disc in the following situations:

- Prior to assessment of new test specimen
- Every 50 cycles, if test specimen was abraded with H18 wheels
- Every 500 cycles, if test specimen was abraded with CH10 wheels and 50 cycles for H18 wheels.

Surface wettability was studied as a function of surface damage done by abrasion. The following steps were undertaken in abrasion durability evaluation. Prior to the mechanical assessment a control sample of each coating per condition type (further defined as condition 1, 2, 3 and 4) was subjected to abrasion in order to provide a preliminary estimate of wear behaviour. Based on the obtained results the coatings

were categorized into groups. Figure 3.4 provides a schematic for the testing routine undertaken to assess the mechanical durability evaluation of the candidate coatings. For example, if the control coating sample starts to fail after 2000 cycles, water contact angle of this coating will be measured after each 500 cycles.

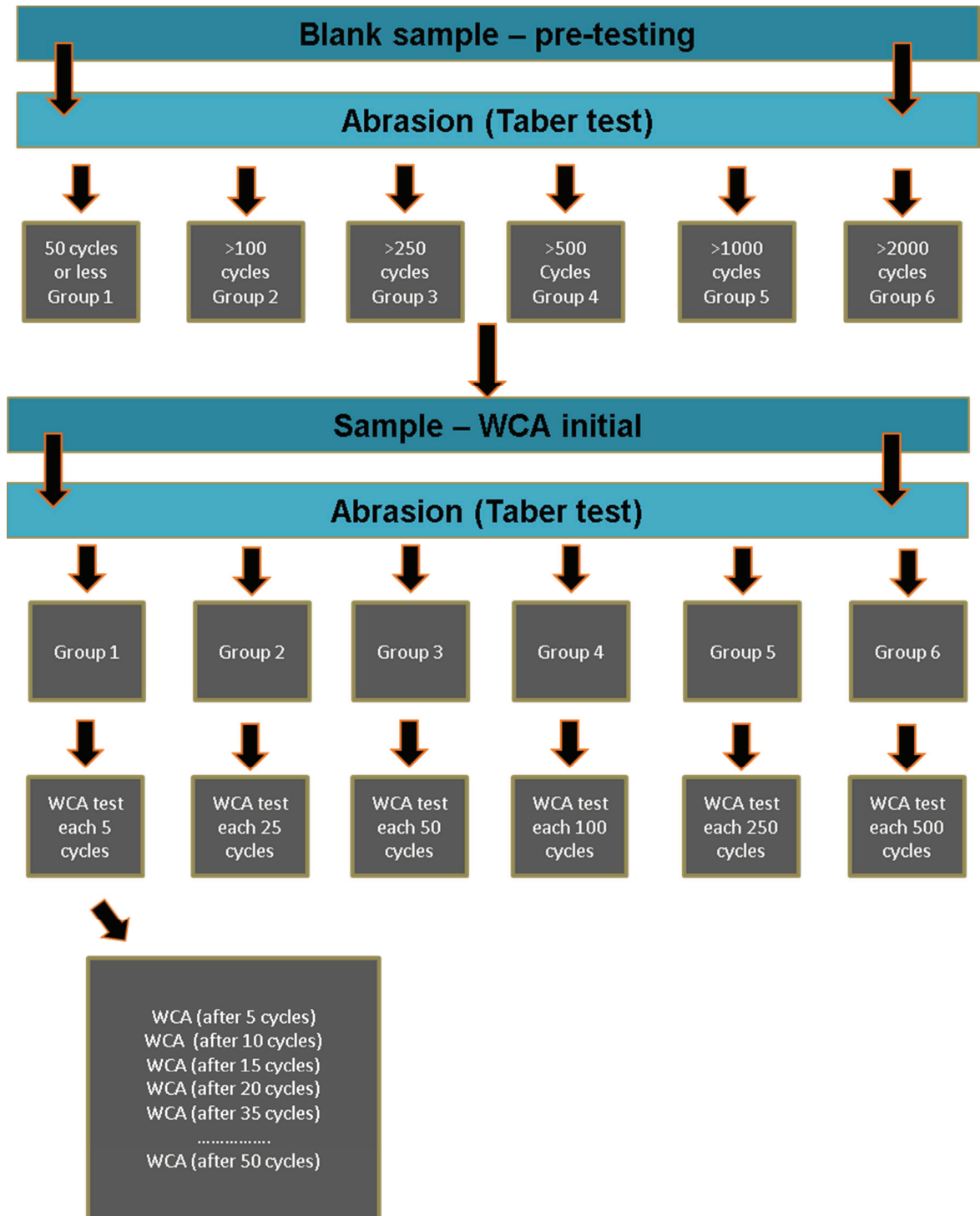


Figure 3.4 Novel approach to test durability of highly repellent surfaces – abrasion and water contact angle testing routine

Coatings were subjected to abrasive damage, until failure of the surface was captured. Final durability point of these coatings was defined and assessed. Final

durability point classification criteria (for coating abrasion group 3) are represented in Figure 3.5. For example, WCA of coating that belongs to group 3 will be measured in 50 cycle intervals and measurements will be carried until failure occurs. The final durability point is therefore the WCA value, which was measured at penultimate interval.

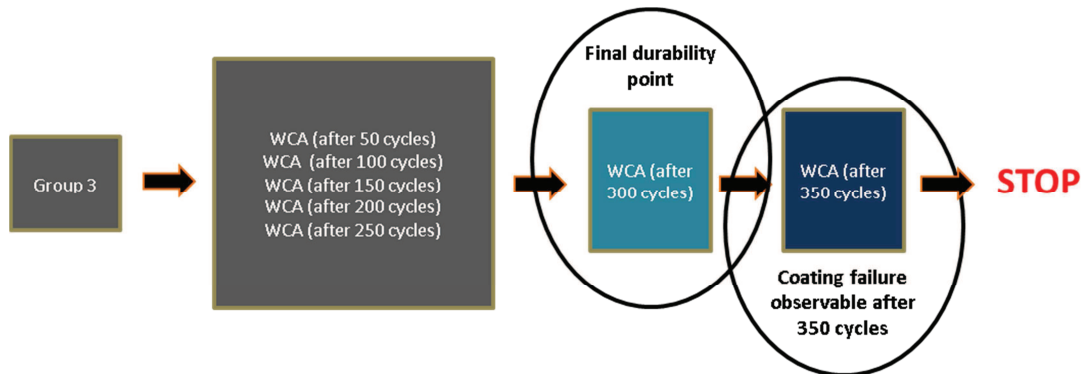


Figure 3.5 Novel approach to test durability of highly repellent surfaces – final durability point definition

Abrasion was performed in four different conditions that increase in aggressiveness in following order (Figure 3.6):

- CS10 wheels, 500g load (hereinafter referred to as cond. 1), CS10 wheels, 1000g load (cond. 2), H18 wheels, 500g load (cond. 3), H18 wheels, 1000g load (cond. 4)

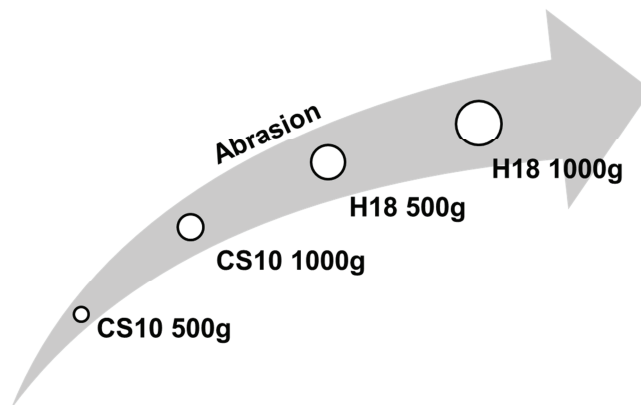


Figure 3.6 Abrasion conditions (types of abrasive wheels and load) applied in rotary Taber test

### Durability – adhesion

Adhesive wear in pristine state was evaluated with PosiTest from DeFelsko with accordance to ASTM D4541 (ASTM D4541-09e1, 2011). A metal dolly of 20 mm diameter was placed on the test area and stuck to the surface using LOCTITE 4061 (ethyl cyanoacrylate) adhesive. After the adhesive was cured (1h drying in lab conditions), a dolly was attached to the pull-off equipment, hydraulic pressure was applied (1 MPa) and increased gradually until the dolly was completely pulled-off

from the surface. The test specification of adhesion testing is provided in detail in Chapter 6.

Due to the fact that adhesion influences chemical durability of the coating, chemical stability was evaluated after the surface was subjected to some specified ageing conditions. Three types of chemicals were used as ageing agents and testing was conducted in the similar manner as presented in ASTM D6943 - 15. All tests were conducted at room temperature. Stability in salt water (4.95% sodium chloride from Sigma-Aldrich in deionised water), IMS (industrial methylated spirits alcohol from ReAgent Chemical) and acidic environment (1% of H<sub>2</sub>SO<sub>4</sub> from Sigma-Aldrich) were studied. Samples were immersed in the described solutions in room temperature for one week (it has been decided that one week of immersion should be enough to test the chemical resistance in selected chemical agents). After the designated time, visual surface failure analysis (ability to maintain film integrity after immersion) and changes in water contact angle were examined.

### **3.3 Classification criteria**

A spider diagram approach was selected as the way to represent in a single graph the behaviour of the coatings against a range of different metrics. The spider diagram is a plot that consists of a sequence of equiangular spokes, called radii, with each spoke representing one of the variables (Chambers J., 1983). The presentation of performance characteristics in the form of spider or radar diagrams has been adopted by many areas of research and industry (de Waal A.A., 2015) (Galindo P.V., 2015) (Daniel C., 2008). The proposed spider diagram approach allows considerable amounts of experimental data to be presented within a single graphical representation. Coating properties that were taken under consideration include: initial wettability (WCA and DCA), gloss and haze (initial values), abrasion resilience (number of cycles required to achieve final durability point in four different conditions), retention of initial water repellency (retention ratio RR under four different abrasive conditions), adhesion strength (in pristine conditions) and chemical durability (retention ratio and quality of surface under three different conditions). Figure 3.7 represents scheme of spider diagram proposed in this study. Further explanation of metrics and axes from spider diagram can be found in Table 3.3.

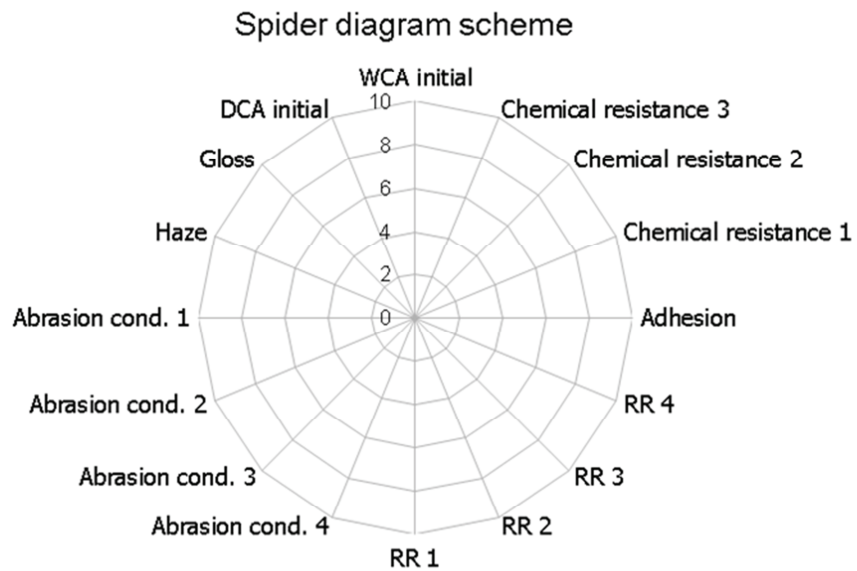


*Figure 3.7 Spider diagram scheme proposed for evaluation of highly repellent surfaces*

Table 3.3 Summary of the properties measured, measurement techniques and accompanying standard procedures

Property	Technique	Standard
Water contact angle (WCA) initial	Drop shape analyser	ASTM D7490
Diiodomethane contact angle (DCA) initial	Drop shape analyser	ASTM D7490
Gloss initial	Glossmeter	ASTM D523
Haze initial	Glossmeter	ASTM E430
Abrasion (cond. 1)	Taber abrader, CS10 wheels/500 g	ASTM D4060
Abrasion (cond. 2)	Taber abrader, CS10 wheels/1000 g	ASTM D4060
Abrasion (cond. 3)	Taber abrader, H18 wheels/500 g	ASTM D4060
Abrasion (cond. 4)	Taber abrader, H18 wheels/1000 g	ASTM D4060
RR (cond. 1)	Drop shape analyser	ASTM D7490
RR (cond. 2)	Drop shape analyser	ASTM D7490
RR (cond. 3)	Drop shape analyser	ASTM D7490
RR (cond. 4)	Drop shape analyser	ASTM D7490
Adhesion strength	Pull-off tester	ASTM D4541
Chemical resistance 1	1 week immersion in 1% $H_2SO_4$	N/A
Chemical resistance 2	1 week immersion in IMS	N/A
Chemical resistance 3	1 week immersion in 4.95% NaCl	N/A

Each branch from diagram was divided into 10 points, so each single property is so scaled that its highest numerical value does not exceed 10. For each property, lower and upper limit were established and implemented. With regard to initial values of WCA, surface that has 90 degrees of WCA (minimum requirements that have to be fulfilled in order to achieve hydrophobicity) was assigned a value of 1 point. On the other hand, surface that displays extraordinary non-wetting properties (150 degrees

and above) was classified as the one with maximum score (10) in this category. With the respect to DCA, pointing system was based on the whole scale of wettability, from superoleophilic (1 point) to superoleophobic surfaces (10 points). Table 3.4 provides classification criteria for initial wettability of highly repellent surfaces.

*Table 3.4 WCA and DCA (initial values) classification criteria for spider diagram*

Point	WCA initial [°]	DCA initial [°]
1	90	10 and less
2	95	30
3	100	50
4	105	70
5	110	90
6	115	110
7	120	120
8	130	130
9	140	140
10	150 and more	150 and more

Visual appearance of coatings was categorized based on gloss and haze values. Gloss describes the perception of a surface appearing ‘shiny’ when light is reflected from it and therefore, surfaces with the higher than 200 GU were assigned 10 points . On the contrary, gloss below 20 GU indicates that surface reflection is poor and classify for 1 point in this category. Haze describes the milky halo or bloom adjacent to the reflected image. When measuring haze values, higher numbers indicate a lower quality surface, while high gloss with zero haze has a deep reflection image with high contrast (10 points). Table 3.5 explains surface categorization with the respect to its visual appearance.

*Table 3.5 Gloss and haze (prisitne state) classification criteria for spider diagram*

Point	Gloss at 20° [GU]	Haze at 20° [HU]
1	20 and less	50 and more
2	50	45
3	70	40
4	90	35
5	110	30
6	130	25
7	150	20
8	170	15
9	190	10
10	200 and more	5 and less

Abrasion pointing scale was divided with respect to type of abrasive material. CS10 resilient wheels offer a mild-medium abrading action likes that of normal handling, cleaning, and polishing and therefore classification criteria for this type of abrasive agent needs to consider high values for upper limit point. Therefore an upper limit

was established for 3500 cycles. The situation will be different when comes to abrasion with H18 wheels. This type of non-resilient wheel provides a medium coarse abrasive action that is able to damage the surface very quickly. The same classification criteria apply for a different loading level. Explanation of these categories can be found in Table 3.6.

Table 3.6 Abrasion classification criteria for spider diagram

Point	CS10 wheels (no. of cycles) 500/1000g load	H18 wheels (no. of cycles) 500/1000g load
1	50 and less	5 and less
2	100	10
3	250	25
4	500	50
5	1000	100
6	1500	150
7	2000	200
8	2500	300
9	3000	400
10	3500 and more	500 and more

Retention ratio is another important parameter associated with durability of highly repellent surfaces. Even if the coating is durable and can withstand many abrasion cycles, it doesn't mean that its wettability characteristics won't change over the time. It was proposed that when coating doesn't change its repellent properties (RR=1) over its lifetime (until final durability point) it is assigned a value of 10 points. Every deviation from initial water contact angle, either an increase or decrease, is not desirable and therefore, the surface that changes its repellency over time should be classified as a poorer performing material.

Adhesion was evaluated in pristine state. It was proposed to classify adhesion as high quality (10 points) when the bonding strength between coating and substrate exceed more than 4 MPa (the value 4 MPa was selected due to the fact that none of the evaluated coatings have reached this level of adhesion strength). Table 3.7 provides classification criteria with the respect to retention rate and initial adhesion strength.

Table 3.7 Retention ratio and adhesion classification criteria for spider diagram

Point	Retention ratio	Adhesion [MPa]
1	$\Delta \pm 80\%$ and more	0.1 and less
2	$\Delta \pm 70\%$	0.5
3	$\Delta \pm 60\%$	1
4	$\Delta \pm 50\%$	1.5
5	$\Delta \pm 40\%$	2
6	$\Delta \pm 30\%$	2.5
7	$\Delta \pm 20\%$	3
8	$\Delta \pm 10\%$	3.5
9	$\Delta \pm 5\%$	3.75
10	1	4 and more

Chemical durability presents the last category of coating evaluation and it's strongly dependent upon initial adhesive strength between coating and substrate. Therefore, in this case classification criteria have to be dependent upon two factors. On the one side, retention ratio of initial water contact angle needs to be evaluated after chemical testing was completed. On the other side, resistance of coatings to separation from substrates should be taken under consideration as well. Retention ratio was classified in the same manner as was done for abrasion testing. With regard to surface quality after chemical testing, it was decided to subtract 1 point for every 20% of affected area. For example, if water contact angle of coating retain 70% from its original value after testing were performed, this coating scores 6 points for chemical resistance in terms of the retention rate. Nevertheless, if the same coating starts to detach from the substrate in more than 20%, 2 points have to be subtracted the scoring, which gives in total 4 points in this testing category.

Table 3.8 Chemical resistance classification (with the respect to retention rate) criteria for spider diagram

Point	Chemical resistance (Retention ratio)
1	$\Delta \pm 80\%$ and more
2	$\Delta \pm 70\%$
3	$\Delta \pm 60\%$
4	$\Delta \pm 50\%$
5	$\Delta \pm 40\%$
6	$\Delta \pm 30\%$
7	$\Delta \pm 20\%$
8	$\Delta \pm 10\%$
9	$\Delta \pm 5\%$
10	1

Table 3.9 Chemical resistance classification (adhesive failure analysis) criteria for spider diagram (based on the idea taken from ASTM D3359)

Classification (points)	Description
0	The edges of the sample are completely smooth; coating is not detached from the surface.
-1	Detachment of the coating at the edges of the sample, the area affected is not greater than 20%
-2	The coating has flaked along the edges, the area affected reaches 40%
-3	The area affected is greater than 40% but do exceed more than 60%
-4	The area affected is greater than 60% but do not exceed more than 80%
-5	The coating is detached from the surface in more than 80%

The spider diagram is to classify materials with respect to 6 categories. Each quarter of this graph represents specified group of coating characteristics (Figure

3.8). First quarter refers to initial characteristics of material and this quarter can be further divided into three separate subgroups. Repellency in pristine state with the respect to WCA values is important group of properties that need to be taken under consideration when selecting easy clean coatings and further referred to as segment 1a of the spider diagram. On the other hand, the initial lipophobic character of the surface is a valuable easy clean surface parameter and should be included as a part of coatings classification criteria (herein referred to as segment 1b). Gloss and haze provides information regarding coating appearance, which might be an important selection criteria for some applications and therefore aesthetic properties are represented by segment 1c. Quarter number 2 collates the mechanical durability of the coatings material under the specified abrasion conditions. The third quarter represents durability of the coating in terms of retaining its initial wetting performance under specified abrasion conditions (indirect durability). The fourth and final quarter refers to another type of failure, strongly dependent upon adhesion strength between coating and substrate (adhesive bonding strength in pristine state and chemical durability in three specified conditions).

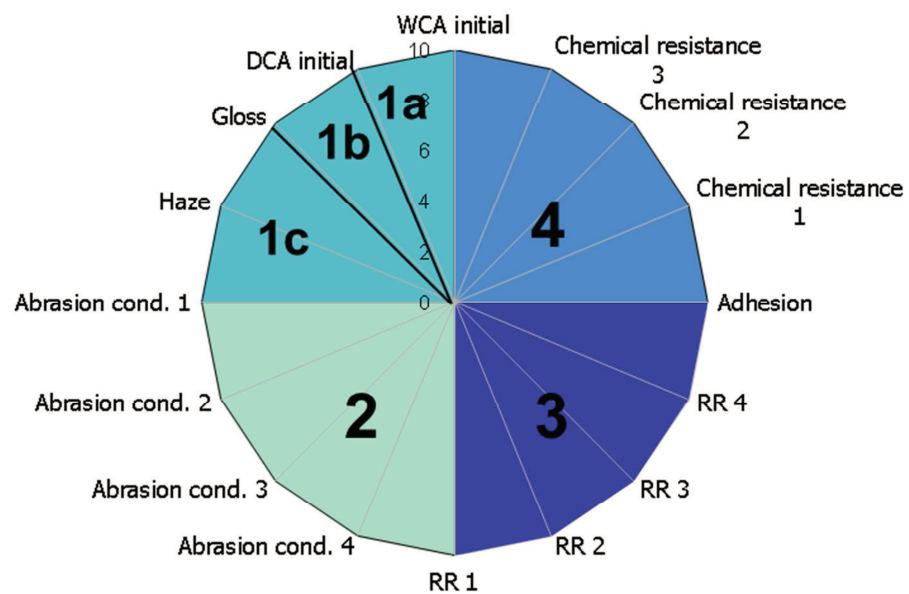


Figure 3.8 Coating classification criteria by materials category

The weighted property assessment was used to compare candidate coatings based on performance requirements. A weighted property value was obtained by dividing the sum of points from each part of spider diagram (1a, 1b, 2, 3 and 4) scored by particular coating by a maximum number of points that can be scored in this specific area of spider diagram. The individual weighted property values are specific for each coating and therefore, they can be used to calculate a

performance index value ( $PI_{Ci}$ ) for each group of properties represented by the segments in the spider diagram (Eq. 3.1).

$$PI_{Ci} = \frac{PG_{Ci}}{MPG_{Ci}} \quad (3.1)$$

The symbol PG corresponds to number of points scored by specific coating (c) in specific group of properties ( $i=1a, 1b, 1c, 2, 3$  or 4 part of spider diagram). MPG is the maximum value that can be scored in this specified group of properties (i.e. MPG for 1a part of spider diagram will be 10, but MPG for 2 part of spider diagram will be 40).

$PG_{1a}$  = Repellency in pristine state

$PG_{1b}$  = Lipophobic characteristics in pristine state

$PG_{1c}$  = Visual appearance in pristine state

$PG_2$  = Ability to resist abrasion (in four specified abrasive conditions)

$PG_3$  = Ability to retain wetting characteristics after abrasion exposure

$PG_4$  = Adhesion performance (in pristine state) combined with chemical durability (chemical resistance in three specified conditions)

Each performance index ( $PI_{Ci}$ ) can be summed and used to establish general performance index of specified coating ( $PI_C$ ) (eq.3.2).

$$PI_C = \sum_{i=1}^n PI_{Ci} \quad (3.2)$$

The performance index shows the technical capability of a coating without regard to its processability. Alternate spider diagrams focussed on processability and encompassing factors such as product cost, solvent content, viscosity, curing time etc. could be produced. Another approach would be to combine the processing and performance characteristics in a single spider diagram. However for this work the focus was only on functional performance.

### 3.4 Plot of performance indices

The wetting characteristics and durability are the key features of easy clean coating systems. The null hypothesis presented in chapter 3 states that there is an inverse relation between repellency and durability. It is commonly believed that a coating system that displays superlative repellent characteristics doesn't have the ability to be durable. Such statement is based on observation that the high nano and micro-scale roughness levels required to enable superhydrophobic behaviour is achieved by having fragile surface structures which are easily damaged leading to a reduction

in repellence. Conversely, lower surface roughness leads to lower values of water contact angles but increased durability. This is consistent with empirical findings but has not yet been proven due to the lack of a suitable test methodology.

The major obstacle that hampered explanation of this hypothesis was a clear definition of coating durability. Since the hypothesis can be only proven by measuring the observed event, durability has to be defined and measurable. Therefore, I propose that performance indexes are used to quantify the variables.

Formulated hypothesis is based on two variables namely initial repellency and durability. There are two questions that should be answered before this hypothesis can be confirmed or rejected. First of all, there is a need to clearly defined what influences durability and following this line of thought, which performance indexes can be used to express coatings durability. The same question applies in the case of wettability performance.

With regard to durability, performance index of abrasion resistance that corresponds to second quarter of spider diagram was proposed to be expressed as measurable result. In case of wettability, two observed events can be connected. On one side, in many scientific works wetting properties of the coating are represented by the value of water contact angle in the pristine state. Nevertheless, it should be considered that these properties will change over time and due to the influence from environment. The repellence ratio unit illustrates such changes in the coating system. Therefore, it is proposed that wettability variable corresponds to average of two performance indexes namely, initial repellency performance index (part 1a of spider diagram) and retention ratio performance index (part 3 of spider diagram).

It is important to have an appropriate plot of performance indices for measuring how well each coating system can meet two main requirements namely, repellency and durability. Figure 3.9 illustrates proposed model of plot of performance indices. That was based on three performance indices (Eq.3.3)

$$\frac{\text{Repellency}}{\text{Durability}} = \frac{\frac{PI_{1a} + PI_3}{2}}{PI_2} \quad (3.3)$$

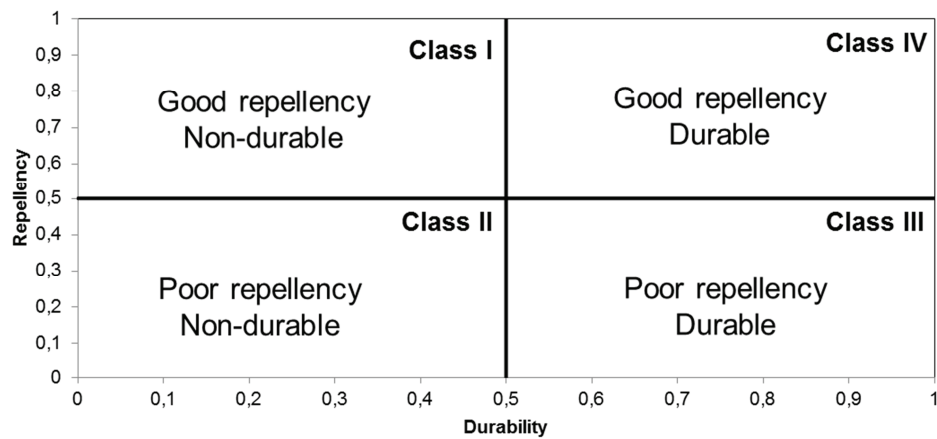


Figure 3.9 Plot of performance indices of easy clean coatings – general principal

The proposed model of plot of performance indices helps to cluster materials into four general categories. Class I and III reflect material behavioural patterns that were presented in null hypothesis that corresponds to inverse relationship between repellency and durability. Class II represents the materials that have not fulfilled the required performance in terms of wettability or mechanical robustness. Class IV illustrates the most desired materials, where highly repellent coatings can be associated with long operational capability. Conventional coatings are not expected to go beyond the behavioural models represented by class I and III. In order to improve performance of easy clean surfaces (develop materials that can be assigned as class IV), it is necessary to find a new way of designing coatings. The focus should be mainly laid on designing roughness profile, due to the fact that surface texture is not only responsible for boosting the value of water contact angle, but it also determines survivability in operational conditions.

### 3.5 Summary

Current approaches to measure durability of highly repellent surfaces are not adapted to real-life applications and don't allow comparison between different families of coatings. A new approach for validating easy clean coatings is proposed.. This novel, modular multi-variate analysis methodology enables assessment of advanced coatings via spider diagrams, performance indices and plot of performance indices approach whilst using many standard test procedures.

The spider diagram approach is proposed in order to illustrate multi-variable properties of the coating within one graph. The key performance characteristics of easy clean coatings were selected and divided into general categories, where each category represents some characteristic group of coating properties. Where necessary, categories were subdivided into relevant categories.. A value

assignment system from 1 to 10 was introduced in order to transfer raw performance data into spider diagram and performance indices. Performance indices for specified group of properties were defined by comparing the assigned value(s) of the key metrics against a theoretical maximum that could be attained in that category.

The designed plot of performance indices was based on the relation between selected coating variables, represented in a form of performance indices. In this study, it was proposed to focus on three general performance indicators of easy clean coatings, namely initial repellence properties, ability to resist abrasion and retention of functional property under aggressive conditions.

The proposed model of coating assessment helps to classify and rank highly repellent surfaces. Due to the validation of performance indices, their durability can be measured and compared. Nevertheless, there are a few conditions that need to be fulfilled prior material evaluation and categorization. First of all, coating system that is subjected to examination, should be cured to the point where its functional properties are fully developed and further surface failure can't be assigned to the lack of cure. Second of all, adhesion between coating and substrate should be enhanced as much as possible, in order to separate synergism of adhesion loss under abrasive wear. In the next chapter, both commercially available and new nanostructured hybrid coating formulations will be described and together with an analysis of their behaviour as evaluated with this new methodology.

## 4 ASSESSMENT OF THE DEGREE OF CONVERSION OF SELECTED COATINGS SYSTEMS

### 4.1 Overview

Growing interest in the use of UV cured coatings has raised the need for improvements in coating manufacturing, testing and characterization. Light induced polymerization has improved significantly in recent years, but further progress is likely to be limited by the lack of verified data on the cure dependent properties of such coating systems. Understanding the mechanisms behind the cure process will give better control over the final properties of the coating. This chapter provides an overview over the curing kinetics in selected easy clean coatings. Surface characterization analysis and degree of conversion were examined using infrared spectroscopy.

### 4.2 Introduction – Fundamentals of UV Radiation Curing

The UV cured coating market, since its introduction in 1970's, has expanded to new applications, thereby displacing traditional thermally dried materials. Unique advantages, such as speed of cure, reduced energy consumption and high quality of final products were very attractive for many industrial applications, including aerospace, automotive, marine, textiles, medical (Stowe R.J., 1993) (Cheng L.L., 2011). UV curing is a photochemical process, where light is used instead of heat to cure materials and therefore, this process practically eliminates the use of solvents. Since the evaporation is reduced and there is reduced loss in coating thickness, lower shrinkage and the risk of cracking can be minimised. So far, UV curing is considered to be the most effective way of transforming the solvent-free resin into solid polymer at the room temperature. Ultraviolet (UV) radiation is characterized by the emission of energy in a portion of the electromagnetic spectrum. Ultraviolet light ranges in wavelength from 100 to 400 nanometers and they cannot be detected by human eye. In general, the UV spectrum can be divided into three transmission bands, namely UVA (400-315nm), UVB (315-280nm) and UVC (280-100nm) (Oldring P.K.T., 1998). UV wavelengths below 200nm exist primarily in vacuum (VUV) and therefore, from industrial point of view they are not very useful. It is also worth noting that UV cure coatings are part of the broader radiation cure. Electron beam (EB) curing is also part of this family. The same coating chemistry is used for both, but with UV cure initiators are used, EB does not require initiators due to the higher energy of the radiation but it does need an EB facility. These are much more

complex, expensive and hazardous than UV lamps and so EB cured coatings are niche compared to UV cured ones and they won't be discussed in this study.

The UV curable system consists of three main components, oligomers, multifunctional monomers and photoinitiator(-s) (Cheng L.L., 2011). Oligomers are generally high in molecular weight (500-5000) and they strongly influence final properties of the coating, such as hardness, scratch, abrasion resistance, flexibility and toughness and chemical stability. Depending on their chemical backbone, they can be divided into three groups, epoxy acrylates, urethane acrylates and polyester acrylates. The acrylate functionality (the number of acrylate bonds per oligomer molecule) varies from 2 to 6. On the other hand, monomers are low in molecular weight and viscosity and therefore they can be used to as functional diluants to reduce the viscosity of oligomers. Monomers also contain double bonds and their functionality varies in the range from 1 to 6. Monofunctional monomers have only one acrylate double bond per molecule and very low viscosity. Hence, they are the backbone of flexible coatings with reduced crosslink density. The viscosity and crosslink density of monomer increases with higher functionality number. The chemical structure and functionality of both oligomer and monomer determine the final degree of polymerization and physical and chemical properties of UV cured coating. The last component of a UV curable system plays a crucial role in the polymerization process by generating free radicals, which initiate radical chain polymerization of the unsaturated monomer or monomers (Monroe B.M, 1993). The reaction starts when photoinitiators absorb the light to form free radicals. These free radicals react with the functional groups of the coating (double acrylate bonds) and the reaction propagates. During the propagation step, molecular weight of polymer increases and coating becomes less flexible and mobile. Finally, two polymer radical chains come together and the reaction is terminated and solid, coherent film is produced. The degree of cross-linking depends on many variables, such as the duration of the exposure to ultraviolet light, intensity and the wavelength of the UV light source. According to the mechanisms by which, the process is initiated, photoinitiators are generally divided into two classes: type I, which undergo cleavage upon irradiation and type II, which forms excited state when they are exposed to UV light. When choosing a photoinitiator, it is important to match its absorption characteristic with spectral output of the lamp (intensity of light at each wavelength over the whole wavelength range emitted by the lamp). A suitable

photoinitiator system must be selected so that its absorptivion will be high in the emission range of the light source.

There are two main models of polymerization: the radical type (for acrylates) and the cationic type (for epoxides and vinyl ethers) (Allen N.S., 1996). Nevertheless, due to the higher reactivity, radical type polymerization has found wider applicability in today's UV curing industry and this model reaction will be presented in this study.

### **4.3 Experimental**

#### *4.3.1 Materials*

Six types of coating were prepared and subjected to further evaluation. All these coatings are UV cured systems and they are based on the acrylate matrix.

#### **TWI formulation A**

Formulation A is the backbone for the next generation of TWI formulations and therefore, it is a reference coating for the further evaluation. The composition of this coating system is based on the aliphatic epoxy diacrylate oligomer (code: CN132, purchased from Sartomer). There are three types of reactive diluents in this formulation, including diacrylate monomer (SR9003, purchased from Sigma-Aldrich), triacrylate monomer (SR454, purchased from Sigma-Aldrich) and tetraacrylate monomer (SR494, purchased from Sartomer). Two types of photoinitiators were used in the system, 1-hydroxycyclohexyl phenyl ketone (184, purchased from Sigma-Aldrich) and benzophenone (BP, purchased from Sartomer). These two photoinitiators were selected on a manner that their absorptivity matches emission range of the light source (Figure 4.1). The match between UV lamp and selected photoinitiators allows for direct correlation of curing effect to radiation intensity of light. In order to improve coating flow properties, two surface control additives were mixed with the other ingredients, TEGO Flow 425 (purchased from EVONIK) and TEGO Wet 270 (also purchased from EVONIK). After all the constituents were mixed together, the resin was placed in an oven at 65°C for 30 min to ensure dissolution of the solid photo-initiators. Table 4.1 provides the composition of formulation A by weight percent.

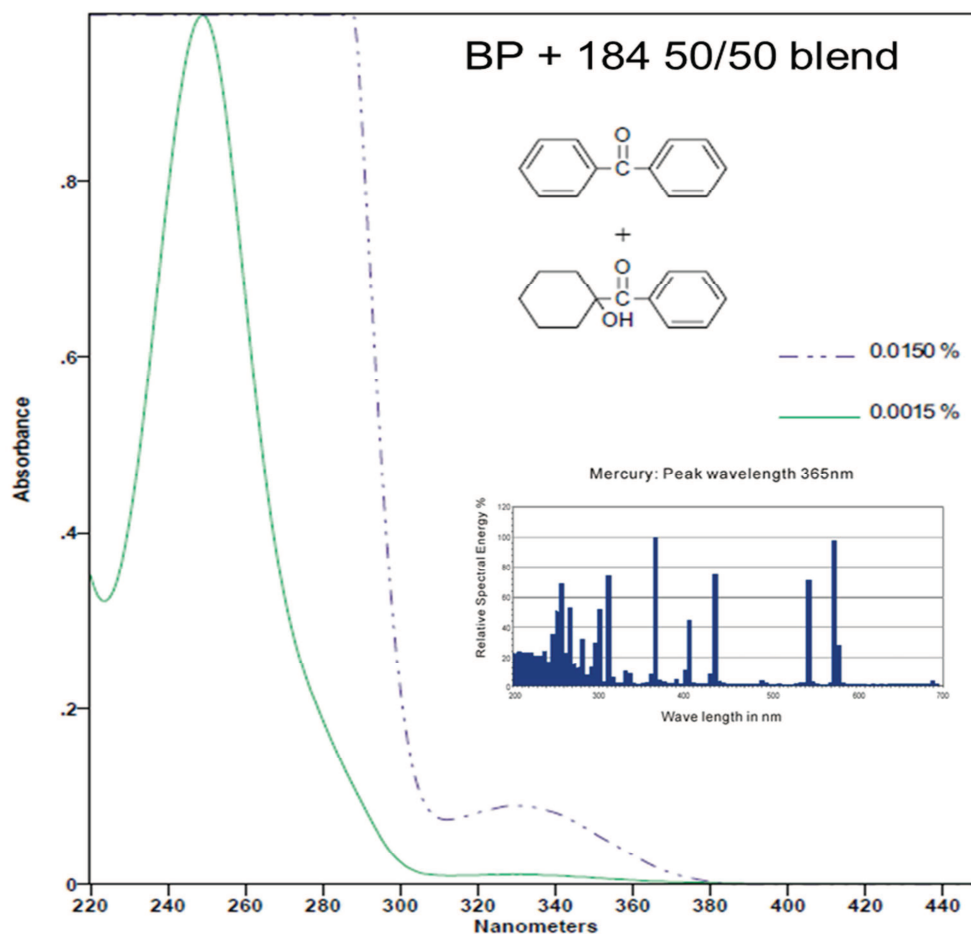


Figure 4.1 BP and 184 emission spectra (Sigma-Aldrich)

Table 4.1 TWI formulation A composition (wt%)

Ingredients	CN132	SR9003	SR454	SR494	184	BP
Formulation A	27	27	27	9	5	5

### TWI formulation B

Formulation B is a derivative of formulation A. In this coating system, SR494 monomer was replaced by Vitolane AZ (supplied by TWI). Composition by weight percent is exactly the same like in the mother formulation (A type). Vitolane AZ is a part of TWI’s Vitolane® technology (described in chapter 3), which offers an affordable way of producing mono-functional silsesquioxane oligomers.

In general, the Vitolane® process involves a two-step hydrolysis/condensation reaction followed by subsequent drying of the resulting formulation (Figure 4.2). At the beginning of the process, hydrolysable inorganic monomer precursor (methacrylate trimethoxysilane) is partially hydrolysed and allowed to undergo limited condensation (i). This step is exothermic as the silane is activated by the generation of silanols via the hydrolysis of the alkoxy groups. Reaction with water

will increase the level of silanol, which will slightly decrease as condensation occurs. In this step, cyclic inorganic oligomers are formed giving the backbone for the building blocks for the final organosilsesquioxanes molecules. In the second part of the process (ii), these inorganic oligomers are quenched by addition of water, which simulates rapid condensation of previously produced structures. At the end of the process, the composition is dried (to remove all volatiles) and can be incorporated into the coating resin formulation. Time and temperature are the key parameters in the degree of condensation. Too short period of time of hydrolysis increases the possibility of residual unreacted alkoxy groups present in the secondary condensation step which can lead to production of high molecular weight resins or even gels. On the other hand, too short a condensation process in the step (i) will lead to incompletely condensed species that can subsequently condense in a more random fashion during the secondary condensation step (ii).

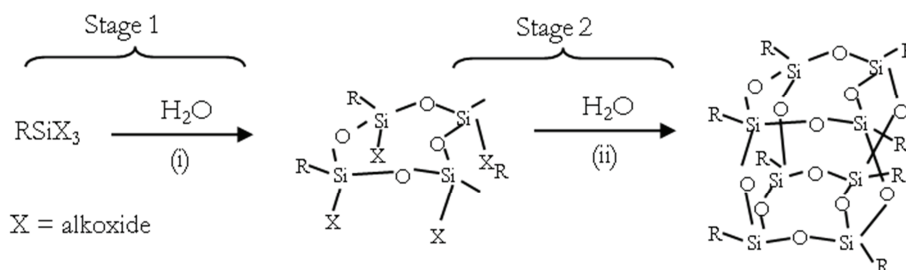


Figure 4.2 Synthesis procedure for mono-functional silsesquioxanes (part of TWI's Vitolane® technology)

For the purpose of this study, methacrylate silsesquioxane was selected as the building block of Vitolane AZ, due to the fact that presence of the methacrylate group in the system will help to incorporate the macromolecule into the acrylate matrix.

### TWI formulation C and D

Formulation C and D are the next generation of formulation B. In addition to the base matrix with Vitolane AZ, these resin systems contain in their composition functionalized silica nanoparticles. These silica nanoparticles were prepared with the Stöber method (description in Chapter 2) and subjected to functionalization. Two types of silica particles size were created (Figure 4.3 and 4.4) and modified hereinafter referred to as TSS4 (~32 nm) and TSS5 (~294 nm).

TSS4 silica Stöber spheres were prepared in the following steps. In vessel A, 84 g of tetraethoxysilane (TEOS, purchased from Sigma-Aldrich) and 150 g of industrial methylated spirit (IMS, purchased from VWR) were thoroughly mixed together. In a separate container, vessel B, 375 g of industrial methylated spirit, 12 g of 25%

ammonium hydroxide (catalyst, purchased from Sigma-Aldrich) and 15 g of deionised water were thoroughly mixed. The contents of vessel A were slowly added to vessel B to ensure homogenous mixing. The mixture was then heated at 65°C for 3 h, and afterwards ammonia was removed using evaporation methods. Dynamic light scattering (DLS) measurement of TSS4 generated by TWI for this study is illustrated in Figure 4.3:

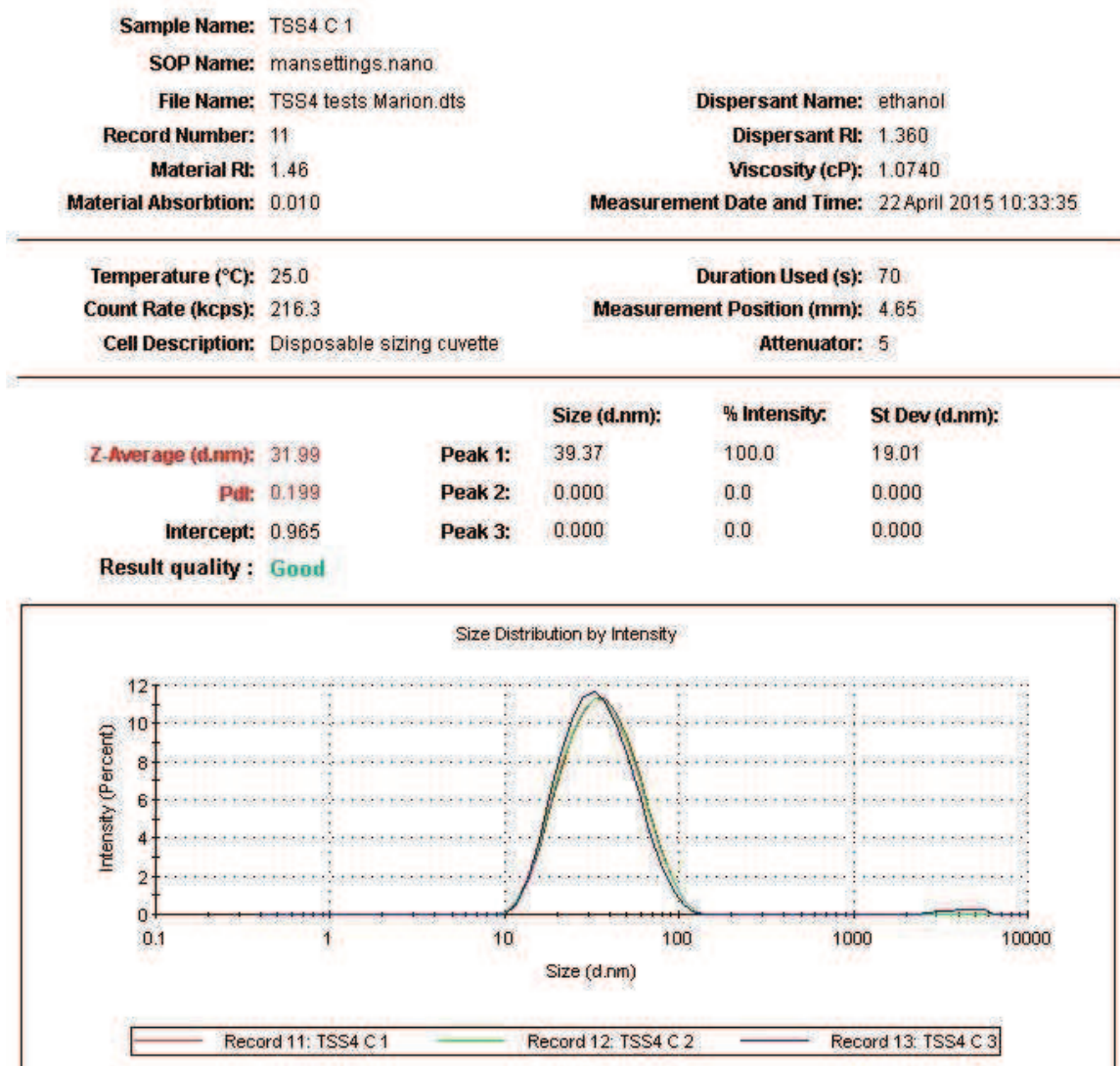


Figure 4.3 Particle size distribution – TSS4 silica Stöber spheres

TSS5 silica Stöber spheres were formulated on a similar manner as TSS4. In vessel A, 29 g of TEOS and 150 g of IMS were thoroughly mixed together. In a separate vessel B, 350 g of IMS, 22.5 g of 25% ammonium hydroxide and 77 g of deionised water were thoroughly mixed. The contents of vessel A were slowly added to vessel B and then mixture was heated at 65°C for 3 h. Ammonia was removed from the mixture by evaporation. Particle size distribution of TSS5 is given in Figure 4.4.

<b>Sample Name:</b> TSS5 clean 03.09 3	<b>Dispersant Name:</b> ethanol
<b>SOP Name:</b> mansettings.nano	<b>Dispersant RI:</b> 1.360
<b>File Name:</b> TSS5.dts	<b>Viscosity (cP):</b> 1.0740
<b>Record Number:</b> 3	<b>Measurement Date and Time:</b> 03 September 2015 15:37:55
<b>Material RI:</b> 1.46	
<b>Material Absorbition:</b> 0.010	

<b>Temperature (°C):</b> 25.0	<b>Duration Used (s):</b> 70
<b>Count Rate (kcps):</b> 255.3	<b>Measurement Position (mm):</b> 0.85
<b>Cell Description:</b> Disposable sizing cuvette	<b>Attenuator:</b> 3

	<b>Size (d.nm):</b>	<b>% Intensity:</b>	<b>St Dev (d.nm):</b>
<b>Z-Average (d.nm):</b> 293.9	<b>Peak 1:</b> 304.2	100.0	64.73
<b>Pdl:</b> 0.006	<b>Peak 2:</b> 0.000	0.0	0.000
<b>Intercept:</b> 0.958	<b>Peak 3:</b> 0.000	0.0	0.000
<b>Result quality:</b> <b>Good</b>			

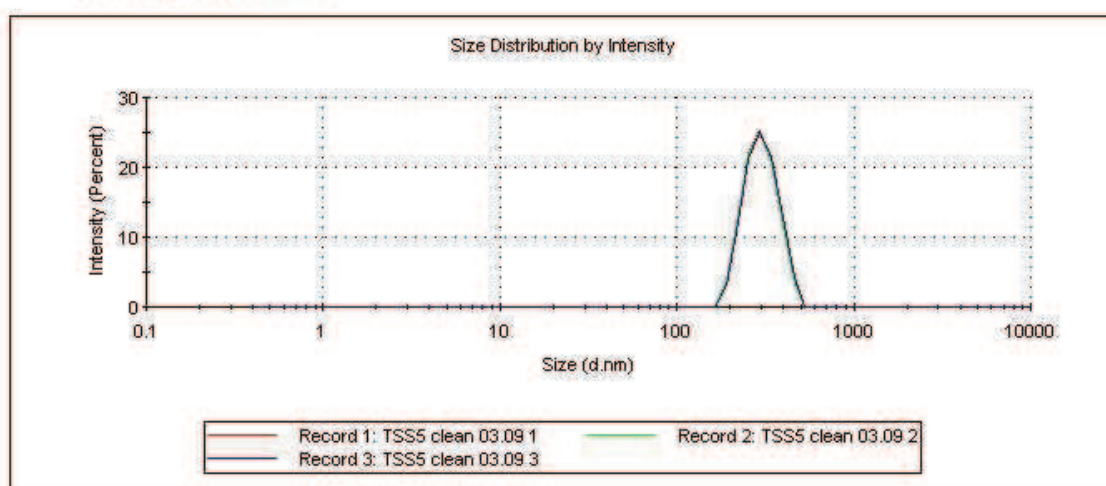
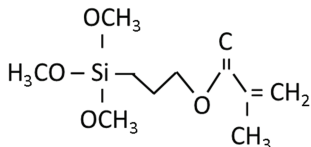
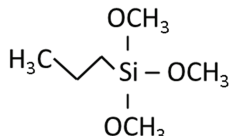
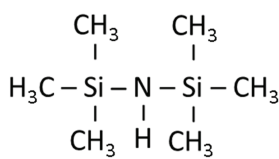


Figure 4.4 Particle size distribution – TSS5 silica Stöber spheres

For the purpose of this study, three types of functionalization (Table 4.2) were chosen in order to tailor the properties of pure silica nanoparticles:

1. MPTMA - 3-(trimethoxysilyl)propyl methacrylate (purchased from Silanes & Silicones Manufacturing) – functionality selected in order to provide compatibility with matrix resin (to provide acrylate species in the system) and to improve the repellent properties of silica.
2. NPTMS - n-propyl trimethoxy silane (purchased from Silanes & Silicones Manufacturing) – functionality selected in order to help silica nanoparticles to improve the hydrophobic character of silica
3. HMDS – hexamethyldisilazane (purchased from Sigma-Aldrich) – functionality that provides another highly repellent species in the system. Besides that, this functionality was used in order to improve the bonding between the coating system and the selected substrate (adhesion promotor)

Table 4.2 Chemical formulas of silica nanoparticles functionalizing agents

Functionalizing agent	Structure
MPTMA	
NPTMS	
HMDS	

The TSS4 silica Stöber spheres were functionalized. A reaction vessel was charged with 186.5 g of TSS4 suspension and 0.4 g of NPTMS and 0.49 g of dibutyltin dilaurate (catalyst). This mixture was heated for 18 hours at 65°C under reflux. In the next step 0.4 g of MPTMA was added and mixture was heated again for 18 hours at 65°C under reflux. At the end, mixture was supplemented by 7.2 g of HMDS and heated once again for 18 hours at 65°C under reflux.

Functionalization of TSS5 was undertaken in the same manner as the functionalization of TSS4. Figure 4.5 illustrates the process of functionalization TSS5.

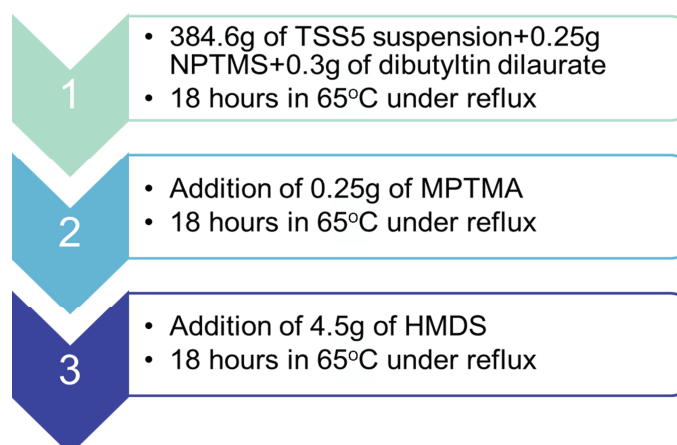


Figure 4.5 Functionalization process of TSS5 Stöber spheres – triple functionalization

After the TSS4 and TSS5 were prepared and functionalized, they were mixed together and added to the coating formulations. In a vessel, 100 g of the triple functionalised TSS4 material was added to 10 g of the triple functionalised TSS5

material. Mixing of two different sizes of nanoparticles was carried out in order to build dual scale roughness, a necessity to achieve high levels of repellence and low roll-off angles. Solvent removal by evaporation in a rotorvap was undertaken until the solid content of the mixture was 50% by weight. The mixture was then added to the matrix mixture (TWI formulation B) and further solvent was removed by evaporation until the solvent content was <10% by weight. The mixture was then deposited onto the substrate and cured.

#### **TWI formulation E**

Formulation E is another variation from formulation B, containing silica nanoparticles in the system. TSS4 silica Stöber spheres were prepared in the same manner as was described above (TSS4 preparation for formulation C and D). Prepared silica nanoparticles were then subjected to further functionalization.

A reaction vessel was charged with 186.5 g of TSS4 suspension and 2 g of NPMTS and 0.49 g of dibutyltin dilaurate. This mixture was heated for 18 hours at 65°C under reflux. In the next step 6 g of MPTMA was added and mixture was heated again for 18 hours at 65°C under reflux.

#### **TWI formulation F**

Formulation F is in general another variation from formulation B, containing functionalized silica nanoparticles (TSS4) in the system. Nevertheless, in this resin the overall amount of photoinitiators in formulation B was decreased from 10 to 1%. Besides that, new functionalization of silica nanoparticles was introduced, namely 1H,1H,2H,2H-perfluorooctyltriethoxysilane (FAS, purchased from Sigma-Aldrich). Description of TWI formulation F has only informative character. Due to the fact that this formulation was created just for the purpose of comparison with other TWI formulations, no surface characterization analysis and degree of conversion of TWI formulation F will be provided within this chapter.

A reaction vessel was charged with 186.5 g of TSS4 suspension and 4 g of FAS and 0.49 g of dibutyltin dilaurate. This mixture was heated for 18 hours at 65°C under reflux. In the next step 4 g of MPTMA was added and mixture was heated again for 18 hours at 65°C under reflux.

Table 4.3 provides summary with regard to TWI formulations composition and functionalization types.

Table 4.3 TWI formulations summary (composition by wt% and functionalities)

Ingredients	A	B	C	D	E	F
Acrylate	100%	91%	36.4%	17.75%	45.5%	36.4%
SSQs	•	9%	3.6%	2.25%	4.5%	3.6%
TSS4	•	•	58.8%	73.5%	50%	60%
F1 TSS4 (MPTMA)	•	•	Yes	Yes	Yes	Yes
F2 TSS4 (NPTMS)	•	•	Yes	Yes	Yes	•
F3 TSS4 (HMDS)	•	•	Yes	Yes	•	•
F4 TSS4 (FAS)	•	•	•	•	•	Yes
TSS5	•	•	1.2%	1.5%	•	•
F1 TSS5 (MPTMA)	•	•	Yes	Yes	•	•
F2 TSS5 (NPTMS)	•	•	Yes	Yes	•	•
F3 TSS5 (HMDS)	•	•	Yes	Yes	•	•
Solid Content	•	•	33.8%	23.8%	46%	56.8%
Solvent type	•	•	IMS	IMS	IMS	IMS

#### 4.3.2 Methods

The substrates used in this study were 0.6 mm thick bare aluminium Q panels made from alloy 3003 H14 (purchased from Q-Lab). Prior to the processing, samples were degreased with acetone. All resins were deposited onto the substrates using a 20 µm wire wound bar. After deposition, coated samples were placed in 65 °C for 20 min in order to give the resin ability to flow into a smooth, uniform thickness.

The curing process was carried out by using 2000-EC Series UV Curing Flood Lamp Systems from DYMAX. The curing system had the basic mercury bulb (H-type bulb with no dichroic IR filter), which emits energy in the short wavelengths (240-270 nm) and the long wavelengths (350-380 nm) (Oldring P.K.T., 1998). A particular advantage of this type of bulb is that they can be used in an oxygen-rich environment and the strong short wavelengths emission (between 250 and 270 nm) make them ideal to match to UV curing photoinitiators. During the curing process short wavelengths work on the specimen surface, while the long ones penetrate more deeply into the coating. In this particular UV curing system, the light source comes from microwave-excited medium pressure mercury plasma. Due to the fact that oxygen in ambient air reduces cross-linking in photoinitiator driven reactions ( a process known as oxygen inhibition), the UV curing process was carried out in the nitrogen atmosphere. The amount of UV arriving at the cured surface (irradiance) was measured with the Dr. Hönle UVA-meter.

In order to measure the degree of conversion for selected coating systems, there is a need to know how much energy was absorbed in the material. Therefore, regular calibration of the UV curing system is crucial. For the purpose of this study calibration was done on a monthly basis with a routine shown in Figure 4.6. Intensity of light was measured using radiometer in the same points at the constant distance from the light source (an average values of intensity of light multiplied by the time that sample spent under UV lamp gave the value of energy absorbed).



Figure 4.6 Calibration procedure of selected UV curing system

Dry film thickness was evaluated using Scanning Electron Microscopy and Elcometer 300 Coating Thickness Gauge. The Elcometer 300 uses eddy current principle. When a single coil carrying low voltage current is placed to the test specimen, small currents are induced in opposition to the original field. This change in fields effectively reduces the voltage across the coil. The variation in voltage is dependent upon the distance from the sample and can be related to coating thickness. Twenty aluminium bare panels were degreased with acetone and coated with TWI formulation B. Three different sizes of spiral bar coaters were used for film application, 10, 20 and 50  $\mu\text{m}$ . Samples were cut onto small pieces (2x1 cm) and eddy current gauge readings were taken. These small pieces were further preceded for SEM sample preparation. All samples were ground flat on P120, P320, P400, P600 and P1200 abrasive paper and finally polished with 3 and 1  $\mu\text{m}$  polishing plates. SEM backscatter images of cross-sectional areas of prepared test specimens were studied. Statistical comparison of dry film coating thickness measured by eddy current gauge and SEM was carried out.

Surface characterization analysis and the degree of polymerization were studied with Fourier Transform Infrared Spectroscopy. The principle of FTIR is based on the interaction between electromagnetic radiation and natural vibrations of the chemical

bonds among atoms that create the matter. Vibrations, rotations of the molecule will result in the absorption band in the infrared spectrum (IR). Nevertheless, in order for the material to absorb radiation in IR region, two conditions must be fulfilled. First of all, the natural vibration must cause change in the dipole moment during vibration. Besides that, there must be resonance among the frequencies of the infrared radiation and molecular vibration. There are two types of molecular vibrations, namely stretching and bending. The first one changes the length of the bond, whereas the second one influences the angle of the bond.

The position of absorption bands in spectrum is represented by wavelength ( $\lambda$ ), which is the distance between two consecutive points that are in the same phase. The number of wavelengths in a given distance along the propagation of the wave is defined as wavenumber ( $\nu$ ). This wavenumber is directly proportional to the energy (E) and frequency ( $\nu$ ) of the radiation (Eq.4.1)

$$E = h\nu = hc\nu = \frac{hc}{\lambda} \quad (4.1)$$

The band intensity can be expressed either in absorbance (A) or transmittance (T). Transmittance represents the ration between intensity of incident light and the intensity of transmitted light (Eq.4.2)

$$T = \frac{I}{I_0} \quad (4.2)$$

On the other hand, Absorbencies (logarithmic) of the reciprocal of the transmittance:

$$A = \log_{10}\left(\frac{1}{T}\right) = \log_{10}\left(\frac{I_0}{I}\right) \quad (4.3)$$

In this study, IR analysis was carried out using 4100 ExoScan Series FTIR from Agilent Technologies. For measuring the degree of polymerization, dedicated sampling probe called attenuated total reflectance (ATR) was used. In this ATR technique, internal reflection occurs when infrared radiation enters a highly refractive material. In this particular spectrometer, diamond crystal was used. The IR beam reflects from the internal surface of the crystal and creates an evanescent wave, which projects orthogonally into the sample in intimate contact with the ATR crystal (Harrick N.J., 1967). Some of the energy of the evanescent wave is absorbed by the sample and the reflected radiation is returned to the detector. This ATR principle is shown graphically in the Figure 4.7.

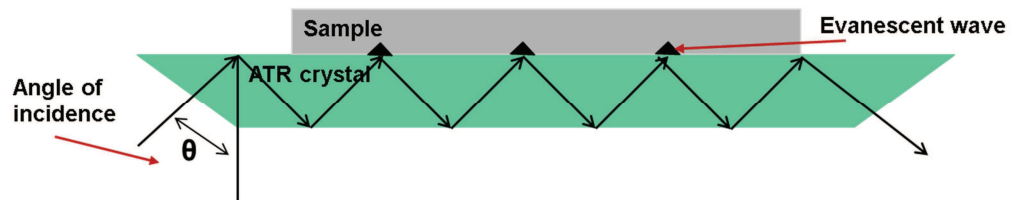


Figure 4.7 The principle of Attenuated Total Reflectance Spectroscopy

The intensity of the evanescent wave decays exponentially with the distance into the crystal surface. The depth of penetration ( $d_p$ ) of the IR beam into the sample is dependent upon the wavelength of infrared radiation, the crystal material and the angle of incident radiation ( $\theta$ ) according to the equation 4.4:

$$d_p = \frac{\lambda}{2\pi n_1 (\sin^2 \theta - n_{21}^2)^{1/2}} \quad (4.4)$$

Where,  $n_1$  is the refractive index of the crystal,  $n_{21}$  is the ratio of the refractive indices between sample and the crystal. Therefore, the value of penetration depth can be tailored either by using lower refractive index materials or by applying smaller incidence angle.

In this study, FTIR-ATR spectra were collected. Each spectrum contained thirty-two scans collected in range  $650\text{-}4000\text{ cm}^{-1}$ , with the resolution of  $4\text{ cm}^{-1}$ , taken with a  $45^\circ$  angle of incidence. In order to measure the intensity that is left after passing thought test specimen, background spectrum (IR intensity with no sample) was collected. Samples data were analysed using Panorama LabCognition software. The baselines of the spectra were corrected and normalized.

Nanoindentation technique was used in this study in order to assess mechanical performance of coatings with different amount of energy absorbed during UV curing process. All measurements were done with Nano Test Platform Three from Micro Materials Ltd (Berkovich indenter,  $0.1\text{mN}$  load,  $1\mu\text{m}$  depth). Hardness  $H$  and elastic modulus  $E$ , evaluated by nanointender, are two relevant parameters, which affect the abrasion wear resistance of the material and designate the durability of the system. It was also found in the literature that the ratio  $H/E$  between hardness  $H$  and elastic modulus  $E$  can be a good indication of determining the tribological properties of material (Oberle T.L., 2000) (Leyland A., 2000).

Visual appearance of prepared formulations was studied with Novo-Gloss IQ Goniometer from Rhopoint Instruments, with the respect to standards ASTM D523-08 and ASTM E430. There is a general rule that if the measurement made at  $60^\circ$  gives a value greater than 70 GU, the default angle should be changed to  $20^\circ$  to optimise measurement accuracy.

## 4.4 Results and discussion

### 4.4.1 Dry film thickness

Dry film thickness measurement data are shown in Table 4.4 and they are displayed in Figure 4.8.

Table 4.4 Thickness measurements carried out with two different techniques (eddy current and SEM) for three different coating thicknesses (10, 20 and 50  $\mu\text{m}$ )

No.	Eddy current [10 $\mu\text{m}$ ]	SEM [10 $\mu\text{m}$ ]	No.	Eddy current [20 $\mu\text{m}$ ]	SEM [20 $\mu\text{m}$ ]	No.	Eddy current [50 $\mu\text{m}$ ]	SEM [50 $\mu\text{m}$ ]
10.1	15.22	12.34	20.1	20.42	22.11	50.1	53.71	51.25
10.2	12.48	14.49	20.2	19.64	18.98	50.2	50.48	56.78
10.3	13.32	12.73	20.3	18.70	21.90	50.3	48.48	47.16
10.4	12.86	13.11	20.4	21.10	20.44	50.4	53.78	49.21
10.5	12.98	12.73	20.5	20.22	21.26	50.5	55.64	54.38
10.6	12.66	13.25	20.6	20.30	19.82	50.6	47.62	51.29
10.7	13.00	14.31	20.7	19.80	20.96	50.7	51.86	57.43
10.8	13.28	12.86	20.8	20.64	21.43	50.8	47.66	45.18
10.9	12.42	13.53	20.9	18.50	19.20	50.9	50.06	53.77
10.10	12.84	13.22	20.10	20.76	20.51	50.10	49.36	52.38

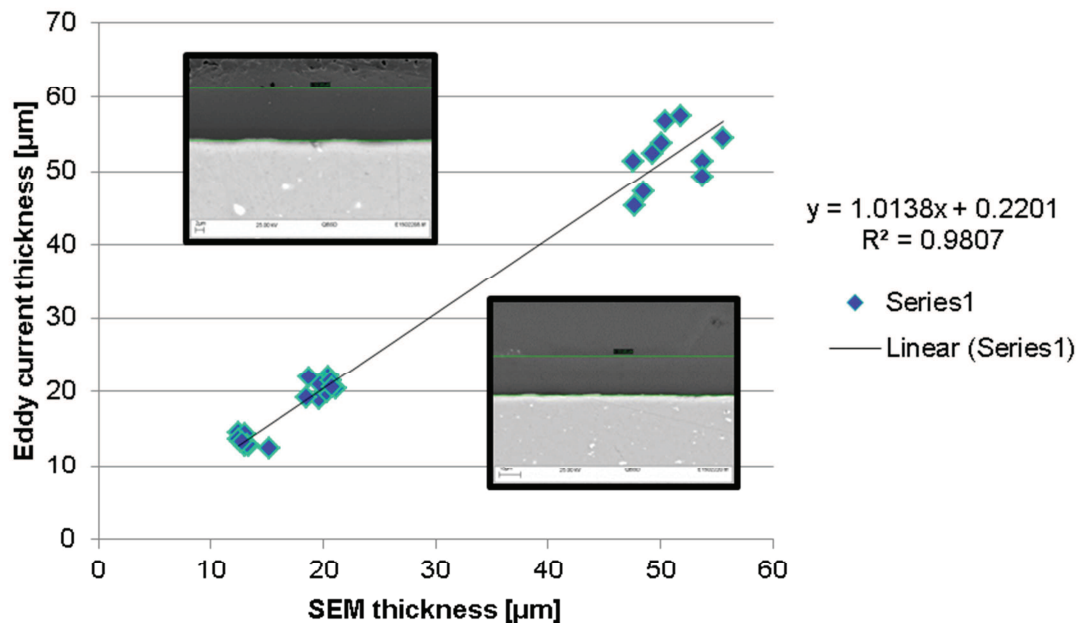


Figure 4.8 Correlation between two techniques for thickness measurements. Two SEM images shows the general principle of thickness evaluation done with microscopic technique

An analysis of variance procedure was used in order to compare mean values obtained from these two measuring techniques. Two hypotheses were created. The null hypothesis ( $H_0$ ) states that there is no difference between the thickness data obtained from these two measuring techniques and therefore, these two methods are comparable (Eq.4.5). In opposition, alternative hypothesis ( $H_1$ ) states that

obtained data is significantly different and these two methodologies cannot be interchangeable (Eq.4.6).

$$H_0: \mu_1 = \mu_2 \quad (4.5)$$

$$H_1: \mu_1 \neq \mu_2 \quad (4.6)$$

ANOVA Tables (4.5, 4.6 and 4.7) present components of variation such as, variation between and within groups, error and residual variation, where SS represents sum of squares, Df is the degree of freedom, MS is mean squares, F ratio is the ratio of two mean square value, p-value represents significance level to assess the null hypothesis and  $F_{crit}$  is a critical value for F distribution (Dougherly C., 2011).

*Table 4.5 ANOVA single factor for thickness measurements obtained by eddy current gauge and SEM for panels coated with 10  $\mu$ m bar*

Source of Variation	SS	Df	MS	F	P-value	F crit
Between Groups	0.08	1	0.08	0.15	0.70	4.41
Within Groups	10.10	18	0.56			
Total	10.18	19				

*Table 4.6 ANOVA single factor for thickness measurements obtained by eddy current gauge and SEM for panels coated with 20  $\mu$ m bar*

Source of Variation	SS	Df	MS	F	P-value	F crit
Between Groups	2.67	1	2.67	3.31	0.09	4.41
Within Groups	14.52	18	0.81			
Total	17.19	19				

*Table 4.7 ANOVA single factor for thickness measurements obtained by eddy current gauge and SEM for panels coated with 50  $\mu$ m bar*

Source of Variation	SS	Df	MS	F	P-value	F crit
Between Groups	5.18	1	5.18	0.44	0.51	4.41
Within Groups	209.85	18	11.66			
Total	215.03	19				

The regression shown in Figure 4.8 indicates a linear relationship which almost has parity ( $R^2$  value close to one) with a slight offset. Nevertheless, taking under consideration the nature of this offset and the errors of measurement, these two

methods can be viewed as practically equivalent. Analysis of variance (ANOVA) has been carried out in order to test the difference in more than two independent means, which comes from two independent groups. Variation between and within the groups have been measured and based on the obtained data, F-statistic has been found. In all of the cases (coatings deposited with 10, 20 and 50  $\mu\text{m}$  bar), the calculated F-value is lower than F-critical (Dougherly C., 2011). Since the critical F is greater than obtained f-value, there are no statistical basics to reject the null hypothesis. Therefore, it can be stated that there are no statistical difference in data obtained by these two methods and they can be used interchangeable. Due to the fact that thickness measurement with eddy current principle is much faster and requires no sample preparation, it was decided that for the purpose of this study this method will be mainly used for thickness evaluation.

The ability to control coating thickness allows for the next step in assessment of degree of conversion. Nevertheless, before degree of conversion can be quantified, it is necessary to find out, what kind of structural changes occurred during UV radiation process.

#### 4.4.2 Structural characterization

The spectra of the prepared formulations/coatings are illustrated in Figure 4.9, 4.10, 4.11, 4.12, and 4.13. The peak assignments are listed in Table 4.8. All peak assignments were taken from IR frequencies database from Panorama LabCognition software.

Table 4.8 Infrared absorption frequencies for selected coating systems (Panorama software library)

Absorption band position [ $\text{cm}^{-1}$ ]	Assignment	Peak intensity
3600-3100	SiO-H	medium
2900-2700	C-H	medium
1730-1700	C=O	medium
1670-1630	C=C	weak-medium
1480-1370	C-H	medium-strong
1200-1100	C-O	strong
1100	Si-C	shoulder
1100-1000	Si-O-Si	very strong
1000-850	SiO-H	strong
810-800	SiO-CH <sub>2</sub> CH <sub>3</sub>	strong
700	C-H	medium

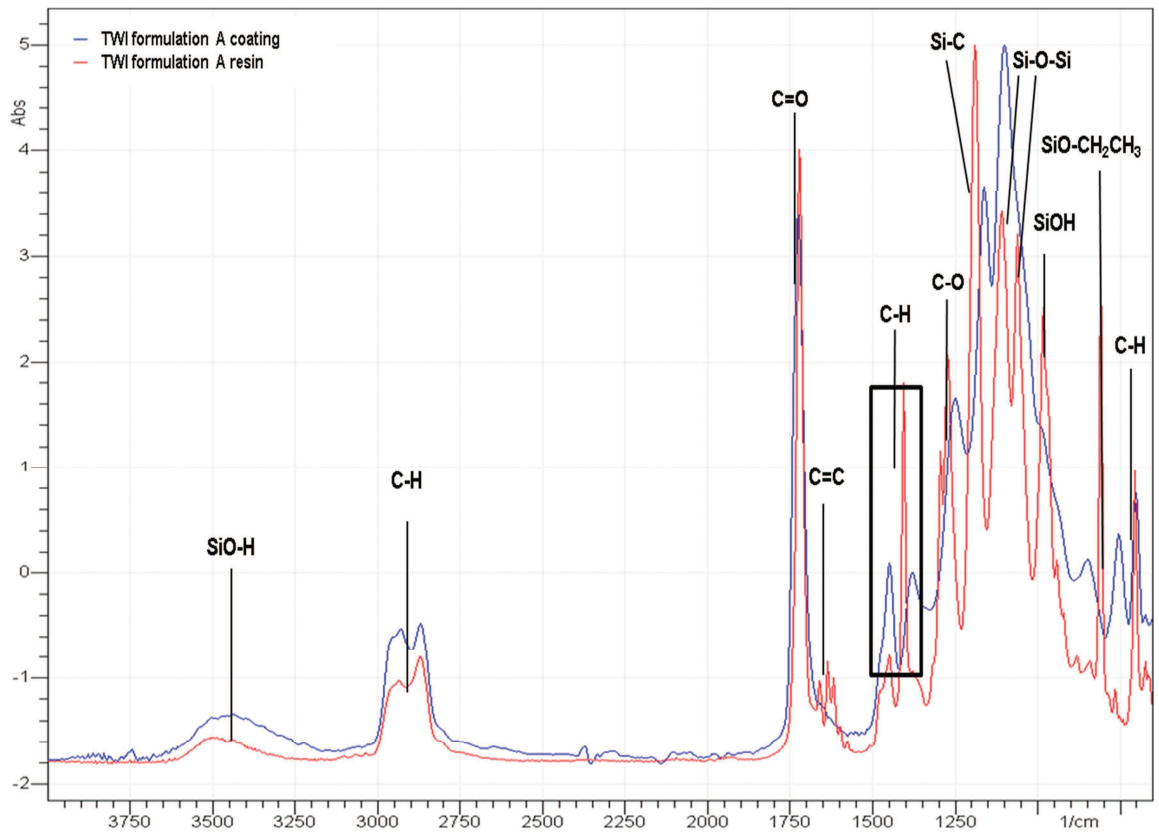


Figure 4.9 FTIR spectra of TWI formulation A measured in range of  $4000-650\text{ cm}^{-1}$  (Abs – absorbance)

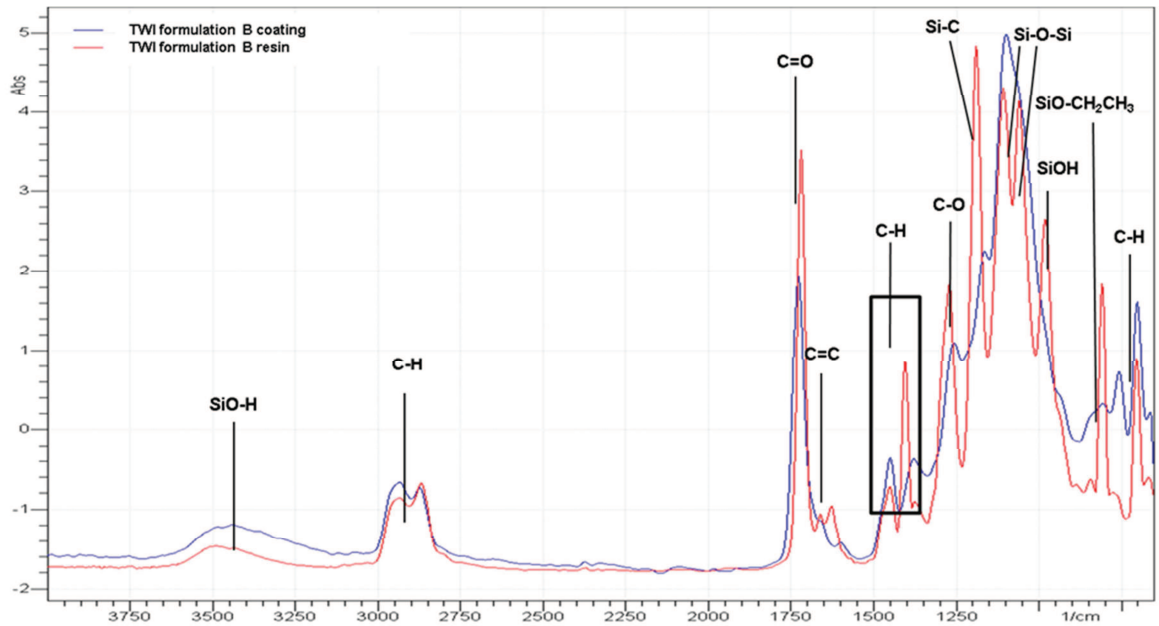


Figure 4.10 FTIR spectra of TWI formulation B measured in range  $4000-650\text{ cm}^{-1}$  (Abs – absorbance)

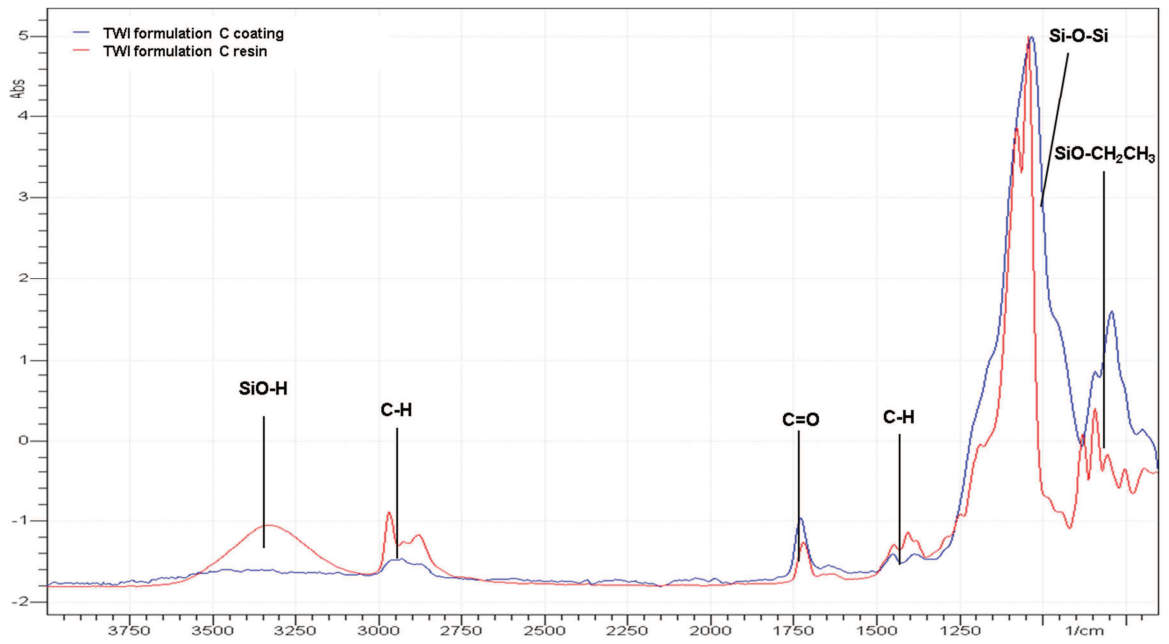


Figure 4.11 FTIR spectra of TWI formulation C measured in a range 4000-650  $\text{cm}^{-1}$  (Abs – absorbance)

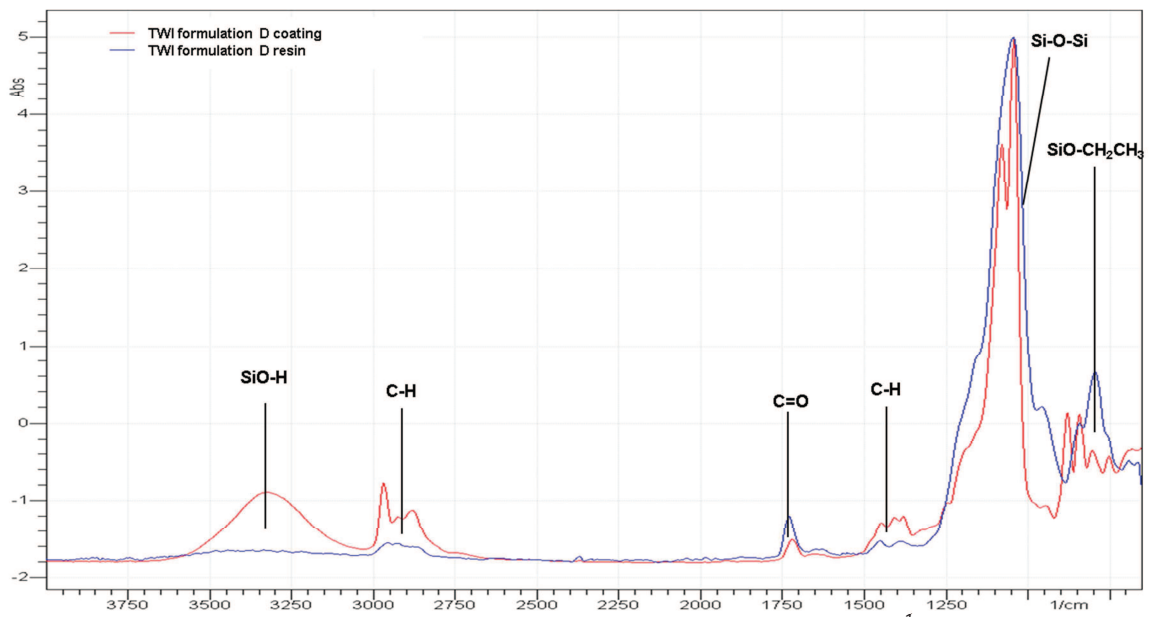


Figure 4.12 FTIR spectra of TWI formulation D measured in range 4000-650  $\text{cm}^{-1}$  (Abs – absorbance)

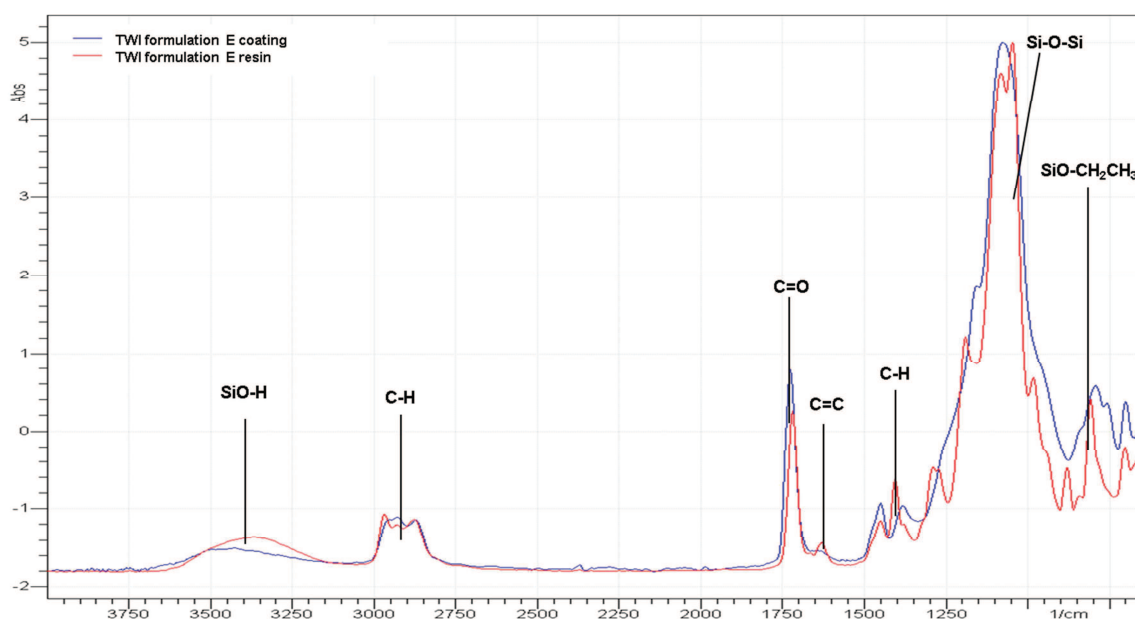
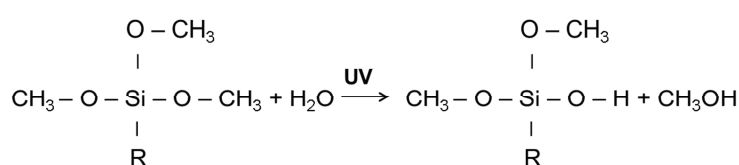
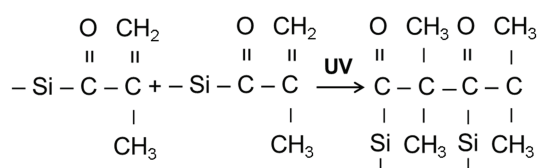


Figure 4.13 FTIR spectra of TWI formulation E measured in a range of 4000-650  $\text{cm}^{-1}$  (Abs – absorbance)

Figures 4.9 to 4.13 illustrate the FTIR spectra of TWI formulations measured in a range of 4000-650 $\text{cm}^{-1}$ . Each figure represents each formulation prior the polymerization process (resin) and after the structure was converted to its final form (hereinafter referred to as coating). Due to the high similarity in composition, spectra of TWI formulations A and B are not significantly different. The peak assignments together with the wavelength and intensity are presented in Table 4.8. The absorption bands between 3600-3100  $\text{cm}^{-1}$  relates to silanol group stretching. Another SiO-H vibration appears at 980  $\text{cm}^{-1}$  and refers to incomplete condensation of SiO-H bonds. The peak intensity increases with higher silica content. The absorption band observed near 1720 and 1630  $\text{cm}^{-1}$  are C=O and C=C respectively. The peak at 1100  $\text{cm}^{-1}$  associated with Si-C bond represents the covalent bonding between polymer chain and the silica network. The Si-O-Si stretching frequencies of siloxanes are characterized by sharp peaks in the region 1100-1000  $\text{cm}^{-1}$ . The C-H group absorption bands occur in the region 2900-2700  $\text{cm}^{-1}$ , 1480-1370  $\text{cm}^{-1}$  and 700  $\text{cm}^{-1}$ . During polymerization of TWI formulation A and B some changes can be observed. First of all, a small rise occurs in Si-OH band in the region 3600-3100  $\text{cm}^{-1}$  and it is caused by the reaction of alkoxy group from MPTMA groups (formulation B) in hydrolysis reaction:



Another change can be observable for C=C peak of methacrylate groups in MPTMA (monomer) or acrylate monomers. During polymerization the double bond between carbon atoms in the region  $1630\text{ cm}^{-1}$  will transform into C-C bond. C-C bends peak appears in the region of  $500\text{ cm}^{-1}$ , which is outside from spectral window and C-C stretches result in a weak band in the region  $1200\text{-}800\text{ cm}^{-1}$  and cannot be valued for interpretation. Due to that fact it is not possible to detect C-C band on 4100 ExoScan Series FTIR. Nevertheless, the consumption of C=C bonds give enough information about the polymerization reaction:



Another significant change in structure of formulations A and B during polymerization relates to the siloxane group. Prior to polymerization, siloxanes show two very sharp infrared bands in the region  $1100\text{-}1000\text{ cm}^{-1}$ . As the siloxane chain becomes longer and/or branched during the reaction, the absorption band of Si-O-Si becomes broader and more complex and Si-O-S peaks start to overlap.

The formulations C and D are more complex derivatives of formulation B. Due to the fact that their composition is not far different than formulation B, their absorption bands should be expected to occur at the same wavenumber. From the Figure 4.11 and 4.12 following peaks can be distinguished: Si-OH in the region  $3600\text{-}3100\text{ cm}^{-1}$ , C=O at  $1720\text{ cm}^{-1}$ , Si-O-Si in the region  $1100\text{-}1000\text{ cm}^{-1}$  and C-H in the region  $2900\text{-}2700\text{ cm}^{-1}$ ,  $1480\text{-}1370\text{ cm}^{-1}$  and at  $700\text{ cm}^{-1}$ . After polymerization, a few changes in the spectrum are observable. As a result of hydrolysis of alkoxy group from TEOS (from silica nanoparticles) and MPTMA (from silica's functional groups and SSQs oligomers), an increase of Si-OH peak in the region  $3600\text{-}3100\text{ cm}^{-1}$  should be expected. Nevertheless, significant decrease of this peak is observed. It might be explained by the presence of hydroxyl groups of IMS in the resin system. When solvent evaporates during the polymerization, the amount of hydroxyl groups in the solution will significantly decrease and therefore, lower absorption band should be expected in the region  $3600\text{-}3100\text{ cm}^{-1}$ . Figure 4.14 confirms that hydroxyl group peak of resin D in the region  $3600\text{-}3100\text{ cm}^{-1}$  is compatible with hydroxyl group from IMS. Nevertheless, it should be noted that the origin of this peak might also come from different sources, such as the Si-OH groups in the Stöber spheres, from hydrolysed but uncondensed alkoxy groups

attached to the silanes, from the water that is present at 1% in the IMS or potentially from the OH associated with the IMS. The change in the region  $1100-1000\text{ cm}^{-1}$  (siloxane group transformation) is related to exactly the same conversion as in the case of TWI formulation A and B.

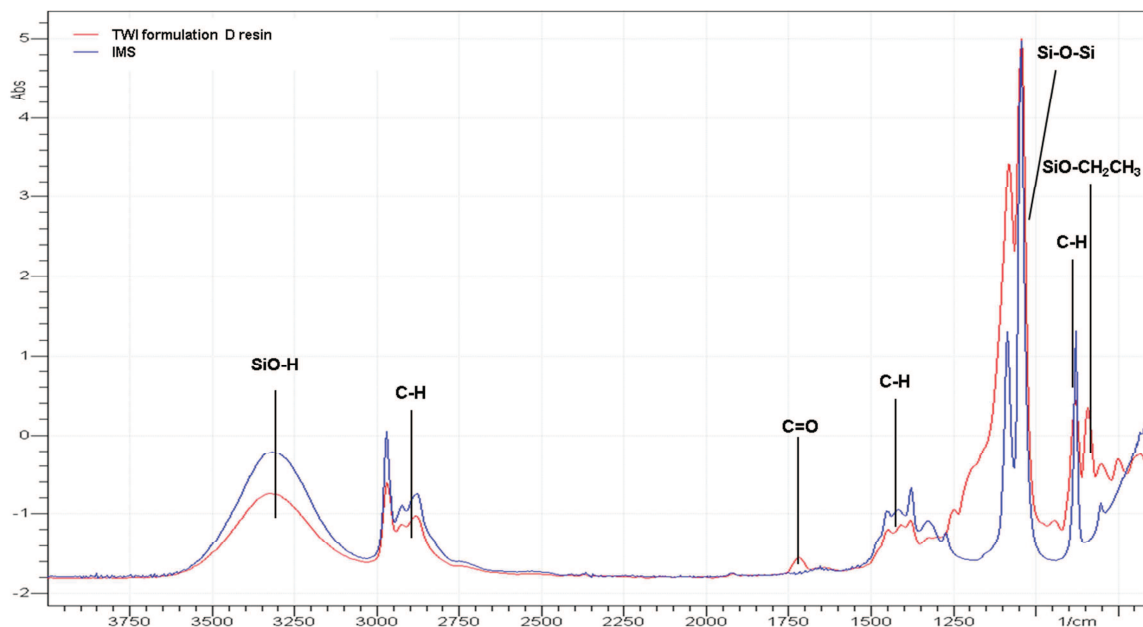


Figure 4.14 FTIR spectra of TWI formulation D resin and IMS measured in a range of  $4000-650\text{ cm}^{-1}$  (Abs – absorbance)

The formulation E is also a derivative of formulation B, but its composition is slightly different than formulation C and D. Nevertheless, there is no significant difference between spectrum of formulation C, D or E. For the formulation E resin, the only observable difference can be spotted at  $1620\text{ cm}^{-1}$ . The peak at  $1630\text{ cm}^{-1}$  corresponds to C=C peak and comes from acrylate and MPTMA groups. After polymerization following changes will take place: C=C absorption band will disappear, siloxane Si-O-Si peaks will overlap and the amount of hydroxyl group in the system will decrease. Due to the fact that formulation E resin contains less amount of solvent, decrease of hydroxyl peaks in the region  $3600-3100\text{ cm}^{-1}$  won't be as significant as in case of resin C and D. Table 4.9 provides the position of absorption bands together with the assignment to the compounds, where these absorption bands occur.

Table 4.9 Correlation between absorption bands and resin composition (F1, F2 and F3 corresponds to functionality type in silica system) (IR frequencies database from Panorama software library)

Absorption band position [cm <sup>-1</sup> ]	Assignment to compound	Assignment to resin composition
3600-3100	MPTMA	SSQs, F1 of silica particles
	TEOS	Silica particles
	HMDS	F3 of silica particles
1730-1700	Acrylate	Matrix
	MPTMA	SSQs, F1 of silica particles
1670-1630	Acrylate	Matrix
	MPTMA	SSQs, F1 of silica particles
1200-1100	MPTMA	SSQs, F1 of silica particles
	NPTMS	SSQs, F2 of silica particles
1100	MPTMA	SSQs, F1 of silica particles
	NPTMS	SSQs, F2 of silica particles
	HMDS	F3 of silica particles
1000-850	MPTMA	SSQs, F1 of silica particles
	TEOS	Silica particles
	HMDS	F3 of silica particles

Understatement of the nature of structural formations during polymerization process and ability to track these changes allows for the assessment of the degree of conversion.

#### 4.4.3 Degree of conversion

In general, the assessment of the degree of conversion is based on the monitoring the consumption one of the reactive functional group. In the following study, TWI formulation B was selected as a model to quantify structural changes during polymerization. The assessment for degree of conversion for TWI formulation B based on chemical rearrangement in its structure is presented in Figure 4.15. In total, 40 samples were prepared (4 samples per specified conditions, each conditions represent different level of energy absorbed) and subjected for further evaluation. Acetone was used to remove any organic contaminants from aluminium surface prior to the bonding. The resin B was deposited onto the substrate using 20 µm bar and placed in an oven at 65°C for 20 min in order to let the coating to planarise. Afterwards, samples were exposed to UV light for various periods of time in order to provide a range of UV flux exposures (energy input).

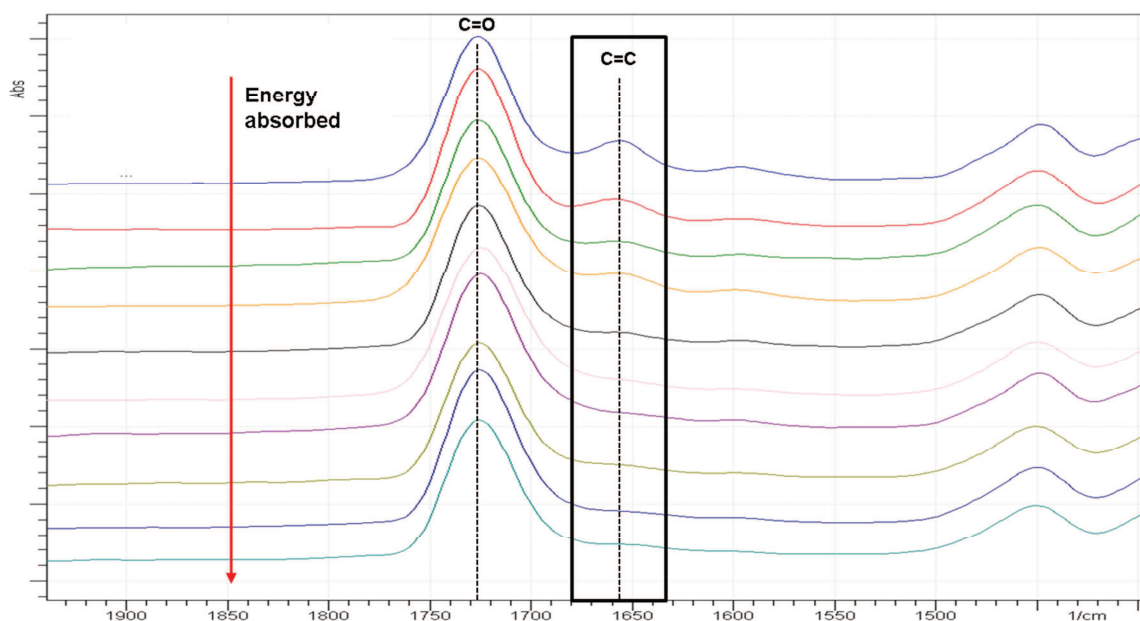


Figure 4.15 FTIR spectra of TWI formulation B for different amounts of energy absorbed measured in a range of 4000-650  $\text{cm}^{-1}$  (Abs – absorbance)

It was found out that the band at  $1630 \text{ cm}^{-1}$  (C=C), attributed to the methacrylate functional group, decreases during irradiation of the sample with the ultraviolet light (Figure 4.15). In order to quantify the amount by which C=C bond peak decreases, it is necessary compare it with a standard peak which does not change with respect to exposure time. For the purpose of this study, two inert peaks were selected as a reference, the carbon oxygen bond C=O ( $1730\text{-}1700 \text{ cm}^{-1}$ ) and C-H peak at  $2870 \text{ cm}^{-1}$  (Figure 4.10).

The size of peak is most frequently determined by area under the peak. The Panorama LabCognition software slices the selected peak area into small trapezoids and then sums the area of these trapezoids. There are two types of area that can be obtained, namely mathematical area (which is algebraic sum of trapezoids) and absolute area (which is the area of sum of absolute values, where absolute value of a real number x is the non-negative value of x without regard to its sign). The software provides also additional information, such as peak height, width, beginning, max and end values. The degree of conversion for the individual spectrum has been calculated based on the equation 4.7 (Tasic S., 2004):

$$X(\%) = \frac{(A_{\text{C=C}}(1630\text{cm}^{-1}) / A_{\text{C=O}}(1720\text{cm}^{-1}))_0 - (A_{\text{C=C}}(1630\text{cm}^{-1}) / A_{\text{C=O}}(1720\text{cm}^{-1}))_t}{(A_{\text{C=C}}(1630\text{cm}^{-1}) / A_{\text{C=O}}(1720\text{cm}^{-1}))_0} * 100\% \quad (4.7)$$

Symbol A indicates the area under peak for the chosen functional groups (C=C with absorbance spectrum at  $1630\text{cm}^{-1}$ , C=O with absorbance spectrum at  $1720\text{cm}^{-1}$ ) before the polymerization and at the given curing time t, respectively. Conversion of

acrylate bond for the different irradiation times for TWI formulation B for the two selected standard peaks is shown in Figure 4.16. Another way to assess the degree of conversion can be done by measuring the decrease in absorbance ratio between selected peaks before and after polymerization (Figure 4.17) according to following equation:

$$Abs_{ratio} = \frac{\left(\frac{H_{C=C}}{H_{C=O}}\right)_t}{\left(\frac{H_{C=C}}{H_{C=O}}\right)_0} \quad (4.8)$$

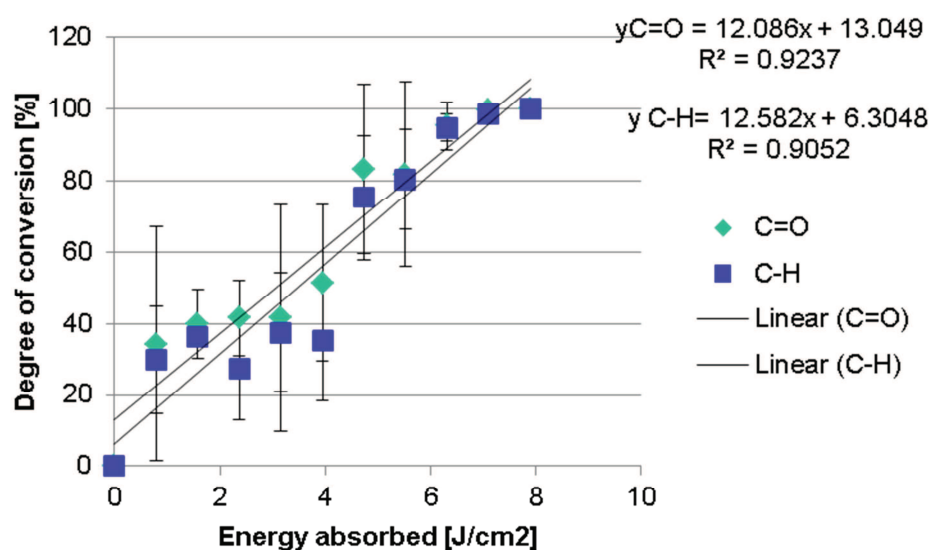


Figure 4.16 Degree of conversion assessment measured based on disappearance of C=C peak– TWI formulation B – C=O and C-H standard peaks

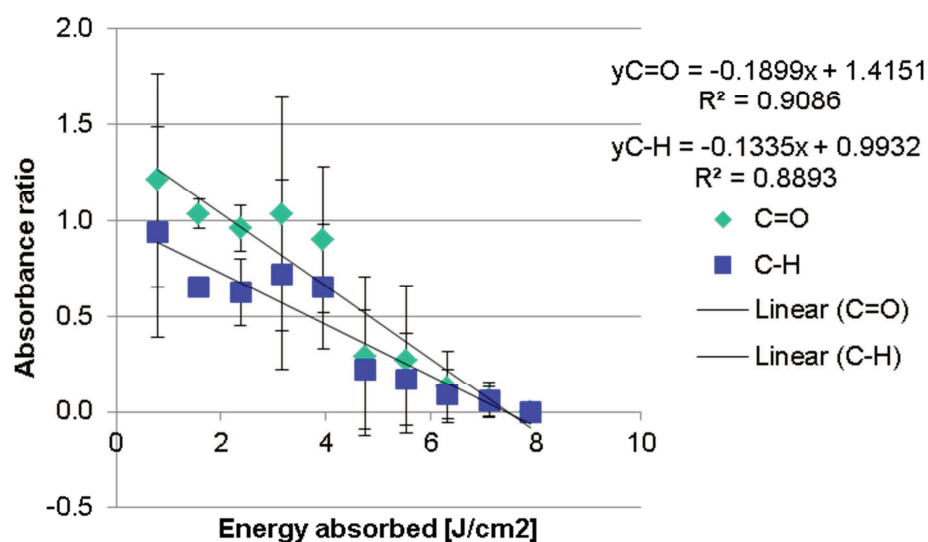


Figure 4.17 Degree of conversion assessment measured based on disappearance of C=C peak – TWI formulation B – absorbance ratio

Calibration curves illustrated in Figure 4.16 show the linearity of formulation B polymerization process. It can be observed that within first stadium of UV curing

process the degree of conversion changes very fast. High values of standard deviations reveal that at this stage reproducibility of the results is very low. The same conclusions arise from the absorbance ratio calibration curves, which confirm the linear manner of UV induced polymerization. Nevertheless, it has to be remembered that degree of conversion for every coating system is strongly dependent upon the thickness of the coating (Figure 4.18). Figure 4.20 illustrates the degree of conversion for TWI formulation B as a function of coating thickness measured with the eddy current principle. As the thickness of coating increases, it limits the penetration of UV light to the aluminium-coating interface. Nevertheless, it can be observed that for the specified energy absorbed, the degree of conversion of coating is not very different for coatings with the thickness in range between 20 and 40  $\mu\text{m}$ . It can be therefore stated that the effect of coating thickness is influencing the degree of conversion by limiting the penetration depth of the UV radiation from the bulb.

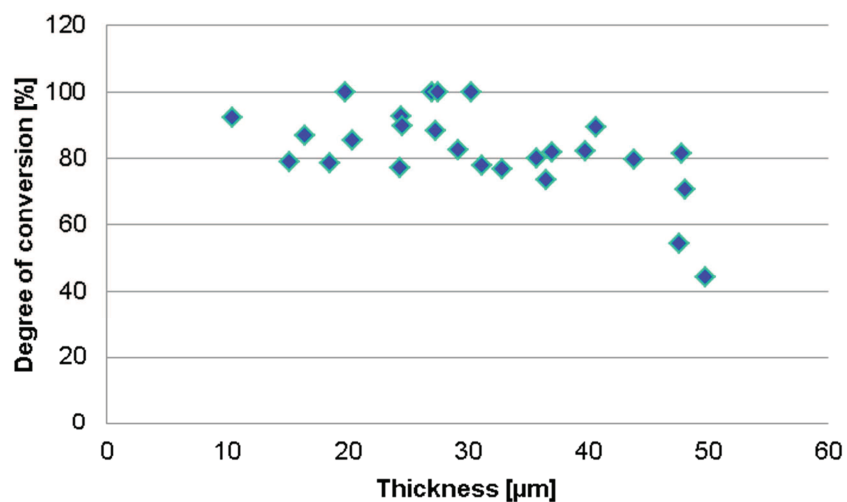


Figure 4.18 Relationship between the coating thickness and the degree of conversion (TWI formulation B, 5.5  $\text{J}/\text{cm}^2$  energy absorbed)

It is generally accepted rule that when polymerization reaches 95%, coatings can be classified as “cured” (Decker C., 2006). Fourier-transform infrared spectroscopy (FTIR) provides a powerful real-time method for monitoring chemical changes. These changes in structural formation can be compared with the evolution of coating properties. Within the UV exposure time, the most significant changes will include progress in mechanical resilience of the coating. One of the ways to track those changes can be done using the nanoindentation technique.

The degree of conversion assessment for TWI formulation B based on changes in mechanical properties is given in Figure 4.19 and in Table 4.10. In total, 10 specimens per condition were prepared and subjected for further evaluation.

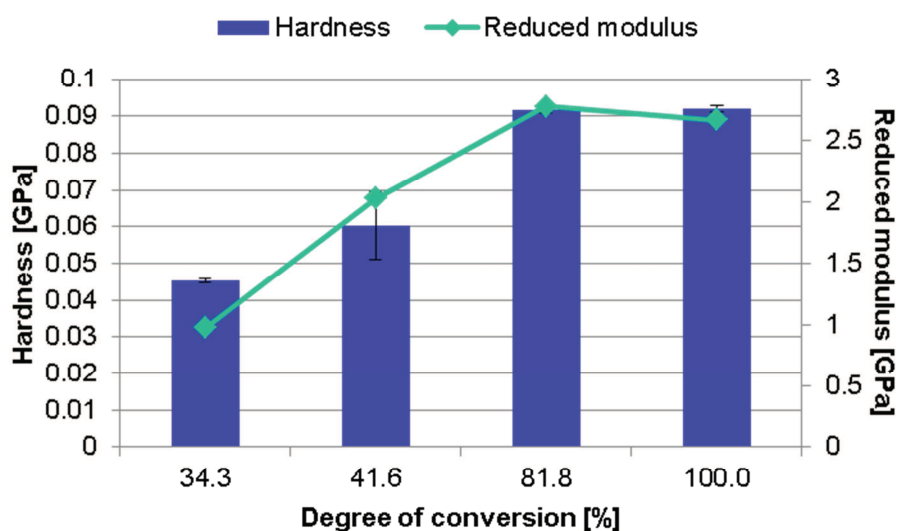


Figure 4.19 Hardness and reduced modulus at 0.1mN load for different degrees of conversion (TWI formulation B)

Table 4.10 H/E and H<sup>3</sup>/E<sup>2</sup> ratio as a function of degree of conversion during UV exposure (TWI formulation B)

Energy absorbed [J/cm <sup>2</sup> ]	34.3	41.6	81.8	100.0
H/E	0.046	0.030	0.033	0.034
H <sup>3</sup> /E <sup>2</sup>	9.70E-05	5.29E-05	1.00E-04	1.09E-04

Figure 4.19 confirms that hardness and elastic modulus of TWI formulation B increases with the longer exposure to UV light (more energy absorbed, higher degree of conversion). A barely visible difference between hardness of samples that reached 81.8 and 100% of conversion (which corresponds to 5.5 and 7.9 J/cm<sup>2</sup> energy absorbed, Figure 4.16) indicates that further UV curing doesn't change this property. Due to the fact that mechanical characteristic of coating is closely related to its chemical rearrangement during UV curing process, these data confirm the results obtained by FTIR. Therefore, it can be assumed that the minimum curing requirements for TWI formulation B will be met, if coating absorbs around 8 J/cm<sup>2</sup> (which corresponds to 100% degree of conversion). With the regard to reduced modulus, the situation appears to be very similar. The highest values of modulus belong to coatings that have been "fully" cured. According to the H/E ratios, the best tribological performance (low E and high H) is performed by the samples that haven't absorbed much energy during UV light exposure and this doesn't correlate with the previously obtained data. It can be probably assumed that at the early stage

of UV exposure, film thickness is stress-free, which results in low elastic modulus.  $H/E$  and  $H^3/E^2$  ratios confirm once again that properties of TWI formulation B don't change anymore when this formulation absorbs more than  $5.5 \text{ J/cm}^2$  of energy. Further investigation regarding degree of conversion can be done based on tracing the changes within optical properties of the coating. Table 4.11 provides the data regarding degree of conversion assessment for TWI formulation B based on changes in optical properties. In total, 4 specimens per condition (each condition corresponds to different levels of energy absorbed, which represents different degree of conversion) were prepared and subjected for further evaluation.

*Table 4.11 Visual appearance as a function of degree of conversion (TWI formulation B)*

Degree of conversion [%]	Gloss 20° [GU]	StDev	Haze 20° [HU]	StDev
0.00	N/A	N/A	N/A	N/A
30.04	120.7	0.78	26.2	0.71
36.40	123.1	0.99	26.1	0.64
27.47	126.3	0.35	26.5	0.35
37.58	123.2	0.92	25.3	0.71
35.30	127.1	1.91	24.8	0.78
75.22	122.4	0.57	16.8	0.78
80.32	113.4	0.14	18.2	0.21
94.86	118.6	0.64	17.3	0.92
98.57	128.7	0.71	17.8	0.78
100.00	123.9	17.2	17.2	10.0

The data of gloss for coatings with different degree of conversion shows very similar values. It is therefore hard to tell at this stage, if these coating properties are not changing anymore despite of amount of energy absorbed. First of all, it can be explained by the coating transparency grade. Since the transparency of the coating is very high, high values of gloss are expected, regardless of the degree of conversion. It can be also explained by the limitation of the depth of penetration of the glossmeter. The glossmeter measures only the light that is reflected from the surface and don't penetrate deeper into the material. Therefore, as soon as the coating is "cured" on the surface, its gloss property will be developed and longer exposure to UV light will not make any difference in terms of gloss. The situation is a little bit different when comes to haze measurements. The haze evaluation is based on how much visible light is diffused or scattered when passing through a material. As a result of that, haze values come not only from the surface, but also from the

area underneath the surface. Furthermore, energy absorbed during UV exposure is dependent upon the depth of penetration of UV light and it decreases exponentially with the depth and the area beneath the surface will always get less energy. It can be easily seen that surfaces with a lower degree of conversion have higher values of haze, which indicates lower quality of surface. Based on haze values included in Table 4.11, it can be stated that for TWI formulation B, visual appearance of the coating reaches its highest value, when haziness of the surface is not higher than 18 HU. Obtained data suggest that optical properties of formulation B are not changing anymore when this coating absorbs more than  $5.5 \text{ J/cm}^2$  (which corresponds to ~80% of degree of conversion).

All the above-mentioned ways for the assessment of the degree of conversion are only applicable for the formulations, in which the disappearance of functional group during polymerization can be traced with FTIR. Therefore, such methodologies for degree of conversion assessment can be used for TWI formulations A, B and E, where the consumption of C=C bond is observed. The situation gets more complicated when FTIR cannot detect changes in any of the active functional groups. . In the case of formulation C and D, FTIR cannot be used any longer as a tool for the assessment of degree of conversion and in this instance there is a need to rely on other methodologies. For the purpose of this study, the reaction with potassium permanganate was used as a replacement methodology for the assessment of the degree of conversion. The reaction with potassium permanganate is based on the oxidation process. If there are residual C=C bonds in the system, potassium permanganate will react with them leading to a change in colour from intensive violet to brown according to the reaction:



Figure 4.20 and 4.21 present the degree of conversion analysis of TWI formulation D done with the use of real-time FTIR and potassium permanganate reaction. Figure 4.20 confirms the applicability of potassium permanganate in the detection of residual reactive C=C bonds in the system.

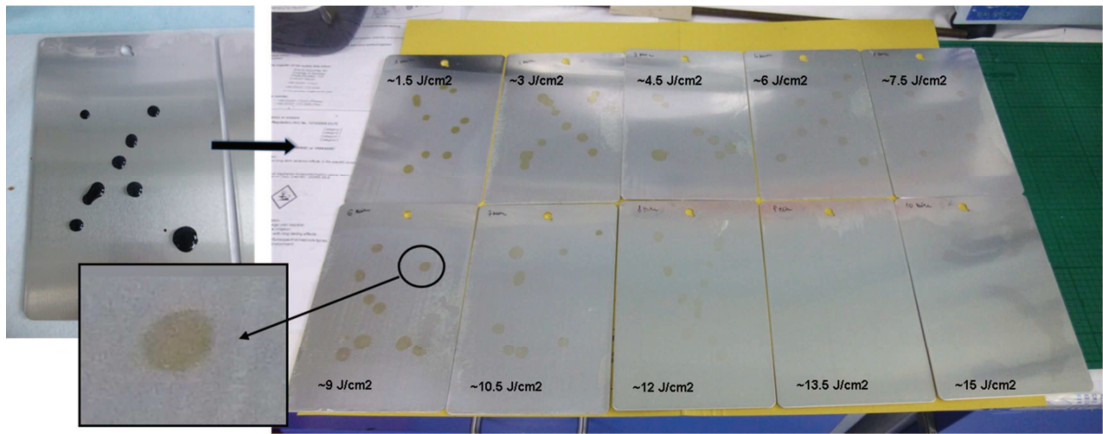


Figure 4.20 Degree of conversion analysis – TWI formulation D – potassium permanganate reaction

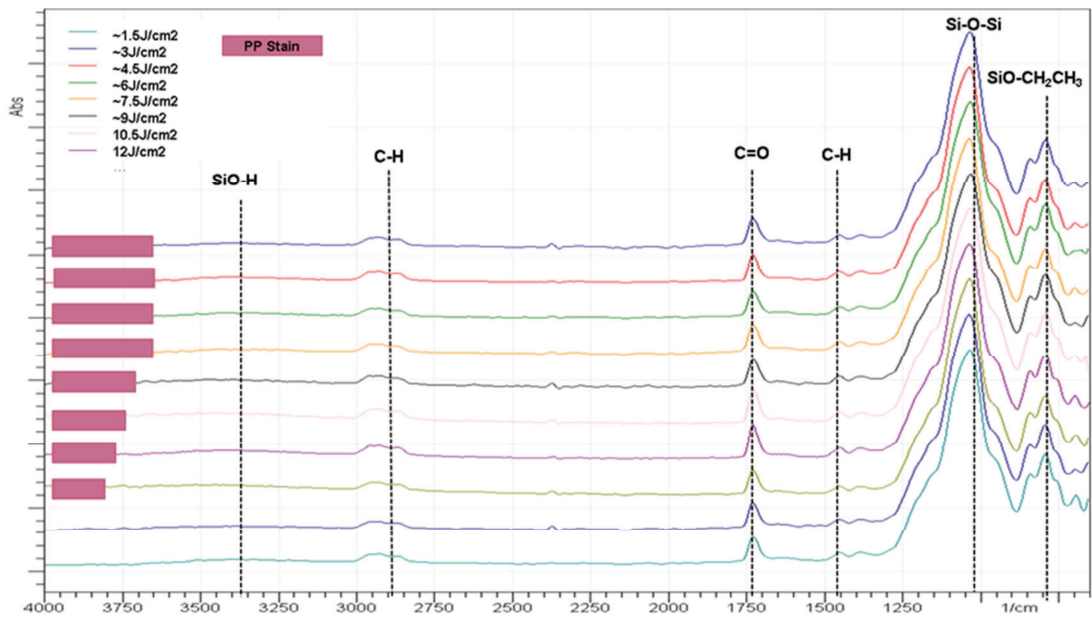


Figure 4.21 Degree of conversion assessment by FTIR and potassium permanganate reaction – TWI formulation D

Figure 4.21 illustrates the comparison of results obtained by measuring the degree of conversion of formulation D with two different approaches. These results prove that real-time FTIR is not capable of tracking polymerization changes for the coatings like formulation D. There is no significant difference between the spectra for different UV exposure times, which indicates that degree of conversion cannot be determined using this method. On the other hand, reaction with potassium permanganate reveals that during polymerization changes in the coating have taken place. Stains from oxidized  $\text{MnO}_2$  appear on the samples, which absorbed less than  $13.5 \text{ J/cm}^2$  during UV light exposure. Nevertheless, the use of potassium permanganate reaction for the assessment of the degree of conversion raises some controversy. The changes in potassium permanganate colour may be the reason of the reaction of any of the other compounds that can be oxidized with  $\text{KMnO}_4$ . Therefore, the same procedure was performed for the other formulation,

in which polymerization changes can be traced with FTIR. The degree of conversion for TWI formulation A has been performed using FTIR and potassium permanganate reaction. Figure 4.22 proves that for selected coating systems reaction with potassium permanganate can be used as a tool for the assessment of degree of conversion.

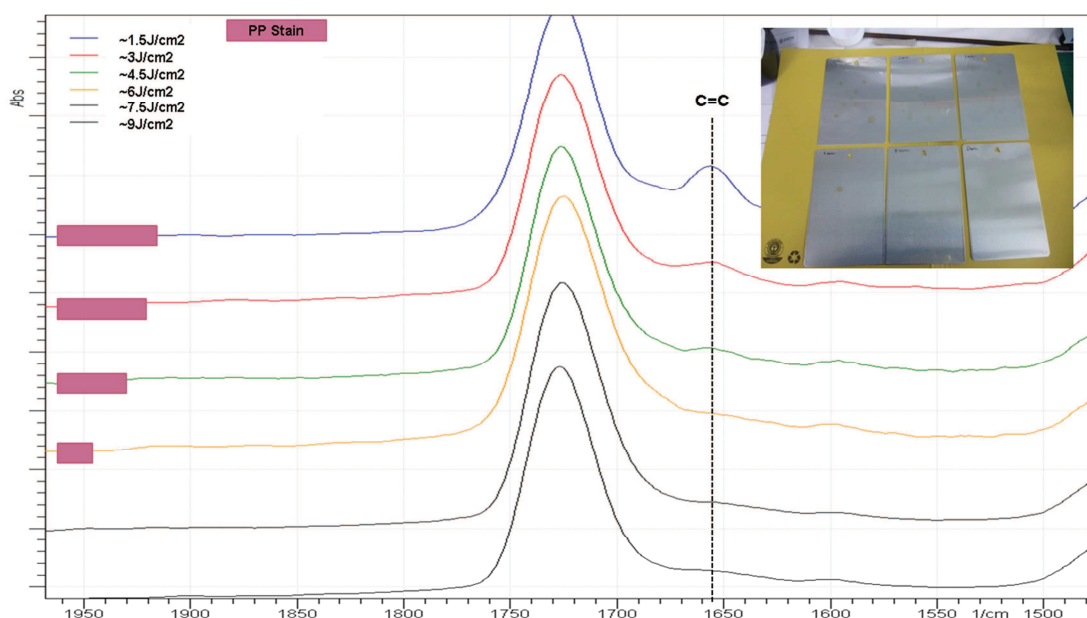


Figure 4.22 Degree of conversion assessment by FTIR and potassium permanganate reaction – TWI formulation A

#### 4.5 Summary

The work presented in this chapter describes the assessment of the degree of conversion in TWI formulations. It was found out that in most of the cases, real-time FTIR is a rapid and accurate methodology for tracing chemical changes that occurs during polymerization. This approach applies to TWI formulation A, B and E, where detection of C=C bond can be a determinant of the degree of conversion. It was found that for TWI formulation B that when this coating absorbs around  $8 \text{ J/cm}^2$ , it reaches its final “cure” stage. The changes of mechanical and optical properties during polymerization seem to be compatible with chemical restructuring. Nanoindentation technique was found to be a good approach for the mechanical assessment of degree of conversion. The hardness and elastic modulus increase with the degree of conversion and become a stable value once the surface reaches some level of chemical transformation. It was found that for TWI formulation B with  $20 \text{ }\mu\text{m}$  thickness that mechanical properties don't change anymore when surface absorbs more than  $5.5 \text{ J/cm}^2$ . With regard to visual appearance of the coating, gloss measurements cannot be used as determinant of the degree of conversion, at least

not in the case of highly transparent coatings. Nevertheless, chemical changes in the coating can be compared with the surface haziness. TWI formulation B develops its optical properties with 75% degree of conversion. Mechanical and optical evaluation of degree of conversion indicates that TWI formulation B doesn't have to be 100% converted, in order to develop its final properties. However, it was decided that for selected coating thickness and UV curing conditions this formulation will be exposed to UV light for enough time to absorb  $8 \text{ J/cm}^2$ .

It was also found out that FTIR cannot be used as indicative technique, when comes to deal with the formulation, in which double bond conversion is not detectable. Therefore, for TWI formulation C and D, reaction with potassium permanganate was used for the assessment of degree of conversion. It was found for formulation D that complete conversion occurs when coating absorbs more than  $13.5 \text{ J/cm}^2$ . However, it was decided that for selected coating thickness and UV curing conditions this formulation will be exposed to UV light for enough time to absorb  $15 \text{ J/cm}^2$ .

Requirements for the amount of energy absorbed during UV light exposure was evaluated only for specific coating thickness and specific types and amount of photoinitiators. Thicker wet film requires more time under UV lamps and therefore, it is crucial to control coating thickness during the process. With regard to thickness evaluation, it was found that measurements done with SEM and eddy current gauge give similar results and these two techniques can be interchangeable.

This chapter provided the methods used for the assessment of the degree of conversion. Prior to evaluation and service, coating needs to be "cured" in order to eliminate failures that might come from the lack of cure. Once "cured" step is fulfilled, coating functional performance can be examined. Due to the fact that lack of adhesion might cause untimely coating failure regardless its final properties, next chapter will focus on investigating ways to enhance the adhesion between aluminium substrate and selected coating.

## 5 ADHESION OF EASY CLEAN COATINGS TO 3003 H14 ALUMINIUM ALLOY

Adhesion of the coating to substrate is one of the main factors that govern durability and lifetime of coating. Surface pre-treatment prior to the coating deposition has a significant effect on the adhesion quality between paint and metal. Very often problems occurring in coating systems are the result of poor surface preparation. Due to the fact that adhesive wear of material may accelerate and reinforce the other types of coating wear, it is important to establish the best possible way to prepare surface. This chapter provides an overview on the surface finish methods. Nevertheless, attention is more focused on the impact of these techniques on the adhesion quality. The overall aim of this chapter is to appoint the most effective available surface pre-treatment technique and to select the best-practise adhesion evaluation method for easy clean coatings.

### 5.1 Introduction – Fundamentals of Coating Adhesion

#### 5.1.1 *Theories of adhesion*

Poor adhesion indicates that coating is not properly attached to the substrate and delamination may occur. A well adhered coating acts like an effective physical barrier, slowing down the material ageing process. According to the Condensed Chemical Dictionary, adhesion is a “phenomenon of the sticking of two surfaces together due to molecular attraction for each other” (Lewis R.J., 2007), while The American College Dictionary states that adhesion as “the molecular force exerted across the surface of contact between unlike liquids and solids which resists their separation” (The American College Dictionary , 1947). It is important to realize that molecular forces or interactions are the fundamental feature of adhesion. Nevertheless, in practise this process is very complicated and it’s hard to refer to only one definition of theory. Adhesion of easy clean coatings to metals can be explained by the model of: mechanical interlocking, electrostatic and adsorption theory (Minford M.D., 1993).

#### **Mechanical interlocking**

This model proposed in 1925 by MacBain and Hopkins postulates adhesion as a result of mechanical keying of the adhesive into the surface irregularities (McBain J.W., 1925). Interlocking adhesives in cavities, pores and asperities of the solid surface prevents the removal of the adhesive from the substrate. Therefore, according to the foregoing theory, a high level of adhesion should be achieved by increasing the interfacial area, for example by increasing surface roughness. It has

been demonstrated several times that even little texturing on a substrate often increases the adhesion bond strength (Evans J.R.G., 1979).

### **Electrostatic theory**

The electrostatic theory came primarily from Derjaguin and co-workers (Derjaguin B.V. S. V., 1967). Authors have suggested that electrostatic and dispersive forces arising from the junction potentials between adhesive and adherent will significantly contribute towards the forces needed to break the bond. In other words, electrostatic forces generated on the double electrical layer at the interface have influence on the adhesion strength (Derjaguin B.V. K. N., 1994).

### **Adsorption (thermodynamic) theory**

The last model of adhesion is generally the most accepted theory. Postulated by Sharpe and Schonhorn is based on the assumption that adhesive will adhere to the substrate because of the interatomic and intermolecular forces established on the interface (Schonhorn H., 1964). Adhesion occurs due to the physically and chemically induced intermolecular interactions, such as ionic, covalent and hydrogen bonds. In this context, strong bonding between adhesive and adherend will enhance adhesion strength. The formation of specific bonding requires an intimate molecular contact at the interface. The process of establishing continuous contact between adhesive and adherent is known as a wetting. Therefore high degree of wetting on the surface can contribute towards stronger adhesion. Sometimes, the bond between the coating and substrate can be enhanced by special adhesion promoter molecules, generally called coupling agents (Plueddemann E.P., 1982).

#### *5.1.2 Factors affecting coating adhesion*

There are several possible sources of weakness in adhesion bonding: surface contamination prior to bonding, poor surface preparation resulting in not proper oxide layer, hydration of the oxide layer, incompatibility of surface preparation technique with adhesive and environment. Environmental considerations are paramount in the adhesive bonding, especially moisture and temperature (Nguyen T., 1995).

### **Coating formulation**

The formulation of coating affects its chemistry and film quality and may be responsible for poor adhesion. Improper coating preparation influences the viscosity

and thus mobility for the adhesive to flow. In extreme cases, due to the high increase in coating viscosity, flow of the coating into the substrate microstructure may be strongly hampered, causing adhesion failure (Martin J. .W., 1994). Besides that, problems with fluid viscosity are responsible for producing a number of voids and pores in the film and therefore, water can diffuse faster to the interface.

### **Coating processing**

All stages in coating processing, from surface preparation to deposition and curing may have an impact on the adhesion quality. Inadequate or insufficient cleaning of the substrate surface will result in mill scale and other surface contaminants (rust, oil, grease, chlorides etc...) that can impair the bonding. Poorly chosen deposition method can prone coating and substrate to mechanical damage, which in turn affects the quality and stability of the interface. Incomplete curing (chemical network formation) results in reduced time for coating to flow and therefore reduced possibilities to fill voids, cavities. Low degree of cross-linking increases chances for water permeability through the surface. On the one hand, if curing process takes too long, thermal degradation of coating will occur (Kunwong D., 1994).

### **Water effect**

Water is considered to be one of the most important environmental factors affecting the quality of adhesion. If the relative humidity is high, deterioration in mechanical properties in coating can occur. Water can also lead to unwanted chemical reactions in the coating as well as the formation of cracks and crazes. Some of the wetting processes are reversible (Ferguson T.P., 2004) (Vanlandingham M.R., 1999), but this reversibility over many cycles causes gradual and permanent changes in structure. There are also irreversible reactions, which tend to be followed by the metal corrosion. In general, Leidheiser and Funke have hypothesized that adhesion failure due to the effect of water occurs by following: water accumulation at the interface, water diffusion and migration through pinholes, pores, defects, and local inhomogeneities, osmotic force, physisorption and condensation reactions and finally destruction of the secondary molecular bonding in the coating (Leidheiser H., 1987).

### **Temperature effect**

Coatings may be subjected to both sub-zero and elevated temperatures during processing and service. Too low temperatures increase the coating viscosity and

reduce its penetration into the substrate (only if the substrate is porous). On the other hand, exposure to high temperatures leads to deterioration in mechanical properties. All organic adhesives degrade at elevated temperatures. The rate of degradation increases with the amount of oxygen present and the primary path for oxygen diffusion is through the coating, which can be relatively high in raised temperatures (Ferguson T.P., 2004).

## **5.2 Experimental**

### *5.2.1 Surface preparation*

In general, with respect to 3003 H14 aluminium alloy finish, there are two types of surface contamination which pre-treatments aim to remove: organic contamination - such as oils, greases etc. and inorganic impurities including rust, oxide films etc. There is a wide choice of surface treatment techniques, which can be divided into three major categories: chemical, mechanical and thermal (energetic). In this study, based on time of preparation, costs and availability, following techniques were selected:

#### **Chemical pre-treatment**

Solvent wiping by hand is the simplest, fastest, and cheapest treatment procedure. This method can effectively wash small areas, but special care needs to be taken during the whole process, because it is easy to re-distribute contaminants. It is advised to change the cloth frequently and wipe the surface in one direction only. In addition, the cleaning solvent should be chosen with care since some of the cleaning chemicals are not compatible with metal and they can harm the surface. For aluminium surface alcohol cleaning agents are the most recommended. Once degreased, the surface must not be touched by hand until coated, in order to avoid grease spots and consequent paint delamination. For the purpose of this project two solvents were selected:

- Acetone – purchased from ReAgent
- IMS - Methylated spirit 99% (74 O.P.) – purchased from VWR

Ultrasonication offers numerous advantages over the manual cleaning methods. Cavitation bubbles generated by high frequency pressure (sound) waves stir the liquid (detergent) and released energies reach and penetrate deep into holes, pores and areas that are unreachable by many cleaning techniques. The removal of contaminants is consistent and uniform regardless the topography of the cleaned surface. Ultrasonication was carried out in thermal bath (Bandelin Sonorex Technik)

in the solution of acetone (purchased from ReAgent). The process was continued for 10 minutes and afterwards, samples were dried in lab conditions for another 5 minutes.

Etching is a controlled corrosion process resulting from electrolytic action between surface areas of different potential (Kehl G.L., 1949). The process involves three steps, transport of reactants to the surface, surface reactions and transport of the products from the surface. Etching is able to clean the surface from contaminants. Additionally, this process removes aluminium oxide presented on the surface in varying amounts or in different forms and replaces it with a new uniform oxide layer. There is a number of etching cleaners and generally they can be divided into three categories: alkaline, mechanical and acid etching. Acid etching removes embedded impurities from the metal and smooth out surface imperfections and in contrast to other etching techniques doesn't change so much the aluminium colour and therefore, this type of etching was chosen in this study. In general, it is a well-established process of deoxidising aluminium substrate, in favour of forming new layer. Taking under consideration compatibility of metal and acid, different acid treatments are selected for different materials. In the case of aluminium, chromic acid etching is favourable technique. The industry standard for this method was established in late 1940s by the FPL (Forest Product Laboratories) (Eickner H.W., 1950). Since then, chromic acid etching was modified several times; nonetheless basic principle of the procedure remains the same. Etching has been carried out according to TWI's etching procedure. Following steps have taken place:

1. Degrease – samples were immersed in the solution of METFIN AK 16 (NST cleaner): non-silicate cleaner that consists of tetrasodium pyrophosphate, sodium hydroxide, sodium metasilicate and distilled water, purchased from Silmid. Immersion was carried out for 15 minutes in thermal bath at 65°C. Prior to the second step samples were rinsed thoroughly in the running tap.
2. Exposures to a sodium dichromate – samples were immersed in sulphuric acid solution in thermal bath at 65°C for 15 minutes. Two reactions take place:



Aluminium oxide is produced and then in the reaction with the sulphuric acid changes to the aluminium sulphate. The first reaction proceeds much faster to

control the amount of aluminium oxide layer on the surface. After the etching procedure, the substrate must be washed with the water. However, it is highly recommended to rinse instead of immerse, because impurities from the surface may contaminate the bath and decrease the quality of adhesion. After etching procedure, samples were dried in 65°C for 30 minutes.

From an industrial perspective anodizing is one of the favoured techniques for aluminium surface preparation, due to its relatively low cost, simplicity, high efficiency and versatility. The purpose of the process is to create on the adherend a porous and stable columnar oxide layer on the top of the simple, planar surface oxide film formed in the etching reaction through the use of a direct current electrical supply. Therefore, anodizing process always follows etching procedure. In the initial stages of anodizing, a dense oxide layer is formed. It has been called the barrier layer due to its high resistance to wear and corrosion. The growth of this layer stops when the high electrical resistance of the oxide reduces the potential of the applied voltage in the electrochemical bath. Future growth is slow and depends on the acid solutions (Brace A.W., 1979). Anodizing is one of the types of electrolysis, where the adherend is the anode and the acid usually acts as an electrolyte. There are a number of acid adherends used in this process and the most popular are: sulphuric acid (SAA), chromic acid (CAA) and phosphoric acid (PAA) (Brace A.W., 1979). Phosphoric Acid Anodizing process (PAA) was established in the mid 1970's in order to improve bond reliability for "metal-bond" structure parts (Marceau J.A., 1978). Today phosphoric acid anodizing is the most widely used anodizing process for general surface preparation of aluminium in aerospace industry. This technique owes its popularity due to the fact that the PAA anodize formed oxide have greater degree of microroughness compared to the CAA and SAA oxides (Venables J.D., 1979).

In this study PAA has been performed according to TWI's anodizing procedure. Prior to anodizing process, all samples have been subjected to TWI's etching routine. Anodization was performed with 10 wt% orthophosphoric acid (purchased from Sigmaaldrich) in the lab temperature (20°C). Anode was attached to the power generator and the voltage was increased gradually up to 10 volts over a period of 60 seconds (the amperage was kept as low as possible). The current was applied for 20 minutes, which is enough time to build up porous oxide film with the thickness around 0.5 µm. After the process, in order to remove residual phosphate from the

surface, all samples were rinsed with the water. Drying was carried out for 30 minutes in 65°C.

### **Non-chemical pre-treatment**

Blast cleaning relies on the mechanical forces obtained by directing and 'blasting' a suitable medium towards the surface to remove the surface contamination and thus clean it (Harris A.F., 1999). Blast cleaning offers the possibility not only to remove the contaminants from the surface, but also to provide special surface topography, in order to achieve good degree of wetting. The parameters, which need to be considered with blasting, are: chosen medium, the particle size, pressure of blast, angles of blast, exposure time and distance between the blast and the adherend. In this study, blast cleaning has been performed using fresh 250 µm (60 mesh) aluminium oxide (purchased from Kramer Industries) with 30 psi applied pressure in a position of 45°, 10 cm away from the nozzle. All processes were carried out in a clean air atmosphere. Prior to grit blasting, all samples were degreased with acetone. After the blast cleaning was completed, ultrasonication was performed (the same procedure as described above) in order to remove any residual media.

In summary, six types of surface preparation were carried out, a total of 10 test specimens were prepared and evaluated per following conditions:

1. Solvent wiping – acetone [Ac]
2. Solvent wiping – IMS [IMS]
3. Ultrasonication [U]
4. Acetone wiping + grit blasting + ultrasonication [Ac+GB+U]
5. Immersion in alkali cleaner + etching [E]
6. Immersion in alkali cleaner + etching + anodizing [E+A]

The influence of the surface preparation methods have been studied with the comparison with plain aluminium samples [PA].

#### *5.2.2 Surface cleanliness verification*

In order to specify a desired level of cleanliness, there is a need to identify the method of measuring surface contamination stage. The method selection should be based on criteria such as type of the contaminants to be monitored, type of substrate being checked, accuracy and precision and level of cleanliness that must be verified. For the purpose of this study Drop Shape Analysis and Fourier-transform Infrared Spectroscopy (FTIR) were chosen as the tools for the verification of sample contamination. The surface of treated aluminium samples were examined using optical microscopy.

## Drop shape analysis

The drop shape analyser (DSA100 from KRÜSS) measures the contact angle of the surface. The process of surface wetting is described in Chapter 2. The advantage of this method is the fact that most of the organic contaminants have hydrophobic character (fats, oils, etc...) and will cause the water droplet to bead up. A contaminated aluminium part will have higher contact angle with water than a pristine surface. Another benefit of this technique is the possibility to define the surface wettability. Nevertheless, this cleanliness verification method is very subjective and not necessarily capable of detecting small contaminants. It is also very time consuming, when comes to measuring large tests area. Moreover, obtained values very often may be not the results of the contamination, but the result of surface topography or other factors.



Figure 5.1 Drop shape analyser from KRÜSS

The optical contact angle measurement system DSA100, from KRÜSS, was used to measure the surface free energy of the coated samples (Figure 5.1). All samples were measured at 10 different points and the average was taken. Deionized water (5 points) and diiodomethane (5 points) were used as standardised test liquids. A fine auto-metered syringe placed 1  $\mu\text{L}$  droplets onto the solid surface of the surface and high resolution image was taken. The droplet volume was small enough that gravitational effects could be neglected. After the equilibrium state was achieved (when there was no visible change in the droplet width), the goniometer was measuring the droplet contact angle each 0.1 s for every 5 s of measurement. The total surface energy was then calculated based on the OWRK method (Owens, Wendt, Rabel and Kaelble) (Owens D., 1969) (Kaelble D.H., 1970).

## **Fourier Transform Infrared Spectroscopy (FTIR)**

FTIR spectroscopy is another technique, suitable for monitoring the quality of surface pre – bond preparation and its principle was described in Chapter 4. The handheld infrared spectrometer (Agilent Technologies ExoScan) configured in diffusive reflectance objective was used to measure the surface of aluminium substrate. Prepared aluminium samples spectra were collected. Background spectrum was also collected before each sample spectrum. One sample spectrum contained 64 scans, taken with the 45° angle of incidence. Spectra were analysed with Panorama software in a range of 650 – 4000  $\text{cm}^{-1}$ . The Savitzky-Golay function has been used as low-pass filter to render visible the relative widths and heights of spectral lines in noisy data without major loss of intensity (smoothing) (Savitzky A., 1964).

## **Optical microscopy**

The light microscope was used to study the surface of prepared test specimen. In this type of microscope, samples are magnified with a convex lens that bends the light rays by refraction. Diverging rays from points within the object (object points) are made to converge behind the convex lens and cross over each other to form image points (focused image) (Keller E., 2006). This distance of the sample from the lens divided into the distance of focused image from the lens determines the magnification. The visibility of magnified samples is dependent upon contrast and resolution. In this study, surface pictures were undertaken with Olympus BX41M metallurgical microscope and they were altered and modified with Essential software.

### *5.2.3 Adhesion measurements*

A total of ten test specimens per each surface preparation technique were fabricated and coated with the TWI formulation B. The degree of adhesion between aluminium and coating was studied. The advantage of the chosen model coating is the fact that formulation B is a coating, which itself poorly adheres to the aluminium surface and all of obtained results will give the true information about the influence of the surface preparation method on the adhesion strength. Generally, adhesion test methods can be divided into two groups, qualitative and quantitative. For the purpose of this study, one representative from each group was selected, qualitative cross cut tape test and quantitative pull – off test. All the measurements were carried out in lab conditions.

### **Cross cut tape test**

Cross cut tape test is one of the most commonly used adhesion measurement method, because is cheap, fast and easy to perform. A lattice pattern was cut on the film down to the substrate (Figure 5.2). Then the test area was brushed in order to remove any residual material, special tape (One-inch (25-mm) wide semitransparent pressure-sensitive tape, supplied by Elcometer, part number T9998894) was applied over the cut pattern and rapidly removed after 60 s with an angle of 180°.

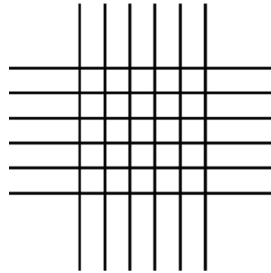


Figure 5.2 *Cross cut tape test cutting pattern*

The rate of adhesion was assessed according to ASTM D 3359 – 97 in the 5 points scale, where 5 points are assigned for a perfectly smooth lattice and 0 points are assigned for the area affected by more than 65%. The main advantage of the tape test is ease of implementation. Also, this evaluation can be classified as a semi-quantitative measure of coating adhesion to the substrate, which may be used in many applications for control or ranking purpose. The predominant limitation of tape test is that it may be not suitable for some types of coatings, like for example coatings with extraordinary repellency. Due to very low energy of the surface, tape may not stick properly and obtained results are not the true values. In addition, there is some concern about achieving reproducibility of the results and using this type of measurement as a guide to performance of the coating under environmental conditions.

### **Pull-off test**

Pull test is the most popular technique in coating adhesion analysis. The method is based on assessing the adhesion of a coating by measuring the tensile stress necessary to detach the coating in a direction perpendicular to the substrate. The adhesion pull-off tester measures the force required to pull a specific diameter of coating away from the metal using hydraulic pressure. The test was performed using the DeFelsko PosiTest analyser (Figure 5.3) according to ASTM D4541. A metal dolly with 20 mm diameter was placed on the test area and stuck to the surface using LOCTITE 4061 (ethyl cyanoacrylate) adhesive. After the adhesive is dried and cured (1h drying in lab conditions), the dolly was attached to the pull-off

equipment, hydraulic pressure was applied and increased gradually until the dolly was completely pulled-off from the surface. The tensile stress required to detach the coating has been shown on the display.

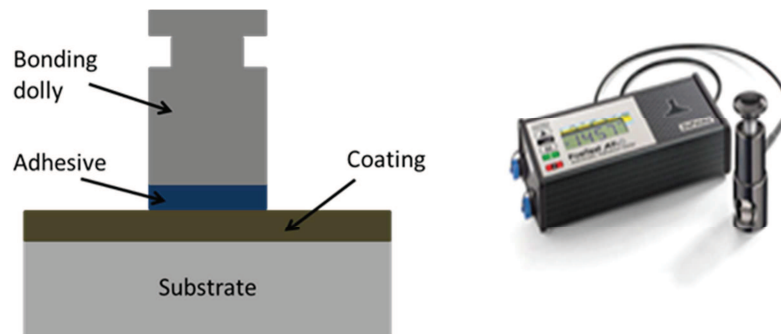


Figure 5.3 Pull-off test setup

## 5.3 Results

### 5.3.1 Surface cleanliness verification

The range of data of the water contact angles for 3003 H14 aluminium alloy prepared in the specified conditions is summarized on box plots in Figure 5.4. Box plots enable to study the distributional characteristics of a group of values as well as the level of the values. In practise, box plots provide a useful way to visualise the range and other characteristics of responses for a large group of data. All values are divided into 4 groups (4Q, four quartiles) and 25% of all values are placed in each group. Furthermore, the median (middle quartile) marks the mid-point of the data and is shown by the line that divides the box into two parts (half the values are greater than or equal to median and half are less). Standard deviations poles are called upper and lower whiskers, which represent values that lie outside of the middle 50%.

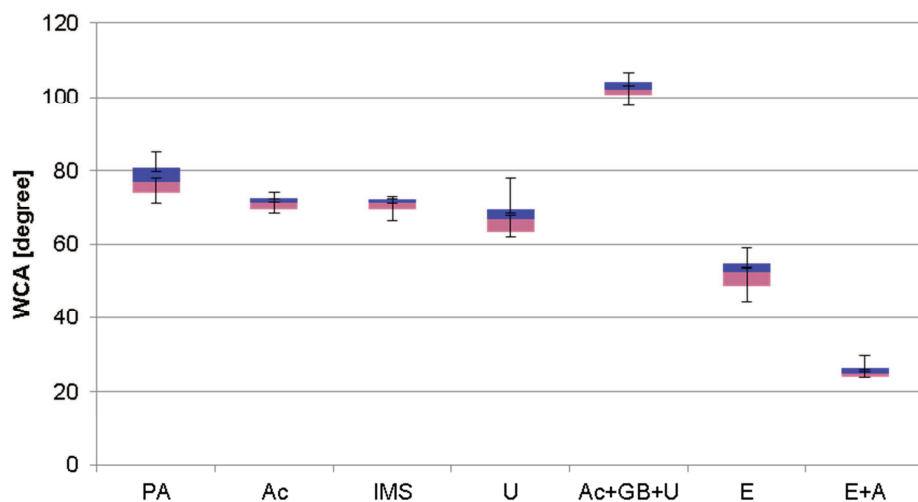


Figure 5.4 Influence of surface preparation technique on water contact angle of 3003 H14 aluminium alloy

All selected surface preparation techniques have some degree of influence on water contact angle. In general, they can be divided onto two groups: the first group corresponds to the pre-treatment techniques that increase the wettability of plain aluminium and the other group represents the methodologies, which decreases water spreading. It can be easily noticed that all chemical pre-treatment methods belong to the first group (where preparation techniques improve the surface wettability), whereas the second group is represented by mechanical cleaning technique (surface wettability is reduced as an effect of surface preparation). While anodizing decrease WCA on aluminium surface by almost 70%, grit blasting helps to increase its value by 30%.

The same routine was carried out regarding diiodomethane contact angle (DCA), in order to measure lipophobic character of the surface. Figure 5.5 shows the range of data of DCA for selected surface preparation techniques (box plot principle).

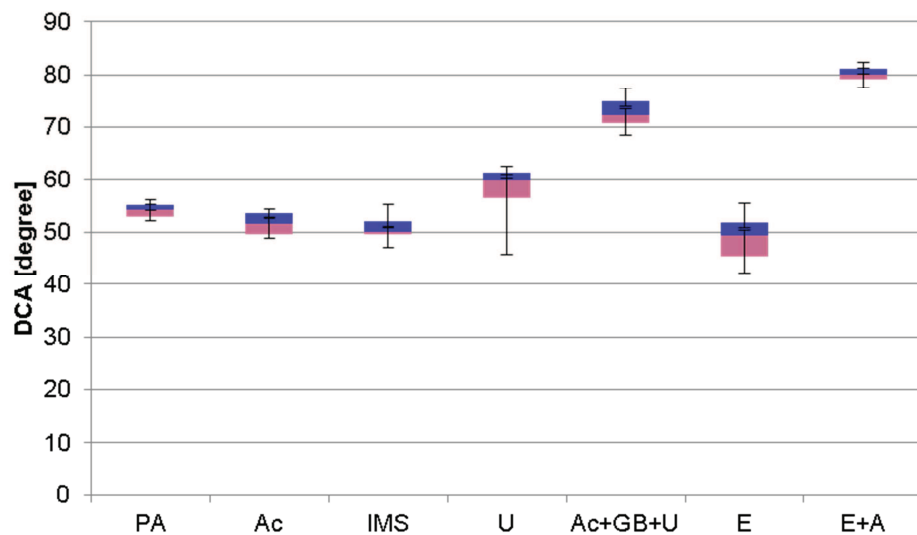


Figure 5.5 Influence of surface preparation technique on diiodomethane contact angle of 3003 H14 aluminium alloy

The obtained results indicate that most of the surface preparation techniques don't have much impact on the contact angle with diiodomethane, since this is not reduced indicating limited wetting. Only anodizing procedure and mechanical pre-treatment enhance the lipophobic character of the aluminium surface. The DCA for grit blasted and anodized surface increased from 54° to 73° and from 54° to 80° respectively.

According to OWRK theory (Eq.5.1) (more explanation can be found in Chapter 2), there are two unknown terms in the equation, namely disperse ( $\gamma_s^d$ ) and polar component ( $\gamma_s^p$ ) of the surface energy of the solid.

$$0.5\gamma_l(1 = \cos \theta) = \sqrt{\gamma_l^d \gamma_s^d} + \sqrt{\gamma_l^p \gamma_s^p} \quad (5.1)$$

Therefore, in order to solve this equation, there is a need to measure the contact angle with two liquids, where one is dominant from a polar perspective ( $\gamma_l^p$ ) and the other from dispersive ( $\gamma_l^d$ ). Diiodomethane has relatively high surface tension ( $\gamma=50.8$  mN/m) and due to its molecular symmetry, this surface tension doesn't have a polar component. On the other hand, water has uneven distribution of electron density and therefore, it has highly polar molecule. Having the values of polar and dispersive components, ORWK equation can be solved and surface energy can be evaluated. The Figure 5.6 represents the average values of surface energy for 3003 H14 aluminium alloy prepared in a number of different ways. Table 5.1 provides information about the effect of surface preparation procedures on the content of polar and dispersive groups at the interface.

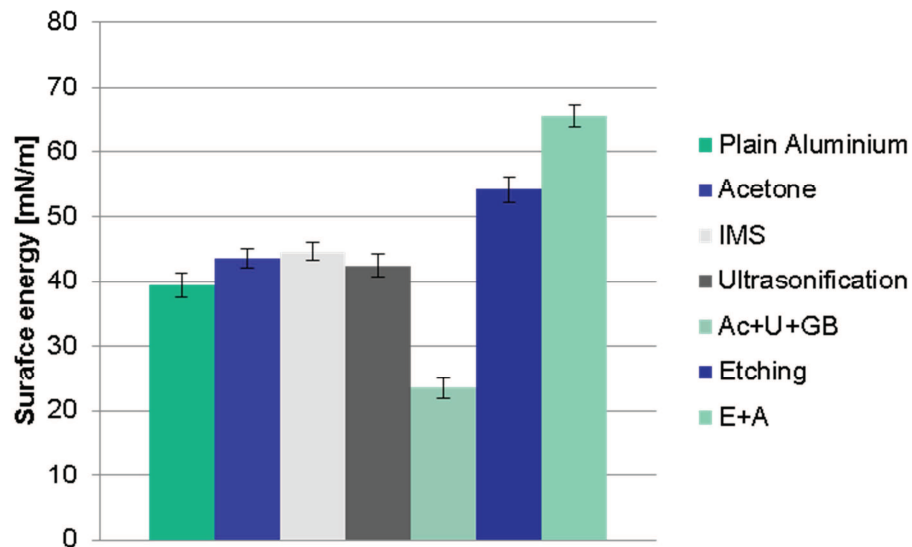


Figure 5.6 Influence of surface preparation technique on total surface energy of 3003 H14 aluminium alloy. Surface energy calculated with OWRK method

Table 5.1 Dispersive and polar components of surface energy after selected surface preparation routines

Surface preparation technique	Polar components [mN/m]	StDev	Disperse components [mN/m]	StDev
Plain aluminium	6.71	0.62	32.74	0.50
Acetone	8.85	0.84	34.81	1.13
IMS	10.74	0.31	33.87	1.70
Ultrasonication	12.63	0.75	29.84	2.05
Acetone+Grit	1.17	0.65	22.32	2.17
Blasting+Ultrasonication				
Etching	18.63	0.52	35.37	4.28
Etching + Anodizing	50.11	0.77	15.41	1.42

Effectiveness of cleanliness methods was further verified with Diffused Reflectance Fourier Infrared Spectroscopy (reflected FTIR). This type of FTIR objective allows collection and analysis of scattered IR energy. Figure 5.7 represents spectra of aluminium samples undertaken after specified surface pre-treatment.

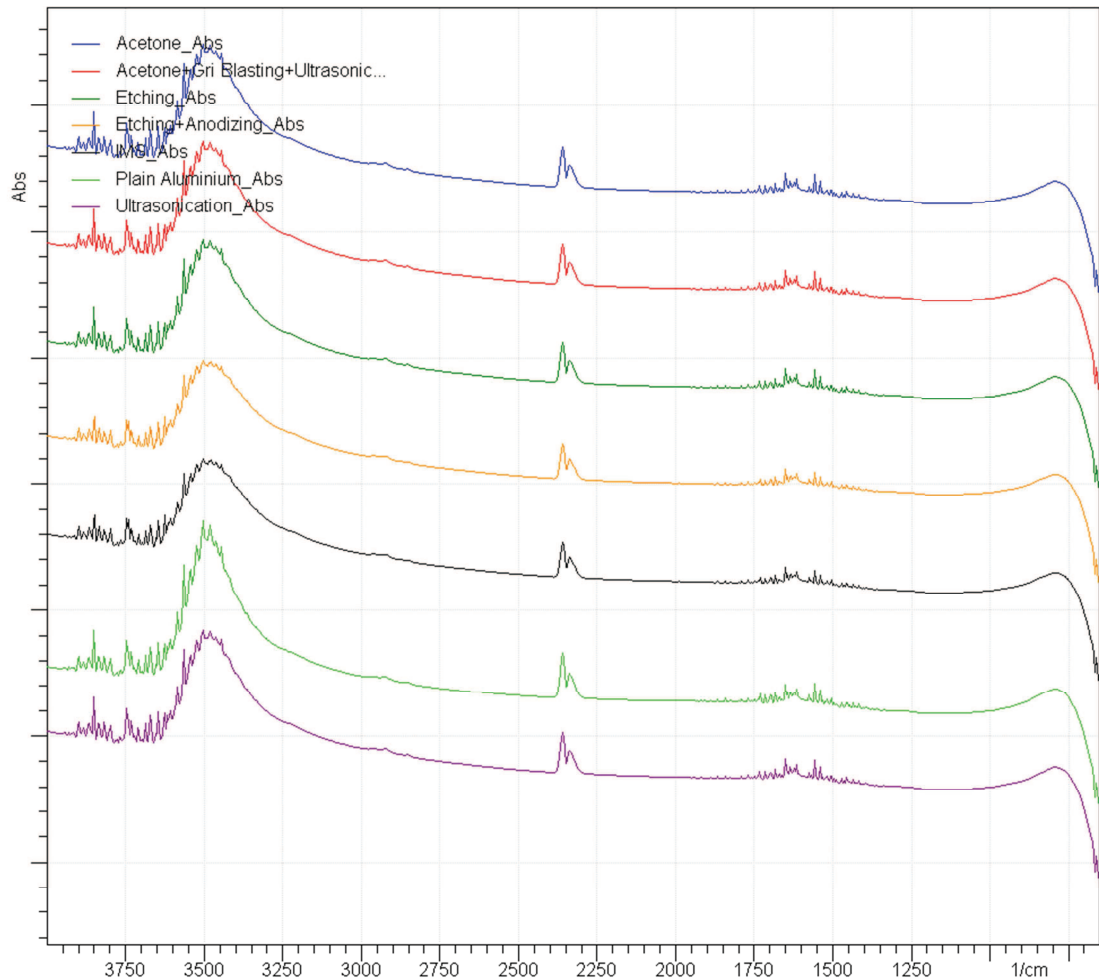


Figure 5.7 Surface cleanliness verification by Diffusive Reflectance Spectroscopy (reflected FTIR, Abs - absorbance)

Surface cleanliness verification done with FTIR has some limitation regarding instrument detection and therefore, low amount of contaminants may be not taken under consideration during measurement. Since all the spectra from Figure 5.7 do not differ between each other, it cannot be excluded that this is a reason of poor detection level of this particular FTIR instrument. To determine the limit of detection for this FTIR spectrometer, series of test samples with different concentration were measured. Industrial methylated spirits (IMS) was dissolved in deionized water with concentration ranging from 4.2 to 42 ppm, in order to check at which IMS level, the instrument will not detect it anymore (Table 5.2).

Table 5.2 Concentrations of IMS dissolved in deionized water

Sample 1	Sample 2	Sample 3	Sample 4	Sample 5	Sample 6	Sample 7	Sample 8	Sample 9	Sample 10
4.2ppm	8.4ppm	12.6ppm	16.8ppm	21ppm	25.2ppm	29.4ppm	33.6ppm	37.8ppm	42ppm

Several spectra of each concentration were collected using  $4\text{ cm}^{-1}$  resolution, 32 spectra were co-added, yielding a 10 seconds data collection time. Obtained spectra are shown in Figure 5.8. With the increase in IMS concentration, two peaks appear in the spectrum. Those two peaks ( $1085\text{ cm}^{-1}$  and  $1045\text{ cm}^{-1}$ ) correspond to C-O stretch bonding from IMS.

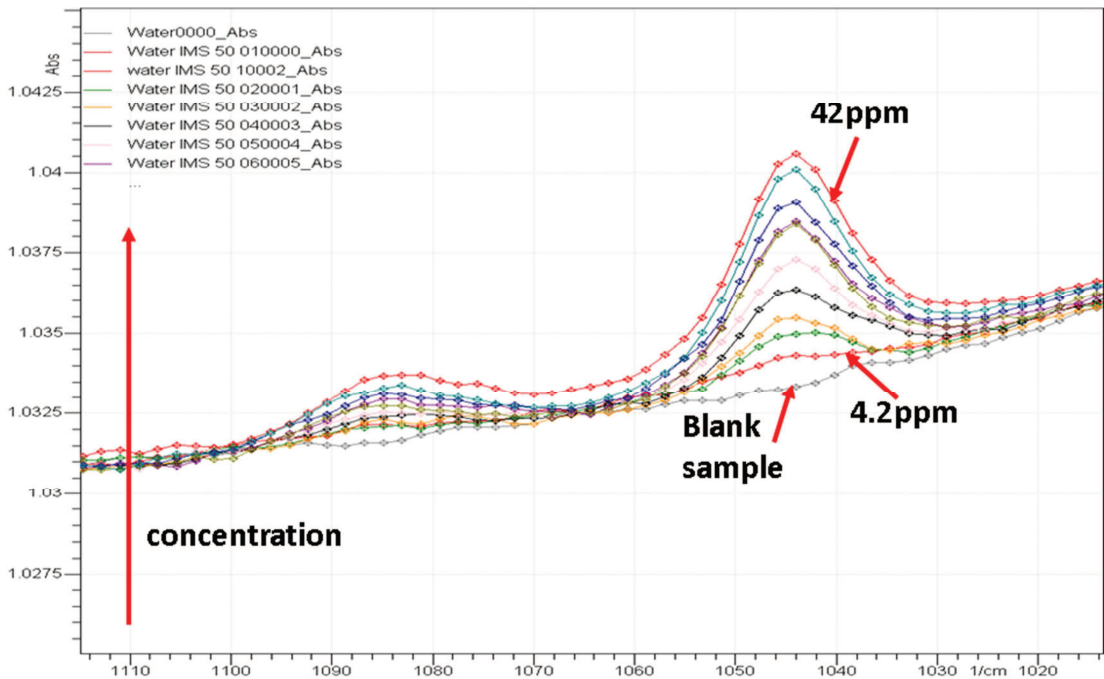


Figure 5.8 Detection limitation for Agilent 4100 ExoScan FTIR (different levels of IMS concentration in water, liquid samples, Abs – absorbance)

### 5.3.2 Adhesion bonding measurements

The second phase of this study was to investigate the influence of surface preparation on the strength of adhesion bonding. A total of ten test specimens per different pre-treatment condition were coated with TWI formulation B and cured under UV lamps until the coating absorbed  $8\text{ J/cm}^2$ , which corresponds to 100% degree of conversion (curing procedures and conditions are presented in Chapter 4). After 24 h from the end of curing, adhesion of prepared samples was studied. Figure 5.9 presents the adhesion class in accordance to ASTM D 3359 – 97 and Figure 5.10 shows adhesion strength evaluated by pull-off tester according to ASTM D4541.

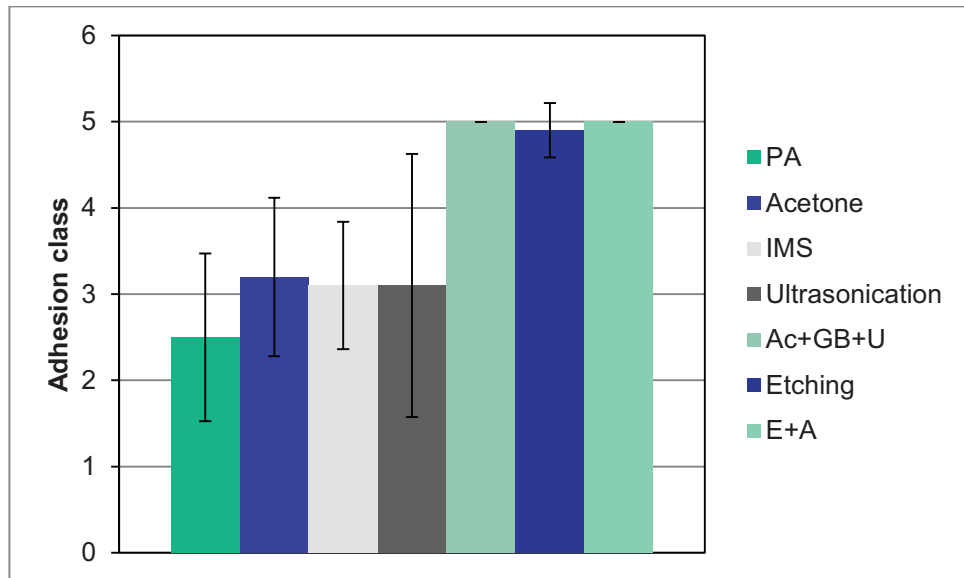


Figure 5.9 The class of adhesion – pristine conditions with accordance to ASTM D 3359 – 97

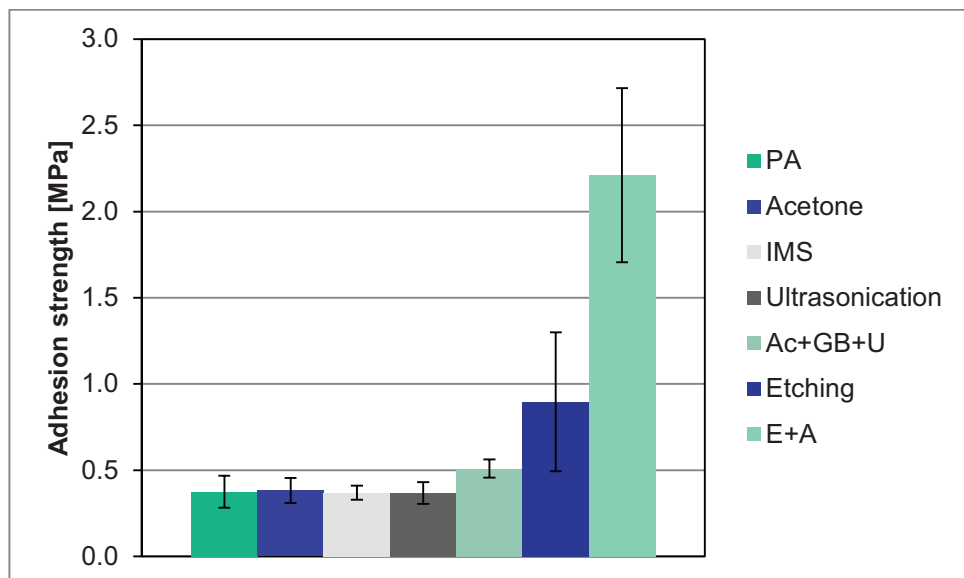


Figure 5.10 Adhesion strength – pristine conditions with accordance to ASTM D4541

As can be seen in Figure 5.9 and 5.10, cleaning surface with solvents or using an ultrasound bath, did not have much influence on the adhesion quality. While all of these techniques slightly increased adhesion class, the results from pull-off test suggest that the bonding strength between coating and aluminium did not change. Grit blasting, etching and anodizing prior to coating deposition turned out to be the most beneficial surface preparation techniques in order to achieve strong adhesion. Investigating the bonding strength of coatings necessitates an artificial ageing program to evaluate their long-term properties. Therefore, the same routine of adhesion analysis was undertaken after selected ageing process. The samples were immersed in deionised water for one week time and left in the lab conditions. Under these conditions, water can reach interface either by diffusion through coating

or by migrating through cracks and voids in coating and eventually reduce the adhesion strength. After designated time, samples were drained with the paper towel, dried for one hour in room temperature and tested. Obtained results are shown in Figure 5.11 and 5.12.

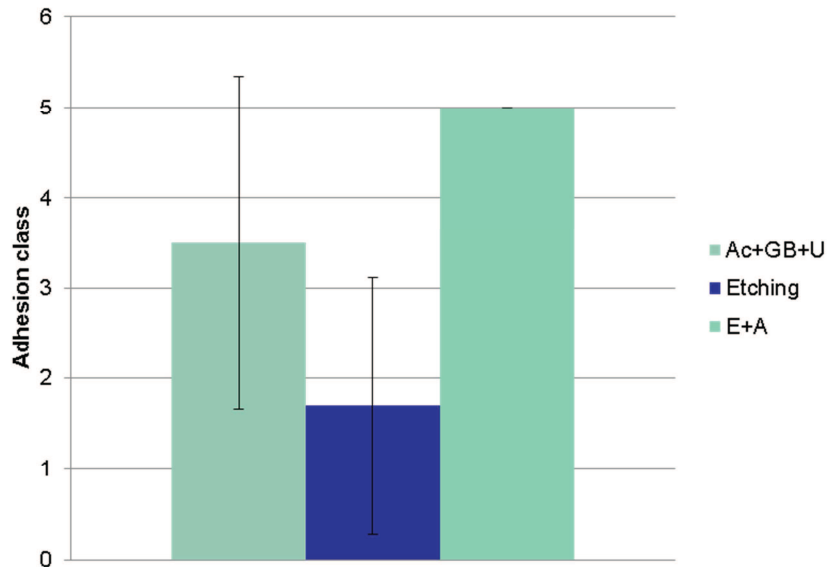


Figure 5.11 The class of adhesion – ageing conditions with accordance to ASTM D 3359 – 97

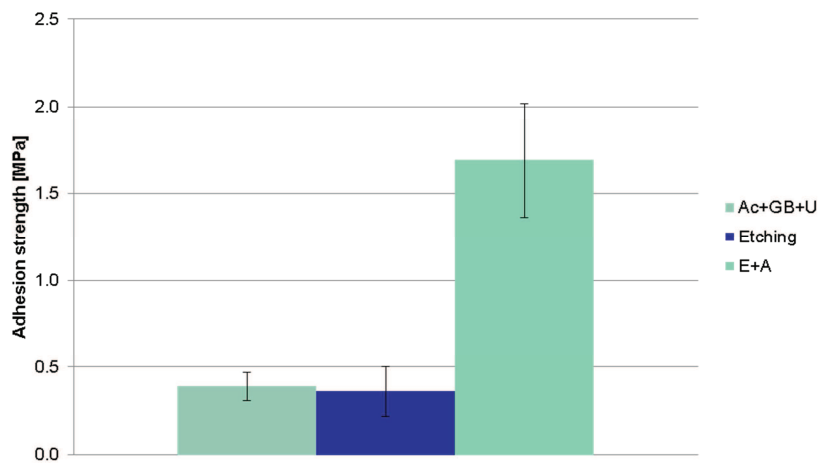


Figure 5.12 Adhesion strength – ageing conditions with accordance to ASTM D4541

Adhesion measurements after ageing conditions confirmed that simple chemical pre-treatments do not guarantee that strong bonding between surface and substrate will be achieved. Enhanced bonding quality can result from mechanically roughening the surface of aluminium through grit blasting or from changed oxide layer through etching. Nevertheless, this study revealed that surface anodizing prior to coating gives the highest values of adhesion strength, even after long-term contact with water.

## 5.4 Discussion

Examining the results from surface cleanliness verification done by drop shape analyser, it can be seen that all of the surface preparation has some influence on structural and surface properties of 3003 H14 aluminium alloy. Those changes can be further referred to adhesion quality between the aluminium and selected coating systems. Surface wettability, as determined by measuring water contact angle on the test specimen can be used to define surface cleanliness. From the Figure 5.4 it can be seen that all selected chemical pre-treatment gives a satisfactory result, in terms of removing organic contaminants. Except the surfaces prepared by grit blasting routine, all samples had the water contact angle lower than 90° and thus they displayed hydrophilic properties. Therefore, it can be assumed that organic contamination is present on these surfaces. Chemical pre-treatment methods involving solvent use, such as simple wiping or more complex ultrasonication result in similar cleanliness level of aluminium surface. The water contact angle of reference samples (untreated aluminium) has the average value of 77.6 degrees. Samples wiped with acetone and IMS decrease this value by 8.13 and 9.19% respectively, while ultrasonication reduces the value by 13.38%. Based on the obtained data, it can be assumed that these surface preparation methods are satisfactory in terms of achieving physical cleanliness. Nevertheless, these processes are insufficient in terms of providing chemical cleanliness, which refers to contamination in the form of oxides and/or silicon. Due to the fact that 3003 H14 aluminium alloy contains both copper and silicon in its composition, an etching process is expected to give more satisfactory results. In this study, it has been found that etching of aluminium decreases water contact angle value by 32.64%. Etching process followed by anodizing routine gives the most satisfactory results, regarding the cleanliness level of the surface. It can be explained by the role of freshly made oxide layer on the aluminium surface. While etching removes the old layer of oxide, anodizing process stimulates the aluminium to undergo further oxidation. When the power is supplied, electrons are pulled from the aluminium into the solution causing the metal to react with water to form an oxide layer on anode, following reactions are taking place:



At the cathode, hydrogen gas is formed and following reaction takes place:



Increased adsorption of ions would result in increased adsorption of water to the surface, and make the surface more hydrophilic, decreasing the surface tension at the interface. This would manifest as an increase in contact angle of the hydrophobic liquids.

The low values of the surface energy on abraded aluminium panels ( $\gamma = 21.89$  [mN/m]) can be explained as a result of change in surface topography (Figure 5.13), which can be correlated with the increase in contact area between the solid/liquid phase. It can be easily observed in Figure 5.13 that only mechanical pre-treatment introduces significant changes to the aluminium structure. As can be seen in Figure 5.13, among selected surface preparation procedures grit blasting is the only one method that changes surface topography on a macroscopic scale (anodizing changes the topography too, but on a microscopic scale).

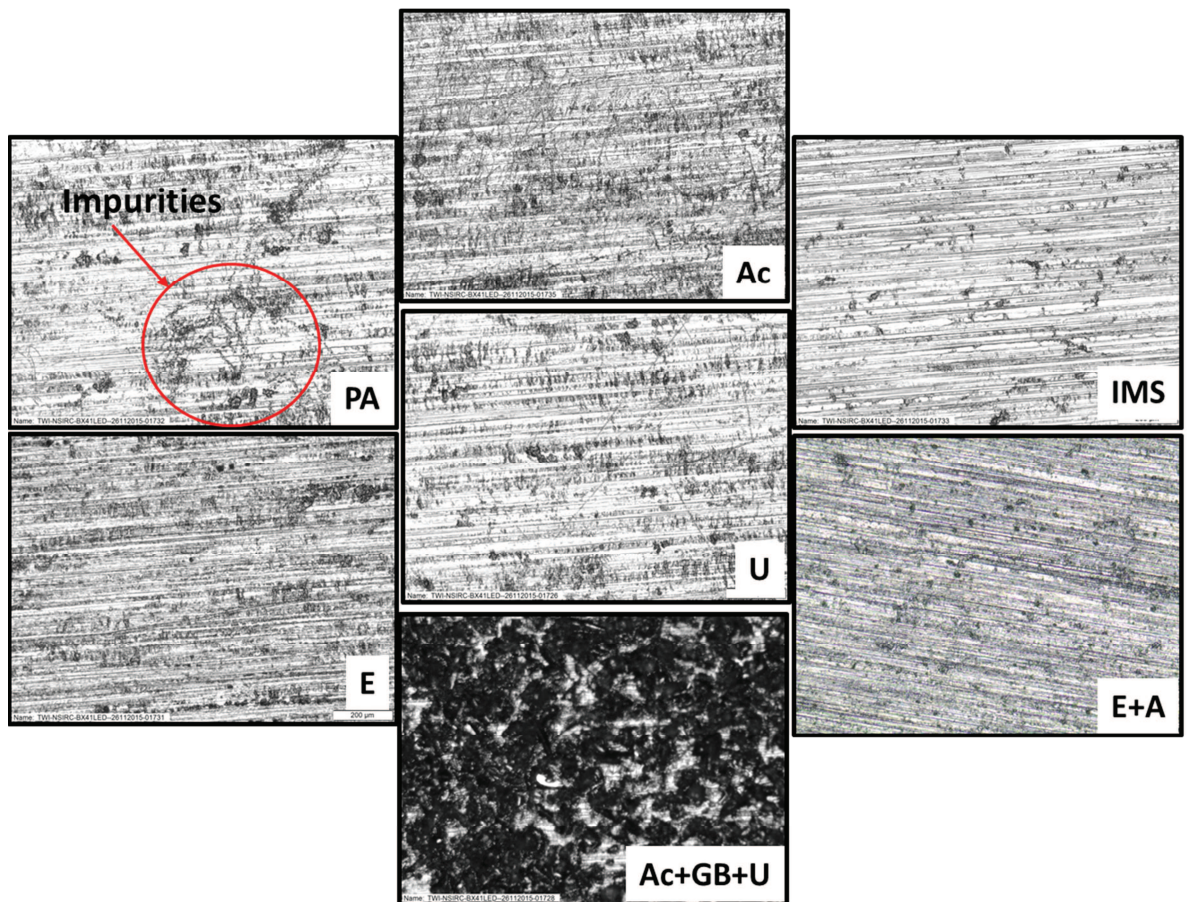


Figure 5.13 The influence of surface preparation on the surface topography (images taken with undertaken with Olympus BX41M metallurgical microscope, 10x magnification)

To understand the chemical nature of the final effect of the surface preparation, further analysis was carried out using FTIR. From the Figure 5.7 it can be read that selected surface preparation have comparable effect in removing organic

contamination. Spectra for different preparation methods have exactly the same shape. Moreover, spectrum for untreated aluminium coincides with spectra for treated aluminium. Based on the obtained results, few explanations can be made. First of all, it is possible that there was not any organic or inorganic contamination on the samples and that's why the spectrum of untreated sample is exactly the same as the spectra of pretreated samples. Nevertheless, it is hard to clearly state that there was no organic contamination on the untreated samples. Optical microscope measurements presented in Figure 5.13 revealed that there was some impurity on untreated aluminium. Therefore, obtained results can be related to the low sensitivity of measuring device that cannot detect small amounts of contaminants. For the reference purposes, contamination detection sensitivity was assessed by tracing the amount of IMS dissolved in deionized water. It was found that for a quick 10 second measurements, the lower level of detection can be found at 4.2 ppm level. Another possible thing that might have happened, it's related to the way how measurements were performed. For the purpose of this study, only small areas of test specimens were scanned with FTIR and therefore, it is possible that these selected areas were free from contamination. More sophisticated surface cleanliness detection could have been done with use of X-ray photoelectron spectroscopy. Nevertheless, contamination detection with XPS is beyond the scope of this thesis.

Adhesion between selected coatings and the 3003 H14 aluminium alloy was assessed based on three model theories, namely mechanical interlocking, electrostatic and adsorption.

According to adsorption theory, stronger adhesion can be achieved by increasing the polarity of the surface and thus, by improving the wettability. Comparing the polar component in surface energy with the adhesion strength, it can be easily seen that increased wettability of the surface prior to bonding benefits towards stronger adhesion. Figure 5.14 shows that in most of the cases durable bonding at the interface can be identified for those surfaces with greater bond polarity.

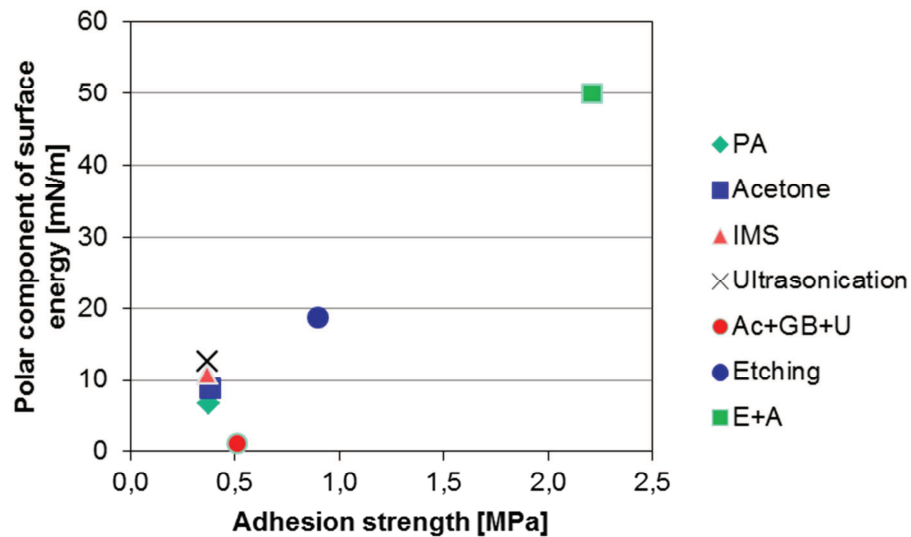


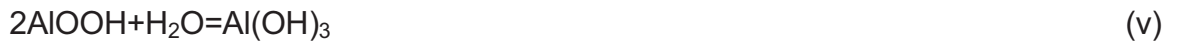
Figure 5.14 Influence of bond polarity on the adhesion strength

Obtained data definitely contributes to the adsorption theory of adhesion. Nevertheless, it can be seen that in one case this theory does not apply. When it comes to the surface prepared by mechanical treatment, stronger adhesion can be achieved even though polarity of the surface it's not so high. Such behaviour of the surface brings in mind another adhesion model, namely mechanical interlocking theory.

According to mechanical interlocking theory, stronger adhesive bonding can be achieved, when the contact area between the surface and adhesive is maximized. Grit blasted surfaces display the larger contact area than the control surfaces due mechanical anchoring between the coating and aluminium and prevents the removal of adhesive from the substrate. Surface texturing can also results in availability of more area for intimate contact and thus, better adhesion can be achieved without changing the polarity of the surface.

The highest adhesion strength was achieved for the surfaces, which were prepared by etching or etching + anodizing process. This explains the importance of the role played by the oxide layer on the aluminium substrate and highlights the final model of adhesion, namely the electrostatic theory. This theory states that if two surfaces are placed in contact, electrons will be transferred from one to the other, which as a result will affect the bonding quality between these two surfaces. On the interface, electrical double layer will be formed and benefits towards the attractive force. It is well known that charge on the aluminium surface is strongly dependent upon its oxidation level. Furthermore, this oxide layer charge will be responsible for hydrophilic ability of the surface. As was shown in early 1935 by Verwey, aluminium

oxide layer created in anodization process, has the tendency to further react with environment, resulting in hydration of outer layer (Verwey E.J.W., 1935). This outer oxide layer is believed to exist in several different forms of hydration ( $Al_2O_3 \cdot xH_2O$ ), depending on the exposure condition, especially in humid environments (reaction iv and v):



Presence of water molecules around aluminium oxide layer increases surface polarity and as a result of that, the surface displays highly hydrophilic character. Nevertheless, it needs to be remembered that longer exposure of aluminium oxide to hydration, results in formation of weak boundary layer, including cohesively weak boehmite ( $Al_2O_3 \cdot 3H_2O$ ) Therefore, it is crucial to strictly control the time between anodizing and coating deposition.

A high degree of adhesion of anodized aluminium can be also explained by the theory of formation of porous aluminium oxide layer (Veneables J.D., 1984). This layer usually exhibits a uniform array of hexagonal cells, where each cell contains a cylindrical pore (O'Sullivan J. P., 1970). The formation of pores at the interface contributes once again towards the mechanical interlocking adhesion model. Textured aluminium oxide is capable of anchoring the coating inside the pores and therefore, it helps to increase the adhesion even for those materials, which are not able to form the bonding with aluminium substrate.

Anodizing is an extensively exploited technique of aluminium surface preparation. The resulting aluminium oxide layer is very resistant to chemical attack, and is only really affected by strong acids or alkalis. In addition, the whole process is easy and quite cheap. However, one of the main disadvantages is that this technique requires multiple steps and is time consuming. In addition, there are number of parameters, which should be controlled carefully, such as applied voltage, temperature, concentration and time of anodizing.

All the adhesion measurements were performed using two techniques, namely semi-qualitative cross-hatch and qualitative pull-off. Nevertheless, it was found that in the case of measuring easy clean coatings, cross-hatch testing may not be adequate. Cross-hatch testing involves the use of tape and therefore, that tape may not stick properly to highly repellent surface. Similar problem appears in the case of pull-off test and poor adhesion might be expected between the coating and the dolly with adhesive (setup illustrated in Figure 3). Nevertheless, some actions were

undertaken in order to enhance the adhesion strength between the coating and adhesive. In this case, mechanical interlocking theory was used and implemented. The surface topography was changed in two places, surface of the coating was slightly abraded with 240 grit abrasive paper and the bottom of the dolly was grit blasted with 250  $\mu\text{m}$  aluminium oxide grit (Figure 5.15). Such modifications in a testing routine helps to increase the adhesion between the adhesive and the coating and therefore, dolly can be properly stuck to the test specimen.

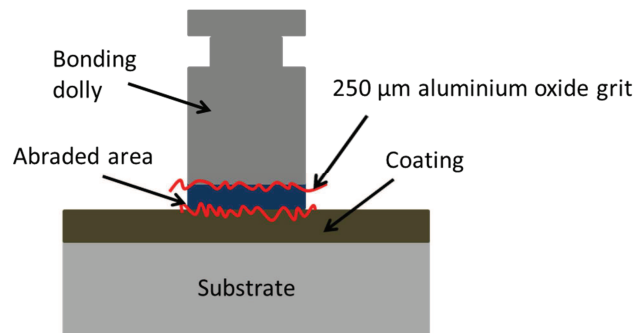


Figure 5.15 Pull-off test setup – version for easy clean coatings

## 5.5 Summary

Effective bonding between dissimilar materials, such as aluminium and coatings is crucial in order to optimise the lifetime of the coating. In this chapter, different chemical, electro-chemical and mechanical pre-treatments designed to modify the surface aluminium to enhance bond quality were studied. It was found out that "satisfactory" bonding cannot be achieved for the aluminium surfaces, which were just degreased. Further surface modification is generally regarded as being required to increase bonding durability. Surface texturing by grit blasting helps to anchor the adhesive in the voids and pores at the interface. This results in stronger adhesion even after the surface was subjected extended periods of exposure to water. The most durable bond between the substrate and the coating was achieved with the phosphoric acid anodizing procedure. The success of the anodizing procedure can be explained by different adhesion models. First of all, freshly made stable oxide is considered important as this can prevent or minimise the formation of a relatively weakly boundary layer. Secondly, the formation of a porous oxide layer changes the structural topography which favours mechanical keying and provides an increased area over which interfacial interactions can occur. Thirdly, the natural tendency of oxide layer to undergo hydration results in increased hydrophilic character of the surface. Such strong interaction between the anodized aluminium and the coating

help to prevent the displacement of the coating by water and therefore, help to enhance its lifetime.

It was also found that adhesion of the coating to aluminium substrate cannot be explained by only one theory of adhesion. All three presented models have some influence on the quality of bonding. As has been found, stronger adhesion can be achieved for those surfaces, on which two or/and more theories of adhesion applies. Therefore, it may be worth to plan surface preparation procedure in manner that allows increasing wettability, increasing contact area and helps to build up effective double layer on the interface at the same time.

With regard to surface cleanliness verification, it was found that both of the methods investigated, surface energy measurements and FTIR, can be used to determine the surface quality prior to the bonding. Nevertheless, it should be remembered that the use of only one methodology may not be enough to obtain necessary information. Besides that, these two techniques for surface cleanliness verification measure only small parts of test specimen and in case of large areas, surface scanning takes a long time and from industrial point of view, such solutions may not be viable.

With regard to adhesion measurements, it was found that the reliability of the cross-hatch test methodology may not longer be applicable for easy clean coatings. The adhesion of highly repellent surfaces can be still measured using standard pull-off test. Nevertheless, some modification needed to be done in the test setup, including increasing the contact area at the interface of the coating.

In this chapter, the knowledge regarding adhesion of easy clean coating system to aluminium alloy 3003 H14 was increased. Due to the fact that etching + anodizing procedure gave the most satisfactory output, it was decided to use this surface preparation routine before the application of all TWI coatings. It was decided as well to use only pull-off test when measuring the adhesion of highly repellent surfaces. Once coating is “cured” and adheres to aluminium substrate, it can be subjected for further evaluation. Following chapter describes validation of selected coating systems with accordance to new assessment methodology.

## 6 ADVANCED EASY CLEAN COATINGS – PERFORMANCE CHARACTERISTICS

This chapter provides performance characteristics evaluation for selected coating systems. Material assessment was conducted with accordance with the novel approach that was introduced in chapter 4. The purpose is to assess the influence of the structure and composition on the coating properties, especially mechanical durability and repellency over the lifetime of the surface.

### 6.1 Introduction

In order to improve the potential of easy clean coatings, it is essential to better understand their behaviour. This understanding will help to complete the classical composition, structure, property relationship. These factors act synergistically and it is not just the composition, which determines the coatings final properties (Danışman S., 2014) (Gangopadhyay S., 2009) (Stein J., 2003). Functional performance is also directly link to the structure and differences in properties can be achieved by changing surface topography (Figure 6.1).

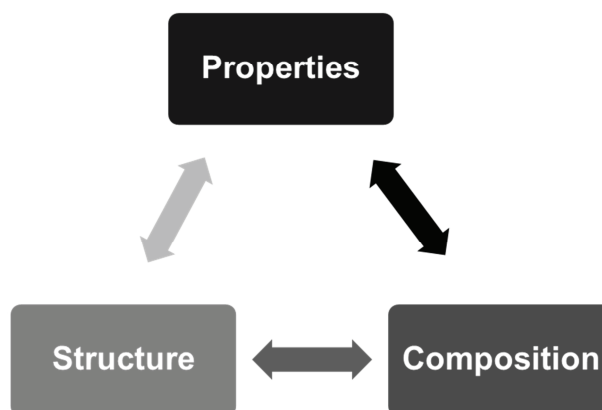


Figure 6.1 Diagram representing the relation between coating composition, structure and property

New advanced coatings and surface treatments that contain nanoparticles in their structure are generally believed to offer the potential to improve the performance of material and therefore, to fill the gap that currently exists on market. Properties of coatings containing nanoadditives can be tailored twofold. On one side, they can be tuned due to the ability to change roughness level by changing the size and loading level of nanoparticles. On the other, nanoparticle functionalization enables a lot of possibilities in terms of changing properties by composition modification.

The purpose of this chapter is to establish the relationship between composition, structure and property for selected coating systems. Six TWI formulations (A, B, C,

D, E and F) were prepared (the resin formulation information can be found in Chapter 4) and deposited onto aluminium substrate (made from 3003 H14 alloy) using 20 µm bar coater. Prior the bonding, aluminium panels were prepared by TWI etching and anodizing procedure (specification is provided in chapter 5). Each system (resin + substrate) was cured under UV lamps until sufficient amount of energy was absorbed (curing regimes are provided in Chapter 4). The composition and structure of the prepared coatings was investigated by determining surface chemistry and surface roughness. Material properties that are investigated within this chapter are combined according to the new assessment methodology and include: adhesion strength, wetting characteristics, visual appearance, and mechanical and chemical resistance.

## **6.2 Experimental**

### *6.2.1 Materials*

Several TWI fabricated coatings were evaluated in this study, referred as formulation A, B, C, D, E and F. Materials description and preparation procedure can be found in Chapter 2 and 4. Two commercial easy clean products were selected and subjected for future evaluation for comparison purposes namely, GP101 (COO-VAR GP101 Anti-Graffiti System from TeaMac) and Never Wet (liquid repellent treatment from Rust-Oleum).

### **Surface preparation**

Aluminium panels (size 102x152x0.6 mm) from Q-lab, made of 3003 H14 alloy were used as model substrate in the following study. In general, two types of pre-treatment were used in order to prepare surface prior the coating:

- Phosphoric acid anodizing (PAA) Boeing procedure (TWI's etching + anodizing procedure) – all TWI's formulated coatings (procedure details described in Chapter 5)
- Wiping with IPA (purchased from ReAgent Chemicals) – commercial products (surfaces were prepared according to manufacturer's application guidance)

### **Deposition**

TWI's coatings were deposited onto aluminium by spiral bar coaters (20 µm thicknesses, purchased from Elcometer). GP101 was applied on the surface by brushing (as recommended by the manufacturer's guidance). Never Wet was

deposited by spraying in three stages process; two layers of base coat were applied followed by the addition of one layer of top coat.

### **Curing/Drying**

All TWI's fabricated materials are UV cured coatings and therefore, they were cured under UV lamps (details about UV curing system and TWI's coatings curing specifications can be found in Chapter 4). GP101 was dried 2 hours in lab conditions (according to manufacturer's guidance). Never Wet coating system was air dried for 15 min for each of base layers, whereas top coat was left for 30 min.

### **Surface chemistry**

Two types of surface characterization techniques were used in order to investigate composition and morphology of prepared coatings namely Fourier Transform Infrared Spectroscopy (FTIR) and Scanning Electron Microscopy (SEM).

FTIR techniques were explained and described in detail in Chapter 4. Spectra were collected with the ATR objective, taken with 45° angle of incidence, with the resolution of 4 cm<sup>-1</sup>. Prior to test specimen measurement, 32 scans were used to collect the single-beam background spectrum. FTIR spectra of coating system of 32 scans were coadded and averaged to obtain single-beam spectrum.

For SEM measurements, small test specimens (1x2 cm) were cut from the coated Q-panel using an aluminium guillotine and a very thin layer of gold sputter coating was applied onto the samples in order to prevent charging during the experiment. An accelerating potential at 20 kV was set for all types of SEM samples. Backscatter and secondary electron detectors were used to study surface topography. Surface chemistry was analysed with SEM/EDX (Energy-dispersive X-ray spectroscopy).

### **Surface roughness**

Wear resistance of material is not an intrinsic property, but depends on coating composition, coating-substrate system, surface roughness and surrounding environment (Luoa D.B., 2011). Therefore, control of surface texturing is necessary in order to establish the role of roughness on the final coating system performance.

For the purpose of this study, surface roughness was measured with an Atomic Force Microscopy (AFM) and surface profilometer (Talysurf Intra from Taylor Hobson). The AFM (Digital Instruments/Veeco Dimension 3000) was operated in tapping mode. In this mode the cantilever is oscillated close to its resonant frequency, while the amplitude of the oscillation is measured. As the cantilever

approaches the surface, the interaction will change the resonant frequency. This change in amplitude is further measured and translated into an image.

The Talysurf Intra profilometer measured the test specimen on a length of 6.1 mm. Roughness measurements data was filtered with accordance to ISO 4288 (ISO 4288, 1996). The filter removes the larger wavelengths that make up waviness and form to leave just roughness. As part of this process the data was broken up into 5 portions (5x0.08 mm).

### **Wetting characteristics**

Three drops of distilled water and three drops of diiodomethane were placed onto the surface of test specimen by fine auto-metered syringe. The measurement of the contact angle was undertaken using optical methods after which an image of the droplet was captured (Figure 6.2). Average values of WCA and DCA were evaluated based on the measurements taken from ten test specimens of each coating. Details regarding wetting measurements undertaken in this study can be found in Chapter 4 and 6.



*Figure 6.2 WCA (left) and DCA (right) measurements principle taken using a DSA100 from KRÜSS*

### **Visual appearance**

Three parameters were selected as indicators for visual appearance quality namely gloss, haze and distinctness of image (DOI). The aesthetic finish of the coated samples was studied with a Novo-Gloss IQ goniometer from Rhopoint Instruments, according to ASTM D523 – 08 (for the gloss) and ASTM E430 (for the haze). Selected instrument strikes the surface with light and uses a diode array to measure the distribution of reflected light  $\pm 6^\circ$  from the specular reflection angle. Each measurement consists of a 256 point profile of the reflected light. Based on this information the goniometer calculates the values of gloss, haze and DOI.

The percentage of light that deviates from the incident beam (greater than 2.5 degrees) on average when passing through sample is defined as haze (ASTM D4449-15, 2015). Therefore, haze was measured by assessing how much light is diffused through the test specimen.

DOI characterize the sharpness of image of objects produced by reflection. It is parameter of a quite high importance in terms of visual appearance. Two different surfaces may exhibit identical value of gloss nonetheless; the visual quality of the surface may be very poor due to low DOI number. The DOI number of a surface is rated from zero to hundred, where a higher number indicates a better quality surface.

Visual appearance measurements were taken from ten test specimens of each coating system.

### **Wear resistance**

The wear resistance of the coating is dependent upon many variables, such as coating, substrate, surface preparation, coating application methodology and environment. Figure 6.3 illustrates the relationship between coating system and its wear resistance.

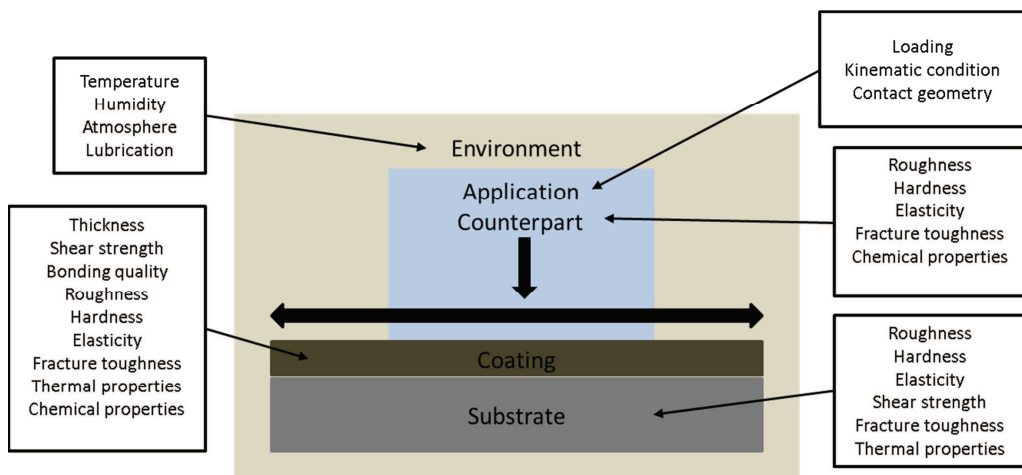


Figure 6.3 Effect of material system parameters on the mechanical performance of a coating

In order to assess the mechanical performance of coatings, rotary abrasion Taber testing was undertaken.

The specification of Taber abrasion measurements is provided in Chapter 4. In total, five samples of each coating per each abrasive condition were examined and analysed.

### **Adhesion**

The coating adhesion to the substrate was measured with several techniques. Quantitative pull-off test and semiquantitative cross cut testing routines were

discussed in Chapter 5. In addition to direct bond strength measurements, wet adhesion loss was evaluated based on and chemical resistance examination (the full description of chemical resistance testing can be found in Chapter 3). In total, ten samples of each coating per each condition were subjected to evaluation.

### 6.3 Results

Table 6.1 summarizes coating application methodology and average thickness. Dry film thickness was controlled with eddy current gauge (measurement specification was provided in Chapter 5) and provided value is based on measurements taken from 10 test specimens.

Table 6.1 Coating application methodology

Coating type	Surface preparation	Deposition	Curing/drying	Thickness [ $\mu\text{m}$ ]
A	Etching + Anodizing	Bar coater (20 $\mu\text{m}$ )	UV, 8 J/cm <sup>2</sup>	21.5 $\pm$ 1.9
B	Etching + Anodizing	Bar coater (20 $\mu\text{m}$ )	UV, 8 J/cm <sup>2</sup>	21.2 $\pm$ 1.5
C	Etching + Anodizing	Bar coater (20 $\mu\text{m}$ )	UV, 15 J/cm <sup>2</sup>	8.3 $\pm$ 2.1
D	Etching + Anodizing	Bar coater (20 $\mu\text{m}$ )	UV, 15 J/cm <sup>2</sup>	7.2 $\pm$ 1.6
E	Etching + Anodizing	Bar coater (20 $\mu\text{m}$ )	UV, 12 J/cm <sup>2</sup>	15.7 $\pm$ 3.4
F	Etching + Anodizing	Bar coater (20 $\mu\text{m}$ )	UV, 40 J/cm <sup>2</sup>	12.3 $\pm$ 1.4
GP101	IPA wiping	Brushing	2h in lab conditions	3.2 $\pm$ 0.2
Never Wet	IPA wiping	Spraying (2xbase, 1x top coat)	Base – 15min, top – 30 min in lab conditions	23.4 $\pm$ 1.5

#### 6.3.1 Initial performance characteristics

The initial coating repellency and lipophobic character is given in Figures 6.5 and 6.6 (box plot principle explained in Chapter 5). Due to the fact that coatings with different topographies were compared and due to gravity effect, all measurements were taken 5 seconds after droplet was deposited on the surface, in order to have readings from equilibrium state.

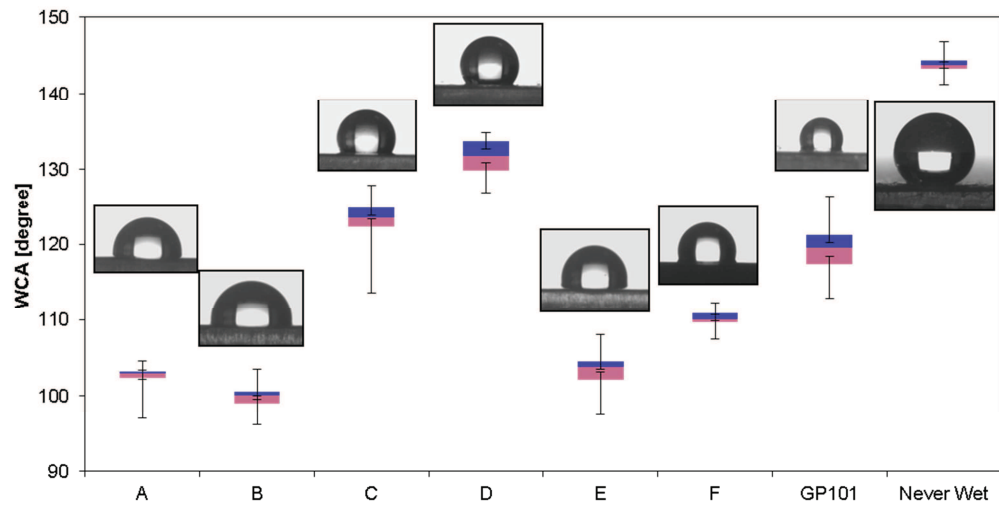


Figure 6.4 Initial wettability characteristics of selected coating systems (box plot principle explained in Chapter 5)

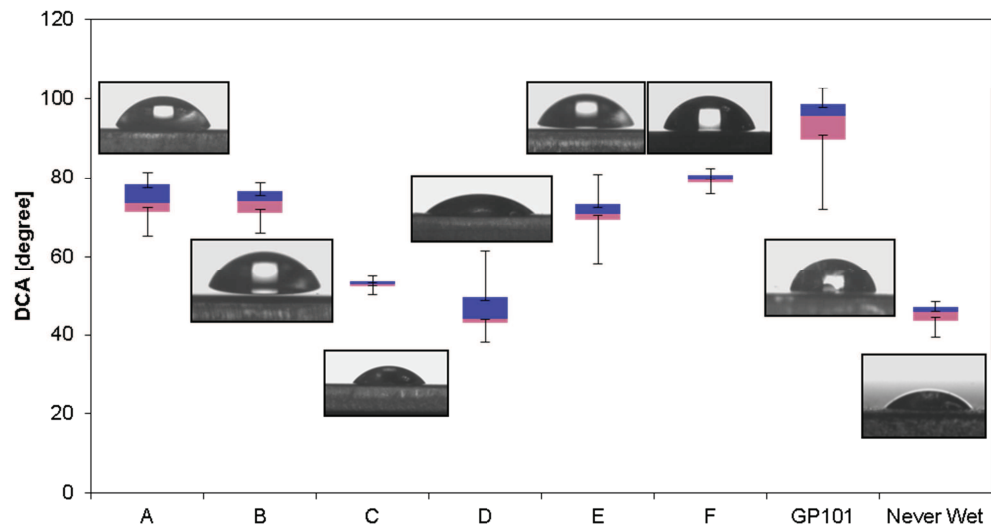


Figure 6.5 Lipophobic characteristics in pristine state of selected coating systems box plot principle explained in Chapter 5)

The average water contact angle values and arithmetic ( $R_a$ ) and geometric means ( $R_q$ ) of the surface profile are given in Table 6.2.

Table 6.2 Surface roughness level, corresponding water contact angle and diiodo contact angle (in selected coating systems, roughness parameters assessed with Talysurf)

Coating type	WCA [degree]	DCA [degree]	$R_a$ [nm]	$R_q$ [nm]
A	102.3	74.3	8.4	10.2
B	103.2	73.8	8.9	10.5
C	121.4	52.8	254.2	324.5
D	128.9	47	394.3	536.5
E	102.5	70.7	9.9	12.6
F	112.3	79.6	216.0	311.4
GP101	118.4	93.3	288.2	355.1
Never Wet	143.9	45.2	8292.3	10959.3

Visual appearance properties, such as gloss, haze and distinctness of image (DOI) are provided in Figure 6.7. Despite the fact that selected surface finish present quite dissimilar values in terms of gloss, it was decided to measure all coatings with 20° geometry. Such approach helps to avoid confusion when surfaces with different optical quality have to be compared.

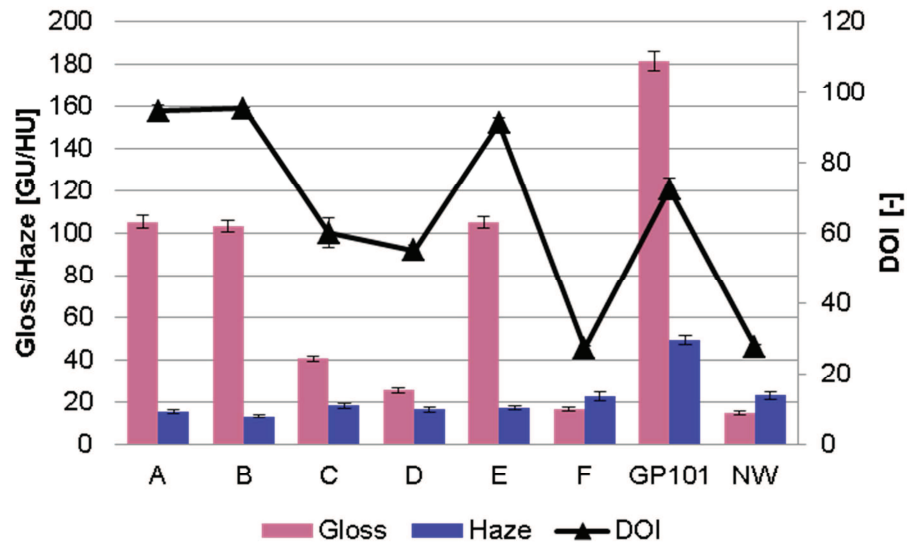


Figure 6.6 Visual appearance (gloss, haze and DOI) taken with 20° geometry of selected coating systems

### 6.3.2 Abrasion resistance and water contact angle retention

Water contact angle as a function of abrasion cycles for selected coating systems are provided in Figure 6.8, 6.10, 6.12, 6.14, 6.16, 6.18 and 6.20. SEM images taken with backscattered detector (500x) in Figure 6.9, 6.11, 6.13, 6.15, 6.17, 6.19, 6.21 and 6.22 represent the changes that were made to the coating as a result of surface abrasion. All changes in the surface were associated with roughness level that is strongly dependent upon abrasion. Arithmetic means of the heights of the surface profile Ra were given in SEM images in the right left corner.

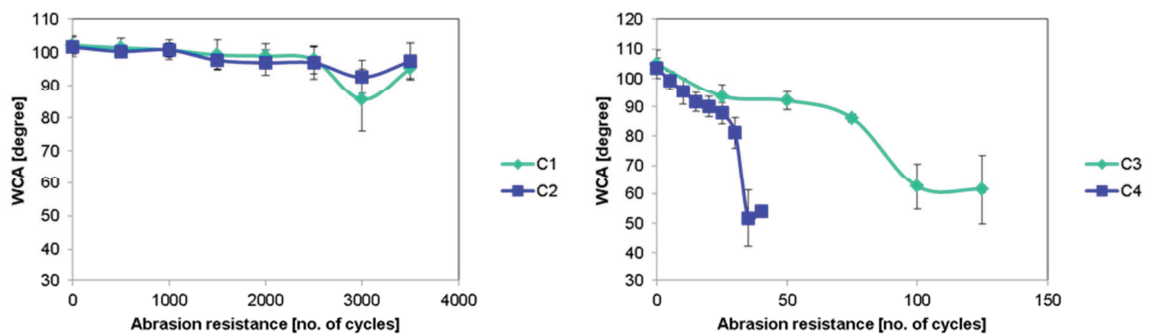


Figure 6.7 Water contact angle retention as a function of abrasion cycles – TWI formulation A (C1 – CS10 wheels/500 g load; C2 – CS10 wheels/1000 g load; C3 – H18 wheels/500 g load; C4 – H18 wheels/1000 g load)

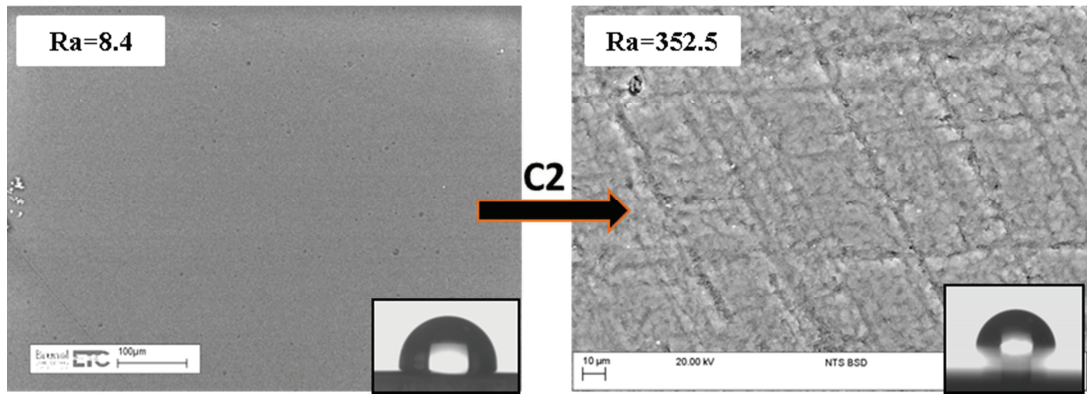


Figure 6.8 SEM images of pristine TWI formulation A (left) and wear scars (right) after abrasion testing (condition 2, 3500 cycles).  $R_a$  represents roughness level in nanometres for specified conditions

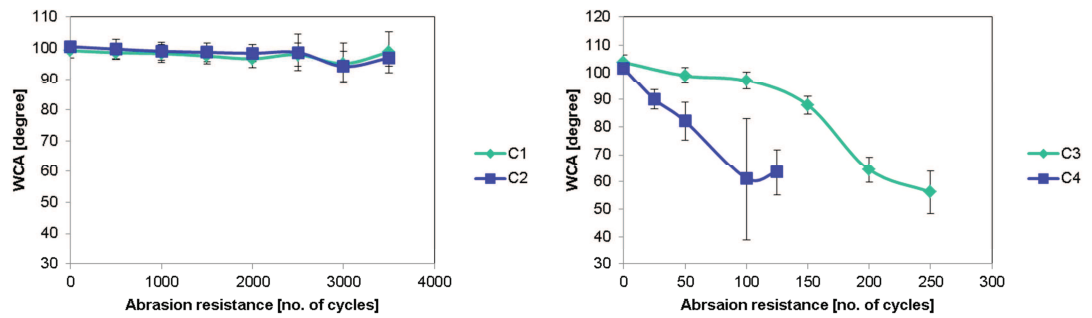


Figure 6.9 Water contact angle retention as a function of abrasion cycles – TWI formulation B (C1 – CS10 wheels/500 g load; C2 – CS10 wheels/1000 g load; C3 – H18 wheels/500 g load; C4 – H18 wheels/1000 g load)

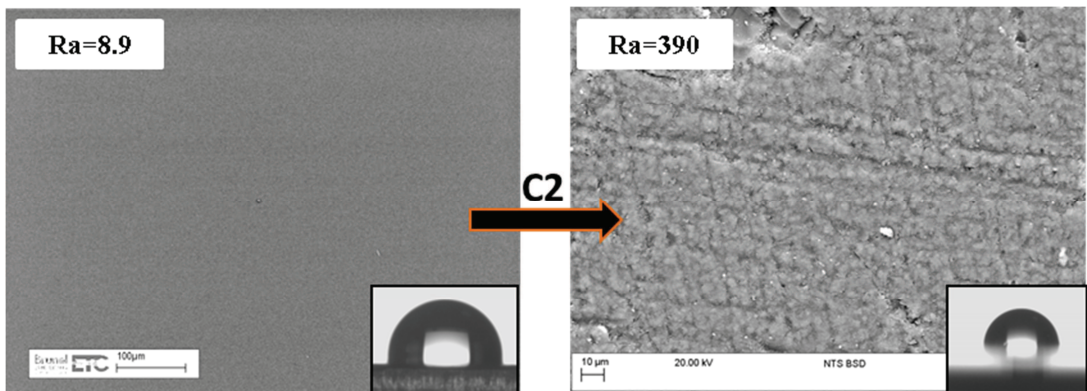


Figure 6.10 SEM images of pristine TWI formulation B (left) and wear scars (right) after abrasion testing (conditions 2, 3500 cycles).  $R_a$  represents roughness level in nanometres for specified conditions

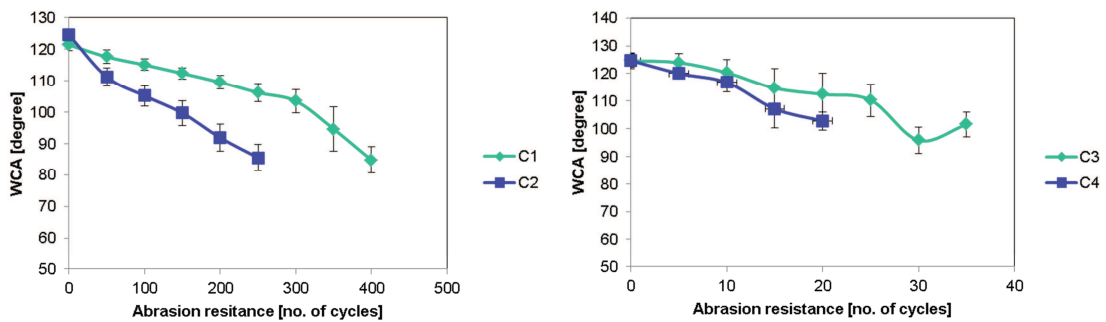


Figure 6.11 Water contact angle retention as a function of abrasion cycles – TWI formulation C (C1 – CS10 wheels/500 g load; C2 – CS10 wheels/1000 g load; C3 – H18 wheels/500 g load; C4 – H18 wheels/1000 g load)

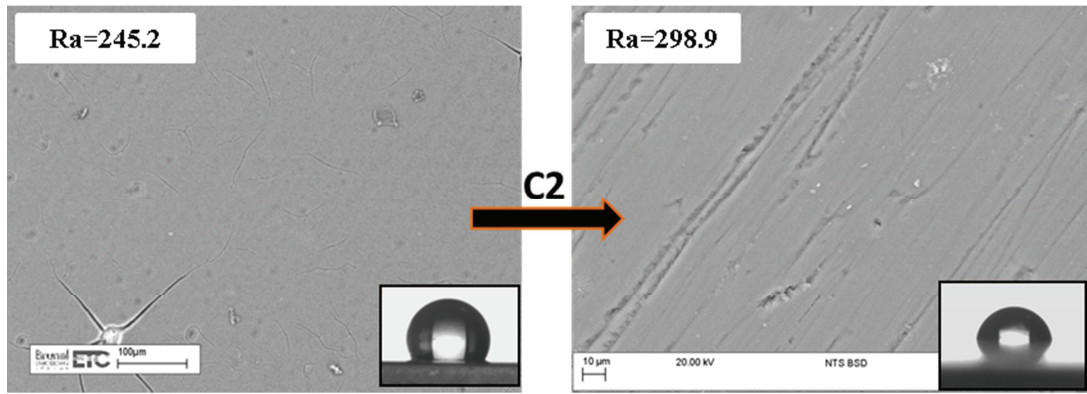


Figure 6.12 SEM images of pristine TWI formulation C (left) and wear scars (right) after abrasion testing (conditions 2, 250 cycles). Ra represents roughness level in nanometres for specified conditions

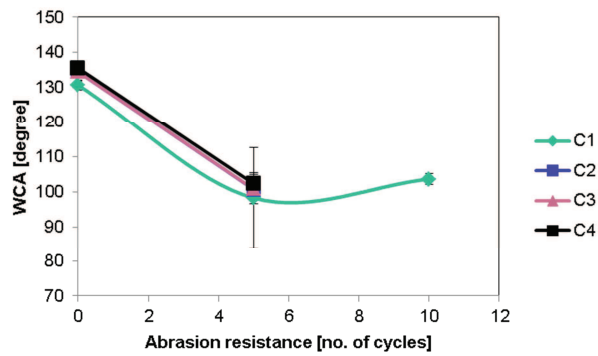


Figure 6.13 Water contact angle retention as a function of abrasion cycles – TWI formulation D (C1 – CS10 wheels/500 g load; C2 – CS10 wheels/1000 g load; C3 – H18 wheels/500 g load; C4 – H18 wheels/1000 g load)

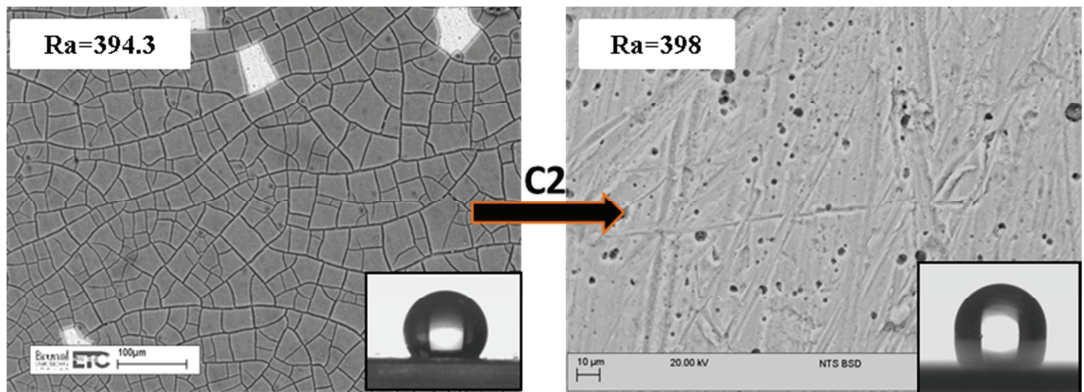


Figure 6.14 SEM images of pristine TWI formulation D (left) and wear scars (right) after abrasion testing (conditions 2, 5 cycles). Ra represents roughness level in nanometres for specified conditions

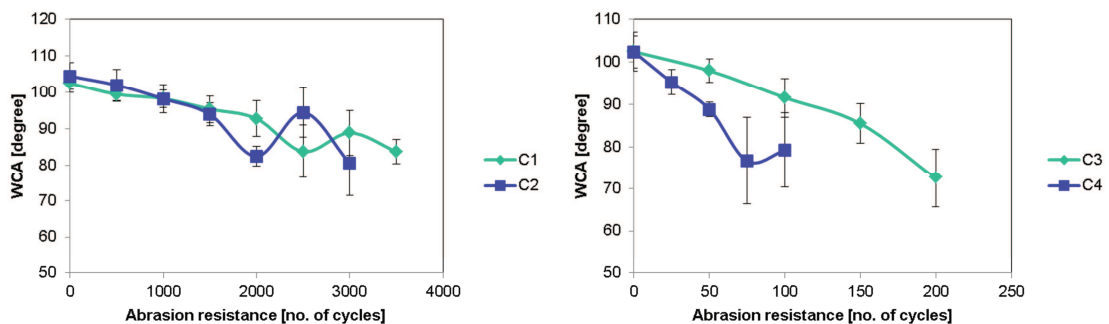


Figure 6.15 Water contact angle retention as a function of abrasion cycles – TWI formulation E (C1 – CS10 wheels/500 g load; C2 – CS10 wheels/1000 g load; C3 – H18 wheels/500 g load; C4 – H18 wheels/1000 g load)

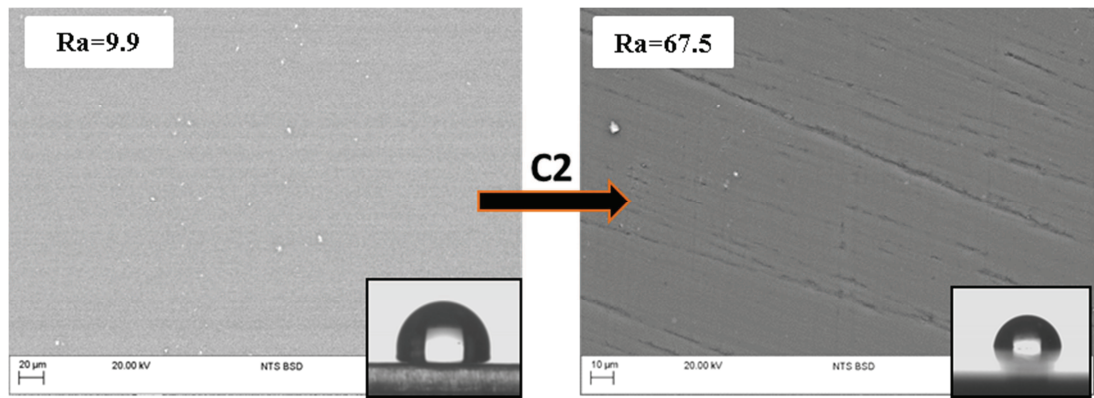


Figure 6.16 SEM images of pristine TWI formulation E (left) and wear scars (right) after abrasion testing (conditions 2, 3000 cycles). Ra represents roughness level in nanometres for specified conditions

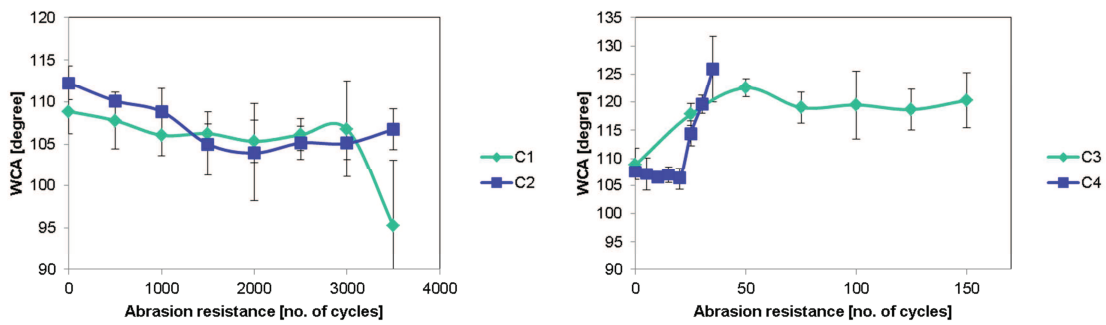


Figure 6.17 Water contact angle retention as a function of abrasion cycles – TWI formulation F (C1 – CS10 wheels/500 g load; C2 – CS10 wheels/1000 g load; C3 – H18 wheels/500 g load; C4 – H18 wheels/1000 g load)

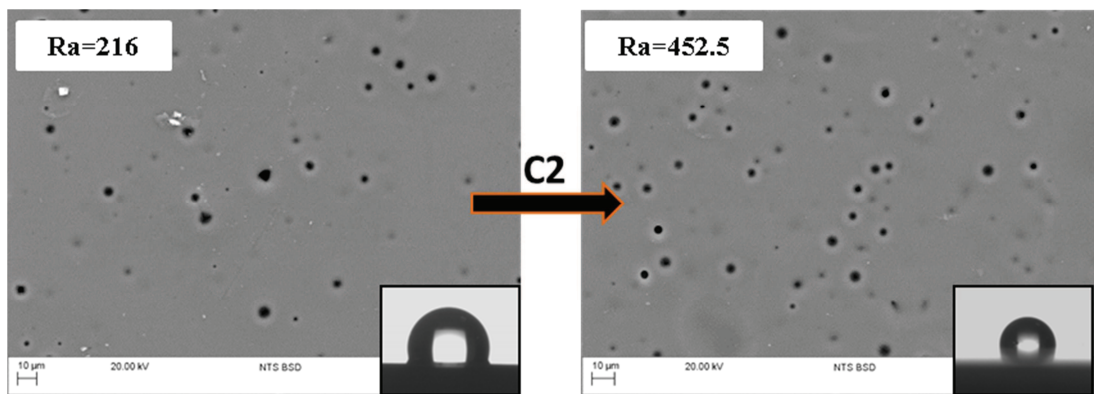


Figure 6.18 SEM images of pristine TWI formulation F (left) and wear scars (right) after abrasion testing (conditions 2, 3500 cycles). Ra represents roughness level in nanometres for specified conditions

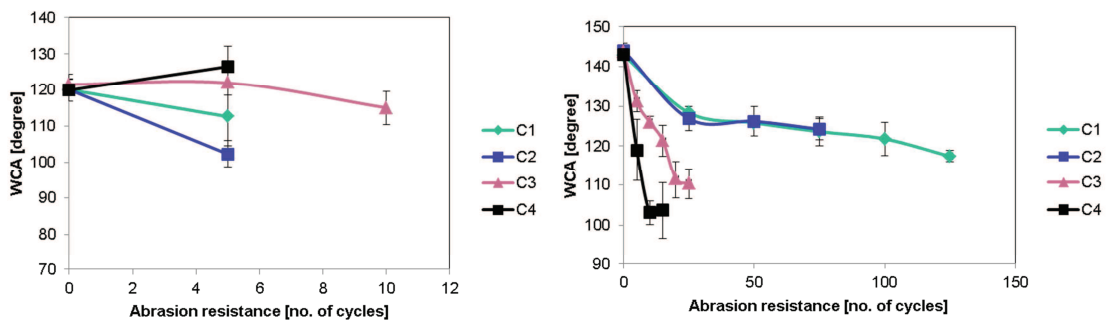


Figure 6.19 Water contact angle retention as a function of abrasion cycles – commercial products GP101 (left) and Never wet (right) (C1 – CS10 wheels/500 g load; C2 – CS10 wheels/1000 g load; C3 – H18 wheels/500 g load; C4 – H18 wheels/1000 g load)

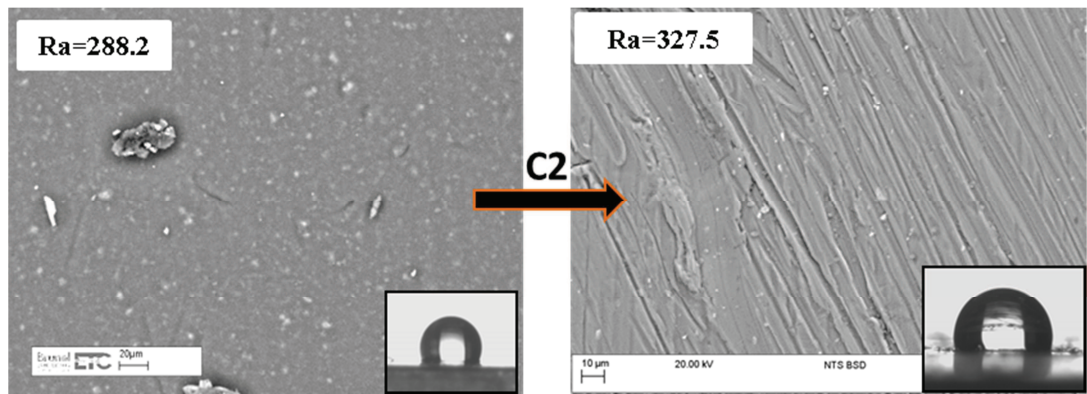


Figure 6.20 SEM images of pristine commercial product GP101 (left) and wear scars (right) after abrasion testing (condition 2, 5 cycles). Ra represents roughness level in nanometres for specified conditions

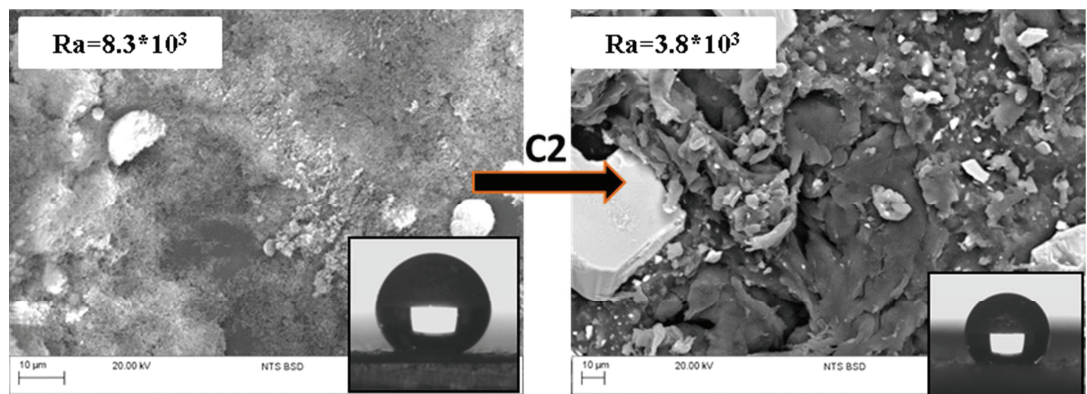


Figure 6.21 SEM images of pristine commercial product Never Wet (left) and wear scars (right) after abrasion testing (conditions 2, 75 cycles). Ra represents roughness level in nanometres for specified conditions

### 6.3.3 Adhesive wear and chemical resistance

The effect of initial adhesion strength as a function of surface intact area after specified ageing conditions are given in Figures 6.24, 6.25 and 6.26. Surface intact area was evaluated based on the following equation:

$$\text{Surface intact area} = 1 - \text{Surface affected area} \quad (6.1)$$

Surface affected area was expressed as a percentage of the coating that was flaked from the surface after specified ageing conditions. Validation of surface quality was done in similar manner as was given in the following standard (ASTM D3359 -09e2, 2009). Figure 6.23 represents example of surface quality assessment for validating the resistance of coatings to separation from aluminium substrate.

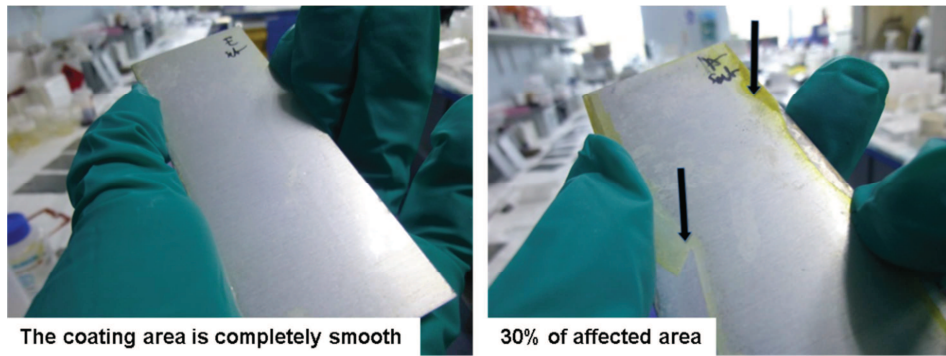


Figure 6.22 Principle for assessing the resistance of coatings to separation from substrates (1 week in 5%NaCl, left – TWI formulation E, right – TWI formulation A)

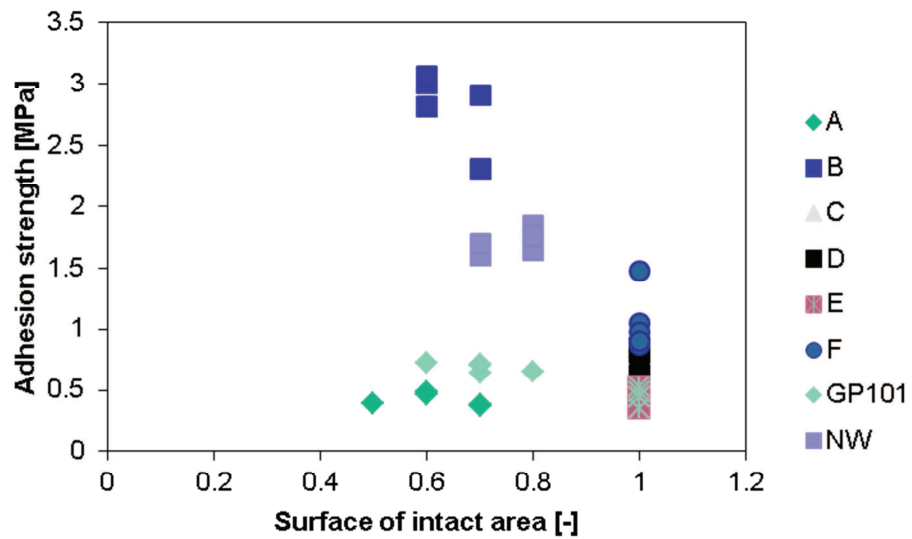


Figure 6.23 Chemical resistance measured in a function of initial adhesion strength and surface quality after specified ageing conditions (1 week in 1% $H_2SO_4$  solution)

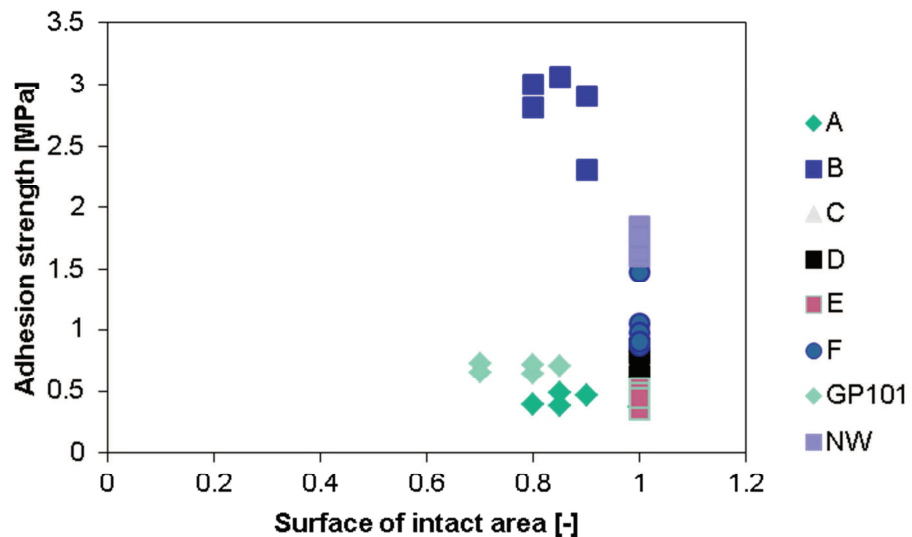


Figure 6.24 Chemical resistance measured in a function of initial adhesion strength and surface quality after specified ageing conditions (1 week IMS solution)

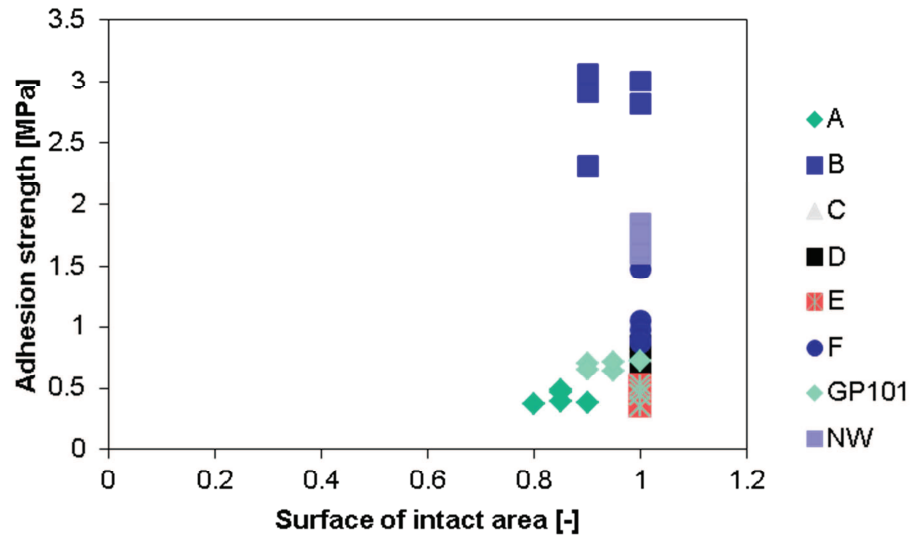


Figure 6.25 Chemical resistance measured in a function of initial adhesion strength and surface quality after specified ageing conditions (1 week 4.95%NaCl solution)

To illustrate the coating chemical durability in conjunction with indirect durability, changes in repellency after ageing were measured. Figure 6.27 presents values of water contact angle in pristine state and exposure to selected chemicals.

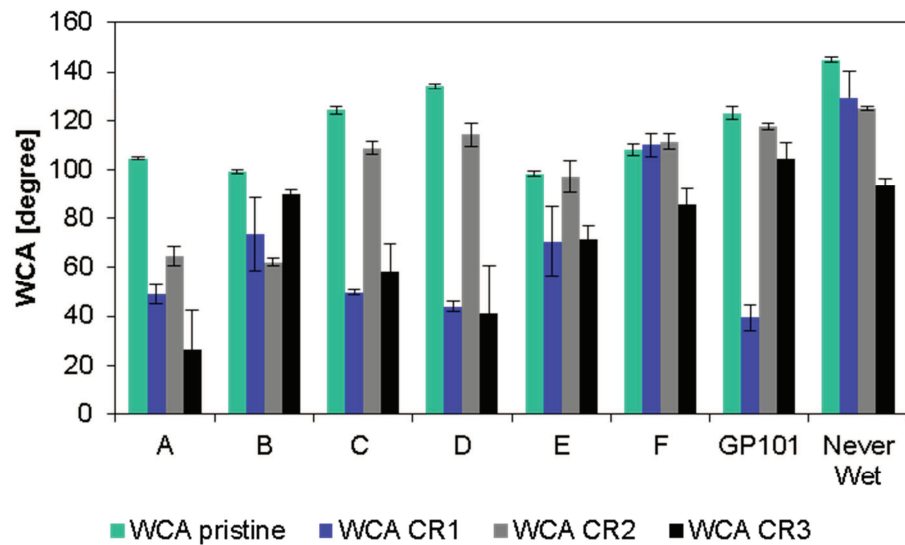


Figure 6.26 Changes in WCA as a result of accelerated chemical ageing process (one week of immersion in: CR1 – 1% $H_2SO_4$ , CR2 – IMS, CR3 – 4.95%NaCl)

## 6.4 Discussion

Examining the results of water contact angle values, it can be seen that all of the selected coatings fulfilled requirements for easy clean properties. All TWI formulations and selected commercial products display more than  $90^\circ$  in the pristine state. Figure 6.4 shows the range of water contact angles values that can be achieved by various coatings. In terms of coating wettability classification they can

be divided into two groups namely, hydrophobic ones, which refers to smooth easy clean coatings and parahydrophobic, where wettability is achieved due to roughness, beyond the effect of the surface chemistry (Marmur A., 2012). None of evaluated surfaces can be classified in superhydrophobic category.

It can be found that amongst the coating systems tested, the lowest WCA values are displayed by the surfaces with quite low roughness level that didn't exceed more than 10 nm. The average WCA of TWI formulations A, B and E do not differ significantly. Addition of silsesquioxane oligomers into the acrylate matrix changes the coating composition, yet this does not affect the surface texture or wetting characteristics. No difference between TWI formulation B and E suggest that further addition of dual functionalized 30 nm silica nanoparticles, will not improve wetting properties. Silica nanoparticles itself are meant to modify the structure. Nevertheless, the value of arithmetic (Ra) and geometric (Rq) mean of surface profile in formulation E are not significantly higher than roughness parameters of formulation B. SEM images (Figure 6.27) confirms that 30 nm silica nanoparticles with dual functionality (MPTMA and NPTMS) representing 46% of formulation do not really change the topography.

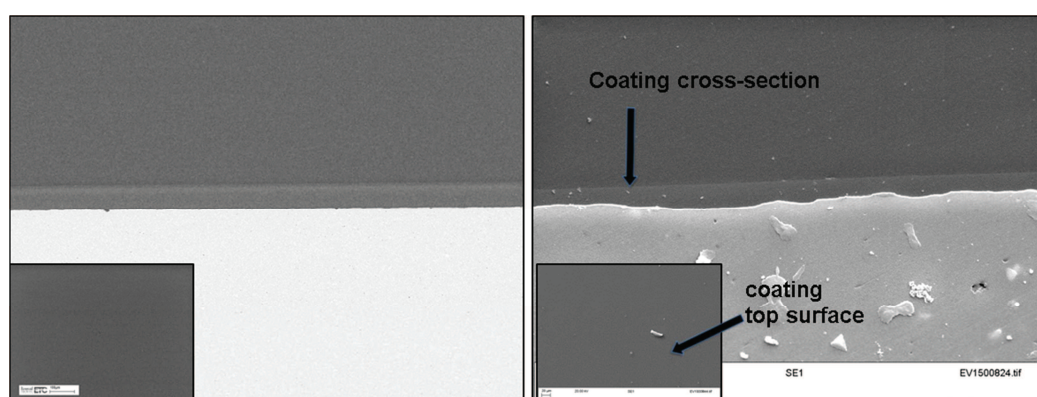


Figure 6.27 SEM images of TWI formulation B (left) and E (right) – cross-sectioning and top surface view (500x magnification, BS detector)

Higher roughness level leads into higher water contact values, which confirms all that extraordinary repellence is achievable by linking together right surface chemistry with right surface hierarchy. The highest contact angles were displayed by TWI formulation D and commercial product Never Wet. These coatings have the highest initial roughness level (Table 6.2). The good non-wetting performance achieved by formulation D comes from nanoparticles triple functionalization with hydrophobic species and also due to the fact that this system has dual hierarchy, created by two different sizes of nanoparticles. In the case of Never Wet, very high roughness level that reaches more than 8  $\mu\text{m}$  definitely contributes towards very

high levels of repellence ( $144^\circ$  of WCA). Unfortunately, the manufacturer does not provide full information about coating composition and therefore, type and influence of hydrophobic species in Never Wet is unknown.

The average WCA of TWI formulation C reaches level of  $121^\circ$ , which is almost  $8^\circ$  lower than formulation D. Since these two coating systems were built from the same components, the difference in WCA values can be inferred to be due to the amount of silica nanoparticles and therefore, to the roughness level. Increasing the amount of triple functionalized nanosilica from 60 to 75% of total composition leads to an increase in Ra value of almost  $0.15\ \mu\text{m}$ .

Nevertheless, arithmetic and geometric means of surface profile may not give the full information about surface roughness level. Very different surface profiles can have the same Ra value (Rodriguez V., 2011). 3D surface parameters calculated from topographical coating map highlight surface's waviness, microroughness and therefore, they can shed more light on coating repellent characteristics (ISO 4287, 1997). With regard to coating functional performance, two of S parameters (The S Parameters provide roughness, spatial and hybrid information for 3D surfaces) might be useful in analysing topography and predicting air-trapping in rough surfaces namely, skewness and kurtosis. Skewness refers to degree of asymmetry of roughness profile, where positive value is associated with peaks predominance in topography, whilst negative characterizes surfaces with valleys majority. Kurtosis describes sharpness of surface profile and  $Ku > 3$  is found in surfaces with sharp summits, where  $Ku < 3$  refers to flatter topography. Some authors have found that surfaces with large positive skewness are able to maintain high values of WCA (Bhushan B J. Y., 2006). Figure 6.28 reveals that coatings with highest values of WCA have also high positive number of skewness such as Never Wet and TWI formulation C. Nevertheless, negative value of skewness of formulation D indicates that surface profile with valleys predominance can trap the air underneath the droplet and boost the value of WCA. The fact that formulation C and D are built from the same components and present similar repellent characteristics with kurtosis higher than 3, yet their skewness parameter is very different indicates that amount of triple functionalized dual size nanosilica in the system influences surface profile. Figure 6.29 illustrates SEM images and AFM profiles of formulation C and D and shows that there are significant differences in the surface profiles of these two coatings. The uneven roughness profile of formulation D might have affected AFM scanning and therefore, some errors in calculating parameters might have occurred.

That would explain high difference in skewness value between formulation C and D. Nevertheless, valleys predominance in surface profile of formulation D could be the effect of high amount of solvent in resin composition. More extensive solvent evaporation during curing might be responsible for re-entrant surface curvature. The effect of solvent amount in resins containing triple functionalized dual size nanosilica on the coating surface profile is beyond the scope of this thesis and may be an interesting topic of further investigation.

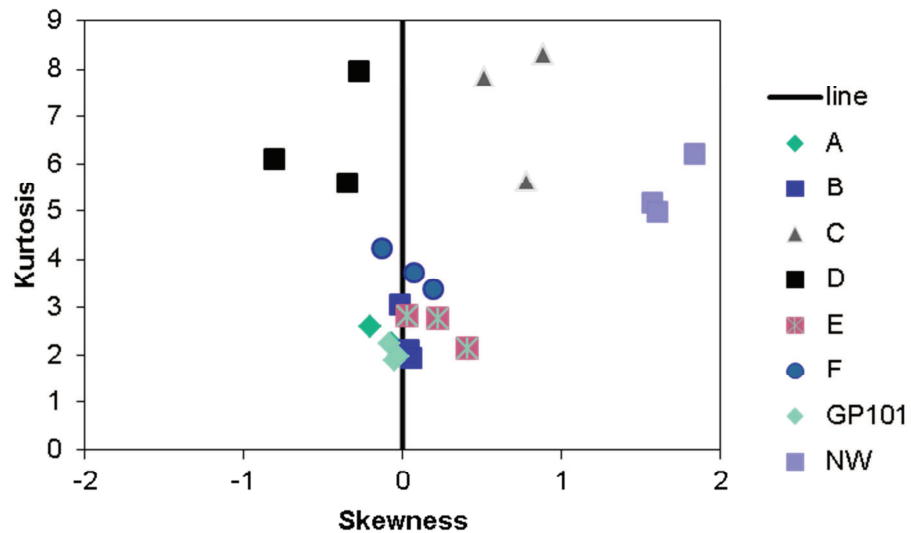


Figure 6.28 Kurtosis and skewness of surface profile of the selected coating systems (pristine state)

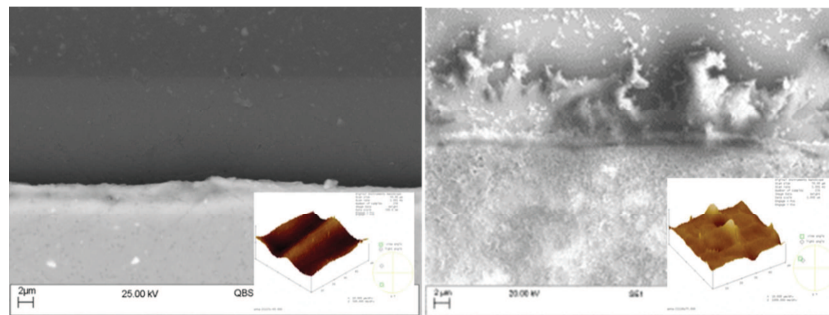


Figure 6.29 SEM cross-sectional images and AFM roughness profile of TWI formulations C (left) and D (right)

TWI formulation A, B, E, F and commercial product GP101 have very similar values of skewness and kurtosis roughness measurements. Since for all of these surfaces skewness is oscillating around zero and kurtosis is not far different than three indicates that roughness profile of these coating systems resemble Gaussian distribution. Coating A, B and E are very smooth ones and therefore, their surface summits are expected to be normally distributed.

The Ra value of formulation F is not far different from the Ra of formulation C, yet its WCA is lower by almost 10 degrees. It seems that air trapping mechanisms cannot be achievable by materials with symmetric surface topography. In the case of

commercial product GP101, the parameters of roughness profile resemble the textural style of formulation F nonetheless, WCA is slightly higher. Since the WCA of GP101 does not reach more than 120 degrees, it can be assumed that surface chemistry plays a dominant role in repellency of GP101. Nevertheless, the role of surface roughness cannot be completely excluded. Unfortunately, the manufacturer does not provide full information about the coating composition and therefore, this assumption cannot be confirmed.

With regard to initial lipophobic character of the coating systems, it can be seen from Figure 6.5 that stronger affinity to oils was found in materials with greater repellency. The diiodomethane contact angles of TWI formulations C, D and commercial product Never Wet sit in the range between 40° and 60°.

In the case of TWI formulations, as expected highest values of DCA are associated with the coating that contains fluorinated component in its structure. 1H 1H 2H 2H-perfluorooctyltriethoxysilane silica functionalizing agent in formulation F provides a low surface tension species in the coating and therefore, hampers affinity to oils. Among selected coating systems, GP101 presents the best oil-repellency characteristics, yet this coating doesn't have a fluorinated component in the system according to its Materials Safety Data Sheet. This most probably corresponds to recently introduced "re-entrant" geometry, which corresponds to surface topography features that bend towards the substrate and form angles with the substrates below 90°. According to Law et al. nonpolar liquid wets the top of structure, yet is highly pinned underneath the re-entrant features (Zhao H. L. K., 2011) (Zhao H. P. K., 2012). Therefore, by manipulating surface geometry, it is possible to control oil penetration (Brown P.S., 2016). Amongst the selected coating systems, the highest values of DCA can be found in surfaces with very symmetrical roughness profile (TWI formulation A, B, E, F, GP101). No significant difference was noticed in the diiodomethane repellence of TWI formulations A, B and E. Since these coatings have very similar texturing profile, it suggests that geometry plays crucial role in wetting by oils and through roughness control, the same lipophobicity can be achieved for surface with different composition.

Coating visual appearance resulting in gloss, haze and DOI is strongly affected by surface composition and geometry. In general, surface reflection and surface topography share a linear relationship, where lower values of gloss are associated with higher roughness level, due to the fact that on rough surfaces light is diffusely scattered in all directions. This statement is confirmed by gloss evaluation of the

coating systems and it's shown in Figure 6.30. Coatings with smooth texturing profile, such as TWI formulation A, B and E represent the group of surfaces with the highest reflections. The value of gloss in these materials is almost identical and just exceeds 100 GU. Based on these findings, it can be stated that controlled addition of SSQs and dual functionalized 30 nm silica nanoparticles into resin matrix do not really affect the reflective properties as long as roughness profile retains its original structure.

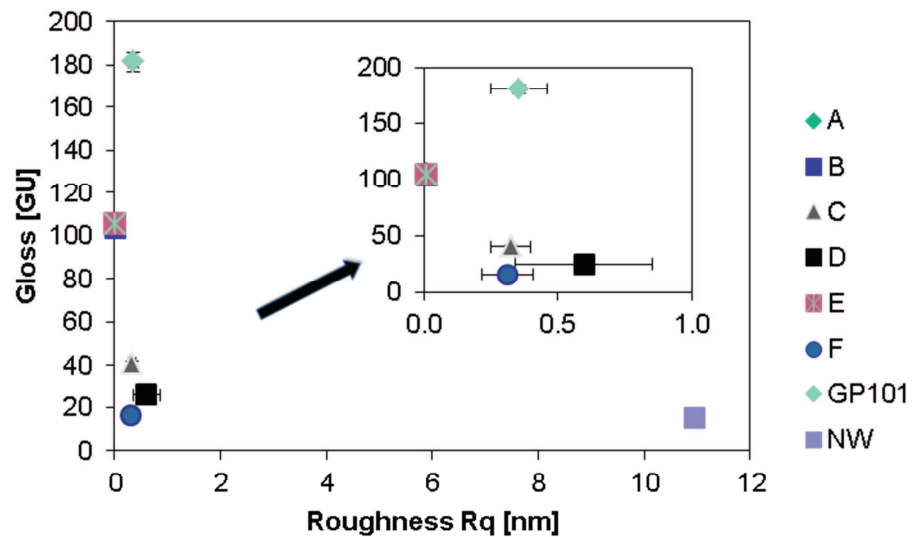


Figure 6.30 Influence of the roughness profile (geometrical mean of surface peaks ( $R_q$ )) on surface reflection (gloss) measured with  $20^\circ$  angle of incidence

The highest value of gloss was found in GP101 coating system and its almost 80 GU higher than in case of TWI formulation A, B and E, despite the fact that this coating cannot be really classified as smooth one. This difference in reflection can be explained twofold. On the one side, high gloss of the rough GP101 coating system is influenced by its composition and corresponding rheological properties. On the other side, gloss is also dependent upon the coating processing conditions. Since all TWI formulations were deposited at the surface, which was previously anodized, it might have lowered the value of gloss in these coating systems. Therefore, the effect of surface preparation type on the gloss of TWI formulations was studied (formulation B was selected as a representative one). Figure 6.31 confirms that anodization of aluminium panel resulting in forming thicker oxide layer on the surface, have the influence on the visual appearance of the coating that was deposited at this surface (oxide layer formation process can be found in Chapter 4). This examination reveals that substrate anodizing prior to deposition decreases gloss value by almost 50%. Taking these results into consideration, it can be stated

that if all of the coatings were deposited on substrate that was prepared in the same manner, the highest reflection values would be coming from the smoother surfaces.

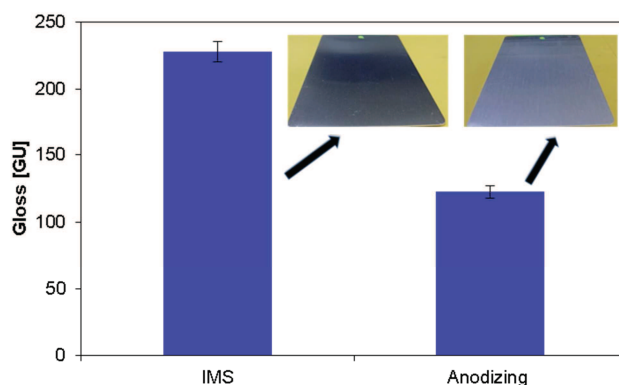


Figure 6.31 Effect of surface preparation conditions on surface reflection in TWI formulation B measured with 20° angle

The low value of gloss of TWI formulations C, D and F are definitely due to the effect of high roughness level. Nevertheless, the difference in reflection from formulation C (gloss 40 GU) and D (gloss 25 GU) might not be only the effect of topography type. It can be also the result of nanoparticles loading level. More nanoparticles in the coating system reduce its transparency, resulting in lower reflection quality. It cannot be also excluded that nanoparticles might not be uniformly dispersed in the coating, they might agglomerate and therefore, reduce the transparency.

In terms of surface haziness, it can be found out that surfaces with higher roughness levels appear to have higher levels of “cloudiness”. In the case of thin films, haze is recognised to be caused by scattering from surface irregularities and therefore surfaces with smoother profile, such as TWI formulation A and B has the lowest value of gloss among selected coating systems. The slightly higher haze value in TWI formulation E is most probably not influenced by roughness, due to the fact that this surface has rather smooth profile that is only 1 nm higher than texture level of formulation A and B. This difference in haze can be therefore explained by the role that silica nanoparticles loading rate plays in coatings visual appearance. Particle concentration, size and the difference between refractive index of bulk material and silica nanoparticles, chemical segregation and clustering due to chemical incompatibility influence the visual quality of coating. Nevertheless, as can be seen in Figure 6.6 in the case of TWI formulations, addition of silica nanoparticles into resin matrix did not affect much haziness of the surface. The highest rise of haze in TWI formulations were notified in the coating system that contains dual functionalized 30 nm silica nanoparticles (TWI formulation F). Since

concentration and size of nanosilica used in formulation E and F are not far different, slightly higher haziness of formulation F finds its explanation in two ways. First of all, higher level of surface irregularities in formulation F can increase the scattering from the coating. On the other side, higher haziness in TWI formulation F might be a direct result from the light scattering caused by the still relatively large nanoparticles or nanoparticles agglomeration. Therefore, this may explain lower visual quality displayed by formulation F.

Commercial product Never Wet is classified as a poor visual quality surface. Low gloss associated with quite high haziness is definitely caused by an extraordinary level of surface roughness level. Nevertheless, lack of information regarding coating composition does not allow further surface visual appearance analysis.

Distinctiveness of Image value seems to be dependent upon surface gloss. The highest values of DOI were found in surfaces with greater reflective properties. In general, DOI is the sharpness and clarity of the image produced by surface reflection and therefore, surfaces with high roughness level should be expected to have low DOI values. The examination of the selected coating systems confirms this statement. The lowest values of DOI shown in Figure 6.6 are associated with coatings, where roughness level  $R_a$  exceeds 200 nm. TWI formulation F and commercial product Never Wet have the least sharp image reflection. In the case of TWI formulation F, such results cannot be explained by the fact that this coating has the lowest concentration of photoinitiators among TWI formulations. The reduced amount of photoinitiators results in extending the amount of energy that needs to be absorbed by the coating during curing process, which has beneficial effect on surface visual appearance (Jančovičová V., 2007). The low value of DOI of TWI formulation F is most probably the effect of surface roughness combined with the value of refractive index of 1H,1H,2H,2H-perfluorooctyltriethoxysilane.

Coating durability assessment was conducted in a function of three variables, such as abrasive wear, ability to retain initial repellent characteristics under constant abrasion and adhesive wear.

When comes to abrasion resistance testing with rotary Taber platform, the ASTM D4060 standard recommends calculating the wear index (WI) for each level of abrasion aging, which is the loss in weight (in milligrams) per thousand cycles of abrasion. Nevertheless, in this study wear index has not been taken into consideration, due to the fact that coatings with different dry film thickness were

compared. Surfaces with thicker film layer result in greater mass loss during abrasion, yet this doesn't mean that these surfaces aren't durable.

Assessing the direct and indirect durability of coatings was evaluated as specified in Chapter 5 under four different testing conditions. TWI formulation A and B exhibits similar retention ratio mechanism in all selected conditions. As can be seen in Figure 6.7 and 6.9, these coatings lose their hydrophobic characteristics when subjected to harsh abrasion (conditions 3 and 4) and this loss is greater when the load is increased. On the contrary, mild abrasive conditions seem to have a little influence on wettability, which indicates that these materials are durable. The high level of mechanical stability of these surfaces comes from a high degree of cross-linking. Nanoindentation examination presented in Chapter 4 reveals that hardness of TWI formulation B increases with the higher degree of cross-linking. Since TWI formulation A and B are not far different, it can be assumed that the same principle will apply for formulation A. Moreover, these two coating systems do not contain solvent and therefore, it is easier to control the size of dry film thickness. The good mechanical resilience of TWI formulation A and B is also a result of smooth surface texture. The arithmetic mean of the surface profile is less than 10nm and there is a practically Gaussian distribution of peaks and heights (Figure 6.32) these factors contribute towards high abrasion resistance.

The surface profile of TWI formulations A and B change when the coatings are subjected to abrasion. Figure 6.8 and 6.10 represent surface texture transformation that has happened under examination in conditions 2. In both of materials, visible marks of abrasion appeared on the surface, yet no signs of cracking or flaking were spotted even after 3500 cycles. The roughness level increased by almost 40 times and according to Figure 6.32, abrasion testing led to a change in the peak and height distribution. Negative skewness values of formulation A and B indicate that more valleys than peaks were observed in surface profile after testing in conditions 2.

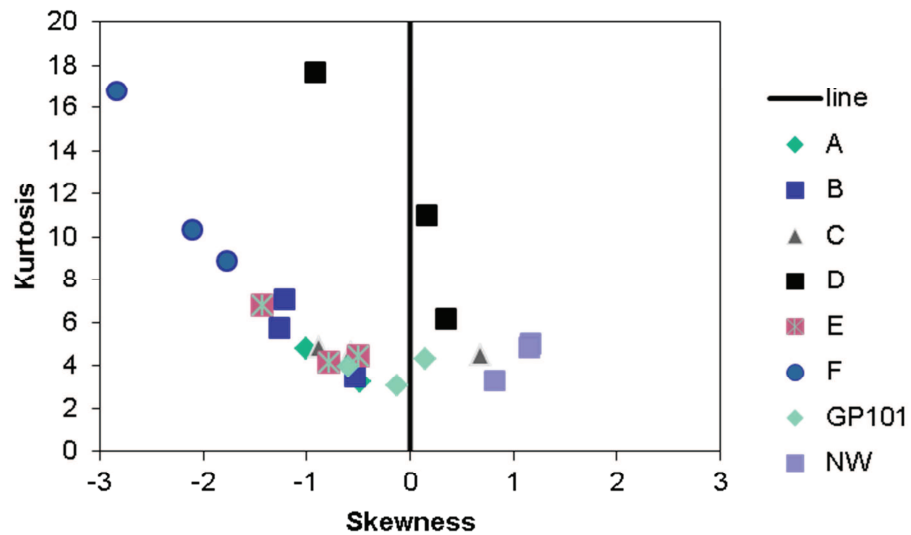


Figure 6.32 Kurtosis and skewness of surface profile in selected coating systems after subjecting them to abrasion condition 2

The wear mechanism underpinning TWI formulations A and B in terms of their loss of non-wetting and the lifetime of the coating practically follow the same pattern. Nevertheless, Figures 6.7 and 6.9 indicates that TWI formulation B is able to withstand twice the time under the same harsh abrasion conditions (conditions 3 and 4). Such behaviour is associated with addition of SSQs into resin matrix that slows down wear processes and helps to extend coatings life longevity. The Vitolane method for manufacturing SSQs produces methacrylate resin that is compatible with most acrylate systems. Each silicon atom has a methacrylate group attached, which in turn can lead to a high cross link-density in the final cured material and therefore, coating mechanical stability will be enhanced. Due to the fact that mild abrasion was performed up to 3500 cycles, it is impossible to exactly asses the lifetime of these surfaces under conditions 1 and 2. Nevertheless, it should be expected that thanks to its inorganic skeleton, TWI formulation B will be more abrasion resistant.

Taking into account TWI formulation C and D, it can be seen that introduction of hierarchical structure in coating system led to decrease in surface mechanical resistance. Abrasive wear of these materials is associated with the loss of wetting characteristics, regardless abrasion conditions type. Faster mechanical wear processes of TWI formulation C in comparison to formulation A and B can be explained by the increase of roughness profile Ra. The arithmetic mean of the surface profile in formulation C reaches 250 nm and there is peak predominance in roughness profile. While these parameters help to boost the value of WCA in pristine state, they are also more sensitive to mechanical damage. Changes in initial

surface roughness profile affect not only coating stability, but also surface repellent characteristics. This explains why retention of initial WCA for TWI formulation C and D reduces much faster than for formulation A and B.

The short lifetime of formulations C and D corresponds as well to the amount of nanosilica used. Higher loading level of nanoparticles is associated with more solvent in coating composition that needs to be used in order to overcome problems with material deposition. The higher amount of solvent results in coating shrinkage during evaporation, which in turn might affect final quality and dry film thickness size of coating. Figure 6.14 shows that high nanoparticles loading level and high solvent content in formulation C results in surface defects, such as crack propagation. The surface finish of formulation D illustrated in Figure 6.14 proves that further loading of silica nanoparticles into resin will result in intensive cracking. Taking into consideration approximation that wet film thickness of formulation C and D was around 20  $\mu\text{m}$  (20  $\mu\text{m}$  bar coater), the dry film thickness was lower due to solvent loss and was  $\sim 8$   $\mu\text{m}$  in case of formulation C and to  $\sim 7$   $\mu\text{m}$  in case of formulation D (Table 6.1) and caused phenomenon called “mud cracking” (Goehring L., 2010). The initial surface defects in TWI formulations C and D strongly affected their ability to withstand any form of abrasion.

The abrasion resistance of TWI formulation E was similar to that of formulations A and B. In this case, the longevity of the coating is mainly due to the effect of synergy between low value of arithmetic means of surface profile ( $R_a=9.9$  nm) and relatively symmetric distribution of valleys and peaks in pristine state (Gaussian like distribution). With regard to retention of repellency of formulation E, slightly faster wear was observable than took place in formulation A and B. This can be identified with the loss of silica nanoparticles in a process of abrasion that may be attributed to crosslink density. Only one of the two functionalization types in formulation E is responsible for crosslinking with acrylate matrix and acts like a coupling agent. Yet, some part of silica nanoparticle is only embedded in a matrix, which makes this part the weakest link when comes to abrasion. Since this part is responsible for boosting repellent characteristics, gradual loss of material will be accompanied by gradual loss of hydrophobicity.

TWI formulation F withstands abrasion as well as formulations A, B and E, despite the fact that both composition and initial surface roughness profile of this coating differs from the other durable TWI surfaces. The overall arithmetic means of surface topography are almost as high as for formulations C and D (Figure 6.18),

nonetheless, mechanical durability is far more superior. It is most probably attributable to the fact that this coating displays high level of uniformity in surface texture profile. The apparent contact area between two surfaces is strongly dependent upon the shape and number of surface asperities and therefore, the load applied to the surfaces will be transferred only through these points of contact. Symmetry in distribution of contact points leads to uniform distribution in stresses in material and greater stability in abrasive environments in comparison to surfaces with high degree of asymmetry. The retention ratio of TWI formulation F resembles the behaviour pattern found in smooth surfaces, such as formulation A and B. Nevertheless, this applies only when formulation F is subjected to polishing-type abrasion (CS10 wheels). The situation changes, when more aggressive type of material starts to abrade the coating (H18 wheels, conditions 3 and 4). Different behaviour under different wear-type modes can be identified with coating composition. Among the TWI coatings, formulation F is the only one that has fluoropolymer component. The C-F bond has a much greater dipole moment than does the C-H bond and therefore, materials with C-F bonding might have greater ability to keep film integrity when exposed to some kinds of wear. Harsh abrasive conditions (conditions 3 and 4) lead to faster and greater changes in surface roughness than in case of mild abrasion (conditions 1 and 2). The combination of highly hydrophobic nature of fluorocarbon and great increase in surface roughness helps to boost the overall repellent characteristics (Wenzel state) and this is why the WCA increases with the time of abrasion in conditions 3 and 4. Nevertheless, changes that happen in surface roughness under harsh abrasive conditions (conditions 3 and 4) are beyond the scope of this thesis.

The commercial product Never Wet has an extraordinary high roughness level ( $R_a=8.3 \mu\text{m}$ ) and does not have the ability to keep film integrity under abrasion and therefore, its lifetime is limited. The repellent properties of this coating system are rapidly lost with the time of contact with abrasive material. The short lifetime under abrasion of Never Wet and its poor ability to retain main functional performance resembles the behavioural pattern of TWI formulation C and D. Nevertheless, the repellency-wear mechanism takes much faster than in any other coating system examined in this study. This can be explained by the fact that this coating is the only one, which losses its initial roughness level under exposure to mechanical damage (Figure 6.21). The great initial repellency of Never Wet is mainly because of the effect of its high value of arithmetic means of surface heights and peak

predominance in surface profile. The rapid loss of surface roughness results in a decrease in its ability to trap air beneath the droplet and therefore, its affinity to water increases.

The GP101 system doesn't have the ability to resist abrasion or retain its initial wetting characteristics. In this case, surface roughness profile resembles the texture of TWI formulation F, yet overall coating durability performance is completely different. The reasons of GP101 failure might be the effect of coating composition (poor quality bonding), thin film layer (Table 6.1) or due to the coating processing. SEM images of GP101 system (Figure 6.22) reveal that there is a lot of debris on the surface. During air drying in lab conditions, impurities could have been absorbed by the coating, which results in high inhomogeneity and therefore, failure processes might take much faster.

With regard to chemical resistance examination, two types of wear mechanisms were observed under exposure to different environments (acid, alcohol, salt). Surface ageing by immersion not only results in loss of adhesion between substrate and coating but also in loss of ability to retain functional performance. It is commonly observed that coatings lose adhesion when subject to moist environments (Lefebvre D. R., 1991). The mechanism under which this process occurs might be the result of water diffusion through the coating because of its permeability to water. Adhesive wear might be also the effect of transport across the interface itself because of disconnections between substrate and coating, resulting from poor surface preparation. In the case of the TWI formulations, all substrates were prepared with etching combined with anodizing procedure. According to findings from Chapter 5, this type of surface preparation was the best-practise available methodology that helps to enhance the adhesion between aluminium and the TWI coatings. Figure 6.33 illustrates how surface preparation procedure influences the ability of the coating to keep integrity with its substrate. In this case, it can be assumed that adhesive failure of TWI formulations doesn't come from poor surface processing.

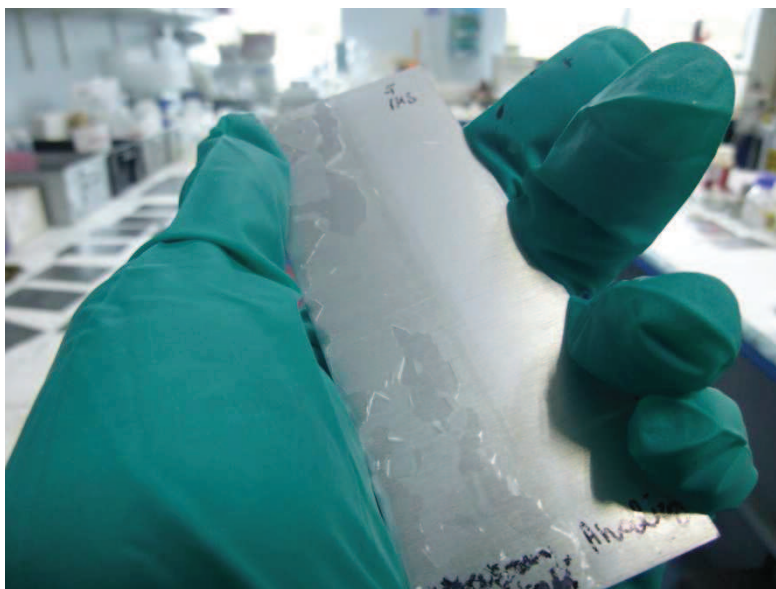


*Figure 6.33 Effect of surface preparation procedure on the interface integrity between aluminium and TWI formulation F (one week of immersion in 5%NaCl solution) – acetone wiping (left side) and etching combined with anodizing (right side)*

The same coating system behaves differently under different chemical ageing conditions. Amongst the selected testing environments, immersion in 1% $H_2SO_4$  turned out to be the most aggressive one in terms of both adhesive wear and repellency-wear. In this condition, a loss of surface integrity was found in TWI formulation A, B and both of selected commercial products (Figure 6.23) and this failure doesn't correspond to initial value of adhesion strength. Poor chemical durability performance of TWI formulation A and commercial GP101 is most probably the effect of weak bonding mechanism between the coating and aluminium. Disconnection at the interface leads into liquid diffusion and loss of overall film integrity, which results in changes in functional performance of coating system. Figure 6.26 shows that exposure to acidic environment in TWI formulation A and commercial GP101 results in increase of surface wettability. Formulation A loses its repellency by more than 50 % (WCA falls from  $104.6 \pm 0.6^\circ$  to  $49 \pm 3.8^\circ$ ), whereas GP101 drops its WCA by  $83.6^\circ$ .

TWI formulation B presents the highest values of initial adhesion strength, yet its superior pristine performance doesn't guarantee coating stability under acidic environment. Nevertheless, loss of film integrity and initial repellency of formulation B is slower than in case of formulation A. Such behaviour can be explained by the role of SSQs in coating composition. Introduction of SSQs in the coating system increases its barrier properties (Nguyen T.A., 2014). Reduction of liquid permeability through surface voids and micropores helps to keep film integrity on a chemical and mechanical manner. Therefore, coating will be able to retain its repellency ability for

extended period of time. This potentially explains why the WCA of TWI formulation B doesn't change much even after exposure to harsh chemical environments (Figure 6.26).

TWI formulations C, D, E and F present excellent properties in terms of surface mechanical integrity. Any degree of material-wear failure was visually observed after chemical resistance testing of these coating systems (Figure 6.23, 6.24 and 6.25). This results from the effect of incorporation of silica nanoparticles into resin that improve coating barrier properties (Deflorian F., 2011). Despite the diffusion reduction, different degree of repellency retention can be observed in these coating systems. TWI formulation C and D suffer from significant loss of their wetting properties in acidic and salty environments (Figure 6.26). Such behaviour can be related to their initial roughness profile. High value of arithmetic means of surface heights and asymmetry of peaks and valleys distribution lead to greater probability of surface failure when exposure to constant liquid floating. TWI formulation E presents almost the same degree of WCA retention as formulation B, which can be related to resemblance in their surface profile. Among selected coatings, TWI formulation F displays the greatest ability to retain repellency under aggressive chemical environments, regardless of its quite high roughness profile. What makes this coating different than others is the presence of C-F chemical bond that undoubtedly contributes to the excellent chemical stability of the material (Kinzig B.J., 1978).

Commercial product Never Wet keeps its repellency under specified ageing condition, whereas its film integrity is only affected by acidic solution. Nevertheless, chemical stability analysis of selected commercial products is beyond the scope of this thesis.

## **6.5 Summary**

The relationship between surface composition and structure influences functional performance of coating system in every aspect of coatings applicability. Exposure to operational conditions affects coatings roughness profile and therefore, wear of surface occurs. Different surface application involves different challenges in terms of durability. Regardless of operational conditions, it was found that coating failure has bimodal nature and can be measured on direct and indirect level. In case of highly repellent surfaces, overall lifetime of the coating represents its direct durability and therefore, correlates to its mechanical wear-mode. Indirect assessment refers to its

ability to retain its functional performance, which is determined by the changing of water contact angle over time.

Influence of different damage conditions on repellency wear-mode and lifetime of selected coating systems were studied according to new assessment methodology. In terms of abrasive wear, the highest survivability was found in coating systems that have low value of arithmetic means of surface profile and symmetric distribution of peaks and valleys (TWI formulations A, B and E). Similar mechanical resilience was found as well in coating material that displays quite high Ra value, but keeps great uniformity in roughness heights (TWI formulation F). On the contrary, surfaces with high Ra value, but asymmetry in peaks and valleys distribution don't have the ability to resist abrasion for a long time (TWI formulation C and commercial product Never Wet). It was found as well that mechanical resistance of the coating is affected by its thickness, processing and cure regime, beyond the effect of surface roughness and composition (TWI formulation D and commercial product GP101).

Abrasive wear lead to a loss of surface repellency in almost all of tested conditions. The greatest changes in surface wettability over time were reported in coating systems with a high level of initial roughness profile and high degree of asymmetry (TWI formulation C and commercial product Never Wet). In these surfaces, the rate of repellency loss occurs in similar manner regardless of type of abrasive material. Different retention behaviour was found in surfaces with smooth, symmetric roughness profiles. In these surfaces, loss of hydrophobic character is less rapid under mild abrasive conditions and increases under exposure to harsh environments.

In terms of adhesive wear, it was found that improvement of coating barrier properties helps to boost surface chemical durability, regardless of initial adhesion strength between the coating and the substrate. Enhancement of barrier properties and good quality bonding between coatings molecules guarantees that adhesive wear and repellency wear occurs slow even in harsh acidic environments (TWI formulation F).

In this chapter key selected coatings properties were examined and analysed, including initial characteristics, abrasion resistance, retention ratio and lifetime in chemical environments. In the following chapter, these raw performance data will be transferred into spider diagram pointing system and performance indices, so that final plot of performance indices can be established.

## 7 CLASSIFICATION OF EASY CLEAN COATINGS

A novel approach for the assessment and comparison of low energy, easy clean coatings is proposed. Two conditions were fulfilled prior the application of this novel routine. It was established that the degree of conversion for the coating system had to reach point at which its functional properties were fully developed. Likewise, the adhesion between coating and aluminium substrate was enhanced by selecting best-practise available surface preparation routine. Once these criteria were accomplished (for TWI formulations), the coating systems were subjected to further evaluation. Commercial products were prepared according to manufacturer's guidance and subjected to testing. This chapter details the methodology that combines the various characterization data of the coating systems into a novel assessment tool that allows comparison between different coating systems. The parent performance data generated during the surface testing is transferred into a spider diagram banding system. Furthermore, these spider diagrams were used in order to establish unique coating performance indices. The final part of this chapter provides global plot of performance indices that relates the repellence characteristics and durability of each coating.

### 7.1 Spider diagrams

The spider diagrams for all the easy clean surfaces tested are listed below. The classification criteria for the spider diagram were evaluated according to banding system presented in Chapter 3. Tables 7.4 - 7.11 provide summaries of performance characteristics of selected coating systems, including raw data and corresponding values in each spider diagram system. Evaluation routines and guidelines regarding number of replicates used for each type of testing were presented in Chapter 3 and 6. Summary of the properties measured, measurement techniques used and accompanying standard procedures (if applicable) are provided in Table 7.1. Table 7.2 and 7.3 provides the general principle of spider diagram banding system. Detailed explanation regarding chemical resistance scoring system can be found in Chapter 3.

Table 7.1 Summary of the properties measured, measurement techniques and accompanying standard procedures

Property	Technique	Standard
Water contact angle (WCA) initial	Drop shape analyser	ASTM D7490
Diiodomethane contact angle (DCA) initial	Drop shape analyser	ASTM D7490
Gloss initial	Glossmeter	ASTM D523
Haze initial	Glossmeter	ASTM E430
Abrasion (cond. 1)	Taber abrader, CS10 wheels/500 g	ASTM D4060
Abrasion (cond. 2)	Taber abrader, CS10 wheels/1000 g	ASTM D4060
Abrasion (cond. 3)	Taber abrader, H18 wheels/500 g	ASTM D4060
Abrasion (cond. 4)	Taber abrader, H18 wheels/1000 g	ASTM D4060
RR (cond. 1)	Drop shape analyser	ASTM D7490
RR (cond. 2)	Drop shape analyser	ASTM D7490
RR (cond. 3)	Drop shape analyser	ASTM D7490
RR (cond. 4)	Drop shape analyser	ASTM D7490
Adhesion strength	Pull-off tester	ASTM D4541
Chemical resistance 1	1 week immersion in 1% $H_2SO_4$	ASTM D6943 - 15
Chemical resistance 2	1 week immersion in IMS	ASTM D6943 - 15
Chemical resistance 3	1 week immersion in 4.95% NaCl	ASTM D6943 - 15

Table 7.2 Summary of spider diagram pointing system

Spider diagram point	WCA initial [°]	DCA initial [°]	Gloss [GU]	Haze [HU]	CS10 wheels (no. of cycles) 500/1000g load	H18 wheels (no. of cycles) 500/1000g load	Retention ratio [%]	Adhesion [MPa]
1	90	10 ≥	20 ≥	50 ≥	50 ≥	5 ≥	Δ±80% ≥	0.1 ≥
2	95	30	50	45	100	10	Δ ± 70%	0.5
3	100	50	70	40	250	25	Δ ± 60%	1
4	105	70	90	35	500	50	Δ ± 50%	1.5
5	110	90	110	30	1000	100	Δ ± 40%	2
6	115	110	130	25	1500	150	Δ ± 30%	2.5
7	120	120	150	20	2000	200	Δ ± 20%	3
8	130	130	170	15	2500	300	Δ ± 10%	3.5
9	140	140	190	10	3000	400	Δ ± 5%	3.75
10	150 ≤	150 ≤	200 ≤	5 ≤	3500 ≤	500 ≤	1	4 ≤

Table 7.3 *Chemical resistance classification (adhesive failure analysis) criteria for spider diagram (additional information to the Table 7.2)*

Classification (points)	Description
0	The edges of the sample are completely smooth, coating is not detached from the surface.
-1	Detachment of the coating at the edges of the sample, the area affected is not greater than 20%
-2	The coating has flaked along the edges, the area affected reaches 40%
-3	The area affected is greater than 40% but do exceed more than 60%
-4	The area affected is greater than 60% but do not exceed more than 80%
-5	The coating is detached from the surface in more than 80%

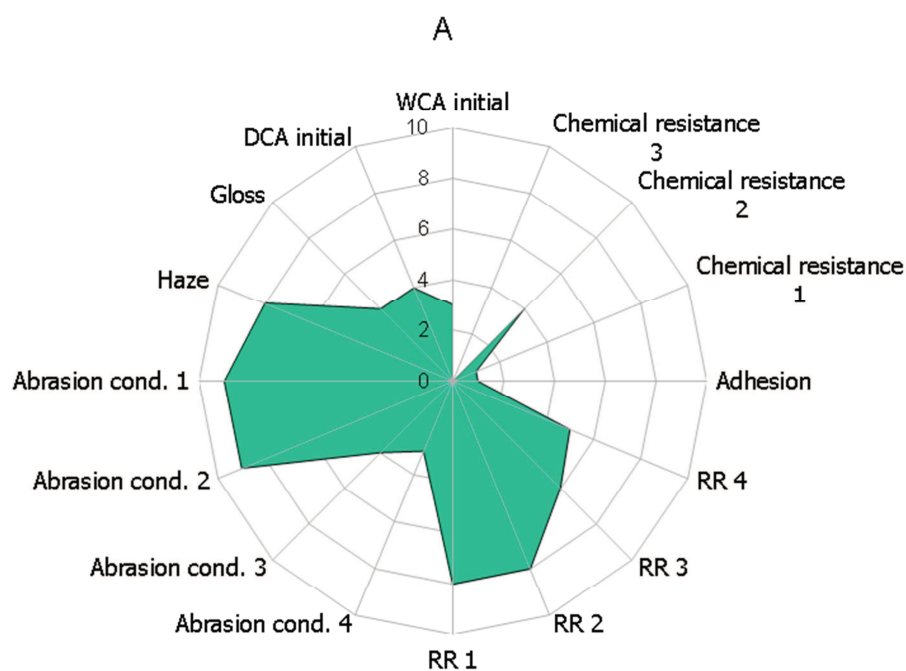


Figure 7.1 TWI formulation A – spider diagram

Table 7.4 TWI formulation A properties represented by numerical value (spider diagram banding) (% AA - % of affected area)

Property	Value	Unit	Points (spider diagram)
WCA initial	102.3	Degree	3
DCA initial	74.4	Degree	4
Gloss initial	105.5	GU	4
Haze initial	15.6	HU	8
Abrasion (cond. 1)	3100	No. of cycles	9
Abrasion (cond. 2)	3100	No. of cycles	9
Abrasion (cond. 3)	75	No. of cycles	4
Abrasion (cond. 4)	29	No. of cycles	3
RR (cond. 1)	0.93	%	8
RR (cond. 2)	0.93	%	8
RR (cond. 3)	0.72	%	6
RR (cond. 4)	0.66	%	5
Adhesion strength	0.41	MPa	1
Chemical resistance 1	0.47+40% AA	%	1
Chemical resistance 2	0.62+10% AA	%	4
Chemical resistance 3	0.25+15% AA	%	0

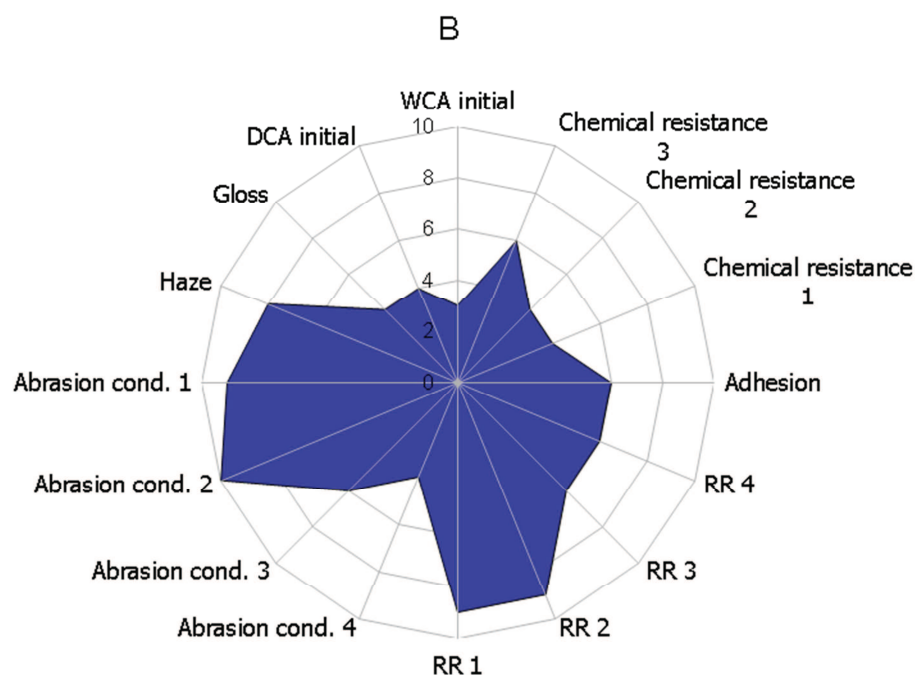


Figure 7.2 TWI formulation B – spider diagram

Table 7.5 TWI formulation B properties represented by numerical value (spider diagram banding) (% AA - % of affected area)

Property	Value	Unit	Points (spider diagram)
WCA initial	103.2	Degree	3
DCA initial	74.7	Degree	4
Gloss initial	103.4	GU	4
Haze initial	13.3	HU	8
Abrasion (cond. 1)	3400	No. of cycles	9
Abrasion (cond. 2)	3500	No. of cycles	10
Abrasion (cond. 3)	150	No. of cycles	6
Abrasion (cond. 4)	70	No. of cycles	4
RR (cond. 1)	1.02	%	9
RR (cond. 2)	0.96	%	9
RR (cond. 3)	0.73	%	6
RR (cond. 4)	0.76	%	6
Adhesion strength	2.7	MPa	6
Chemical resistance 1	0.74+40% AA	%	4
Chemical resistance 2	0.63+20% AA	%	4
Chemical resistance 3	0.90+10% AA	%	6

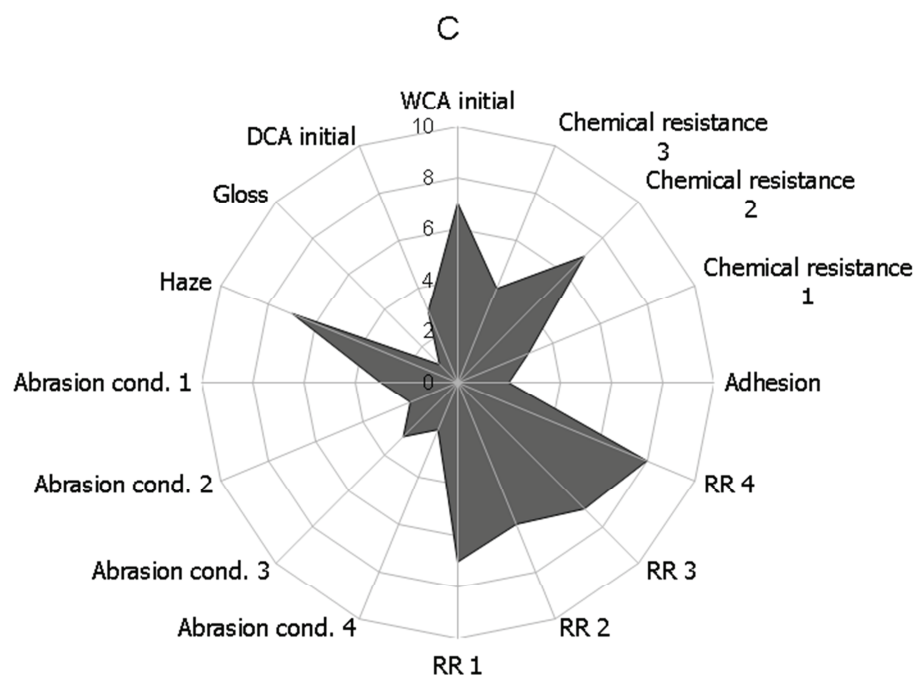


Figure 7.3 TWI formulation C – spider diagram

Table 7.6 TWI formulation C properties represented by numerical value (spider diagram banding) (% AA - % of affected area)

Property	Value	Unit	Points (spider diagram)
WCA initial	121.4	Degree	7
DCA initial	51.2	Degree	3
Gloss initial	40.8	GU	1
Haze initial	18.4	HU	7
Abrasion (cond. 1)	360	No. of cycles	3
Abrasion (cond. 2)	170	No. of cycles	2
Abrasion (cond. 3)	28	No. of cycles	3
Abrasion (cond. 4)	13	No. of cycles	2
RR (cond. 1)	0.80	%	7
RR (cond. 2)	0.77	%	6
RR (cond. 3)	0.85	%	7
RR (cond. 4)	0.91	%	8
Adhesion strength	0.8	MPa	2
Chemical resistance 1	0.40	%	3
Chemical resistance 2	0.88	%	7
Chemical resistance 3	0.47	%	4

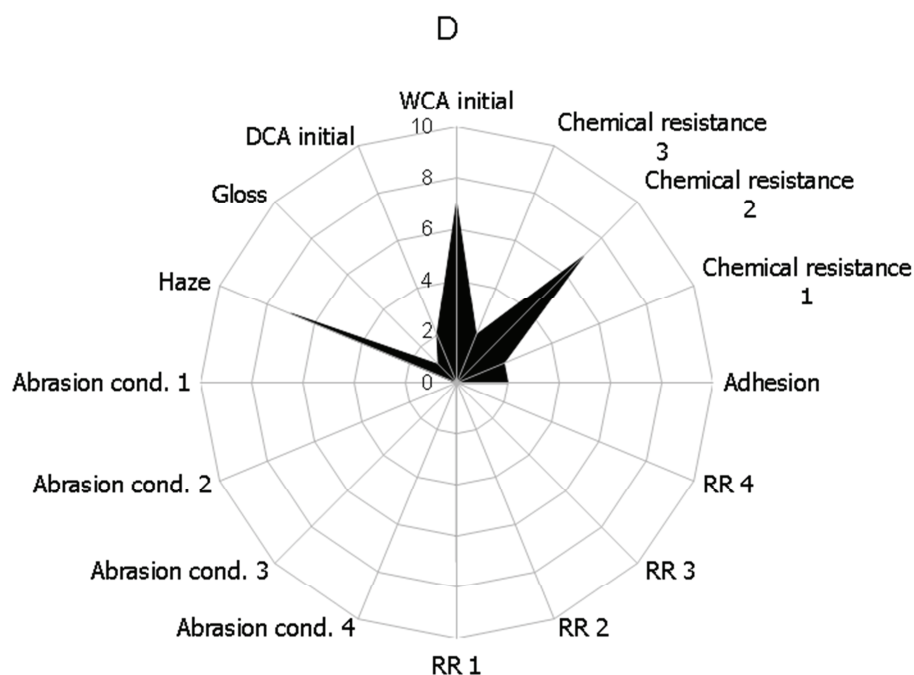


Figure 7.4 TWI formulation D – spider diagram

Table 7.7 TWI formulation D properties represented by numerical value (spider diagram banding) (% AA - % of affected area)

Property	Value	Unit	Points (spider diagram)
WCA initial	128.9	Degree	7
DCA initial	46.7	Degree	2
Gloss initial	25.7	GU	1
Haze initial	16.4	HU	7
Abrasion (cond. 1)	3	No. of cycles	0
Abrasion (cond. 2)	0	No. of cycles	0
Abrasion (cond. 3)	0	No. of cycles	0
Abrasion (cond. 4)	0	No. of cycles	0
RR (cond. 1)	0.8	%	7
RR (cond. 2)	0	%	0
RR (cond. 3)	0	%	0
RR (cond. 4)	0	%	0
Adhesion strength	0.7	MPa	2
Chemical resistance 1	0.33	%	2
Chemical resistance 2	0.85	%	7
Chemical resistance 3	0.31	%	2

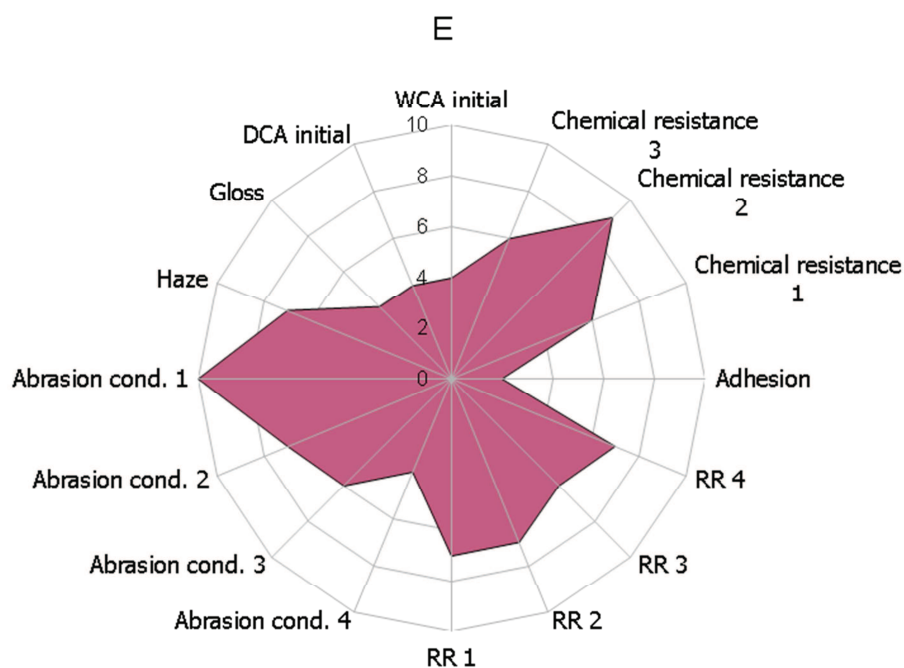


Figure 7.5 TWI formulation E – spider diagram

Table 7.8 TWI formulation E properties represented by numerical value (spider diagram banding) (% AA - % of affected area)

Property	Value	Unit	Points (spider diagram)
WCA initial	102.5	Degree	4
DCA initial	72.8	Degree	4
Gloss initial	105.4	GU	4
Haze initial	17.2	HU	7
Abrasion (cond. 1)	3500	No. of cycles	10
Abrasion (cond. 2)	2300	No. of cycles	7
Abrasion (cond. 3)	100	No. of cycles	6
Abrasion (cond. 4)	60	No. of cycles	4
RR (cond. 1)	0.82	%	7
RR (cond. 2)	0.87	%	7
RR (cond. 3)	0.74	%	6
RR (cond. 4)	0.83	%	7
Adhesion strength	0.6	MPa	2
Chemical resistance 1	0.72	%	6
Chemical resistance 2	0.99	%	9
Chemical resistance 3	0.73	%	6

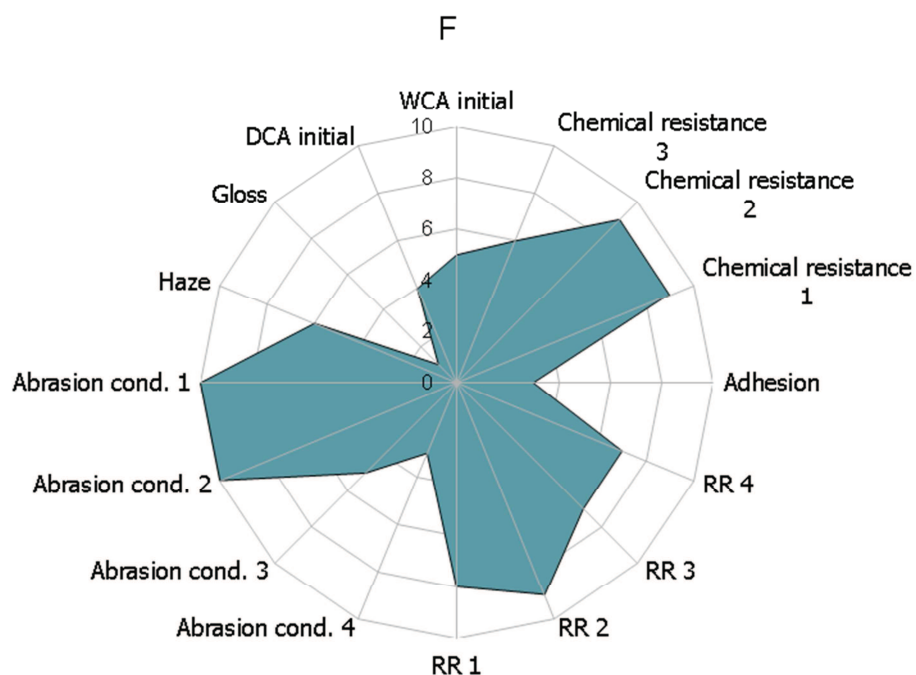


Figure 7.6 TWI formulation F – spider diagram

Table 7.9 TWI formulation F properties represented by numerical value (spider diagram banding) (% AA - % of affected area)

Property	Value	Unit	Points (spider diagram)
WCA initial	112.3	Degree	5
DCA initial	83.6	Degree	4
Gloss initial	16.6	GU	1
Haze initial	22.9	HU	6
Abrasion (cond. 1)	3500	No. of cycles	10
Abrasion (cond. 2)	3500	No. of cycles	10
Abrasion (cond. 3)	115	No. of cycles	7
Abrasion (cond. 4)	29	No. of cycles	3
RR (cond. 1)	0.91	%	8
RR (cond. 2)	0.95	%	9
RR (cond. 3)	1.11	%	7
RR (cond. 4)	1.11	%	7
Adhesion strength	1.1	MPa	3
Chemical resistance 1	1.02	%	9
Chemical resistance 2	1.03	%	9
Chemical resistance 3	0.85	%	6

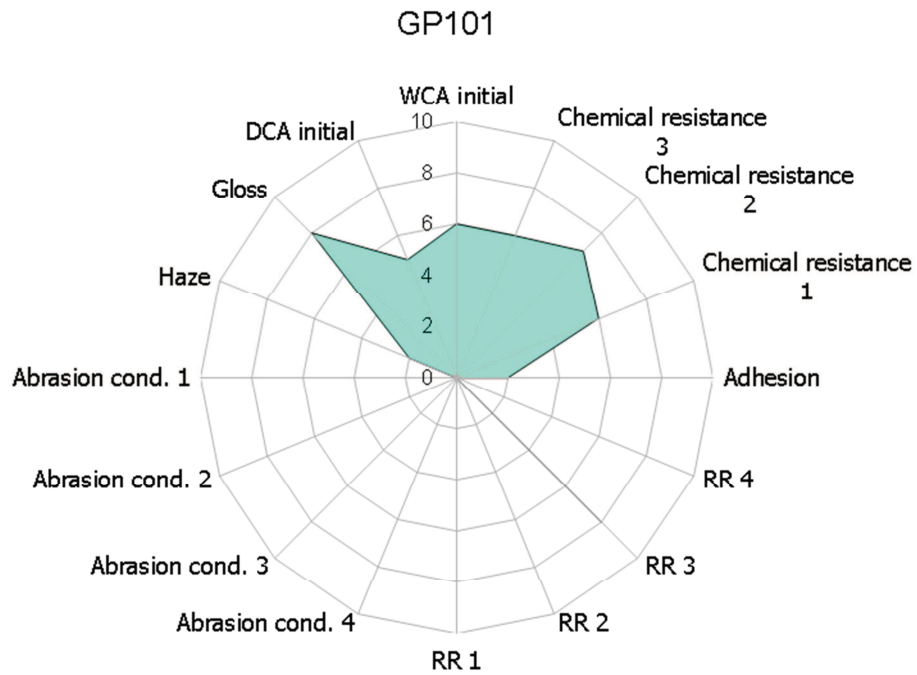


Figure 7.7 GP101 Anti-graffiti system – spider diagram

Table 7.10 TWI formulation GP101 properties represented by numerical value (spider diagram banding) (% AA - % of affected area)

Property	Value	Unit	Points (spider diagram)
WCA initial	118.4	Degree	6
DCA initial	90.7	Degree	5
Gloss initial	181.5	GU	8
Haze initial	49.2	HU	2
Abrasion (cond. 1)	0	No. of cycles	0
Abrasion (cond. 2)	0	No. of cycles	0
Abrasion (cond. 3)	4	No. of cycles	0
Abrasion (cond. 4)	0	No. of cycles	0
RR (cond. 1)	0	%	0
RR (cond. 2)	0	%	0
RR (cond. 3)	1.02	%	9
RR (cond. 4)	0	%	0
Adhesion strength	0.7	MPa	2
Chemical resistance 1	0.32+30% AA	%	6
Chemical resistance 2	0.96+20% AA	%	7
Chemical resistance 3	0.85+5% AA	%	6

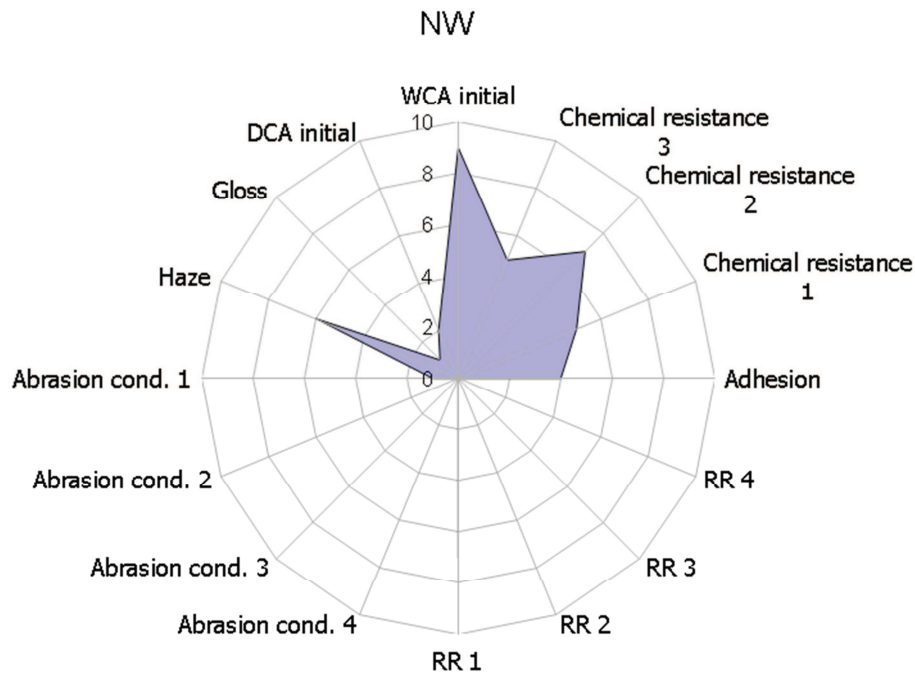


Figure 7.8 Never Wet system – spider diagram

Table 7.11 TWI formulation Never Wet properties represented by numerical value (spider diagram banding) (% AA - % of affected area)

Property	Value	Unit	Points (spider diagram)
WCA initial	143.9	Degree	9
DCA initial	46.9	Degree	2
Gloss initial	14.9	GU	1
Haze initial	23.2	HU	6
Abrasion (cond. 1)	90	No. of cycles	1
Abrasion (cond. 2)	45	No. of cycles	0
Abrasion (cond. 3)	18	No. of cycles	0
Abrasion (cond. 4)	6	No. of cycles	0
RR (cond. 1)	0.85	%	7
RR (cond. 2)	0	%	0
RR (cond. 3)	0	%	0
RR (cond. 4)	0	%	0
Adhesion strength	1.7	MPa	4
Chemical resistance 1	0.89+30% AA	%	5
Chemical resistance 2	0.86	%	7
Chemical resistance 3	0.64	%	5

## 7.2 Performance profile and Figures of Merit

Spider diagrams were used to create unique coating performance index that consists of six separate indices assigned for specific group of properties. Table 7.12 provides performance indices for eight types of coating systems validated in this study. Graphic scheme of proposed evaluation criteria is given in Figure 7.9. Calculations were made in a following manner:

$$PI_{Ci} = \frac{PG_{Ci}}{MPG_{Ci}} \quad (7.1)$$

The symbol PG corresponds to number of points scored by specific coating (c) in specific group of properties (i=1a, 1b, 1c, 2, 3 or 4 part of spider diagram). MPG is the maximum value that can be scored in this specified group of properties (i.e. MPG for 1a part of spider diagram will be 10, but MPG for 2 part of spider diagram will be 40, since it's a combination of four abrasion conditions).

PG<sub>1a</sub> = Repellency in pristine state

PG<sub>1b</sub> = Lipophobic characteristics in pristine state

PG<sub>1c</sub> = Visual appearance in pristine state

PG<sub>2</sub> = Ability to resist abrasion (in four specified abrasion conditions)

PG<sub>3</sub> = Ability to retain wetting characteristics after abrasion exposure (in four specified abrasion conditions)

PG<sub>4</sub> = Adhesion performance combined with chemical durability (adhesion in pristine state together with chemical resistance in three specified conditions)

Each performance index (PI<sub>Ci</sub>) can be summed and used to establish general performance index of specified coating (PI<sub>C</sub>) (Eq.7.2):

$$PI_C = \sum_{i=1}^n PI_{Ci} \quad (7.1)$$

Table 7.12 Performance indices for selected coating systems

Coating	PI <sub>1a</sub>	PI <sub>1b</sub>	PI <sub>1c</sub>	PI <sub>2</sub>	PI <sub>3</sub>	PI <sub>4</sub>	PI <sub>C</sub>
A	0.3	0.4	0.6	0.625	0.675	0.15	<b>2.75</b>
B	0.3	0.4	0.6	0.725	0.75	0.5	<b>3.28</b>
C	0.7	0.3	0.4	0.25	0.7	0.4	<b>2.75</b>
D	0.7	0.2	0.4	0	0.175	0.325	<b>1.80</b>
E	0.4	0.4	0.85	0.6	0.55	0.575	<b>3.38</b>
F	0.5	0.4	0.35	0.7	0.775	0.675	<b>3.40</b>
GP101	0.5	0.6	0.1	0	0.25	0.475	<b>1.93</b>
Never Wet	0.9	0.2	0.35	0.025	0.175	0.525	<b>2.18</b>

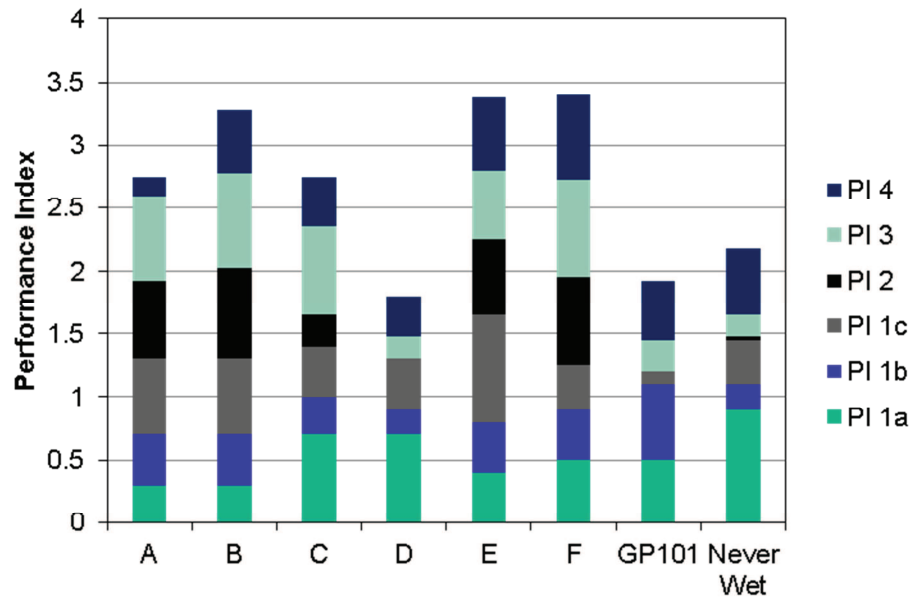


Figure 7.9 Coating performance profile based on the six separate performance indices associated with the selected group of key properties

Figures of merit for performance characterization of highly repellent surfaces for different application scenario are listed below. Figure 7.10 indicates general support for null hypothesis and illustrates a trade-off between wetting characteristics and durability for the easy clean coating systems investigated. This particular scenario represents coating durability as mechanical resistance under different abrasive conditions.

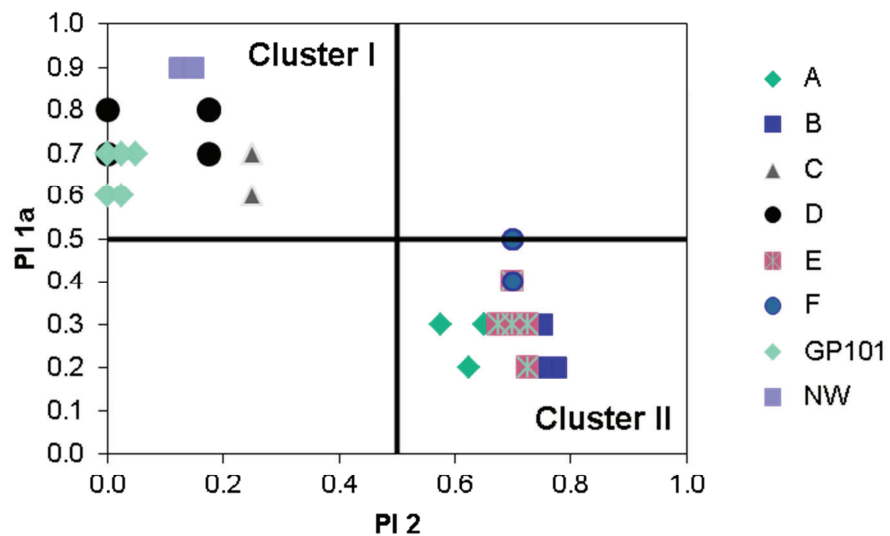


Figure 7.10 Plot of performance indices for easy clean coatings (for five test specimens per coating type). Relation between pristine WCA ( $PI_{1a}$  – performance index for initial repellency) and mechanical durability ( $PI_2$  – performance index for abrasion resistance (combination of four specified abrasion conditions))

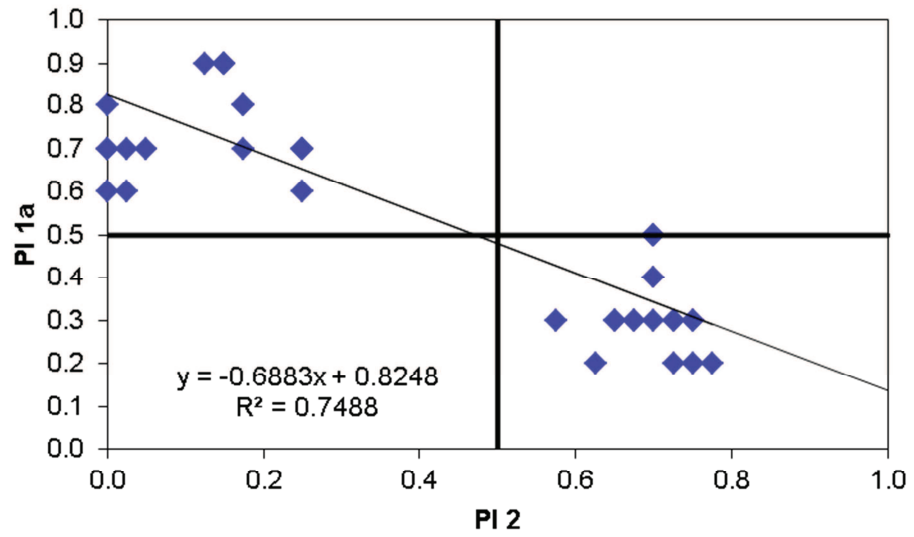


Figure 7.11 Support for null hypothesis – inverse relationship between initial WCA (PI<sub>1a</sub>) and mechanical durability (PI<sub>2</sub>) (for all selected coating systems without distinction between families of coating)

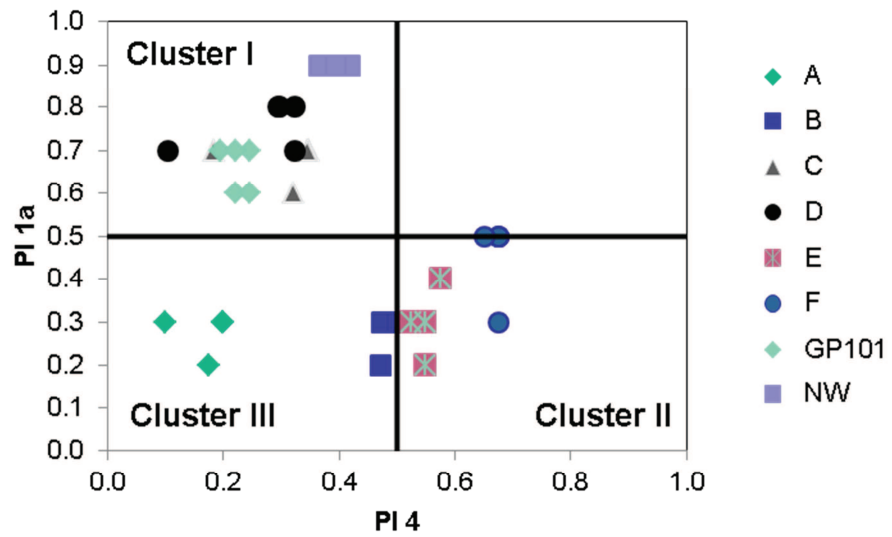


Figure 7.12 Plot of performance indices for easy clean coatings. Relation between pristine WCA (PI<sub>1a</sub> – performance index for initial repellency) and chemical durability (PI<sub>4</sub> – performance index for adhesion performance under chemical degradation)

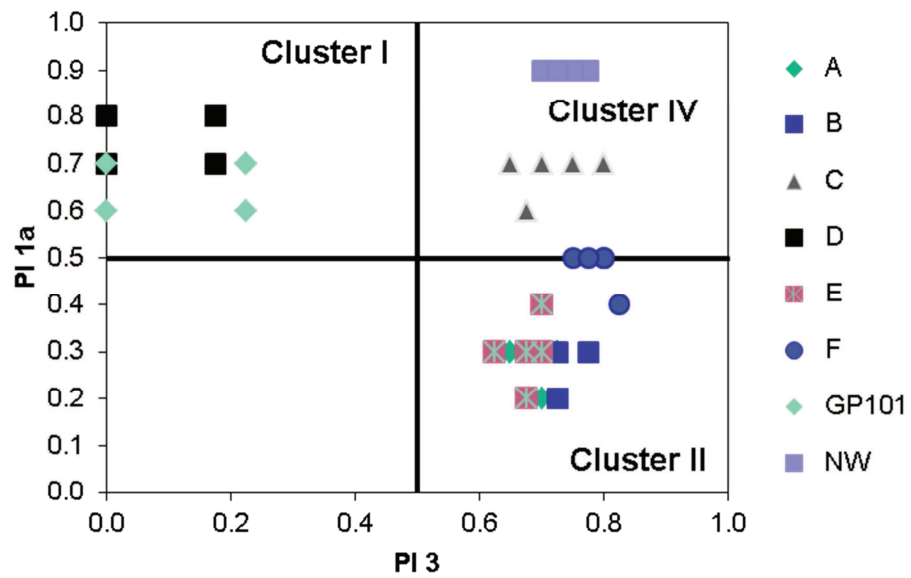


Figure 7.13 Plot of performance indices for easy clean coatings. Relation between initial repellency (PI<sub>1a</sub>) and indirect durability referred as ability to retain initial repellency under abrasive conditions (PI<sub>3</sub>)

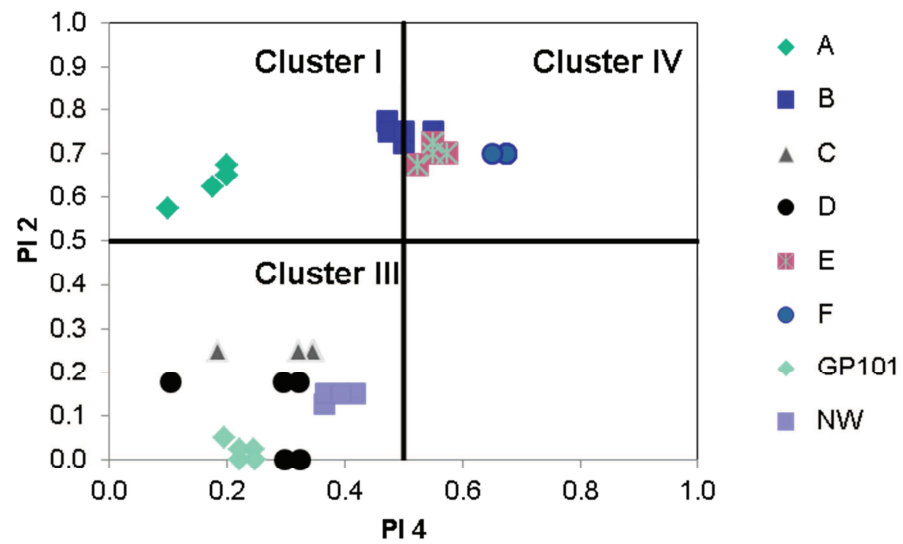


Figure 7.14 Plot of performance indices for easy clean coatings. Relation between mechanical durability under abrasive conditions (PI<sub>2</sub>) and chemical durability (PI<sub>4</sub> – performance index for adhesion performance under chemical degradation)

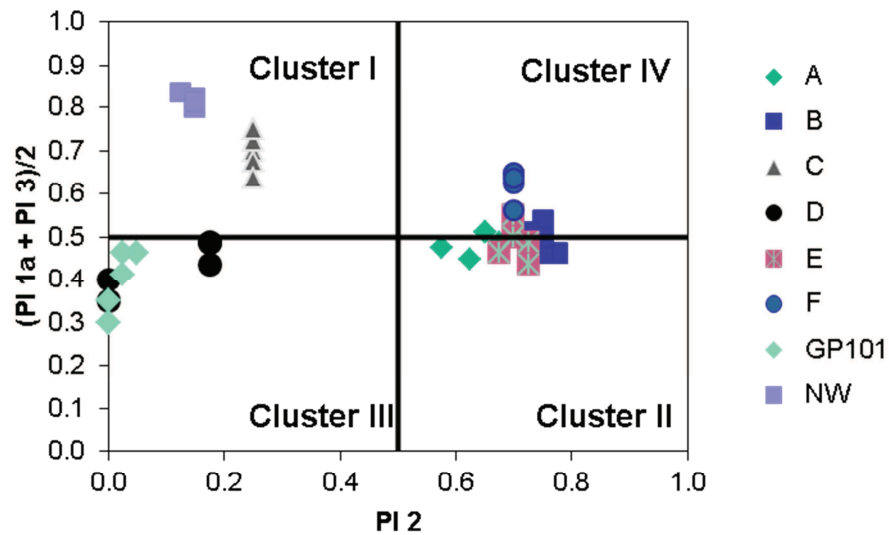


Figure 7.15 Plot of performance indices for easy clean coatings. Relation between coating repellent characteristics over lifetime (average of initial WCA ( $PI_{1a}$ ) and retention ration under abrasive condition ( $PI_3$ )) and mechanical durability under abrasive conditions ( $PI_2$ )

### 7.3 Discussion

The range of possible applications of highly repellent surfaces is enormous and different applications involve different challenges in terms of coating durability and retention of functional performance. The diversity of wear mechanisms that occur in material under its operation conditions makes it almost impossible to perform a full and representative durability assessment of candidate coating systems. Nevertheless, it should be noted that more in-depth study of coating and surface behaviour in a variety of potential harmful environments will bring benefits in terms of coating lifetime assessment. It should be noted as well that in real-world conditions, failure occurs due to synergy between different wear mechanisms. Erosion, abrasion, thermal effects etc. can all affect the surface performance as a separate phenomenon, but very often they overlap and affect the material concurrently. To address all of these aspects, it is imperative to develop an improved quality control tool for assessment of highly repellent surfaces that is suitable for use in different industrial environments. Such an approach has been presented in a form of spider diagrams, performance indices and Figures of merit. The shaded area on spider diagram provides a form of “coating performance map”. Therefore, the usefulness of the coating or material for some specific applications can be directly pre-assessed. Figures 7.1-7.8 illustrate performance maps of the selected coating systems examined in this work. It can be immediately seen that each coating system has its own unique map. Materials with similar composition and surface roughness parameters display very similar shape of shaded area on a

spider diagram (i.e. TWI formulation A and B, see Figure 7.1 and 7.2). Nevertheless, it can be seen that any changes in surface structure or its composition will result in map shape deviations (i.e. TWI formulation A – parent material and TWI formulation C, D, E and F – derivative materials, see Figure 7.3, 7.4, 7.5 and 7.6). This correlates to surface structure-composition-property relationships that was investigated in Chapter 6 and confirms the value of the spider diagram approach. It shows on an easy way how to track the influence of changes in structure and composition on a final performance of the coating.

Spider diagrams are a very useful tool when comes to performance characteristics of single coating system. It is still possible to apply on graph performance characteristics of few coating systems. Nevertheless, shaded areas of different materials may be overlapping and many surfaces compared within one graph will hamper the benefits of such methodology. Therefore, there is a need to bring spider diagram results to more effective graphical way of coatings comparison. The presented spider diagrams were the step towards the creation of coating performance indices. Each performance index represents one specific property (like  $PI_{1a}$  indicating only initial repellency of the coating) or combines some specific group of related properties (like  $PI_2$  explains coating behavioural pattern under different abrasive conditions). Figure 7.9 illustrates performance indices approach taken into practise. Such a methodology allows for a simultaneous graphical representation of general performance characteristics of specified coating systems and its performance indices with regard to different group of properties. The performance index graph is useful not only for comparing the similarity between materials, but also for analysing the variables responsible for similarities and relation among variables in order to assess synergy between them. Looking into Figure 7.9 it can be seen that TWI formulation B, E and F are very similar in terms of the number of overall performance index of coating. Further analysis allows us to state that regardless this overall similarity, these formulations behave in a different manner. Performance indices of initial repellency ( $PI_{1a}$ ) of TWI formulation B has the lowest value among B, E and F systems, yet its performance index of visual appearance ( $PI_{1c}$ ) as well as performance index of retention ratio ( $PI_3$ ) recompense it. This graphical approach makes interpretation easier and permits for quicker decision making when it comes to coating selection. Another advantage of performance indices is that they can be used to establish a plot of performance indices. In many selection processes only few performance indicators will be necessary and

sufficiently relevant to make a selection decision and there is no need to provide full available information regarding coating functionality. In this case, it is important to have appropriate plot of performance indices that displays the relationship between these key indicators. In this study, classification of the coating system is based on quantitative measures of two of the performance characteristics, namely repellency and mechanical durability. Such model of plot of performance indices was proposed (Chapter 3) and brought into practise (Figure 7.10). Taking into consideration its applicability, it can be readily seen that durability of easy clean surfaces, even those based on very different chemistries can be directly compared. Besides that, the range of abrasion resistance of individual coating systems can be read from the graph.

The proposed plot of performance indices allows for tracking performance characteristics under changes that were introduced into coating structure or composition. Due to the fact that performance indices may correspond to a few values simultaneously, it is sometimes difficult to accurately assess coating performance based only on plot of performance indices. Such situation takes place when material mechanical durability is analysed. Performance index of abrasion resistance ( $PI_2$ ) is an average value of coating lifetime assessment under four different abrasive conditions. Therefore,  $PI_2$  itself can't be correlated to singular abrasive environment. It might happen that a particular coating system will be very durable under mild conditions and poorly respond in harsh environments, yet its  $PI_2$  will have the same value as for the surface present quite good durability in all of measured conditions. Nevertheless, the general ability of coating abrasion resistance can be easily read from proposed plot of performance indices. This may be the starting point for the designing a graph for predicting behavioural pattern of easy clean coatings. An example of the proposed mechanisms of process optimisation by the use of this graph is presented in Figure 7.16. The idea of such approach is to be able to roughly assess coating performance when some modifications were made to its composition of surface roughness. This will lead to a reduction in the number of development iterations, ultimately saving cost and development time.

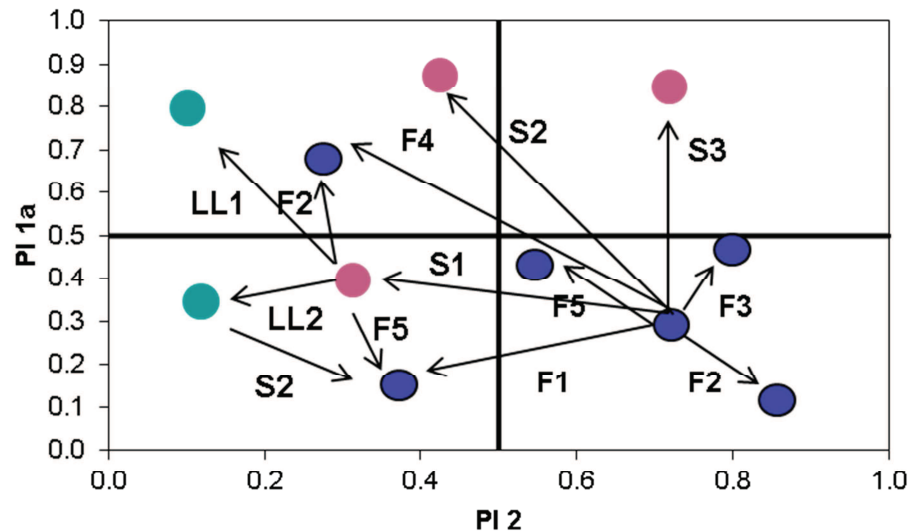


Figure 7.16 Proposed model of graph predicating behavioural pattern of easy clean coatings. F1-5 refers to changes in type of silica nanoparticles functionality, S1-3 symbolises type of silica nanoparticles size and LL1-2 corresponds to silica nanoparticles loading level

The graph model form Figure 7.16 gives the ability to design desirable materials and surface treatments by approach. In a presented model, only three variables are taken under consideration, such as nanoparticle functionality, size and loading level. Nevertheless, it should be noted that this model will be true for coating systems that undergo the same substrate preparation routine and they reach the same level of degree of conversion. In the case of selected coating systems, this model can be designed for all TWI formulations, due to the fact that they are based on the same matrix, they were subjected to the same procedure of substrate treatment and they were cured to the point, at which their functional properties were fully developed. Plot of performance indices methodology proposed in this study not only can be used to design material by approach but also can serve as guideline for surface classification. Initial ranking procedure was established in Chapter 4. The idea was to divide every plot of performance indices into four quarters and each quarter represents material with similar functional performance, regardless their composition and coating processing routine. However, there are some criteria that that need to be established before any of coating system can be evaluated and its functional characteristics can be compared on plot of performance indices. This is mainly referring to coating processing, such as surface preparation, curing/drying regime and dry film thickness. It has to be assumed that prior to surface evaluation, all those three parameters were fulfilled on the best possible manner. This especially applies for the examination of commercial products and in this study refers to GP101 and Never Wet. Since these products are available on the market, it can be

expected that all the information provided by manufacturer regarding the processing routine are the ones that gives the best variation of this products. Such assumption eliminates the problem of comparing coatings with different dry film thickness or preparation routines.

The purpose of this study was to respond to the technological gap regarding a universal classification system for the evaluation of the durability of easy clean coatings. The first step to achieve that was to define durability and transfer it into measurable variable. In this work, durability was classified in a number of different ways, namely abrasive resilience, adhesive resistance and chemical stability. Besides that, durability was presented as variable with bimodal nature with its direct and indirect level. For the purpose of this study, indirect durability refers only to ability of the coating to retain its original repellency. Nevertheless, this methodology can be extended in the future, by incorporating other aspects of coating performance, such as ability to retain initial lipophobicity or visual appearance.

Figure 7.10 illustrates the transfer from starting point of this work into practise. The null hypothesis presented in Chapter 2 states that there is an inverse relationship between coating wetting characteristics and its durability. New approach to measure durability of highly repellent surfaces introduced in this study supports the null hypothesis statement within the population of materials examined (Figure 7.11). If  $PI_{1a}$  is considered as a determinant of coating initial repellency and  $PI_2$  corresponds to mechanical durability presented in a form of abrasive resistance, the null hypothesis statement can be measureable. The graphical illustration of the selected easy clean surfaces performance presented in Figure 7.11 reveals that these coatings fall into two general clusters. Materials belonging to cluster I refer to surfaces with very good repellency in pristine state, but having poor durability, or retention of repellent behaviour. Cluster II is populated by mechanically stable surfaces, where the initial repellency fulfils requirements for easy clean coatings ( $WCA > 90^\circ$ ) but it's not satisfactory for anti-soiling applications. According to Figure 7.11 the initial repellency and coating durability has an almost linear relationship. Nevertheless, such linearity is observed only when mechanical resilience is taken under consideration. When it comes to different durability scenarios, different correlations are observable in plot of performance indices. Consideration of chemical resistance ( $PI_4$ ) versus initial repellency ( $PI_{1a}$ ) indicated that the appearance of two characteristics clusters (cluster I – highly repellency, chemically non-durable; cluster II – repellent on a fair level, chemically durable) (Figure 7.12).

In addition, another cluster has appeared which characterises coatings with fair repellency and poor chemical durability. The observation of the relation between initial wettability of the surface ( $PI_{1a}$ ) and its ability to retain this property under abrasion ( $PI_3$ ) showed another type of cluster, which corresponds to materials with great anti-soiling characteristics over the whole lifetime (Figure 7.13). An analysis of the relation between surface repellency and different scenarios of durability reveals that this relationship has a very complex nature. Each wear mechanism is unique and for coating selection purposes, it would be highly recommended to consider every durability scenario as separate phenomenon.

The proposed model of coating performance assessment provides practical way of durability evaluation of highly repellent surfaces. The general understanding of surface characteristics that can be obtained from the plot of performance indices may be of great value for materials development and research. The inherent versatility of this novel approach allows it to be adapted to different substrates, different coatings technologies and different durability scenarios. The use of performance indices makes the interpretation easier and permits for a quick pre-assessment of coating lifetime. The number and nature of performance indices will be dependent upon the information that needs to be obtained from materials that are subjected to evaluation. Performance indices don't have to be represented only by performance characteristics but can be also used as indicator for coating processability and cost.

Progress in terms of developing a successful methodology for evaluation and comparison of highly repellent surfaces allows for the further development of advanced material. Novel testing criteria helps to rank and compare different easy clean coatings and therefore, the technological gap regarding evaluation methodology isn't an obstacle anymore. In this case, there is a need to ask the question whether durable surfaces with extraordinary repellency can be produced. Analysis of figures of merit has the ability to answer this question. First of all, there is a need to answer what defines a successful coating system and which parts of plot of performance indices clusters the most desirable surfaces. Regardless the type of performance indices used in the graph, the most advanced surfaces can be found in right top corner of plot of performance indices.

Analysis of future perspective in terms of material development was performed on a basis of final plot of performance indices (Figure 7.15). This graph correspond to three types of performance indices that were mainly characterized in this work,

namely initial repellency ( $PI_{1a}$ ), abrasion resistance ( $PI_2$ ) and ability to retain wetting characteristics under abrasive conditions ( $PI_3$ ). Coating wettability should not only be characterized by the value in pristine state, but also by its value over the whole lifetime. It was therefore decided to evaluate coating repellency as an average value taken from two performance indices,  $PI_{1a}$  and  $PI_3$ . A plot of performance indices linking surface repellency with its durability showed four clusters of materials that correspond to four coating classes.

- Cluster I was formed by two types of materials, TWI formulation C and commercial product Never Wet. Their repellent characteristics were generally kept on high level over the whole lifetime of the coating (Figure 7.13). Nevertheless, abrasion resistance was quite poor and therefore, these surfaces can't be designated for harsh environments ( $PI_2 < 0.5$ ).
- Cluster II contained TWI formulations A, B, E. Surfaces that belong to this cluster displayed great mechanical robustness, yet their repellent properties were not satisfactory enough ( $(PI_{1a} + PI_3)/2 < 0.5$ ). There is also another behavioural pattern that characterises this group of materials. Despite their medium level of repellency in pristine state, they can retain this property over the whole lifetime (Figure 7.13).
- Cluster III was represented by the surfaces not really desirable for the industrial application of highly repellent surfaces. Both of performance indicators  $(PI_{1a} + PI_3)/2$  and  $PI_2$  were much lower than 0.5. These surfaces suffered from the lack of durability on indirect level. Regardless their great initial wetting characteristics, they weren't able to retain it (Figure 7.13). Two materials were found in this cluster, TWI formulation D and commercial product GP101
- Cluster IV contained only one type of coating. TWI formulation F was embedded in this cluster. This part of plot of performance indices corresponds to materials that have the most desirable properties and definitely can be adopted in industrial applications of easy clean coatings.

Surfaces that belong to some particular cluster aren't only similar in terms of functional performance. Evaluation of selected coating systems provided in Chapter 6 revealed that surface roughness influences materials performance often much more than its composition. Therefore, clusters from plot of performance indices don't represent only surfaces with similar performance but also with similar roughness level and type:

- Cluster I characterized surfaces with high value of arithmetic means of surface highs and asymmetric distribution of peaks and valleys in roughness profile. In these surfaces, the distribution has leptokurtic character with peak predominance. Type of roughness in pristine state is not the only factor that ties surfaces from cluster I. When these surfaces were exposed to damaging conditions, their texturing had the tendency to change in the same manner. After specified abrasion conditions (CS10 wheels, 1000 g load), surface roughness of materials from cluster I still preserved peak predominance (Chapter 6, Figure 6.35). Nevertheless, as a result of abrasion, the sharpness of roughness profile decreased and the distribution of peaks and valleys had more mesokurtic character.
- Cluster II represented surfaces with symmetric distribution of peaks and valleys with mesokurtic character and rather low value of arithmetic means of surface profile. Materials that belong to this cluster underwent the same changes upon abrasive conditions. Exposure to damaging conditions (abrasive conditions 2) increased overall roughness profile and introduced some level of asymmetry. After abrasion the texture had platykurtic distribution with valleys predominance.
- Cluster III represented surfaces where roughness could not be correlated with performance. All coatings that belong to this group have different type of surface texture. The poor performance of these coatings was rather a result of such textural variability.
- Cluster IV was characterized by only one type of coating and therefore, it's not possible to definitely state whether materials that belong to this group have resemblance in terms of surface roughness. Nevertheless, TWI formulation F had this sort of texturing type that can't be assigned to cluster I or cluster II. This coating had quite high value of arithmetic means of surface profile and symmetric distribution in pristine state. Exposure to abrasion affected the quality of texture in this material exactly in the same manner as it did in case of materials from cluster II.

According to the plot of performance indices (Figure 7.14) and roughness profile analysis, two desirable trends in roughness profile were observable. Mesokurtic distribution and symmetry in terms of peaks and valleys number in roughness profile in pristine state seemed to be the key to create durable materials. In many applications, material damage is strongly dependent upon the height and shape of

the highest asperities above the mean line. The predominance of sharp peaks in the surface roughness makes the material more fragile when placed into contact with other surfaces. This is the reason why TWI formulation C and commercial product Never Wet weren't durable under abrasive conditions. The loss of initial roughness pattern that helps to boost value of water contact angle in pristine state causes the loss of repellency as well. A high value of an arithmetic mean of surface heights definitely helps to increase anti-soiling properties of material, yet may also speed up wear mechanisms under abrasion. TWI formulation F was classified as durable surface despite its high value of Ra. Therefore, it can be stated that surfaces with high value of arithmetic means of surface heights are capable of being mechanically robust, but only if the distribution of these heights is symmetric. It should be assumed as well that there is a borderline in terms of Ra value at which the transition from durable to non-durable surface would be observed. An investigation of mechanical resilience of surfaces with symmetric mesokurtic distribution of asperities but different Ra value (from low to very high) could be interesting area for the future work. Figure 7.17 illustrates coating roughness trends and its influence on performance characteristics presented on a plot of performance indices (final plot of performance indices presented in Figure 7.15)

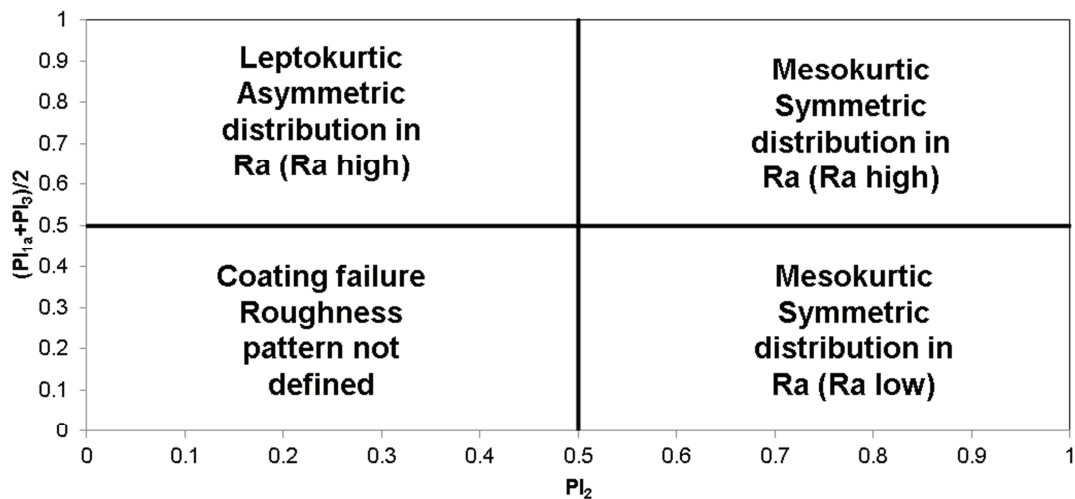
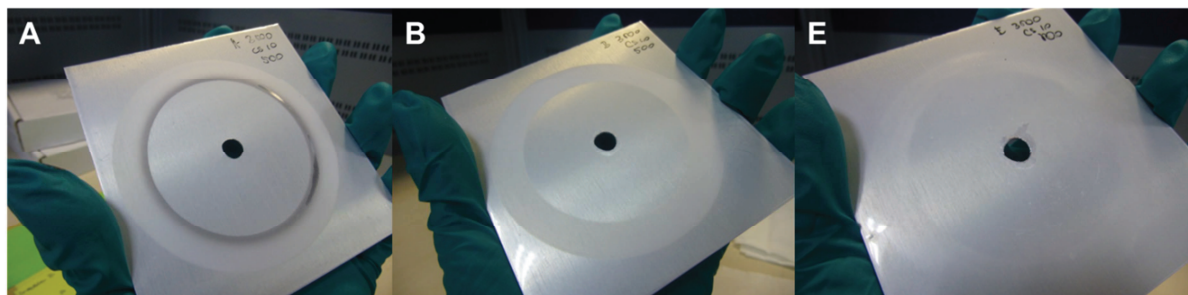


Figure 7.17 Roughness profile trends of selected coating systems and its influence on performance characteristics presented on a plot of performance indices (average of initial WCA ( $PI_{1a}$ ) and retention ratio under abrasive condition ( $PI_3$ )) and mechanical durability under abrasive conditions ( $PI_2$ )

Taking into consideration only one class of coating family presented plot of performance indices can be also used for tracing the influence of changes in material composition. The analysis of TWI formulations performance gave the ability to investigate the impact of inorganic building blocks addition on the overall performance of the coating system. An in-depth examination of TWI formulations

was presented in Chapter 6. In summary, a few specific conclusions can be drawn. The addition of mono-functionalized (MPTMA) SSQs (9%wt) into resin matrix (TWI formulation A) caused an increase in the mechanical and chemical and indirect durability, yet no significant changes in surface repellency was observed (Figure 7.13 and 7.14). The introduction of dual-functionalized (MPTMA, NPTMS) silica nanoparticles (30 nm, 50%wt, 46% solid content) in the coating system (TWI formulation B) had little effect on overall durability and wetting characteristics. This can be explained by the fact that these compositional changes didn't affect the surface topography. In terms of examination, the influence of composition on coating behaviour, only TWI formulations A, B and E can be compared. The reason for that is the fact that these coatings belong to the same family and in practise they aren't different in terms of surface roughness. Therefore, all of the changes in properties can be referred to composition modifications. The Figure below illustrates the influence of coating composition on quality of surface under specified abrasive conditions (CS10 wheels, 1000 g load).



*Figure 7.18 Effect of coating composition in TWI formulations A, B and E on quality of surface under abrasive conditions (CS10 wheels, 1000g load and 3500 cycles)*

This study has demonstrated that controlled incorporation of inorganic building blocks, such as SSQs and functionalized silica nanoparticles (30 nm size) into resin formulation has the potential to reinforce this resin, suggesting that coating lifetime could be substantially improved by this approach. On the other hand, introduction of dual-size silica nanoparticles (30 and 300 nm size) into resin matrix may be the reason for accelerated coating failure. Nevertheless, there is a possibility that the incorporation of different combination of dual-size nanoparticles with various functionalities and different loading level may have diverse influences on the functional performance of the coating system. Such modifications of coating systems would be very interesting direction for further work and new testing criteria developed in this study enables the development of next generation of materials. In terms of performance comparison of TWI coatings with similar easy clean surfaces that can be found in literature, some conclusions can be made. With

regards to repellency, it has been found that reported anti-soiling coatings containing silica nanoparticles have higher values of WCA, usually reaching more than  $150^\circ$  (Dodiuk H. R. P., 2008) (Schaeffer D.A., 2015) (Mahadik S.A., 2013) (Qu M., 2015). Nevertheless, extraordinary repellency of these reported surfaces is a result of very high roughness level, similar to the one presented by Never Wet, where leptokurtic asymmetric distribution in peaks and valleys, is accompanied by high Ra value. With regards to abrasion resistance, it can be definitely stated that durability of easy clean coatings is rather hard to compare, if these coatings haven't been evaluated in the same manner. That's why, it is so important to introduce single standardised durability evaluation methodology, so that all easy clean coatings can be compared and classified.

#### **7.4 Summary**

A new approach for durability evaluation of highly repellent surfaces was used to classify selected coating systems. The concept of spider diagrams helps to analyse multivariate properties within single coating system and to create coating "performance map". The introduction of performance indices that refer to single material property or whole group of properties allows not only for comparison of different properties within single coating system, but also for comparison between different families of coating.

Due to the fact that the developed methodology permits to translation of the durability of coating system into measurable property, the original null hypothesis can be examined. The investigation of mechanical durability of selected easy clean coatings supported the null hypothesis, which stated that there is an inverse relation between initial repellency and abrasion resistance. Nevertheless, comparison of coating wetting characteristics over its whole lifetime with its mechanical durability revealed that behavioural pattern of some of the tested materials diverge from inverse relationship. In general, final plot of performance indices shown that there are four types of behavioural pattern in selected easy clean coatings and they are strongly dependent upon initial surface roughness. Changes of surface composition in evaluated repellent surfaces were found not to have very significant influence on material performance. In terms of surface topography, the best performance (repellency and durability together) was achieved by TWI formulation F, where quite high value of arithmetic mean of surface heights was combined with mesokurtic symmetric distribution of surface asperities.

In terms of relation between initial repellency of coating and different variation of durability (chemical, indirect), the inverse relationship is not so significant anymore and there are materials that behave in unconventional way. It was found that controlled incorporation of inorganic building blocks into resin matrix brings the ability to design materials that behave beyond conventional patterns.

The presented plot of performance indices opens a promising new direction in materials development, where advanced coatings and surface treatments can be developed by design, reducing the number of development iterations, ultimately leading to reduced cost and development time. New assessment criteria can be used as a basis for development of a standard, which would allow direct comparison between different families of highly repellent surfaces.

## 8 CONCLUSIONS AND RECOMMENDATION FOR FUTURE WORK

### 8.1 Conclusions

The lack of a recognized standard procedure that enables comparison between various easy clean coatings was an obstacle in effective development of advanced materials. During this project a novel approach for the evaluation of the durability of highly repellent surfaces was developed. This new methodology helps to investigate coating performance via spider diagrams, performance indices and plot of performance indices approaches. Spider diagrams were used in order to plot multivariate data within one graph. Key coating parameters were selected and clustered into groups in spider diagram. In general, four groups of properties were identified, including initial performance, abrasion resistance, ability to retain repellency under abrasion and chemical durability. Initial performance group were further divided into three subgroups, such as repellency in pristine state, initial lipophobic character and visual appearance of the coating. All these selected coating properties were converted into spider diagram scale, where particular values were assigned to points. Based on the groups and subgroups of properties from spider diagram model, six performance indices of material were identified. Each performance index was obtained by dividing the number of points scored by material in particular group (or subgroup) of spider diagram by maximum points that can be scored in this particular group (or subgroup). Finally, the selected performance indices were compared via plot of performance indices approach.

Six TWI formulations and two commercial products were prepared and subjected to evaluation according to new testing methodology. All TWI materials had common UV cured acrylate matrix but they were different in terms of inorganic building blocks size, functionality and loading level. Commercial products GP101 and Never Wet were prepared according to manufacturer guidance.

Prior to the examination, the cure regime of TWI products was assessed with FTIR and potassium permanganate reaction. Fourier Transform Infrared Spectroscopy was used to trace the consumption of C=C bonding and it was found that this technique can be applicable only for materials that didn't have silica nanoparticles in their structure. In case of formulations containing silica nanoparticles, disappearance of C=C can be assessed with potassium permanganate reaction. Surfaces were cured to the point at which their functional properties were fully developed, so that further surface failure couldn't be identified with lack of cure. It

was found that formulations that contain silica nanoparticles in order to be “cured” they need to absorb more energy than their non-nanoparticle analogues.

Aluminium alloy 3003 H14 was used as a substrate in this study. The TWI etching + anodizing procedure was found to be the most successful available methodology of enhancing adhesion strength between coating and substrate. This process was the most effective due to the fact that adhesion was enhanced by three phenomena that occurred at the interface, namely chemical bonding, mechanical interlocking and force attraction.

Examination of the selected coating systems revealed that there is strong relation between material composition, roughness and property. The best repellent characteristics in pristine state were achieved by surfaces with dual scale roughness. This dual scale roughness also correlated with poor visual appearance. A high value of water contact angle for the coating in a pristine state didn't guarantee that repellent characteristics would be constant over the whole lifetime of the coating. The durability of easy clean coatings was assessed on a direct and indirect level, due to the fact that abrasive wear, adhesive wear is always associated with wear of functional performance. Mechanical properties of the coatings seemed to be strongly correlated to surface roughness. The best abrasion resilience was found in coating systems with mesokurtic symmetric distribution of surface asperities. Results from abrasion resistance indicated that the same coating system behave in a different manner under varying abrasion conditions. The results confirmed that in general, greater abrasion resistance can be found in coating systems with smoother symmetric texture profile. Nevertheless, similar abrasion resistance was associated with surfaces with quite high roughness level, yet very symmetric distribution of surface asperities. Beyond the effect of surface roughness, mechanical resilience was found to be strongly dependent upon coating processing, thickness and curing regime.

Examination of indirect coating durability (retention of initial repellence) revealed that water contact angle decreases with longer exposure to abrasion, yet the rate of loss is dependent upon initial surface roughness and the nature of the abrasive material. Surfaces with dual scale roughness were found to lose their repellency gradually under all types of selected abrasive conditions. Coatings with smooth symmetric surface topography kept very well their anti-soiling properties under mild abrasion, yet harsh damaging conditions accelerated the process of loss of repellency.

Abrasive and adhesive wear, together with initial performance and retention of repellence characteristics of selected coating systems were transferred into spider diagrams and appropriate figures of merit were generated. The application of novel methodology for evaluation of highly repellent surfaces confirmed that different highly hydrophobic surfaces can be compared and categorized. The FoM that relates repellency and mechanical resilience of the coatings supported the null hypothesis, which states that there is an inverse relation between coating repellence and durability. Nevertheless, it was shown that controlled addition of novel inorganic building blocks into resin matrix can improve overall coating performance by linking mechanical robustness with desired wetting characteristics.

The findings open a promising new direction in materials development, where advanced coatings and surface treatments can be designed by approach, reducing time and cost of research. Progress in testing and classification criteria of highly repellent coatings enables further development of next generation of materials. Proposed ranking of easy clean coatings will help to select right coating for right application. Furthermore, this novel evaluation methodology can serve as basis for standard that would allow acceleration of research from laboratory to industrial level.

## **8.2 Recommendation for future work**

Industrial adoption of easy clean coatings would bring a lot of benefits in many materials applications. Improvement of the mechanical stability of highly repellent surfaces would definitely accelerate the transfer from laboratory to market. A new approach for testing and ranking these types of materials significantly facilitates the progress of development of advanced coatings and surface treatments. Nevertheless, there are a number of possible directions for extending the scope of this thesis.

In order to extend the applicability of novel testing criteria, performance indices can be established for different types of surface durability. Erosive-wear, corrosive-wear and thermal-wear modes would be recommended for future investigation. Another thing that should be taken under consideration is the evaluation of synergy of wear mechanisms. It is well-known that some of the wear mechanisms can overlap and accelerate the failure of the coating system. In this case performance indices should be established as well for the synergic effect of few kinds of wear, such as abrasion under elevated and sub-zero temperatures, abrasive and erosive wear together, chemical stability under abrasive conditions etc. With regard to indirect durability, other aspects of coating properties can be included in further investigation.

Lipophobic character and visual appearance can be examined under mechanical or chemical damage.

Investigation of the functional performance of selected coating systems revealed that there is a strong relation between composition, structure and property. It would be very beneficial to extend this knowledge. Change of surface roughness could be evaluated under abrasive conditions 1, 3 and 4 and under exposure to chemicals agents. Besides that, more surface parameters should be also involved in future analysis, such as the influence of the geometric features such as distance between surface asperities or the shape of re-entrant features on the repellence and mechanical resilience of surfaces.

Surface roughness was found to be of great importance in specifying the function of surface, especially when mechanical resistance and repellency are taken under consideration. It would be worth to evaluate different coating families according to the same routine that was presented in this study and investigate if surfaces with similar texture profiles have similar behavioural patterns. The ability to control final roughness by self-assembly approach may be the successful way of producing desired advanced material. In this case, it is important to learn how much of surface performance can be achieved by the surface texturing only.

In this study it was found that materials with lower value of arithmetic means of surface heights are more robust under abrasive conditions. Nevertheless, some of coatings with higher Ra values and symmetric mesokurtic distribution presented similar behaviour pattern when exposed to mechanical damage. It would be worth to investigate, which Ra value is associated with surface transition from durable to non-durable.

Changes in coating composition were found to not have very significant influence on final performance of coating. Nevertheless, there two TWI formulations, where final properties may not be only dependent by changes in surface roughness but also by changes in coating composition. Improvement in repellent characteristics of TWI formulation F over the anti-soiling properties of TWI formulation E can be associated with the rise of Ra value in formulation F. Yet, it is more probable that these changes were the effect of modification in silica nanoparticles functionalization, where NPTMS was exchanged for FAS. Therefore, further investigation of relation between silica functionalization type and material properties should be pursued. Due to the fact that among selected coating systems, formulation F offered the best

performance in terms of combination between repellency and durability, it would be worth to lay more focus on it.

New effective way of surface preparation is also required. In this study it was established that among selected pre-treatment methods, TWI's etching + anodizing procedure was the most successful one. Nevertheless, this process involves the use of chromic acid and it's likely to be limited in future. Therefore, it would be worth to explore the advantages of alternative types of surface preparation. Mechanical anchoring by grit blasting was found to be quite effective way for enhancing adhesion at the interface. It is probable that grit blasting combined with another method of surface preparation (i.e. coupling agents) might give as good final results as TWI's etching + anodizing procedure.

References(n.d.).

- Abbasi F., M. H. (2001). Modification of polysiloxane polymers for biomedical applications: a review. *Polymer International*(1279-1287).
- Adamson A.W., A. (1976). *Physical Chemistry of Surfaces*. New York: Wiley-Interscience.
- Aizenberg J., A. M. (2011). *Patent No. US 9121306 B2*.
- Allen N.S. (1996). Photoinitiators for UV and visible curing of coatings: mechanisms and properties. *Journal of Photochemistry and Photobiology A: Chemistry*(101-107).
- Anderson D.N., R. A. (1997). Tests of the performance of coatings for low ice adhesion. *NASA Technical Memorandum 107399 AIAA-97-0303*.
- Andriot M., D. J. (2008). Silicones in industrial applications. In *Silicon – Based Inorganic Polymers*. Nova Science.
- Antonini C., I. M. (2011). Understanding the effect of superhydrophobic coatings on energy reduction in anti-icing systems. *Cold Regions Science and Technology*(58-67).
- Arkles B. (2001). Commercial applications of sol-gel-derived hybrid materials. *MRS Bulletin*(402-408).
- Arkles B. (2006). Hydrophobicity, Hydrophilicity and Silanes. *Paint & Coatings Industry*(114-124).
- Assink R.A., K. B. (1994). 1H NMR studies of the sol-gel transition". *MRS Spring Meeting Proceedings*.
- ASTM D3359 -09e2. (2009). Standard Test Methods for Measuring Adhesion by Tape Test.
- ASTM D4449-15. (2015). Standard Test Method for Visual Evaluation of Gloss Differences Between Surfaces of Similar Appearance. ASTM.
- ASTM D4541-09e1. (2011). Standard Test Method for Pull-Off Strength of Coatings Using Portable Adhesion Testers.
- ASTM D523-08. (2008). Standard Test Method for Specular Gloss.
- ASTM E430-11. (2011). Standard Test Methods for Measurement of Gloss of High-Gloss Surfaces by Abridged Goniophotometr.
- Bayer I.S., B. A. (2009). Transforming anaerobic adhesives into highly durable and abrasion resistant superhydrophobic organoclay nanocomposite films: A new hybrid spray adhesive for tough superhydrophobicity. *Applied Physics Express*(125003-125006).
- Bhushan B, J. Y. (2006). Micro- and nanoscale characterization of hydrophobic and hydrophilic leaf surfaces. *Nanotechnology*(2758-2772).
- Bhushan B, J. Y. (2009). Lotus-like biomimetic hierarchical structures developed by the self-assembly of tubular plant waxes. *Langmuir*(1659 – 1666).
- Bhushan B, N. M. (2010). The rose petal effect and the modes of superhydrophobicity. *Phil. Trans. R. Soc*(4713-4728).

- Bhushan B., K. K. (2008). Biomimetic hierarchical structure for self-cleaning. *Appl. Phys. Lett.*(093101 – 093103).
- Blaaderen A., G. J. (1992). Monodisperse colloidal silica spheres from tetraalkoxyhanes: Particle formation and growth mechanism. *Journal of Colloid and Interface Science*(481-501).
- Bogush G.H., T. M. (1988). Preparation of monodisperse silica particles: Control of size and mass fraction. *Journal of Non-Crystalline Solids*(95-106).
- Boinovich L., E. A. (2010). Analysis of long-term durability of superhydrophobic properties under continuous contact with water. *Applied Materials and Interfaces*(1754-1758).
- Boinovich L.B., E. A. (2013). Anti-icing potential of superhydrophobic coatings. *Mendeleev Communications*(3-10).
- Boldridge D. (2010). Morphological characterization of fumed silica aggregates. *Aerosol Science and Technology*(182-186).
- Brace A.W., S. P. (1979). *The Technology of Anodizing Aluminium*. Technicopy Limited.
- Brinker C.J., S. G. (1990). *Sol-gel Science: The Physics and Chemistry of Sol-gel Processing*. Academic Press.
- Brown L. H. (1972). Silicones in protective coatings. In *Treatise on Coatings Vol. 1, Part III*. Marcel Dekker.
- Brown P.S., B. B. (2016). Durable, superoleophobic polymer–nanoparticle composite surfaces with re-entrant geometry via solvent-induced phase transformation. *Scientific Reports*.
- Butt H., G. K. (2003). *Physics and Chemistry of Interfaces*. Wiley.
- Cademartiri L., O. G. (2009). *Concepts of Nanochemistry*. John Wiley & Sons.
- Calvert P. (2001). Inkjet printing for materials and devices. *Chem. Mater.*(3299-3305).
- Cao M., G. D. (2015). Water-repellent properties of superhydrophobic and lubricant-infused “slippery” surfaces: A brief study on the functions and applications. *ACS Appl. Mater. Interfaces*.
- Cassie A.B.D. (1948). Contact angles. *Discussion of Faraday Society*(11-16).
- Chambers J., C. W. (1983). *Graphical Methods for Data Analysis*. Wadsworth.
- Cheng L.L., S. W. (2011). Synthesis and photoinitiating behavior of benzophenone-based polymeric photoinitiators used for UV curing coatings. *Progress in Organic Coatings*(355-361).
- Cho H., K. D. (2013). A simple fabrication method for mechanically robust superhydrophobic surface by hierarchical aluminum hydroxide structures. *Current Applied Physics*(762-767).
- Cho W.K., C. I. (2008). Fabrication of hairy polymeric films inspired by geckos: Wetting and high adhesion properties. *Adv. Funct. Mater.*(1089-1096).

- Dalili, N. E. (2009). A review of surface engineering issues critical to wind turbine performance. *Renewable and Sustainable Energy Reviews*(428-438).
- Daniel C. (2008). Materials and processing for lithium-ion batteries. *The Journal of The Minerals, Metals & Materials Society*(43-48).
- Danişman S., S. S. (2014). Relation between coating parameters and structural and mechanical properties of magnetron sputtered TiAlN coatings. *Arabian Journal for Science and Engineering*, 36(5025-5034).
- Davison C., D. G. (2013). Addressing fouling build-up through advanced coatings. *Transactions of the Institute of Metal Finishing*(233-236).
- de Gennes P.G. (1985). Wetting - statics and dynamics. *Reviews of Modern Physics*(827–863).
- de Waal A.A., v. d. (2015). The role of performance management in creating and maintaining a high-performance organization. *Journal of Organization Design*.
- Decker C. (2006). *Photopolymerization and Ultraviolet Curing of Multifunctional Monomers*. Wiley-VCH.
- Deflorian F., F. M. (2011). Study of the effect of organically functionalized silica nanoparticles on the properties of UV curable acrylic coatings. *Progress in Organic Coatings*(44-51).
- Deng, M. L. (2012). Candle soot as a template for a transparent robust superamphiphobic coating. *Science*(67-70).
- Derjaguin B.V., K. N. (1994). Electrical phenomena accompanying the formation of new surfaces, and their role in adhesion and cohesion. *Progress in Surface Science*(95 – 104).
- Derjaguin B.V., S. V. (1967). Electronic theory of adhesion. *J. Appl. Phys.*(4606-4616).
- Dodiuk H., K. S. (2012). Do self-cleaning surfaces repel ice. *Journal of Adhesion Science and Technology*(701-714).
- Dodiuk H., R. P. (2008). Durable ultra-hydrophobic surfaces for self-cleaning applications. *Polymers for Advanced Technologies*(1684-1691).
- Dong H., C. M. (2013). Extraordinary drag-reducing effect of a superhydrophobic coating on a macroscopic model ship at high speed. *Journal of Materials Chemistry A*(5886-5891).
- Dougherty C. (2011). *Induction to Econometrics*. OXFORD.
- Drelich J., C. E. (2011). Hydrophilic and superhydrophilic surfaces and materials. *Soft Matter*(9804-9828).
- Drexler K.E., D. (1986). *Engines of creation • The coming era of nanotechnology*. Anchor Books.
- Drobny J.G. (2001). *Technology of Fluoropolymers*. Boca Raton.
- Durand G.G., T. A. (2014). Durable anti-fouling/anti-icing coatings. New strategy development. *20th International Congress on Surface Treatments in the Aeronautics and Aerospace Industries*.

- ECHA. (n.d.). Retrieved from <https://echa.europa.eu/addressing-chemicals-of-concern/restrictions/substances-restricted-under-reach/-/dislist/details/0b0236e1807e2bc1>.
- ECHA European Chemical Agency. (2014). *ANNEX XV RESTRICTION REPORT Perfluorooctanoic acid (PFOA), PFOA salts and PFOA-related substances*.
- Eickner H.W., S. W. (1950). A study of methods for preparing clad 24S-T3 aluminium alloy surfaces for bonding. *Forest Prod. Lab. Report No. 1813A*.
- Ejenstam L., O. L.-M. (2013). The effect of superhydrophobic wetting state on corrosion protection--the AKD example. *J. Colloid Interface Sci.*(56-64).
- EPA (Environmental Protection Agency). (2012). *2010 – 2015 PFOA Stewardship Programme*.
- European Commission. (2015). *Towards a review of the EC Recommendation for a definition of the term “nanomaterial”*.
- Evans J.R.G., P. D. (1979). Adhesion of polyethylene to metals: The role of surface topography. *The Journal of Adhesion*(177-191).
- Feng L., Z. Y. (2008). Petal Effect: A superhydrophobic state with high adhesive force”. *Langmuir*(4114-4119).
- Ferguson T.P., Q. J. (2004). Moisture and temperature effects on the reliability of interfacial adhesion of a polymer/metal interface. *54th Electronic Components and Technology Conference Proceedings*(1752-1758).
- Foscante R.E., M. N. (1997). Epoxy polysiloxane coating and flooring compositions. *Patent US 5618860 A*.
- Fowkes F.M. (1964). Attractive forces at interface. *Ind. Eng. Chem*(40-52).
- Galindo P.V., V. E. (2015). How corporations deal with reporting sustainability: Assessment using the multicriteria logistic biplot approach. *Systems*(6-26).
- Gallo V., L. G.-E. (2012). Serum perfluorooctanoate (PFOA) and perfluorooctane sulfonate (PFOS) concentrations and liver function biomarkers in a population with elevated PFOA exposure. *Environmental Health Perspectives*(655-660).
- Gangopadhyay S., A. R. (2009). Composition and structure–property relationship of low friction, wear resistant TiN–MoS<sub>x</sub> composite coating deposited by pulsed closed-field unbalanced magnetron sputtering. *Surface and Coatings Technology*, 203(1565–1572).
- Gao L., M. T. (2006). Contact angle hysteresis explained. *Langmuir*(6234-6237).
- Gelling V.J., W. M. (2001). Electroactive-conducting polymers for corrosion control: 4. Studies of poly (3-octyl pyrrole) and poly (3-octadecyl pyrrole) on aluminum 2024-T3 alloy. *Progress in Organic Coatings*(149-157).
- Gibbs J.W. (1873). A method of geometrical representation of the thermodynamic properties of substances by means of surfaces. *Transactions of the Connecticut Academy of Arts and Sciences*(382-404).

- Gnanasekaran D., M. K. (2009). Developments of polyhedral oligomeric silsesquioxanes (PaSS), pass nanocomposites and their applications: A review. *Journal of Scientific & Industrial Research*(437-46).
- Goehring L., C. R. (2010). Evolution of mud-crack patterns during repeated drying cycles. *Soft Matter*.
- Good R.J., G. (1979). Contact angles and the surface free energy of solids. *Surface and Colloid Science*(1-29).
- Harrick N.J. (1967). *Internal Reflection Spectroscopy*. John Wiley & Sons Inc.
- Harris A.F., B. A. (1999). The effect of grit-blasting on surface properties for adhesion. *International Journal of Adhesion & Adhesives*(445-452).
- Heinrich A., R. R. (1991). *Aircraft icing handbook*.
- Hench L.L., W. J. (1990). The sol-gel process. *Chem. Rev.*(33-72).
- Hohne S., B. C. (2009). Superhydrophobic alumina surfaces based on polymer-stabilized oxide layers. *Macromolecular Chemistry and Physics*(1263-1271).
- Hong X., G. X. (2007). Application of superhydrophobic surface with high adhesive force in no lost transport of superparamagnetic microdroplet. *J. Am. Chem. Soc.*(1478-1479).
- Hoyt J.W. (1985). Turbulent-flow interactions and drag reduction. *AIP Conference Proceedings*(95-115).
- Iler R.K. (1979). *The Chemistry of Silica: : Solubility, Polymerization, Colloid and Surface Properties and Biochemistry of Silica*. Wiley.
- ISO 4287. (1997). Geometrical Product Specifications (GPS) - Surface texture: Profile method - Terms, definitions and surface texture parameters.
- ISO 4288. (1996). Geometrical Product Specifications (GPS) -- Surface texture: Profile method -- Rules and procedures for the assessment of surface texture.
- Izumi K., T. H. (1993). Hydrolysis of trifunctional alkoxy silanes and corrosion resistance of steel sheets with alkoxy silane-derived films. *J. Mater. Sci. Lett.*(724-727).
- Jančovičová V., K. J. (2007). Influence of photoinitiator and curing conditions on polymerization kinetics and gloss of UV-cured coatings. *Chemical Papers*(383-390).
- Jin H., T. X. (2013). Preservation of superhydrophobic and superoleophobic properties upon wear damage. *Applied Materilas and Interfaces*(485-488).
- Jones B. (2008). Fluoropolymers for coating applications. *JCT Coatings Tech.*(44-48).
- Jung S., D. M. (2011). Are superhydrophobic surfaces best for icephobicity? *Langmuir*(3059-3066).
- Kaelble D.H. (1970). Dispersion-polar surface tension properties of organic solids. *J. Adhesion*(66-81).

- Kanagasabapathy S., B. R. (2012). Hydrophobic coating compositions for drag reduction. *US 20120142814 A1*.
- Karlović I., N. D. (2010). The influence of surface topography of UV coated. *Journal of Graphic Engineering and Design*.
- Kawakami Y., C. Y. (2006). Design of polysiloxane materials for electronic applications. *Molecular Crystals and Liquid Crystals*(507-520).
- Kehl G.L. (1949). *The Principles of Metallographic Laboratory Practice*. McGraw-Hill.
- Keijman J.M. (2002). Inorganic-organic hybrid coatings in the protective coatings industry. *SSPC (The Society for Protective Coatings) Conference Proceedings*.
- Keller E., G. ., (2006). *Light Microscopy*. Cold Spring Harbor Laboratory Press.
- Khlebtsov B.N., K. V. (2008). Determination of the size, concentration, and refractive index of silica nanoparticles from turbidity spectra. *Langmuir*(8964–8970).
- Kickelbick G. (2007). *Hybrid Materials: Synthesis, Characterization, and Applications*. Wiley-VCH Verlag GmbH & Co. KGaA.
- Kim P., K. M. (2013). Hierarchical or not? Effect of the length scale and hierarchy of the of the surface roughness on omniphobicity of lubricant-infused substrates. *Nano Letters*(1793–1799).
- Kinziga B.J., R. H. (1978). Factors contributing to the properties of fluoropolymer barrier films. *Tribology Translations*.
- Kissa, E. (1994). *Fluorinated Surfactants and Repellents*. Marcel Dekker, Inc.
- Koch K., B. B. (2010). Multifunctional plant surfaces and smart materials. *Springer Handbook of Nanotechnology F*(1399-1436).
- Kulinich S.A., F. M. (2011). On ice-releasing properties of rough hydrophobic coatings. *Cold Regions Science and Technology*(60-64).
- Kunwong D., S. N. (1994). Curing behavior and cured film performance of easy-to-clean UV-curable coatings based on hybrid urethane acrylate oligomers. *Journal of Polymer Research*(1-12).
- Laforte J.L., A. M. (1998). State-of-the-art on power line de-icing. *Atmospheric Research*(143-158).
- Lafuma A., Q. D. (2003). Superhydrophobic states. *Nat. Mater.*(457-460).
- Lakshmi R.V., B. T. (2012). Fabrication of superhydrophobic and oleophobic sol-gel nanocomposite coating. *Surface & Coatings Technology*(3888-3894).
- Lane J. M., I. A. (2009). Forces between functionalized silica nanoparticles in solution. *Physical Review E*.

- Lefebvre D. R., T. K. (1991). Degradation of epoxy coatings in humid environment: The critical relative humidity for adhesion loss. *Journal of Adhesion Science and Technology*, 5(201-227).
- Leidheiser H., F. W. (1987). Water disbondment and wet adhesion of organic coatings on metals: A review and interpretation. *Journal of the Oil and Colour Chemists Association*(121-132).
- Lewis R.J. (2007). *Hawley's Condensed Chemical Dictionary*. Wiley – Interscience.
- Leyland A., M. A. (2000). On the significance of the H/E ratio in wear control: a nanocomposite coating approach to optimised tribological behaviour. *Wear*(1-11).
- Li B., Z. J. (2013). Durable superhydrophobic surface prepared by spray coating of polymerized organosilane/attapulgite nanocomposites. *ChemPlusChem*(1503-1509).
- Li Y., L. L. (2010). Bioinspired self-healing superhydrophobic coatings. *Angewandte Chemie*(6129-6133).
- Lichtenhan J.D., S. J. (n.d.). Process for the formation of polyhedral oligomeric silsesquioxanes. *US 6972312 B1*.
- Lim H.M., L. J. (2010). Comparative Study of Various Preparation Methods of Colloidal Silica. *Engineering*.
- Liu X., Z. J. (2012). Clam's shell inspired high-energy inorganic coatings with underwater low adhesive superoleophobicity. *Advanced Materials*(3401-3405).
- Luo D.B., F. V. (2011). A systematic approach for the selection of tribological coatings. *Wear*(2132– 2143).
- Lyklema J. (1991). *Fundamentals of Interface and Colloid Science*. Academic Press.
- Mahadik S.A., F. P. (2013). Durability and restoring of superhydrophobic properties in silica-based coatings. *Journal of Colloid and Interface Science*.
- Makkonen L. (2012). Ice adhesion – theory, measurements and countermeasures. *Journal of Adhesion Science and Technology*(413-445).
- Malavasi I., B. I. (2014). Assessing durability of superhydrophobic surfaces. *Surface Innovations*.
- Malkov A.A., S. E. (2006). The Influence of titanium oxide nanocoatings on the surface quality of glass products for electronic devices. *Glass Physics and Chemistry*(70-74).
- Mammeri F., L. B. (2005). Mechanical properties of hybrid organic–Inorganic materials. *J. Mater. Chem.*(3738-3811).
- Manczyk K., M. K. (2008). Anti-graffiti protective coatings. *Polimery*(830-835).
- Marceau J.A., F. R. (1978). Method for Providing Environmentally stable Aluminium Surfaces for Adhesive Bonding and Product Produced. *US Patent 4,127,451*.
- Marmur A. (1994). Thermodynamic aspects of contact angle hysteresis. *Adv. Colloid Interface Sci.*(121-141).

- Marmur A. (2004). The Lotus Effect: superhydrophobicity and metastability. *Langmuir*(3517-3519).
- Marmur A. (2012). Hydro- hygro- oleo- omni-phobic? Terminology of wettability classification. *Soft Matter*.
- Martin J. .W., S. S. (1994). *Methodologies for Predicting the Service Lives of Coating Systems*. DIANE Publishing.
- McBain J.W., H. D. (1925). On adhesives and adhesive action. *J. Phys. Chem.*(188 – 204).
- Menini R., F. M. (2009). Elaboration of Al<sub>2</sub>O<sub>3</sub>/PTFE icephobic coatings for protecting aluminum surfaces. *Surface & Coating technology*(1941-1946).
- Menini R., F. M. (2011). Advanced icephobic coatings. *Journal of Adhesion Science and Technology*(971-992).
- Messori M., T. M. (2006). Perfluoropolyether-based organic-inorganic hybrid coatings: Preparation and surface characterisation. *Polymer*(1055-1062).
- Milionis A., B. I. (2013). Combination of lithography and coating methods for surface wetting control. *Nanotechnology and Nanomaterials*.
- Min J., A. M. (2008). The role of interparticle and external forces in nanoparticle assembly. *Nature: Materials*(527-538).
- Minford M.D. (1993). *Handbook of Aluminium Bonding Technology and Data*. CRC Press.
- Monroe B.M, W. G. (1993). Photoinitiators for free radical initiated photoimaging systems. *Chemical Reviews*(435-448).
- Mowrer N. R. (2003). *Polysiloxane coatings innovation*. Amerton Int.
- Nahum T., D. H. (2014). Superhydrophobic durable coating based on UV-photoreactive silica nanoparticles. *Journal of Applied Polymer Science*.
- Napierska D., T. L. (2010). The nanosilica hazard: another variable entity. *Particle and Fibre Toxicology*(7-39).
- Neumann A.W., G. R. (1979). Techniques of measuring contact angles. In *Surface and Colloid Science*. Springer.
- Nguyen T., B. D. (1995). Method for measuring water diffusion in a coating applied to a substrate. *Journal of Coatings Technology*(37-46).
- Nguyen T.A., G. Ø. (2014). Effects of hydrophobic polyhedral oligomeric silsesquioxane coating on water vapour barrier and water resistance properties of paperboard. *Journal of Sol-Gel Science and Technology*(237-249).
- Nosonovsky M. (2011). Materials science: slippery when wetted. *Nature*.
- Nosonovsky M., N. (2007). Multiscale roughness and stability of superhydrophobic biomimetic interfaces. *Langmuir*(3157–3161).

- Nowak B.M., N. (1993). Hybrid nanocomposite materials—between inorganic glasses and organic polymers. *Adv. Mater.*(422-433).
- NRC (National Research Council). (2006). *A Matter of Size: Triennial Review of the National Nanotechnology Initiative*. National Academies Press.
- O’Sullivan J. P., W. G. (1970). The morphology, mechanisms of formation of porous anodizing film on aluminium surface. *Proceedings of Royal Society of London A*(511-543).
- Oberle T.L. (2000). On the influence of thermal properties on wear resistance of rubbing metals at elevated temperatures. *Journal of Tribology—ransaction of the ASTM*(657-660 ).
- OCHA. (n.d.). Retrieved from <https://www.osha.gov/SLTC/hexavalentchromium/>.
- Oldring P.K.T. (1998). *Chemistry & Technology for UV & EB Formulation for Coatings, Inks & Paints, Speciality Finishes*. Wiley.
- Owens D., W. R. (1969). Estimation of the surface free energy of polymers. *J. Appl. Polym. Sci*(1741-1747).
- Parkin L.P., P. R. (2005). Self-cleaning coatings. *J. Matter. Chem.*(1689-1695).
- Pazderova M., B. M. (2011). Tribological behaviour of composite coatings. *Conference Proceedings of The 11th Conference on the Mechanical Behaviour of Materials*.
- Pham D.C., N. K. (2011). Wetting behavior and nanotribological properties of silicon nanopatterns combined with diamond-like carbon and perfluoropolyether films. *Nanotechnology*.
- Pham Q.T., C. C. (2013). Thermal stability of organofunctional polysiloxanes. *Thermochimica Acta*(114-123).
- Plueddemann E.P. (1982). *Silane coupling agents*. Plenum Press.
- Qu M., H. J. (2015). Fabrication of Mechanical Durable Polysiloxane Superhydrophobic Materials. *Journal of Nanomaterials*.
- R. Valeri. (2009). Photocurable acrylic coating compositions having good adhesion properties to a subsequent coating and corresponding coated substrates. *US 20090311518 A1*.
- Rabea A.M., M. M. (2012). Surface analysis and anti-graffiti behavior of a weathered polyurethane-based coating embedded with hydrophobic nano silica. *Applied Surface Science*(4391-4396).
- Random House Webster’s College Dictionary. (2005).
- Remer M., S. G. (2014). Dynamic contact of droplet with superhydrophobic surface in conditions favour icing. *Journal of Physics: Conference Series*.
- Roach P., S. N. (2008). Progress in superhydrophobic surface development. *Soft Matter*(224-240).
- Rodriguez V., S. J. (2011). Roughness measurement problems in tribological testing. *International Journal of Sustainable Construction & Design*.

- Sanchez C., B. P. (2011). Applications of advanced hybrid organic-inorganic nanomaterials: from laboratory to market. *Chem. Soc. Rev.*(696-753).
- Sanchez C., R. F. (1994). Design of hybrid organic-inorganic materials synthesized via sol-gel chemistry. *New J. Chem.*(1007-1047).
- Savitzky A., G. M. (1964). Smoothing and differentiation of data by simplified least squares procedures. *Analytical Chemistry*(1627-1639 ).
- Schaeffer D.A., P. G. (2015). Optically transparent and environmentally durable superhydrophobic coating based on functionalized SiO<sub>2</sub> nanoparticles. *Nanotechnology*.
- Schmidt H., P. G. (1986). Glass sealings by sol – gel derived organically modified silicates. *Collect. Pap. Int. Congr. Glass*(429-436).
- Schonhorn H., S. L. (1964). Surface energetics, adhesion, and adhesive joints. *Advances in Chemistry Series, Amer. Chem. Soc.*(189 – 201).
- Schottner G. (2001). “Hybrid sol-gel-derived polymers: applications of multifunctional materials. *Chem. Matter.*(3422-3435).
- Schutzius T.M., T. M. (2011). High strain sustaining, nitrile rubber based, large-area, superhydrophobic, nanostructured composite coatings. *Composites: Part A*(979-985).
- Scott D.W., S. (1946). Thermal rearrangement of branched-chain methylpolysiloxanes. *J. Am. Chem. Soc.*(356-358).
- Shevchenko V.Y., M. A. (2003). The structural diversity of the nanoworld. *Glass Physics and Chemistry*.
- Singh P., V. R. (2000). Formation and aging of incipient thin film wax-oil gels. *AIChE Journal*(1059-1074).
- Smietana M., B. W. (2010). Nanocoating enhanced optical fibre sensors. *Advances in Materials Science for Environmental and Nuclear Technology*(275-286).
- Smitha V.S., J. K. (2013). UV curable hydrophobic inorganic-organic hybrid coating on solar cell covers for photocatalytic self-cleaning application. *J. Matter. Chem. A*.
- Sørensen P.A., K. S.-J. (2009). Anticorrosive coatings: a review. *Journal of Coatings Technology and Research*(135-176).
- Spori D. (2010). Structural Influences on Self-cleaning Surfaces. *DISS ETH NO.: 18942*.
- Srinivasan S., C. W. (2013). Drag reduction for viscous laminar flow on spray-coated non-wetting surfaces. *Soft Matter*(5691-5702).
- Steele A., B. L. (2012). Adhesion strength and superhydrophobicity of polyurethane/organoclay nanocomposite coatings. *Journal of Applied Polymer Science*(E445-E452).
- Steidl N., M. A. (2003). Pure cleanness. *European Coatings Journal*(63).

- Stein J., T. K. (2003). Structure-property relationships of silicone biofouling-release coatings: Effect of silicone network architecture on pseudobarnacle attachment strengths. *The Journal of Bioadhesion and Biofilm Research*, 19(87-94).
- Stöber W., F. A. (1968). Controlled growth of monodisperse silica spheres in the micron size range. *Journal of Colloid and Interface Science*(62-69).
- Stowe R.J. (1993). High peak irradiance microwave – powered UV lamps for processing of coatings, inks and adhesives. *Ultraviolet Technology IV*(375-385).
- Tasic S., B. B. (2004). Synthesis of new hyperbranched urethane-acrylates and their evaluation in UV-curable coatings. *Progress in Organic Coatings*(321-328 ).
- Taylor A. (2014). *A review and evaluation of the durability of low surface energy coatings*. TWI Industrial Member 1047/2014.
- Taylor A. (2011). *Patent No. US7910216B2*.
- Taylor A., B. L. (2011). Analysis of Vitolane® method for the synthesis of methacrylate functionalised resin. *TWI's Member Report 19361.01/2011/1400.3*.
- Taylor A., D. G. (2015). *Functionalisation methods for metal oxides particles*.
- Taylor A., H. D. (1993). The chemical synthesis and crystallisation sequence of mullite. *Journal of Non-Crystalline Solids* 1(1-17).
- Teng H., T. (2012). Overview of the development of the fluoropolymer industry. *Appl. Sci.* (496-512).
- Teo B.K., S. X. (2006). From top-down to bottom-up to hybrid nanotechnologies: Road to nanodevices. *Journal of Cluster Science*(529-540).
- The American College Dictionary* . (1947). Random House.
- Tjong S.C., C. H. (2004). Nanocrystalline materials and coatings. *Materials Science Engineering R – Reports*(1-88).
- Townsin R.L. (2003). The Ship Hull Fouling Penalty. *Journal of Bioadhesion and Biofilm Research*(9-15).
- UNEP (United Nations Environmental Programme). (2006). *Annual Report*.
- Uyanik M., A. E. (2006). Heat-resistant hydrophobic–oleophobic coatings. *J. Appl. Polym. Sci.*(2386-2392).
- Van Oss C.J., G. R. (1988). Additive and nonadditive surface tension components and the interpolation of contact angles. *Langumir*(884-891).
- Vanlandingham M.R., E. R. (1999). Moisture diffusion in epoxy systems. *Journal of Applied Polymer Science*(787-798).

- Vasiliev L.L., V. (2013). Heat Transfer Enhancement in Heat Pipes and Thermosyphons Using Nanotechnologies (Nano-Coatings, Nano-Liquids, and Nano Composites as the HP Envelope). *Conference Proceedings of The 11th International Heat Pipe Symposium*.
- Venables J.D., M. D. (1979). Oxide morphologies on aluminium prepared for adhesive bonding. *Appl. Surf. Sci.*(88).
- Veneables J.D. (1984). Adhesion and durability of metal-polymer bonds. *Journal of Materials Science*.
- Verho T., B. C. (2011). Mechanically durable superhydrophobic surfaces. *Advanced Materials* 5, pp. 673-678.
- Verma G., S. S. (2013). Hydrophobic self-cleaning coating based on siloxane modified waterborne polyester. *International Journal of Scientific Engineering and Technology*(192-200).
- Verwey E.J.W. (1935). Electrolytic conduction of a solid insulator at high fields for the formation of the anodic oxide film on aluminium. *Physica*(1059-1063).
- Voronkov M.G., L. V. (1982). Polyhedral oligosilsesquioxanes and their homo derivatives. *Topics in Current Chemistry*(199-236).
- Vu C., L. F. (2005). High Performance UV Multi-Layer Coatings Using Inorganic Nanoparticles. *RadTech Europe 2005 Conference & Exhibition*.
- Wang F.J., L. S. (2013). Superhydrophobic surfaces with excellent mechanical durability and easy repairability. *Applied Surface*(397-400).
- Wang S., J. L. (2007). Definition of superhydrophobic states. *Adv. Mater.*(3423-3424).
- Wen J.Y., W. G. (1996). Organic/inorganic hybrid network materials by the sol-gel approach. *Chemistry of Materials*(1667-1681).
- Wenzel R.N. (1936). Resistance of solid surfaces to wetting by water. *Ind. Eng. Chem*(988-994).
- Whitesides G.M., G. B. (2002). Self-assembly at all scales. *Science*(2418-2421).
- Wojdyla A., D. G. (2014). Advanced low energy durable coatings. *International Journal of Energy Research*(165-171).
- Wu L.Y., N. S. (2011). Quantitative test method for evaluation of anti-fingerprint property of coated surfaces. *Applied Surface Science*(2965-2969).
- Wu X., R. R. (2008). Development of low-VOC 2K waterborne polyurethane anti-graffiti coatings. *JTC Coatings Tech*(66-72).
- Young T., Y. (1805). An essay on the cohesion of fluids. *Phil. Trans. R. Soc.*(65-87).
- Zhang F.Z., Z. L. (2008). Corrosion Resistance of Superhydrophobic Layered Double Hydroxide Films on Aluminum. *Angewandte Chemie – International Edition*(2466-2469).
- Zhang S. (2003). Building from the bottom up. *Materials Today*.

- Zhang X., L. X. (2012). Easy-to-clean property and durability of superhydrophobic flaky -alumina coating on stainless steel in field test at a paper machine. *Applied Surface Science*(3102-3108).
- Zhao H., L. K. (2011). Fabrication, surface properties, and origin of superoleophobicity for a model textured surface. *Langmuir*(5927–5935).
- Zhao H., P. K. (2012). Effect of surface texturing on superoleophobicity, contact angle hysteresis, and “robustness”. *Langmuir*(14925–14934).
- Zheng S.X., L. J. (2010). Inorganic - organic sol gel hybrid coatings for corrosion protection of metals. *Journal of Sol-Gel Science and Technology*(174-187).
- Zhou S., D. X. (2013). Fabrication of ambient-curable superhydrophobic fluoropolysiloxane/TiO<sub>2</sub> nanocomposite coatings with good mechanical properties and durability. *Progress in Organic Coatings*(563-570).
- Zhu W., T. D. (2012). Multifunctional composite multilayer coatings on glass with self-cleaning, hydrophilicity and heat-insulating properties. *Thin Solid Films*(201-211).
- Zhu X., Z. Z. (2011). Robust superhydrophobic surfaces with mechanical durability and easy repairability. *Journal of Material Chemistry*(15793-15797).
- Zimmermann J., R. F. (2007). Long term environmental durability of a superhydrophobic silicone nanofilament coating. *Colloids and Surfaces A: Physicochemical and Engineering Aspects*(234-340).
- Zisman W.A., Z. (1964). Relation of the equilibrium contact angle to liquid and solid constitution. *Adv. Chem. Ser.*(1-51).